



UNIVERSITAT DE  
BARCELONA

## Prognostic markers and therapeutic targets for metastatic renal cell carcinoma

Mariona Bartrolí Comellas



Aquesta tesi doctoral està subjecta a la llicència *Reconeixement- SenseObraDerivada 4.0. Espanya de Creative Commons.*

Esta tesis doctoral está sujeta a la licencia *Reconocimiento - SinObraDerivada 4.0. España de Creative Commons.*

This doctoral thesis is licensed under the *Creative Commons Attribution-NoDerivatives 4.0. Spain License.*

**UNIVERSITAT DE BARCELONA**  
**FACULTAT DE FARMÀCIA I CIÈNCIES DE L'ALIMENTACIÓ**  
**DEPARTAMENT DE BIOQUÍMICA I BIOLOGIA MOLECULAR**  
**PROGRAMA DE DOCTORAT EN BIOMEDICINA**

**PROGNOSTIC MARKERS AND THERAPEUTIC TARGETS  
FOR METASTATIC RENAL CELL CARCINOMA**

**MARIONA BARTROLÍ COMELLAS**

**2018**





UNIVERSITAT DE BARCELONA

FACULTAT DE FARMÀCIA I CIÈNCIES DE L'ALIMENTACIÓ

DEPARTAMENT DE BIOQUÍMICA I BIOLOGIA MOLECULAR

PROGRAMA DE DOCTORAT EN BIOMEDICINA

**PROGNOSTIC MARKERS AND THERAPEUTIC TARGETS**

**FOR METASTATIC RENAL CELL CARCINOMA**

MARIONA BARTROLÍ COMELLAS

2018

Memòria presentada per Mariona Bartrolí Comellas per optar al grau de Doctor/a per la  
Universitat de Barcelona

Dr. Oriol Casanovas Casanovas

Dr. Francesc Viñals Canals

Mariona Bartrolí Comellas

Director

Tutor

Autor





# TABLE OF CONTENTS

<b>LIST OF ABBREVIATIONS</b> .....	<b>7</b>
<b>LIST OF FIGURES</b> .....	<b>13</b>
<b>LIST OF TABLES</b> .....	<b>17</b>
<b>SUMMARY</b> .....	<b>19</b>
<b>RESUM</b> .....	<b>23</b>
<b>INTRODUCTION</b> .....	<b>27</b>
<b>1. METASTASIS</b> .....	<b>29</b>
1.1 <i>Local invasion</i> .....	31
1.2 <i>Intravasation</i> .....	32
1.3 <i>Survival in the circulation</i> .....	34
1.4 <i>Arrest at a distant organ site</i> .....	37
1.5 <i>Extravasation</i> .....	37
1.6 <i>Initial survival in a foreign microenvironment and micrometastasis formation</i> .....	39
1.7 <i>Distant/metastatic colonization</i> .....	40
1.8 <i>Challenges in metastatic research</i> .....	41
<b>2. CLONAL HETEROGENEITY</b> .....	<b>42</b>
2.1 <i>Metastasis progression models</i> .....	43
2.2 <i>Metastasis progression genes</i> .....	44
2.3 <i>Clonal heterogeneity influences cancer treatments and outcomes</i> .....	46
<b>3. RENAL CELL CARCINOMA</b> .....	<b>47</b>
3.1 <i>RCC Classification</i> .....	48
3.1.1 <i>Clear Cell Renal Cell Carcinoma</i> .....	50
3.2 <i>Histopathological classification: Nuclear grade classification</i> .....	50
3.3 <i>Clinical classification of RCC: Tumor-Node-Metastasis staging</i> .....	51
3.4 <i>Clonal heterogeneity in Renal Cell Carcinoma</i> .....	53
<b>4. MODELING METASTASIS IN THE MOUSE</b> .....	<b>54</b>
4.1 <i>Patient-derived xenograft mouse models</i> .....	54
<b>5. PREVIOUS DATA</b> .....	<b>55</b>



5.1 Spontaneous generation of two variants of a ccRCC Patient-derived orthoxenograft mouse model .....	55
5.2 Metastatic potential of Ren 50 and Ren 50M tumors .....	58
5.3 Molecular characterization .....	60
5.3.1 Exome sequencing analysis of the human biopsy, Ren 50 and Ren 50M tumors ..	60
5.3.2 Fluorescent <i>In Situ</i> Hybridization analysis of Ren 50 and Ren 50M tumors, together with Ren 50M lung metastases .....	62
5.3.3 RNA sequencing and Gene Set Enrichment Analysis of Ren 50 and Ren 50 tumors .....	66
<b>OBJECTIVES .....</b>	<b>71</b>
<b>MATERIALS AND METHODS .....</b>	<b>75</b>
<b>1. IN VITRO.....</b>	<b>77</b>
1.1 Cell culture.....	77
1.1.1 Cell line maintenance .....	77
1.1.2 Cell lines.....	77
1.1.3 Mycoplasma test .....	78
1.1.4 Cell line treatments .....	79
1.1.5 Cell counting .....	79
1.1.6 Cell freezing and cryopreservation.....	79
1.2 Molecular analysis.....	80
1.2.1 RNA detection.....	80
1.2.1.1 RNA extraction of cells.....	80
1.2.1.2 Obtention of cDNA from RNA .....	80
1.2.1.3 Real-Time Quantitative PCR .....	81
1.2.2 Protein detection.....	82
1.2.2.1 Preparation of protein lysates from cell culture .....	82
1.2.2.2 Quantification of protein extracts.....	82
1.2.2.3 Conditioned media generation and trichloroacetic acid protein precipitation .....	83
1.2.2.4 Protein analysis by western blotting.....	83
1.2.2.5 Protein detection by immunocytofluorescence.....	85
1.2.3 Cell transfections and infections .....	86
1.2.3.1 Handling of bacteria .....	86

1.2.3.2 Bacterial transformation using heat shock and competent cells .....	86
1.2.3.3 Obtaining plasmidic DNA from bacterian cultures .....	87
1.2.3.4 Large scale DNA preparations.....	87
1.2.3.5 Characterization of the plasmid genome by DNA digestion with restriction enzymes.....	87
1.2.3.6 Lipofectamine DNA Transfection.....	88
1.2.3.7 Cumate system.....	89
1.2.3.7.1 Lentiviral production using polyethylenimine-mediated transfection .....	90
1.2.3.7.2 Lentiviral infections .....	91
1.2.3.8 Cell Sorting.....	92
<b>1.3 In vitro assays.....</b>	<b>92</b>
1.3.1 Migration assays .....	92
1.3.1.1 Wound healing assay .....	92
1.3.1.2 Transwell migration assay .....	93
1.3.2 Invasion assays .....	93
<b>2. IN VIVO .....</b>	<b>94</b>
2.1 <i>Animals and conditions</i> .....	94
2.2 <i>Patient-Derived Orthoxenograft Mouse Model from a RCC Human Biopsy</i> .....	94
2.3 <i>Cell lines mouse models</i> .....	95
2.3.1 Kidney tumors.....	95
2.3.2 Intravenous – Tail vein injection.....	95
2.4 <i>Tumor and organ collection</i> .....	95
2.5 <i>Paraffin inclusion</i> .....	96
2.6 <i>Determination of tumor burden</i> .....	96
2.7 <i>Invasion studies</i> .....	96
2.8 <i>Metastasis determination</i> .....	97
2.9 <i>Vorapaxar treatment</i> .....	97
2.10 <i>Molecular analysis</i> .....	99
2.10.1 RNA detection.....	99
2.10.1.1 RNA extraction of tumor samples and cDNA obtention .....	99
2.10.1.2 Real-Time Quantitative PCR .....	99
2.10.2 Protein detection.....	100
2.10.2.1 Tissue protein extraction and quantification.....	100

2.10.2.2 Protein analysis by western blotting.....	100
2.10.2.3 Immunohistochemistry in paraffinized sections .....	100
<b>3. CLINICAL VALIDATION: IN SILICO ANALYSES.....</b>	<b>101</b>
<b>4. STATISTICAL ANALYSIS .....</b>	<b>102</b>
<b>RESULTS .....</b>	<b>103</b>
<b>1. METASTATIC CANDIDATES .....</b>	<b>105</b>
1.1 Carboxypeptidase E.....	105
1.2 Coagulation pathway.....	107
<b>2. EXPRESSION VALIDATION.....</b>	<b>113</b>
2.1 Expression of CPE, F13A and F2R in Ren 50 and Ren 50M tumors.....	113
2.2 Protein expression heterogeneity of CPE, F13A and F2R in the orthotopic mouse and in Ren 50M tumors.....	115
2.3 CPE, F13A and F2R expression in Ren 50 and Ren 50M lung metastases .....	118
<b>3. FUNCTIONAL VALIDATION.....</b>	<b>120</b>
3.1 Carboxypeptidase E.....	120
3.1.1 CPE expression in RCC cell lines.....	124
3.1.2 Generation of a CPE-expressing cell line .....	125
3.1.3 Effects of CPE expression in 786O- cells.....	131
3.1.4 CPE secreted protein detection and its effects <i>in vitro</i> .....	133
3.1.5 Effects of CPE expression in <i>in vivo</i> models of 786O-.....	137
3.2 Coagulation Pathway.....	141
3.2.1 Coagulation Factor XIII.....	142
3.2.1.1 F13A expression in RCC cell lines.....	144
3.2.1.2 Generation of a F13A-expressing cell line.....	145
3.2.1.3 Generation of F13A-expressing tumors .....	146
3.2.1.4 Effects of F13A expression in 786O- tumors.....	146
3.2.1.5 CPE expression by F13A-expressing tumors.....	148
3.2.2 Coagulation Factor II Thrombin Receptor or Protease-Activated Receptor 1.....	149
3.2.2.1 F2R expression in RCC cell lines.....	151
3.2.2.2 F2R protein expression in SN12C cells and tumors .....	151
3.2.2.3 Effects of F2R inhibition in <i>in vivo</i> models of SN12C .....	152
3.2.2.4 Effects of F2R inhibition in SN12C cells .....	157

<b>4. CLINICAL VALIDATION .....</b>	<b>160</b>
4.1 <i>Expression of CPE, F13A1 and F2R in ccRCC tumors compared to other cancer types and the main RCC subtypes .....</i>	<i>160</i>
4.2 <i>Evaluation of CPE, F13A and f2r IN rcc tissue samples.....</i>	<i>163</i>
4.3 <i>Evaluation of survival in ccRCC patients with overexpression of CPE, F13A1 and F2R</i>	<i>163</i>
4.4 <i>Correlation between CPE, F13A1 and F2R gene expression and their correlating genes in ccRCC patients .....</i>	<i>167</i>
<b>DISCUSSION .....</b>	<b>171</b>
<b>1. METASTASIS, CLONAL HETEROGENEITY AND REN 50/50M MODEL .....</b>	<b>173</b>
<b>2. MODELLING METASTASIS IN THE MOUSE .....</b>	<b>179</b>
<b>3. METASTATIC candidate genes .....</b>	<b>181</b>
3.1 <i>Carboxypeptidase E .....</i>	<i>181</i>
3.2 <i>Coagulation pathway .....</i>	<i>186</i>
3.2.1 <i>Coagulation Factor XIII.....</i>	<i>188</i>
3.2.2 <i>Coagulation Factor II Thrombin Receptor or Protease-activated Receptor 1 .....</i>	<i>189</i>
<b>CONCLUSIONS .....</b>	<b>197</b>
<b>REFERENCES .....</b>	<b>201</b>



## LIST OF ABBREVIATIONS

<b>%</b>	Percentage
<b>∞</b>	Infinity
<b>Δ</b>	Delta
<b>°C</b>	Centigrade degrees
<b>μg</b>	Microgram
<b>μl</b>	Microliter
<b>μm</b>	Micrometer
<b>μM</b>	Micromolar
<b>aa</b>	Aminoacids
<b>AAALAC</b>	Association for Assessment and Accreditation of Laboratory Animal Care
<b>AJCC</b>	American Joint Committee on Cancer
<b>APS</b>	Ammonium persulfate
<b>BCA</b>	Bicinchoninic acid
<b>BM</b>	Basement membrane
<b>BSA</b>	Bovine serum albumin
<b>Myc</b>	MYC Proto-Oncogene, BHLH Transcription Factor
<b>Ca<sup>2+</sup></b>	Calcium
<b>CCIT-UB</b>	Centres Científics i Tecnològics de la Universitat de Barcleona
<b>ccRCC</b>	Clear Cell Renal Cell Carcinoma
<b>cDNA</b>	Complementary DNA
<b>CEIC</b>	Centre Ètic d'Investigació Clínica
<b>chr</b>	Chromosome
<b>Chi<sup>2</sup></b>	Chi square
<b>cm</b>	Centimeter
<b>CMV</b>	Cytomegalovirus
<b>CNAG</b>	Centro Nacional de Análisis Genómico
<b>CO<sub>2</sub></b>	Carbon dioxide
<b>Const</b>	Constitutive
<b>CPE</b>	Carboxypeptidase E
<b>Cpm</b>	Counts per million
<b>CSIC</b>	Consell Superior d'Investigacions Científiques

## List of abbreviations

---

<b>CSP</b>	Constitutive secretory pathway
<b>Ct</b>	Threshold cycle
<b>CTC</b>	Circulating tumor cell
<b>CRC</b>	Colorectal cancer
<b>DAB</b>	3,3'-Diaminobenzidine
<b>DAPI</b>	4',6-Diamidino-2-phenylindole dihydrochloride
<b>dH<sub>2</sub>O</b>	Distilled water
<b>ddH<sub>2</sub>O</b>	Bi-distilled water
<b>ddNTP</b>	2',3' dideoxynucleotides
<b>DMEM</b>	Dulbecco's Modified Eagle's Medium
<b>DMSO</b>	Dimethyl sulfoxide
<b>DNA</b>	Deoxyribonucleic acid
<b>DOAC</b>	Direct oral anticoagulants
<b>DPX</b>	Distyrene, plasticiser and xylene
<b>ECM</b>	Extracellular matrix
<b>EDTA</b>	Ethylenediaminetetraacetic acid
<b>EMT</b>	Epithelial-mesenchymal transition
<b>F2R</b>	Coagulation Factor 2 Thrombin Receptor
<b>FXIII/F13</b>	Blood Coagulation Factor XIII/13
<b>FAK</b>	Focal Adhesion Kinase
<b>FBS</b>	Fetal bovine serum
<b>FC</b>	Fold change
<b>FDA</b>	Food and Drug Administration
<b>FDR</b>	Fold discovery rate
<b>FISH</b>	Flourescent <i>In Situ</i> Hybridation
<b>G</b>	Gauge
<b>g</b>	Gram
<b>GDP</b>	Guanosine diphosphate
<b>GEMSA</b>	Guanidinoethylmercaptosuccinic acid
<b>GFP</b>	Green flourescent protein
<b>GTP</b>	Guanosine triphosphate
<b>GPCR</b>	G-protein coupled receptor
<b>GSEA</b>	Gene Set Enrichment Analysis

<b>h</b>	Hour
<b>H&amp;E</b>	Hematoxylin and eosin
<b>H<sub>2</sub>O<sub>2</sub></b>	Hydrogen peroxide
<b>HCC</b>	Hepatocellular Carcinoma
<b>HCl</b>	Chloridric acid
<b>HEPES</b>	4-(2-hydroxyethyl)-1-piperazineethanesulfonic acid
<b>HIF</b>	Hypoxia-inducible Factor
<b>HRP</b>	Horseradish peroxidase
<b>ICGC</b>	International Cancer Genome Consortium
<b>ICO</b>	Institut Català d'Oncologia
<b>IDIBELL</b>	Institut d'Investigació Biomèdica de Bellvitge
<b>IgG</b>	Immunoglobulin G
<b>IGV</b>	Integrative Genomic Viewer
<b>Ind</b>	Inducible
<b>IRB</b>	Institut de Recerca Biomèdica
<b>ISUP</b>	International Society of Urological Pathology
<b>ITGB3</b>	Integrin Subunit Beta 3
<b>IV</b>	Intravenous
<b>Kan</b>	Kanamycin
<b>Kb</b>	Kilobase
<b>KDa</b>	Kilodalton
<b>Kg</b>	Kilogram
<b>KH<sub>2</sub>PO<sub>4</sub></b>	Potassium phosphate monobasic
<b>KIRC</b>	Kidney Renal Clear Cell Carcinoma
<b>KIRP</b>	Kidney Renal Papillary Cell Carcinoma
<b>Km</b>	Michaelis constant
<b>L</b>	Litre
<b>LB</b>	Lysogeny broth
<b>KMWH</b>	Low-Molecular-Weight Heparin
<b>lnRNA</b>	Long-non-coding ribonucleic acid
<b>LOH</b>	Loss of heterozygosis
<b>Met</b>	Metastatic
<b>MET</b>	Mesenchymal-epithelial transition



## List of abbreviations

---

<b>mg</b>	Milligram
<b>min</b>	Minute
<b>ml</b>	Milliliter
<b>mm</b>	Millimeter
<b>mm<sup>2</sup></b>	Square millimeter
<b>mm<sup>3</sup></b>	Cubic millimeter
<b>mM</b>	Millimolar
<b>MMP</b>	Matrix metalloprotease
<b>mRNA</b>	Messenger ribonucleic acid
<b>miRNA</b>	Micro ribonucleic acid
<b>MolSigDB</b>	Molecular Signatures DataBase
<b>NaCl</b>	Sodium chloride
<b>Na<sub>2</sub>HPO<sub>4</sub></b>	Monosodium phosphate
<b>NCDB</b>	National Cancer Data Base
<b>NIS</b>	National Inpatient Sample
<b>ng</b>	Nanogram
<b>NK</b>	Natural killer
<b>nm</b>	Nanometer
<b>Non-met</b>	Non-metastatic
<b>O/N</b>	Over night
<b>OCT</b>	Optimum Cutting Temperature compound
<b>OT</b>	Orthotopic
<b>PAGE</b>	Polyacrylamide gel electrophoresis
<b>PAR</b>	Protease-Activator Receptor
<b>PEBC</b>	Programa d'Epigenètica i Biologia del Càncer
<b>PBS</b>	Phosphate buffered saline
<b>PCR</b>	Polymerase chain reaction
<b>PDX</b>	Patient-derived xenograft
<b>PDOX</b>	Patient-derived orthoxenograft
<b>PEI</b>	Polyethylenimine
<b>PES</b>	Polyethersulfone
<b>PFA</b>	Paraformaldehyde
<b>pg</b>	Picogram

<b>PGL</b>	araganglioma
<b>PHEO</b>	pheochromocytoma
<b>proCURE</b>	Programa contra la Resistència Terapèutica del Càncer
<b>Puro</b>	Puromycin
<b>RCC</b>	Renal Cell Carcinoma
<b>RER</b>	Rough endoplasmic reticulum
<b>RIPA</b>	Radioimmunoprecipitation assay buffer
<b>RNA</b>	Ribonucleic acid
<b>RNAseq</b>	Ribonucleic acid sequencing
<b>rpm</b>	Revolutions per minute
<b>RPMI</b>	Roswell Park Memorial Institute
<b>RSEM</b>	Reservoir Sampling based Ensemble Method
<b>RSP</b>	Regulated secretory pathway
<b>RT</b>	Room temperature
<b>RT-qPCR</b>	Real-time quantitative PCR
<b>s</b>	Second
<b>SciPY</b>	Python Scipy library
<b>SD</b>	Standard deviation
<b>SDS</b>	Sodium dodecyl sulfate
<b>SERPINE1</b>	Serpin Family E Member 1
<b>SOC</b>	Super optimal broth
<b>SPF</b>	Specific pathogen free
<b>Src</b>	SRC Proto-Oncogene, Non-Receptor Tyrosine Kinase
<b>TAE</b>	Tris-acetate-EDTA
<b>TBS</b>	Tris-buffered Saline
<b>TCA</b>	Trichloroacetic acid
<b>TCGA</b>	The Cancer Genome Atlas
<b>TEM</b>	Transendothelial migration
<b>TEMED</b>	Tetramethylethylenediamine
<b>TFPI</b>	Tissue Factor Pathway Inhibitor
<b>TGN</b>	Transgolgi
<b>TNM</b>	Tumor-node-metastasis
<b>Tris</b>	Tris(hydroxymethyl)aminomethane

<b>TPBS</b>	Triton-phosphate buffered saline
<b>TTBS</b>	Tween-tris-buffered saline
<b>UV</b>	Ultraviolet
<b>V</b>	Volt
<b>VEGF</b>	Vascular Endothelial Growth Factor
<b>VHIO</b>	Vall d'Hebrón Institut d'Oncologia
<b>VHL</b>	Von Hippel-Lindau
<b>VTE</b>	Venous thromboembolism
<b>WHO</b>	World Health Organization

## Amino acids

<b>F</b> Phe, phenylalanine	<b>S</b> Ser, serine	<b>Y</b> Tyr, tyrosine	<b>K</b> Lys, lysine	<b>W</b> Trp tryptophan
<b>L</b> Leu, leucine	<b>P</b> Pro, proline	<b>H</b> his, histidine	<b>D</b> Asp, aspartic acid	<b>R</b> Arg, arginine
<b>I</b> Ile, isoleucine	<b>T</b> Thr, threonine	<b>Q</b> Gln, glutamine	<b>E</b> Glu, glutamic acid	<b>G</b> Gly, glycine
<b>M</b> Met, methionine	<b>A</b> Ala, alanine	<b>N</b> Asn, asparagine	<b>C</b> Cys, cysteine	<b>V</b> Val, valine

## Nucleotides

<b>A</b> adenine	<b>T</b> thymine	<b>G</b> guanine	<b>C</b> cytosine	<b>U</b> uracil
------------------	------------------	------------------	-------------------	-----------------

## LIST OF FIGURES

Figure 1. Metastasis cascade.....	30
Figure 2. Schematic representation of tumor local invasion.....	32
Figure 3. Schematic representation of intravasation process.....	33
Figure 4. Schematic representation of platelet biology.....	35
Figure 5. Schematic representation of tumor cells survival in the circulation.....	36
Figure 6. Extravasation of renal tumor cells into lung tissue.....	38
Figure 7. Extravasation.....	39
Figure 8. Linear and parallel progression models of tumor evolution and metastasis formation.....	44
Figure 9. Metastatic progression genes.....	46
Figure 10. Renal Cell Carcinoma.....	50
Figure 11. PDOX mouse model of RCC.....	56
Figure 12. The orthotopic mouse presented both micrometastases and macrometastases in the lung...56	
Figure 13. Schematic representation of Ren 50 and Ren 50M mouse orthoxenograft lines.....	57
Figure 14. Ren 50M did metastasis at a higher frequency compared to Ren 50.....	58
Figure 15. Ren 50 always showed micrometastases, whereas Ren 50M mice presented more lesions in the lungs, including both micrometastases and macrometastases.....	59
Figure 16. Results from exome sequencing analysis revealed shared mutations between the human biopsy, Ren 50 and Ren 50M tumors. In addition, we observed specific mutations for each group ...	61
Figure 17. Results from exome sequencing revealed an accumulation of mutations in chromosomes 8, 15 and 18.....	62
Figure 18. Centromer of chromosome 8 and 8q24 analysis showed the same copy number expression pattern between them. Nevertheless, more copies of 8q24 were quantified.....	63
Figure 19. Schematic representation of isochromosomes.....	64
Figure 20. Ren 50M tumors showed a tendency of an accumulation of chromosome 15. Differences were statistically significant when comparing both groups to metastases, which presented a clear accumulation of this chromosome.....	65
Figure 21. Ren 50M tumors showed a slight accumulation of chromosome 18. Differences were statistically significant when comparing both groups with metastases, which presented a clear accumulation of this chromosome.....	65
Figure 22. Results from RNA Sequencing of Ren 50 and Ren 50M tumors showed an accumulation of alterations in the expression of genes from chromosomes 8, 15 and 18.....	67
Figure 23. Results from GSEA showed that Ren 50/50M samples highly correlated with the Regulation of body fluid levels signature.....	68
Figure 24. Schematic representation of cumate system.....	89
Figure 25. Schematic representation of lentiviral vectors.....	90

Figure 26. Mechanism of action of Vorapaxar .....	98
Figure 27. <i>CPE</i> RNA was only detected in Ren 50M tumors.....	105
Figure 28. Coagulation pathway.....	109
Figure 29. <i>F13A1</i> and <i>F2R</i> were almost not expressed in Ren 50 tumors and highly expressed in Ren 50M .....	110
Figure 30. Ren 50 mice presented reddish skin, which could be related to coagulation pathway alterations.....	110
Figure 31. Ren 50M tumors showed dilated vessels compared to long and thin vessels present in Ren 50 .....	111
Figure 32. Ren 50 tumors presented both phenotypes, whereas Ren 50M predominantly presented phenotype 2. Phenotype 1 was associated to non-metastatic animals and most of metastatic animals presented phenotype 2 .....	112
Figure 33. There was almost no relative <i>CPE</i> , <i>F13A1</i> and <i>F2R</i> expression in Ren 50 tumors and a very high expression in Ren 50M.....	114
Figure 34. Protein analyses confirmed absence of <i>CPE</i> , <i>F13A</i> and <i>F2R</i> protein expression in Ren 50 tumors and high expression in Ren 50M .....	115
Figure 35. Immunohistochemistry staining of our candidates confirmed protein expression heterogeneity in the orthotopic mouse and also in advanced passages of Ren 50M .....	116
Figure 36. When comparing the staining of the three proteins, they had some common areas but not all of them were completely overlapped .....	117
Figure 37. Only Ren 50M metastases presented <i>CPE</i> , <i>F13A</i> and <i>F2R</i> protein expression.....	118
Figure 38. Molecular model of <i>CPE</i> protein .....	121
Figure 39. Functionality of <i>CPE</i> .....	123
Figure 40. None of the renal cell lines presented <i>CPE</i> relative RNA and protein expression.....	125
Figure 41. <i>CPE</i> expression was not detected in cells transfected with the pCMV3-Empty vector. Almost no expression was either detected in cells transfected with the pCMV3- <i>CPE</i> vector .....	126
Figure 42. 786O- CYMR cells did not show full infection efficiency of the <i>CPE</i> and Blank vectors .....	127
Figure 43. Cell sorting of 786O- CYMR, CYMR Blank and CYMR <i>CPE</i> cells.....	128
Figure 44. After cell sorting, we obtained three populations of 786O- CYMR Blank and <i>CPE</i> clearly differing in GFP expression .....	129
Figure 45. 786O- CYMR Blank cells did not show <i>CPE</i> expression neither at RNA level, nor at protein level. <i>CPE</i> Constitutive cells expressed both <i>CPE</i> RNA and protein in a constitutive way. The expression slightly increased after cumate induction. <i>CPE</i> Inducible cells did almost not present expression and it was clearly upregulated with the addition of cumate.....	130
Figure 46. <i>CPE</i> highest levels were obtained after 72h of cumate incubation. Its expression was completely reversed after 24h of its removal.....	131
Figure 47. <i>CPE</i> expression did not increase the migration capacity of 786O- cells.....	132

---

Figure 48. CPE expression did not increase either the migration or the invasion capacity of 786O- cells .....	133
Figure 49. CPE-expressing cells secreted the protein into the media .....	134
Figure 50. Soluble CPE did not change cell migration capacity .....	134
Figure 51. CPE acted as a chemoattractant or as a ligand by increasing the invasion potential of 786O- cells .....	135
Figure 52. Cells invaded through Matrigel® regardless of the presence of CPE in pretreated mediums	136
Figure 53. Effects in invasion produced by soluble CPE were not reversed with an inhibitor of its enzymatic activity .....	137
Figure 54. CPE Constitutive cells seemed to have the ability to generate more macrometastases than Blank cells when being injected through tail vein .....	138
Figure 55. CPE Constitutive cells did not generate more lung metastasis than Blank cells when they were intravenously injected .....	139
Figure 56. CPE-expressing tumors did not show an increase in the invasive phenotype .....	140
Figure 57. CPE expression was not enough to enhance the metastatic potential of 786O- tumors.....	140
Figure 58. Schematic representation of FXIII activation and its role in coagulation .....	143
Figure 59. F13A expression could not be detected in any of the renal cell lines tested .....	144
Figure 60. Only cells transfected with the pCMV3- <i>F13A1</i> vector expressed the protein .....	145
Figure 61. Only 786O- tumors generated with pCMV3- <i>F13A1</i> transfected cells expressed F13A protein .....	146
Figure 62. F13A-expressing tumors did not show an increase of the invasion capacity .....	147
Figure 63. F13A-expressing tumors did not show any metastatic advantage compared to controls .....	147
Figure 64. There was a crosslink between F13A and CPE <i>in vivo</i> .....	148
Figure 65. Schematic representation of thrombin-mediated PAR1 activation .....	150
Figure 66. RCC4- and SN12C cell lines presented the highest <i>F2R</i> RNA expression .....	151
Figure 67. Both SN12C cells and tumors expressed F2R protein.....	152
Figure 68. F2R inhibition did not reduce the number of affected lung lobes but showed a reduction of the total metastasis area density.....	153
Figure 69. F2R inhibition did not affect tumor growth.....	154
Figure 70. F2R inhibition with Vorapaxar showed a decrease in the invasive phenotype .....	154
Figure 71. F2R inhibition showed a decrease in invasion.....	155
Figure 72. F2R inhibition demonstrated a reduction of the metastatic capacity of SN12C tumors by reducing the number of lung colonies and their size.....	156
Figure 73. F2R inhibition reduced metastasis .....	157
Figure 74. F2R inhibition changed SN12C cells phenotype .....	158
Figure 75. F2R inhibition did not change the migration capacity of SN12C cells .....	158
Figure 76. F2R inhibition drastically decreased the invasion capacity of SN12C cells.....	159

Figure 77. ccRCC is one of the cancer types showing the highest expression ranking of *CPE*, *F13A1* and *F2R* .....161

Figure 78. *CPE*, *F13A1* and *F2R* expression is higher in ccRCC compared to the other two main RCC subtypes.....162

Figure 79. *CPE*, *F13A1* and *F2R* were expressed in nearly the third RCC tissue samples .....163

Figure 80. ccRCC patients with an overexpression of *CPE* and *F13A1* present significant worse survival rates. On the contrary, *F2R* gene expression do not change ccRCC patient overall survival.....165

Figure 81. Patients presenting an overexpression of genes involved in the coagulation pathway tend to present worse survival .....166

Figure 82. Data from TCGA demonstrated a correlation between *CPE*, *F13A1* and *F2R* in patients.....168

Figure 83. Data from TCGA demonstrated a correlation between *CPE*, *F13A1* and *F2R* correlating genes in patients .....169

Figure 84. Schematic representation of Ren 50 and Ren 50M, probably generated from a polyclonal metastasis .....175

## LIST OF TABLES

Table 1. WHO Classification of kidney tumors .....	49
Table 2. Renal Cell Carcinoma classification.....	51
Table 3. Stages of RCC .....	52
Table 4. Mediums used for cell culture. ....	77
Table 5. Cell lines derived from human kidney tissues used.....	78
Table 6. Oligonucleotides used for the detection of mycoplasma contamination. ....	78
Table 7. Specific probes used in Taqman® analyses.....	81
Table 8. Primary antibodies used for the Western blot detections. ....	85
Table 9. Primary antibodies used for protein detection by immunocytofluorescence.....	86
Table 10. Restriction enzymes used to confirm correct plasmid genomes. ....	88
Table 11. pCMV3 vectors used to transfect 768O- cell line. ....	88
Table 12. Lentiviral plasmids used to generate lentiviruses.....	90
Table 13. Primary antibodies used for protein detection by immunohistochemistry .....	101
Table 14. <i>CPE</i> gene was one of the all genome with a highest fold change when comparing Ren 50M to Ren 50 tumors. Its expression in the metastatic group was extremely high .....	106
Table 15. Twelve genes from the <i>Regulation of body fluid levels</i> signature of GSEA were enriched in our data set. <i>F13A1</i> and <i>F2R</i> were two of the genes with a highest fold change and also high gene expression levels in Ren 50M tumors .....	108





# **SUMMARY**



Targeting cancer metastasis has gained considerable importance in the recent years when aiming to increase patients' overall survival. In Renal Cell Carcinoma (RCC), the discovery of metastatic biomarkers and targets is still required, as most patients present metastatic disease at the time of diagnosis.

Therefore, the aim of this thesis is the discovery of new biomarkers and targets of metastatic RCC using two variants of a patient-derived orthoxenograft (PDOX) animal model of clear cell RCC (ccRCC). Indeed, PDOX models have recently gained significant relevance for studying the progression of cancer and metastasis, due to their better mimicking of the histology, the metastatic capacity and treatment responses of human cancers. To this purpose, previous results had sequenced the two variants of this PDOX model, both at DNA and at RNA level, and had performed a FISH analysis.

Firstly, Carboxypeptidase E (CPE), which was one of the highest expressed genes in the metastatic variant, has demonstrated to play a role in invasion when it is secreted to the medium, even though its overexpression alone is not sufficient to generate metastasis *in vivo*. In addition, it has showed a clear association to ccRCC and an inverse correlation with the overall survival of these patients. Secondly, we have studied two molecules of the coagulation pathway due to its relevance as one of the most upregulated pathways at RNA level. On the one hand, Factor XIII (FXIII or F13) has shown to be related to CPE *in vivo*, despite the overexpression of both molecules is not sufficient to develop all the metastatic cascade. However, it also affects the overall survival of ccRCC patients, highlighting these two molecules as possible biomarkers for this type of cancer. On the other hand, Coagulation Factor II Thrombin Receptor (F2R or PAR1) has demonstrated to play a role in metastasis, since its inhibition reduces both the early and late phases of this process. With the use of F2R inhibitors and the clinical association of the coagulation pathway to worse prognosis, this thesis opens new opportunities for the treatment of metastasis and cancer malignization.

In summary, we have discovered new metastatic biomarkers and targets which, together with further validations, especially in the clinical setting, are proposed to be useful for RCC patients in the future.



**RESUM**



Durant els últims anys, l'estudi de la metastasi ha guanyat importància amb l'objectiu d'augmentar la supervivència dels pacients amb càncer. En el càncer renal (RCC), el descobriment de biomarcadors metastàtics i dianes terapèutiques encara és necessari degut a que la majoria de pacients presenten metastasi en el moment del diagnòstic.

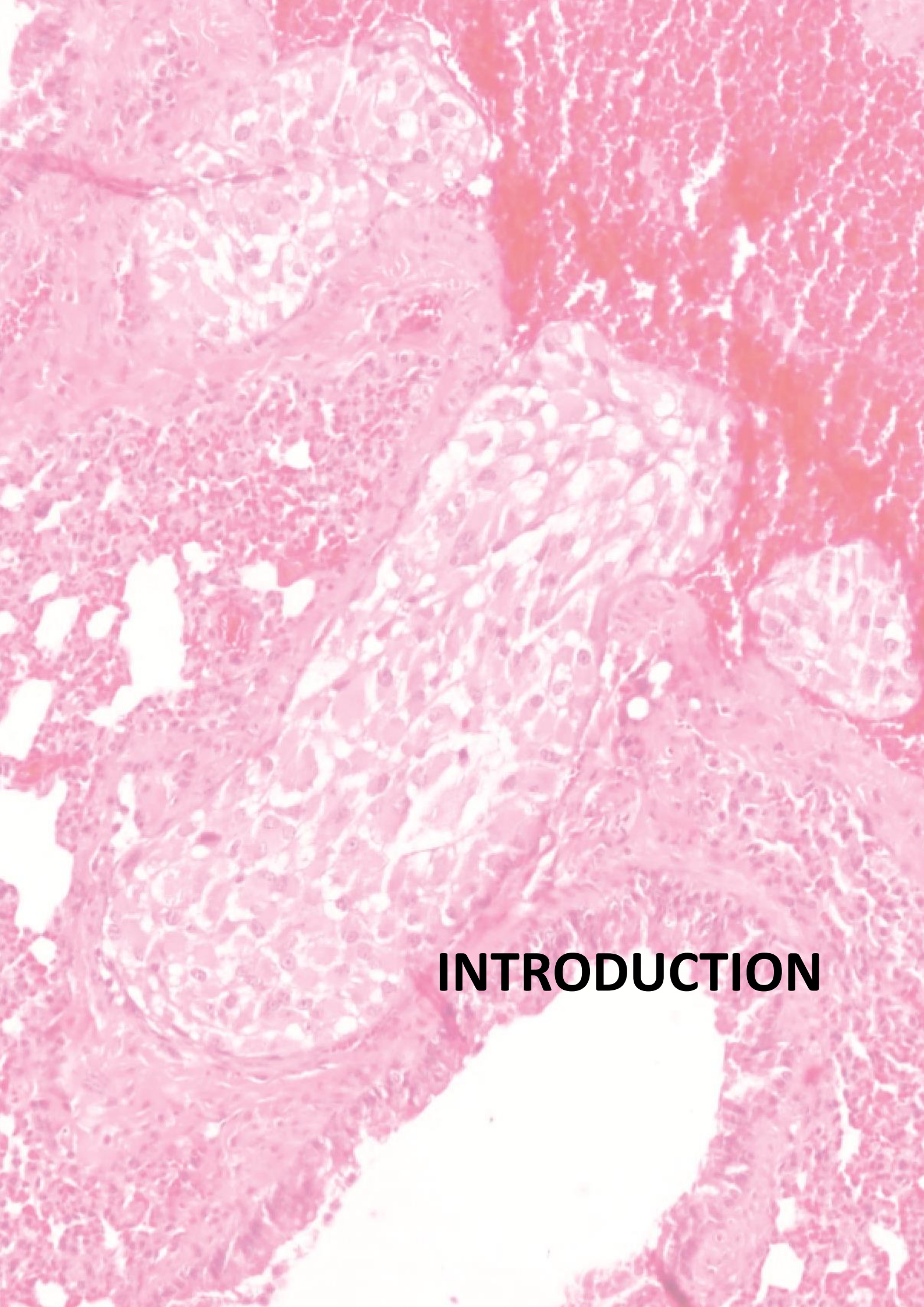
Així doncs, l'objectiu d'aquesta tesi ha estat el descobriment de nous biomarcadors i dianes terapèutiques pel càncer renal metastàtic a través de dues variants d'un model animal orthoxenograft (PDOX) de càncer renal de cèl·lula clara (ccRCC). Els models PDOX han guanyat molta importància durant els últims anys en l'estudi de la progressió del càncer i la metastasi, ja que mimetitzen la histologia, la capacitat metastàtica i la resposta als tractaments. Amb aquest objectiu, prèviament s'havien seqüenciat les dues variants d'aquest model PDOX tant a nivell de DNA com de RNA, juntament amb un anàlisi FISH.

En primer lloc, la Carboxipeptidasa E (CPE), un dels gens més expressats en la variant metastàtica, ha demostrat ser important en la invasió quan és secretada al medi, tot i que només la seva sobreexpressió no és suficient per generar metastasi *in vivo*. A més, ha demostrat una clara associació amb el ccRCC i una correlació inversa amb la supervivència d'aquests pacients. En segon lloc, hem estudiat dues molècules de la cascada de coagulació després de veure que era una de les cascades més alterades pel que fa els nivells de RNA. Per una banda, hem demostrat que el Factor XIII (FXIII o F13) està relacionat amb CPE *in vivo*, malgrat que l'expressió de les dues molècules no és suficient per a que es desenvolupi tot el procés metastàtic. Tot i així, el F13 afecta la supervivència de pacients amb ccRCC, la qual cosa suggereix que aquestes dues molècules podrien ser possibles biomarcadors d'aquest tipus de càncer. Per altra banda, el Receptor del Factor de Coagulació II (F2R o PAR1) ha demostrat jugar un paper important en la metastasi, ja que la seva inhibició redueix les fases inicials i finals d'aquest procés. L'ús d'inhibidors de F2R, juntament amb el fet que la cascada de coagulació es relaciona amb el pronòstic dels pacients, fa que aquesta tesi obri noves oportunitats per al tractament de la metastasi i la malignització del càncer.

En resum, hem descobert nous biomarcadors i dianes terapèutiques que, juntament amb futures validacions, sobretot en la part clínica, poden ser útils per als pacients metastàtics de ccRCC.







# **INTRODUCTION**



## 1. METASTASIS

Cancer consists of a neoplasm, which is an alteration of cell proliferation and very often also of cell differentiation, that is expressed by an abnormal mass of tissue named tumor. Nowadays, cancer is a major cause of human mortality and thanks to its early diagnosis and new treatment options, survival rate has improved. However, the incidence and prevalence of cancer continues to increase. According to one of the last studies on cancer distribution worldwide, 14 million of new cases are detected every year (UK, 2012) and 8.8 million deaths caused by cancer were reported by the World Health Organization (WHO) in 2015 (World Health Organization, 2018).

The metastatic spread of cancer cells to distant parts of the body represents the major cause of cancer-related deaths, being one of the most life-threatening pathologic events. Concretely, more than 90% of deaths are a consequence of the metastases and not due to the primary tumor (Gupta and Massagué, 2006).

Tumors with an epithelial origin represent an average of 80% of life-threatening cancers because of their capacity to metastasize in distant organs (Valastyan and Weingberg, 2011). Metastases show an organ-specific pattern of spread depending on the type of cancer because of the dependence on the *seed* (cancer cell) and on the *soil* (secondary organ). This theory was hypothesized for the first time in 1889 by Stephen Paget in Lancet (Fidler, 2003; Paget, 1889). However, lungs are one of the most typical places where tumor cells metastasize in solid tumors. One of the reasons for this specific high prevalence is probably due to the fact that our entire cardiac output circulates through the lung-capillary network (Gupta and Massagué, 2006).

The metastatic cascade is a biological multistep complex process with multiple restrictive bottlenecks. This process is initiated by local invasion, in which epithelial tumor cells detach from the primary tumor and invade through the surrounding basement membrane (BM) and degrade the extracellular matrix (ECM). Thereafter, cells intravasate into the blood vessels' lumina. Intravasation is easier thanks to the thin-walled venules, such as lymphatic channels, which offer very little resistance to

penetration by tumor cells. Furthermore, this step is allowed by the formation of leak new blood vessels from preexisting ones, a process called angiogenesis. The next step is the systemic dissemination. While tumor cells are in circulation, they need to fight and survive against the mechanical flow and the immune system components present in blood. Once in a distant organ, they must be able to extravasate into the parenchyma of distant tissues, survive in a new niche, establish and outgrow, forming firstly micrometastases, and finally generating metastatic colonization, leading to clinically detectable macroscopic metastases (Figure 1) (Lambert et al., 2017; Valastyan and Weingberg, 2011).

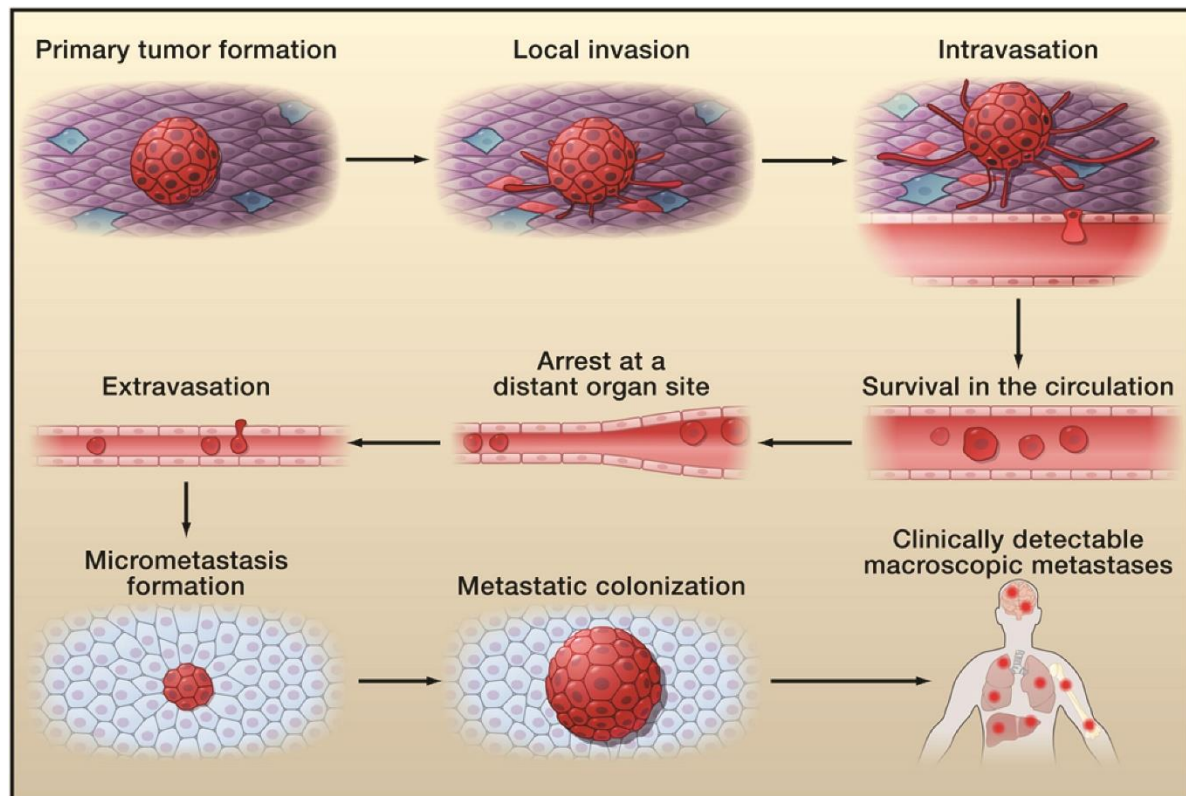


**Figure 1. Metastasis cascade.** Tumor cells escape from their primary site of growth, survive in the circulation and finally colonize a second distant organ forming metastases. Image has been adapted from (Valastyan and Weingberg, 2011).

## **1.1 LOCAL INVASION**

The first step of the metastasis cascade is the local invasion of the tumor into the surrounding tumor-associated stroma and, afterwards, into the normal tissue parenchyma.

The BM is a thin layer of specialized ECM, which is composed of several glycoproteins and proteoglycans. This membrane supports the structure on which epithelial and endothelial cell layers grow, playing essential roles in organizing epithelial tissues. Thereafter, in tumors at early stages, the BM acts by preventing invasion into the subjacent stroma. However, when cells progress into malignancy, they are able to disrupt regulatory mechanisms and induce proteolytic activities on this BM and the interstitial ECM. One of the most common effects is the secretion of ECM remodelers, mainly comprising metalloproteinases (MMPs) (Figure 2) (Gupta and Massagué, 2006; Lu et al., 2012; Valastyan and Weingberg, 2011).

Once tumor cells have degraded the BM, they enter into the stroma. It is composed of a variety of tumor-associated tumor cells, such as endothelial cells, fibroblasts, pericytes, macrophages and other immune cells. However, this composition is able to adapt and change depending on the state of the tumor progression. These stromal cells can also induce a high number of signaling pathways which enhance the aggressiveness of the tumor (Figure 2) (Pietras and Ostman, 2010).

Since the adult epithelial cells from which they arise are normally polarized and non-motile, tumor cells undergo an epithelial-to-mesenchymal transition (EMT), which consists of a gain of stem cell-like behavior. This reversible phenotype is characterized by the loss of epithelial features, like intercellular adhesion and epithelial polarization, prompted by a switch of cadherin proteins. The downregulation of the epithelial protein E-cadherin, an essential mediator of both cell-cell adhesions and the maintenance and homeostasis of polarized epithelial monolayers, is required for an efficient cell migration. In parallel, an upregulation of the mesenchymal cell-cell adhesion protein N-cadherin takes place. This switch leads to a drastic change in adhesive affinity of tumor cells, from

epithelial to mesenchymal cells, such as fibroblasts or vascular endothelial cells. Hence, invasion and the following intravasation are promoted (Brabletz, 2012; Chaffer et al., 2016; Yilmaz and Christofori, 2009).

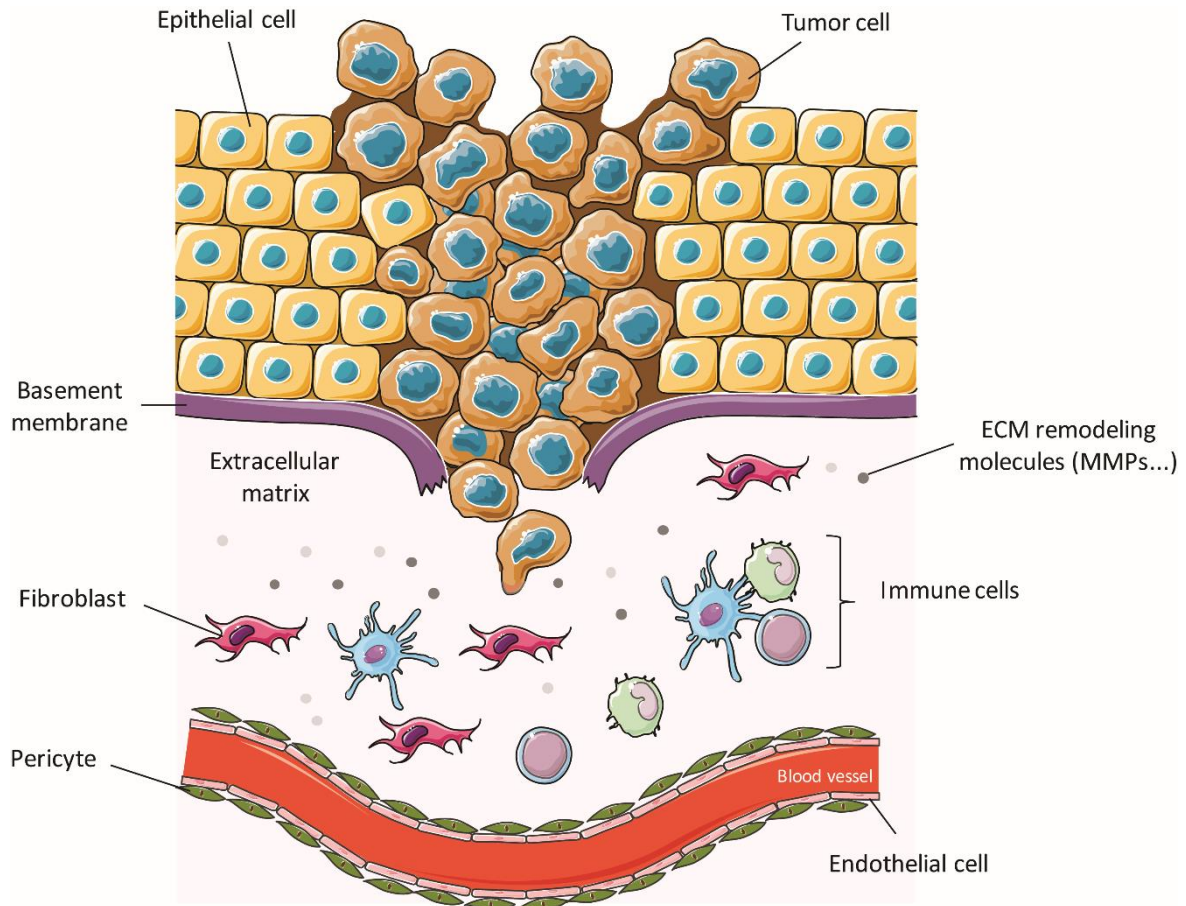


**Figure 2. Schematic representation of tumor local invasion.** Local invasion of the primary tumor into the surrounding parenchyma starts with the degradation of the BM and the following entrance into the stroma, composed of ECM proteins and a variety of cells, such as fibroblasts, immune cells, pericytes and endothelial cells.

## 1.2 INTRAVASATION

After local invasion, tumor cells continue to metastasize by entering into the lumina of lymphatic or blood vessels in order to gain access to distant parts of the body. However, metastasis formation in all solid organs is mostly through the hematogenous circulation (Gupta and Massagué, 2006).

This process is facilitated by the formation of new vessels created from pre-existing ones, a process called angiogenesis. Angiogenesis, whilst providing vascular support by increasing the amounts of available oxygen and nutrients to the developing mass, not only influences the growth of the primary tumor, but is also associated with the systemic dissemination of tumor cells. Many of the mechanisms involved in the formation of these new blood vessels imply the presence of high levels of the Vascular Endothelial Growth Factor (VEGF) and the consequent activation of its signaling pathway. Therefore, an increase of vascular permeability occurs, hence facilitating tumor cell intravasation (Figure 3) (Moserle and Casanovas, 2013).

During intravasation, the disruption of the endothelial junctions by cancer cells is required in order to cross the endothelium in a process known as transendothelial migration (TEM) (Figure 3). This can occur differently depending on the way that cells transmigrate. When tumor cells disrupt EC junctions and squeeze between them it is called paracellular TEM. It has been demonstrated that this is the preferred route by cells *in vitro*. However, small evidence suggests that they can also use the second route, termed transcellular TEM. In this case, tumor cells migrate directly through a single EC cytoplasm. *In vivo* models are not still able to demonstrate which route is used in this context, or whether it depends on the vascular bed or the cancer cell type (Reymond et al., 2013).

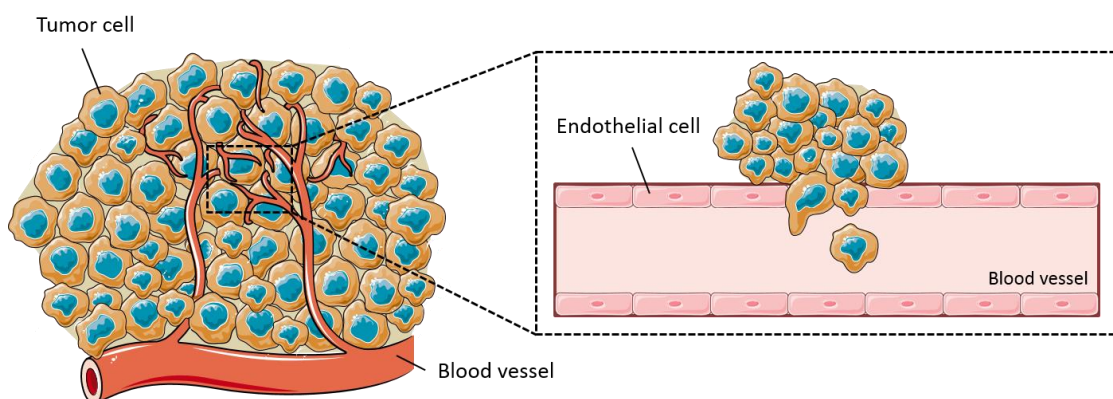


**Figure 3. Schematic representation of intravasation process.** During tumor formation, new capillaries sprout from pre-existing vessels, resulting in a new capillary network, a process known as angiogenesis. The creation of these new leak vessels facilitates the intravasation of tumor cells and their entrance into the bloodstream through the disruption of endothelial junctions. Figure has been adapted from (Reymond et al., 2013).



### **1.3 SURVIVAL IN THE CIRCULATION**

Once in the bloodstream, circulating tumor cells (CTCs) have lost their integrin-mediated adhesion to the ECM, which is a requirement for epithelial cells to survive. These interactions induce a recruitment of different molecules, such as focal adhesion kinase (FAK) and adaptor proteins, thus inducing survival pathways.

When tumor cells detach, they normally undergo anoikis, a form of cell death caused by apoptosis triggered by loss of anchorage to substratum. Tumor cells present a number of mechanisms in order to avoid this process.

On one hand, tumor cells can form microaggregates. In parallel, FAK can be recruited by endosomal integrins from detached cells, thus inducing downstream signaling pathways promoting anoikis resistance. In other cases, anoikis can also be suppressed through the upregulation of some tyrosine kinases or the acquisition of mutations in anti-apoptotic and pro-survival pathways (Strilic and Offermanns, 2017).

In circulation, tumor cells also need to survive through the hemodynamic shear forces, as well as withstand the oxidative stress and protect themselves against immune-mediated responses, mostly started by natural killer cells (Gupta and Massagué, 2006).

In order to overcome all of these perils, tumor cells take advantage of blood coagulation. Cancer patients often present signs of thrombosis and enhanced coagulation parameters, mainly due to the generation of thrombin and the subsequent abnormally high platelet activation and aggregation rates (Lima and Monteiro, 2013; Xie et al., 2005).

In homeostasis, platelets are activated during thrombus formation. This activation is mostly due to the binding of thrombin, which also cleaves fibrinogen and induces fibrin formation, to the G protein-linked protease-activated receptors (PARs) present on their surface. Upon the activation of these receptors, a rapid reorganization of their cytoskeleton occurs with a subsequent change in their shape, thus maximizing platelet adhesion through adhesion molecules, such as integrins. At the same time, platelet

granules containing active proteases, growth factors, matrix proteins and chemokines are released (Figure 4) (Gay and Felding-Habermann, 2011).

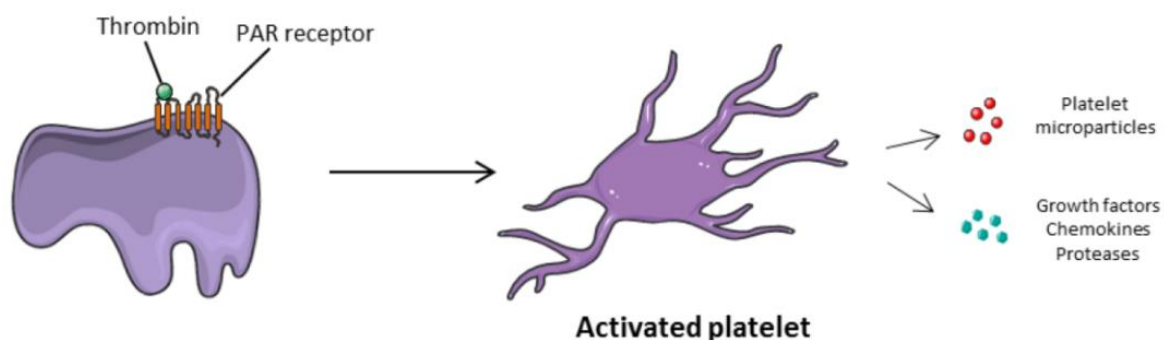


**Figure 4. Schematic representation of platelet biology.** During thrombus formation in physiological conditions, thrombin activates G protein-linked PARs present on platelets' surface, therefore leading to their activation. This produces shape changes that enhance platelet adhesion during thrombus formation, as well as the liberation of molecules such as growth factors, chemokines or proteases. This figure has been adapted from (Gay and Felding-Habermann, 2011).

During cancer progression, high levels of platelet activation lead to an increase of their adhesiveness and a release of granules and microparticles, which facilitates the cohesion of heteroaggregates formed with tumor cells, together with fibrinogen and fibrin molecules (Gay and Felding-Habermann, 2011). Coagulation Factor XIII (FXIII) is responsible for the stabilization of fibrin/platelet thrombi associated with tumor cells by physically shielding them from NK cell-mediated lysis and also by downregulating NK functions through the engagement of released immune modulators from platelets. Furthermore, FXIII-stabilized fibrin matrices will facilitate tumor cell migration out of vessels, which will be later necessary for metastasis to succeed (Palumbo et al., 2008).

Therefore, tumor cells shield themselves by co-opting with activated blood platelets, thereby avoiding physical hemodynamic forces and evading immune-mediated mechanisms for clearance (Figure 5) (Gay and Felding-Habermann, 2011; Nieswandt et al., 1999; Tesfamariam, 2016).

In addition, platelet-induced coagulation steps can also activate PAR receptors present in tumor cells. This fact promotes procoagulant activity, releasing tissue factor and FVIIa,

which triggers thrombin activation. Hence, thrombin will activate PAR receptors on platelets and tumor cells, thereby enhancing invasion and metastasis in a feedback loop (Figure 5) (Gay and Felding-Habermann, 2011; Nash et al., 2002; Tesfamariam, 2016).

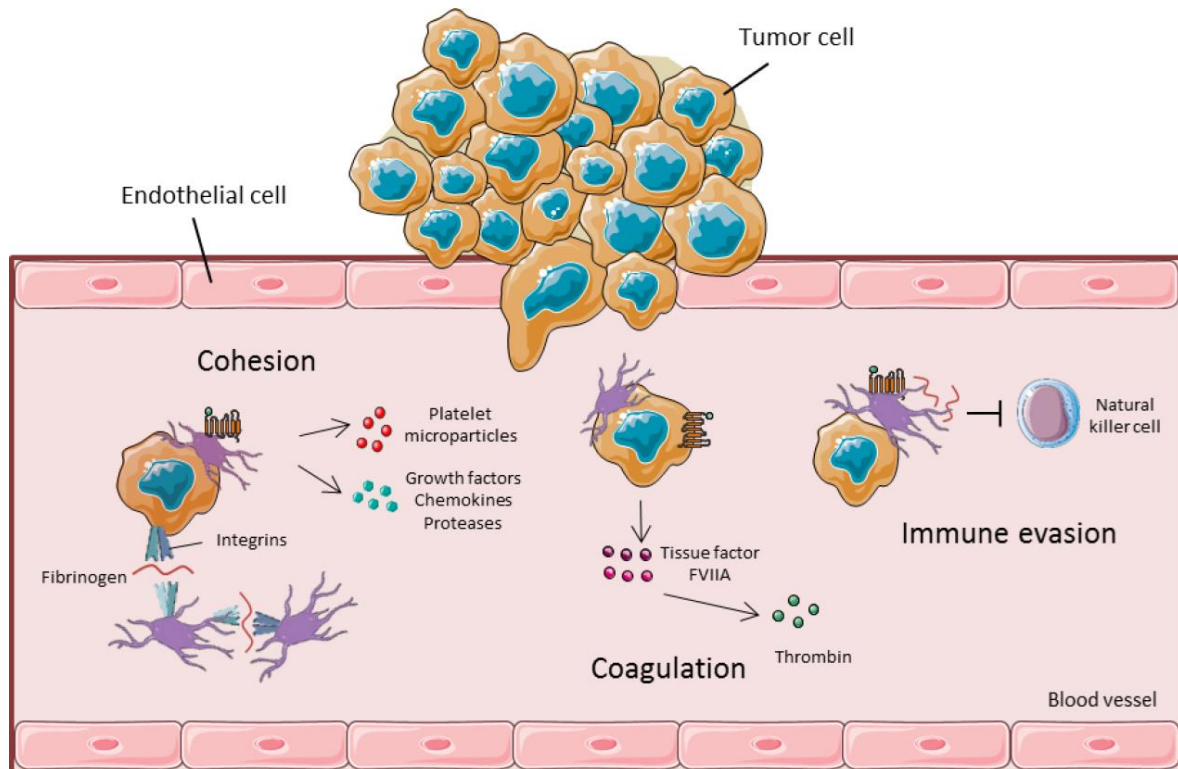


**Figure 5. Schematic representation of tumor cells survival in the circulation.** Once platelets become activated, they form heteroaggregates with tumor cells shielding them against the immune system. These interactions are mediated mostly by integrins,  $\alpha v\beta 3$  on tumor cells and  $\alpha IIb\beta 3$  on activated platelets. Platelet activation also triggers PARs activation in tumor cells, leading to thrombin activation, which will bind PARs on their surface and activate again the pathway in a feedback loop. This figure has been adapted from (Gay and Felding-Habermann, 2011).

In sum, stimulation of the coagulation system, and especially platelet activation, have been demonstrated to play essential roles in the hematogenous metastatic progression of cancer, thereby facilitating the survival of tumor cells in circulation and reducing the progression-free survival, as well as the overall survival, in a variety of cancer patients.

## 1.4 ARREST AT A DISTANT ORGAN SITE

Arrest of CTCs in distant organs is a required step for hematogenous metastasis. Despite the ability of CTCs to generate metastases in distant secondary sites, it has been reported that, depending on the cancer type, disseminating tumor cells show a preference to certain target organs (Obenauf and Massagué, 2015). This *Seed and Soil* theory of cancer spread, postulated for the first time by Paget, proposes a non-random pattern for metastasis, in which the specificity of metastatic places depends on the cross-talk between the metastasizing cancer cells and the specific organ microenvironment (Fidler, 2003; Paget, 1889).

It is not well known what exactly promotes these predilections to lodge in certain tissues. It is postulated that the initial trapping events could be caused by tropism prompted by an arrest of CTCs within capillary beds, due to the restrictions applied by circulation patterns. In parallel, it is also believed that cells that are permanently arrested are those with a genetically specificity that regulates the interactions between them and the luminal walls of the microvasculature of specific organs. In addition, it is known that endothelial cells present in the vasculature of target organs express specific cell surface receptors and growth factors which influence the phenotype of the metastatic cells (Chambers et al., 2002; Fidler, 2003; Labelle and Hynes, 2012; Valastyan and Weingberg, 2011). At the same time, adhesion molecules expressed by tumor cells can also contribute to their arrest at the metastatic sites. For instance, the expression of the  $\alpha_v\beta_3$  integrin by tumor cells has been shown to contribute to the arresting of tumor cells in the lung (Wang et al., 2004).

## 1.5 EXTRAVASATION

Once CTCs are lodged in the small capillaries of the secondary organ, they need to extravasate into the surrounding parenchyma by penetrating the endothelial cell and pericyte layers. Tumor cells may initiate intraluminal growth in order to form a microcolony with the ability to rupture vessel walls, which vary depending on the target

organ. In lung metastases, tumor cells will need to cross the endothelial barrier of the lung capillaries, which have tight junctions and a basement membrane (Figure 6).

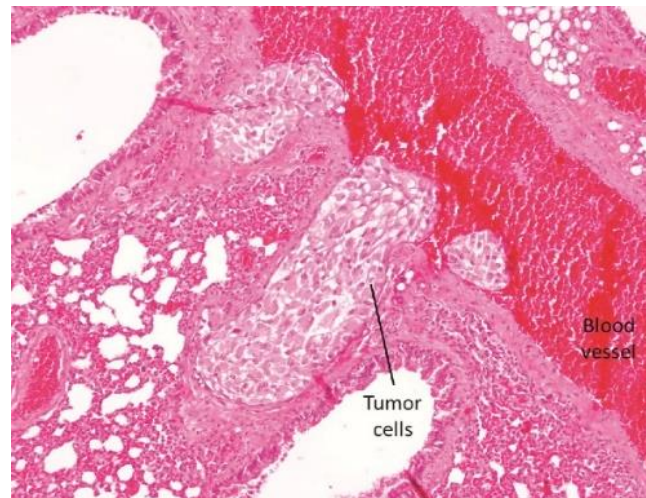


**Figure 6. Extravasation of renal tumor cells into lung tissue.** Picture of a hematoxylin-eosin staining (10X). We can observe three groups of ccRCC cells extravasating from a blood vessel into the lung parenchyma.

As in the intravasation process, extravasation also requires TEM of cancer cells. Even though these processes seemed to be very similar, they are clearly different due to the fact that cancer cells approach the endothelium from opposite sides. Furthermore, these two steps differ mechanistically, being vessel permeability one of the main barriers. The neovasculature in primary tumors is tortuous and leaky, whereas in the destination sites vessels are likely to be highly functional, therefore presenting a stronger barrier for cells to traverse (Massagué and Obenauf, 2016a; Reymond et al., 2013; Valastyan and Weingberg, 2011). In order to facilitate this process, tumor cells secrete molecules and factors, such as angiopoietins, metalloproteases or VEGF (Weis and Cheresh, 2005). These molecules, along with their downstream counterparts, like members of the Src kinase family (Criscuoli et al., 2008), have the capability to disrupt the endothelial cell-cell junctions and induce a vascular hyper-permeability in these secondary sites.

In order to facilitate the attachment to the endothelium, tumor cells can also interact with platelets and leukocytes and form heteroaggregates, thus supporting the adhesion and thereby contributing to metastasis. Evidence suggests that these interactions can be

mediated by integrins, as well as by selectins, mucins, CD44 and other intracellular adhesion molecules (Figure 7) (Gay and Felding-Habermann, 2011).

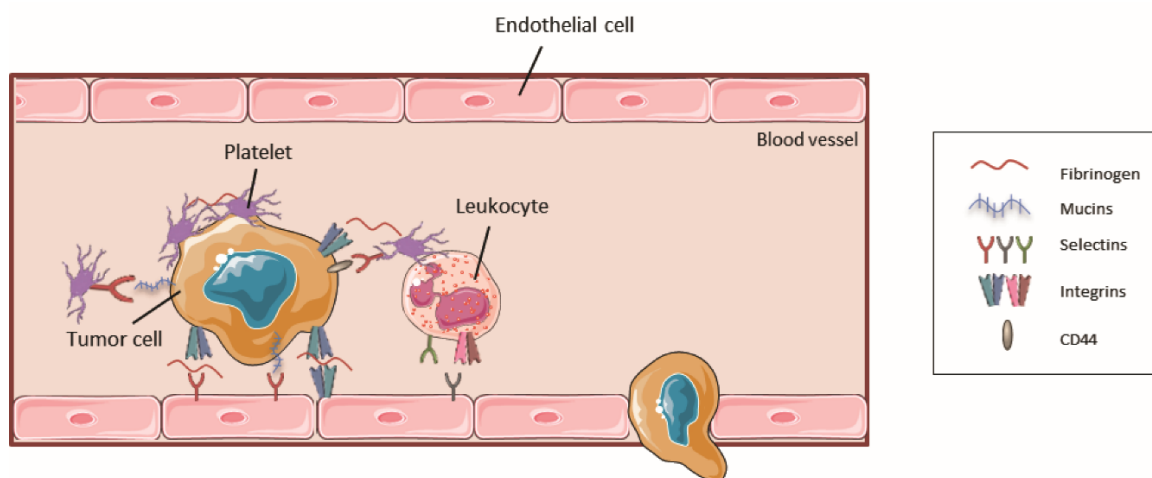


**Figure 7. Extravasation.** Circulating tumor cells can interact with activated platelets and leukocytes, forming heteroaggregates with a higher capability to attach to endothelial cells. Through these interactions, tumor cells extravasate into the parenchyma of the new tissue. This figure has been adapted from (Gay and Felding-Habermann, 2011)

## 1.6 INITIAL SURVIVAL IN A FOREIGN MICROENVIRONMENT AND MICROMETASTASIS FORMATION

After extravasating and settling in the secondary site, tumor cells must adapt to the microenvironment present in the new foreign tissue. This normally differs greatly from the one in the primary tumor, including differences in ECM constituents, stromal cell types, growth factors, cytokines and even the microarchitecture of the tissue itself (Peinado et al., 2017).

Aiming to solve this problem, tumor cells try to establish a pre-metastatic niche, which comprises the preconditioning sites of metastasis preceding the engraftment into that tissue (Peinado et al., 2017, 2011; Psaila and Lyden, 2009). The mobilization of hematopoietic progenitors, such as VEGFR1, from the bone marrow to these future sites of metastasis is required to generate a viable niche. This induces MMP9 expression in endothelial cells and macrophages, resulting in a stimulation of a variety of integrins and the liberation of molecules that have been sequestered in the ECM (Kaplan et al., 2005).

Mature monocytes and macrophages also secrete factors, chemokines and matrix-degrading enzymes. These modulate the local microenvironment and mediate chemoattraction of other inflammatory cells, helping the formation of the pre-metastatic niche (Hiratsuka et al., 2006; Pollard, 2004). In addition, endothelial progenitor cells are mobilized (Gao et al., 2008) and mesenchymal cells give rise to fibroblasts, which are essential components of the tumor stroma and facilitate the angiogenic recruitment of endothelial cells and pericytes (Kalluri and Zeisberg, 2006). Altogether, these changes make the tissue more compliant for the establishment of the metastatic tumor cells into the new microenvironment.

Despite their success in surviving in the new microenvironment and persisting, the vast majority of metastatic tumor cells are still not guaranteed to be able to proliferate and form large macroscopic metastases. Most of them will die, and some of them can enter into a state of dormancy. In this process, cells undergo growth arrest, becoming inactive in proliferation. However, this interval is sometimes needed in long latent metastases, acting as a delayed adaption and allowing them to survive and colonize the distant organ afterwards (Giancotti, 2013; Nguyen et al., 2009; Reymond et al., 2013).

## **1.7 DISTANT/METASTATIC COLONIZATION**

Metastatic colonization is the endpoint of the invasion-metastasis cascade, being the most complex and rate-limiting phase. It has been demonstrated that, both in patients and in animal models, tumors can shed millions of cells to the vasculature every day. Nevertheless, only a tiny minority of surviving CTCs present in blood samples are in the end able to develop metastasis in the secondary niche. There is a big challenge in detecting these cells in the blood due to the presence of only 1 CTC against  $10^6$ - $10^7$  of surrounding normal peripheral mononuclear blood cells. However, their detection is very relevant, as the presence of CTCs in patients has been related to a decrease of both progression-free survival and overall survival in different types of cancer (Joosse et al., 2015; Strilic and Offermanns, 2017).

As some previous steps, macrometastasis formation requires an angiogenic switch. Therefore, the assembly of a functional vasculature is required to enable further cellular expansion and progression from micrometastases to macrometastases (Holmgren et al., 1995).

This last step also involves the acquisition of traits that allow tumor cells to outgrow in the target organ. Some of them can be present since the beginning of the metastatic cascade, although they can play different roles regarding the process in which they are involved. Nevertheless, not all of them have necessarily to be present in the primary site. In fact, it remains unclear when tumor cells acquire these advantageous traits (Giancotti, 2013). For instance, as EMT has been demonstrated to play essential roles in primary tumor invasion, one of the crucial processes for macrometastasis formation is the induction of re-differentiation through a mesenchymal-epithelial transition (MET). This explains the epithelial phenotype present in a high proportion of metastases in a variety of cancers, resembling to their primary tumors. Furthermore, the differentiation state of metastasis has been associated to the clinical outcome (Brabletz, 2012).

At the end, as the last previous steps, programs governing metastatic colonization depend on the identity of the organ being targeted, as well as the tissue of origin of the disseminating primary tumor cells (Gupta and Massagué, 2006; Nguyen et al., 2009).

## **1.8 CHALLENGES IN METASTASIC RESEARCH**

Tumor metastasis is the major cause of cancer deaths and is still a fairly unascertained process. Enhancing the knowledge about the molecular mechanisms involved, together with the best therapeutic strategies, are needed to improve the prevention and treatment of metastatic cancer to finally obtain better therapeutic outcomes.

Numerous limitations are found in metastasis research. From general to specific processes, we firstly find the heterogeneity between tumors. Despite of classifying different tumors into the same type of cancer, it has been demonstrated that they show differences in mutational landscapes and also differ in genetic expression profiles.



In addition to intertumoral heterogeneity, intratumor clonal heterogeneity poses an even harder challenge, since it becomes even more relevant when it is found between the primary and the secondary sites. This heterogeneity leads to major failure rates in treatment responses and increases the complexity to find robust biomarkers.

Finally, the complex interaction network between heterogeneous populations and also between cancer cells and the microenvironment constitutes an additional hurdle for metastatic research.

## **2. CLONAL HETEROGENEITY**

Cancer progression is an evolutionary process in which natural selection acts on the phenotypic variability as a result of the accumulation of genetic, genomic and epigenetic alterations. Therefore, tumors are formed by multiple cell populations with genomic and phenotypical differences, which change throughout tumor evolution (Nowell, 1976; Podlaha et al., 2012).

Metastasis is a highly inefficient process and all steps described in section 1 end up becoming a competition for clonal selection. Thus, clones with the most advantageous biological traits will endure the environmental stresses they suffer (Massagué and Obenauf, 2016b; Turajlic and Swanton, 2016).

After decades of study, conventional models suggest that metastasis originates from a single tumor cell from the primary tumor that enters into the circulation and seeds monoclonal metastases. However, in recent years, it has been demonstrated that metastases can contain multiple clones. Different analyses of both experimental models and patient samples in different types of cancer, such as breast cancer (Aceto et al., 2014; Cheung et al., 2016), pancreatic cancer (Maddipati and Stanger, 2015) and prostate cancer (Gudem et al., 2015), have demonstrated the existence of an interclonal cooperation between subclones. This cooperativity seems to provide a more efficient travelling and seeding in secondary sites compared to the single cell metastatic spread (Caswell and Swanton, 2017; Cheung and Ewald, 2016).

## **2.1 METASTASIS PROGRESSION MODELS**

Metastatic subclones can be originated both at early and late stages during cancer progression. Depending on this, two main models have been described. Both models consider that primary tumors and metastases have the ancestral cell in common, so they are clonally related. However, differences in the relative timing of appearance of the metastatic precursor population determine their clonal heterogeneity.

The first one defines a linear progression model, in which the metastasis-competent clone arises late in tumor progression. Therefore, metastatic clones seeded at the secondary site are advanced primary clones, or subclones, which present minimal genetic divergence with the primary tumor.

Conversely, the second one describes a parallel progression model. In this case, metastases are formed and disseminated at early stages, hence accumulating high levels of genetic divergence due to the parallel evolution both in the primary tumor and in the metastases (Figure 8) (Caswell and Swanton, 2017; Turajlic and Swanton, 2016).

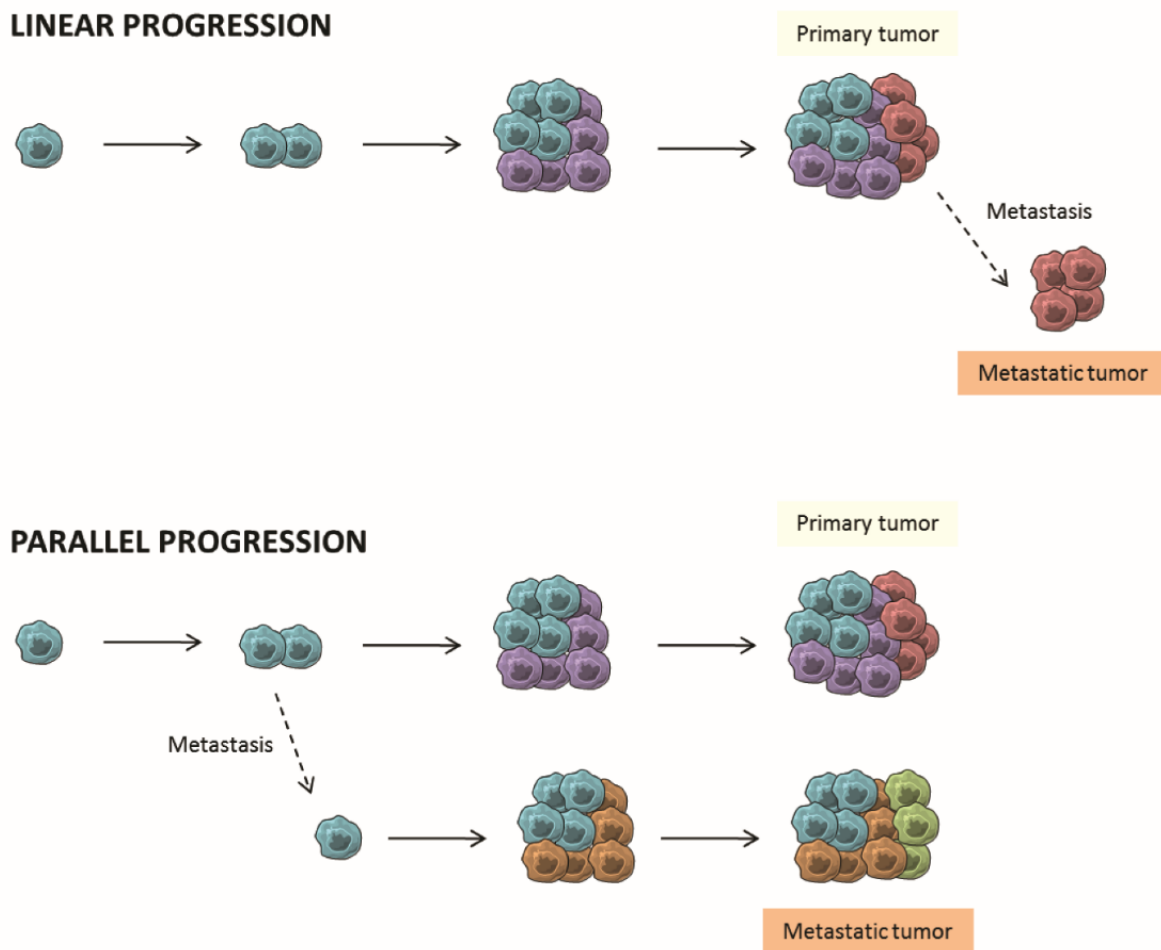


**Figure 8. Linear and parallel progression models of tumor evolution and metastasis formation.** In the linear progression model (upper panel), metastases are formed by late stage tumor cells, whereas in the parallel progression model (lower panel), cells are disseminated from early states of tumor evolution. In this case, both primary tumor and metastasis are progressing in parallel, gaining multiple and different subclonal populations. This figure has been adapted from (Caswell and Swanton, 2017).

## 2.2 METASTASIS PROGRESSION GENES

During clonal evolution, different types of alterations accumulate, and the genes involved can be classified into three main groups: metastasis initiation, metastasis progression and metastasis virulence genes.

Metastasis initiating genes, as indicated by its name, are involved in the early steps of the metastatic process, thus providing an advantage in primary tumors. The expression of these genes is mostly related to invasive features observed in processes such as ECM degradation, EMT or cell motility. Their expression has been described to predict poor prognosis in some types of cancers.

The second group is represented by the metastasis progression genes. Their expression can already be present at early stages, even though they might exert their role in the last steps. Furthermore, their biochemical functions may differ depending on whether they are expressed in the primary tumor or in the metastases. Nevertheless, their selection in the primary tumor may inadvertently benefit the growth at the distant organ. This group of genes is generally involved in the capacity of cells to intravasate through the capillary walls and their survival in the newly invaded parenchyma.

The third and last group is composed of the metastasis virulence genes. These genes are related to the last steps of the metastatic process, being relevant for metastatic infiltration, survival and colonization of the distant organ. As described above, two major determinants for these last steps are the *seed* and the *soil*. Therefore, the expression of these genes normally varies and depends on the type of cancer and the target organ. Their expression arises at plausibly high frequencies at some point during malignant progression, resulting from stochastic alterations due to genomic instability. Nevertheless, they could become stabilized by providing a selective advantage to tumor cells in the new niche. In consequence, these genes cannot be selected during primary tumor evolution and are not useful as predictor metastatic markers in primary sites (Figure 9) (Nguyen et al., 2009; Nguyen and Massagué, 2007).

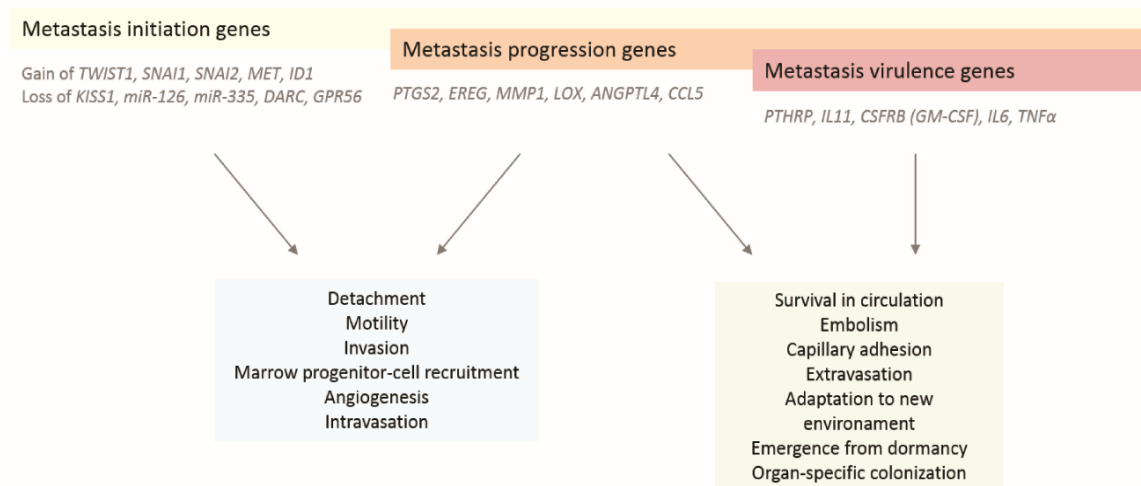


**Figure 9. Metastatic progression genes.** The first group is composed of metastasis initiation genes, which are involved in the early steps of the metastatic cascade. The second group is represented by metastasis progression genes, which are mainly involved in intravasation and tumor cell circulation. However, they can have functions in different processes across metastasis progression. The last group represents the metastasis virulence genes and is involved in the last steps of the cascade. Image has been adapted from (Nguyen et al., 2009; Nguyen and Massagué, 2007)

### 2.3 CLONAL HETEROGENEITY INFLUENCES CANCER TREATMENTS AND OUTCOMES

Clonal heterogeneity results from intrinsic tumor adaptation, as well as from external factors such as treatments, which exert selective pressures on the tumor. Therefore, once a patient is submitted under a treatment, most of the clones composing the tumor will die. However, some cancer cells with advantageous genetic profiles may remain and will be able to proliferate and survive, leading to a relapse of the disease. Consequently, intratumor heterogeneity may foster the selection of resistant subclones (Figure 8) (Venkatesan and Swanton, 2016).

Nowadays, highly variable interpatient treatment responses represent one of the most challenging problems, driving research interest on personalized medicine.

One of the most relevant handicaps to choose the most suitable treatment is the presence of intratumor genetic heterogeneity. Genomic studies in a variety of cancers have demonstrated the existence of regionally diverse mutational landscapes both in primary tumors and in metastases. The problem arises when personalized medicine

strategies normally depend on results from a single site tumor-biopsy evaluation, thus underestimating the mutational burden within a tumor. In order to solve this problem, it has been suggested that treatments should target a *trunk* event in the early clonal evolution. Therefore, it would target something in common between the primary tumor and the metastases, thus contributing to finding more reliable biomarkers and therapeutic approaches (Sankin et al., 2014; Yap et al., 2012).

### **3. RENAL CELL CARCINOMA**

Renal Cell Carcinoma (RCC) is one of the 10 most common cancers, accounting for 2% of all cancer diagnoses and cancer-related deaths worldwide. Every year, nearly 300,000 new cases are diagnosed and more than 100,000 deaths are reported, most of which occurring in developed countries. This type of cancer represents, on average, over 90% of all kidney malignancies that occur in adults of both sexes. It affects more men than women at a ratio 2:1 during the most frequent ages (41-60), and nearly equally divided in older patients (Hsieh et al., 2017).

Kidney cancer is a group of malignancies arising from the epithelium of the proximal renal tubules. This part of the nephron acts as a filtrate pH regulator by exchanging hydrogen ions in the interstitium for bicarbonate ions in the filtrate (Polascik et al., 2002).

One of the most important genetic events in the development of ccRCC is the inactivation of the tumor suppressor gene von Hippel-Lindau (VHL). The VHL gene codifies for a ubiquitin-ligase protein involved in the degradation of Hypoxia-Inducible Factor 1 $\alpha$  (HIF1- $\alpha$ ) and HIF2- $\alpha$  through oxygen and iron sensing mechanisms. Thereafter, tumors associated to an inactivation of this gene often present a high level of vascularization and an overproduction of mRNAs responsive to hypoxia and to different angiogenic factors (Linehan et al., 2010).

Data from one of the most important studies of metastasis distribution in RCC from the National Inpatient Sample (NIS) reported that the most common sites of metastasis are

the lungs (45%), followed by bones (30%), lymph nodes (22%) and liver (20%). In a low incidence, adrenal and brain metastases were also found (9% each) (Gong et al., 2016).

### **3.1 RCC CLASSIFICATION**

RCC is made up of many different subtypes with histological differences and distinctive genetic and molecular alterations. They also present different clinical courses and therapy responses.

The classification for Renal Cell tumors was revised for the last time at the WHO Consensus Conference in Zurich, Switzerland, in 2015. The review was published in 2016 as the fourth edition of the WHO classification of urogenital tumors (Moch et al., 2016b) and summarizes both the prior version for renal classification and the newly published one. In this last version, mainly grounded on morphological and cytogenetic features, a classification of more than 10 different renal cancers was determined, with the recognition of five new RCC subtypes. The most typical ones are: Clear Cell Renal Cell Carcinoma (70-80% of the cases), Papillary Carcinoma (15-20%) and Chromophobe (5%) (Table 1) (Moch et al., 2016a).

WHO Classification of tumors of the kidney
<b>Renal Cell tumors</b>
Clear Cell Renal Cell Carcinoma
Multilocular cystic renal neoplasm of low malignant potential
Papillary Renal Cell Carcinoma
Hereditary leiomyomatosis and Renal Cell Carcinoma-associated Renal Cell Carcinoma*
Chromophobe Renal Cell Carcinoma
Collecting duct carcinoma
Renal medullary carcinoma
MiT family translocation Renal Cell Carcinomas
Succinate dehydrogenase-deficient Renal Carcinoma*
Mucinous tubular and spindle Cell Carcinoma
Tubulocystic Renal Cell Carcinoma*
Acquired cystic disease-associated Renal Cell Carcinoma*
Clear cell papillary Renal Cell Carcinoma*
Renal Cell Carcinoma, unclassified
Papillary adenoma
Oncocytoma

**Table 1. WHO Classification of kidney tumors.** Table adapted from (Moch et al., 2016a). Newly recognized subtypes of epithelial renal tumors are highlighted with an \*.

In search for a more successful management and also in order to apply beneficial treatments to RCC patients, identification and differentiation of subtypes is completely necessary. It is well known that they differ histologically. However, their mechanistic differences are not well defined yet. Analyses from 488 RCC from the three major histologic subtypes revealed that the differences observed in histology are explained by differences in mutations, chromosomal copy number alterations and variable expression patterns of mRNA, miRNA and lncRNA (Ricketts et al., 2018).



### 3.1.1 Clear Cell Renal Cell Carcinoma

Clear Cell RCC (ccRCC) is the most frequent RCC and accounts for most cancer-related deaths. It was named after the clear or eosinophilic cytoplasm, and it represents between the 70-80% of the cases. Its appearance is due to the presence of lipids and glycogen that get dissolved during the histological processing. It is also characterized by a delicate thin-walled vascular network (Figure 10B) (Rini et al., 2009).

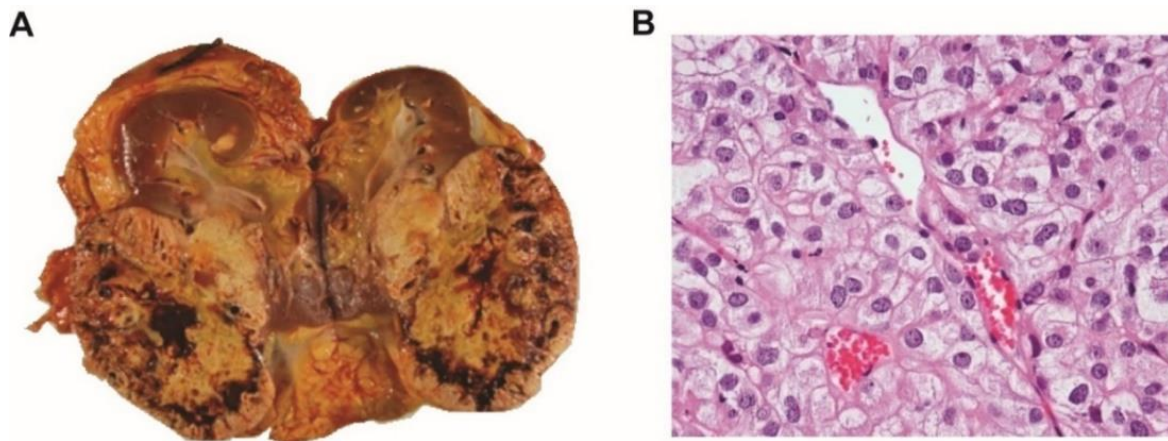


**Figure 10. Renal Cell Carcinoma.** A) Picture from a kidney tumor of a patient. B) Hematoxylin-eosin staining of a ccRCC tumor (20X). Tumor cells present a clear phenotype and the tumor has a delicate vascular network.

## 3.2 HISTOPATHOLOGICAL CLASSIFICATION: NUCLEAR GRADE CLASSIFICATION

Many grading systems have been determined for RCC during the last years. The Fuhrman system is the most popular and widely used classification. It is based on the nuclear size, shape and nucleolar prominence of tumor cells. This classification uses four grades and it correlates with patient prognosis, being the highest grades related to worse prognosis (Fuhrman et al., 1982). However, this system cannot be applied for the chromophobe subtype and it has not been validated for most of the new RCC subtypes. Owing to these reasons, since the revisions by the International Society of Urological Pathology (ISUP) in 2012 and the WHO in 2016, the WHO/ISUP grading system shown in Table 2 is the recommended grading system of use (Moch et al., 2016a; Samaratunga et al., 2014).

GRADE	DESCRIPTION
Grade 1	Nucleoli are absent or inconspicuous and basophilic at 400X magnification
Grade 2	Nucleoli are conspicuous and eosinophilic at 400X magnification and visible but not prominent at 100X magnification
Grade 3	Nucleoli are conspicuous and eosinophilic at 100X magnification
Grade 4	There is extreme nuclear pleomorphism, multinucleate giant cells, and/or rhabdoid and/or sarcomatoid differentiation

**Table 2. Renal Cell Carcinoma classification.** Table adapted from (Moch et al., 2016a)



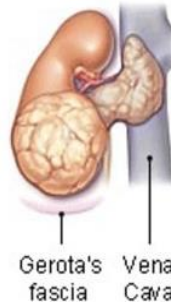
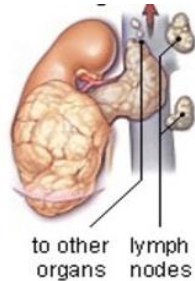
### 3.3 CLINICAL CLASSIFICATION OF RCC: TUMOR-NODE-METASTASIS STAGING

In order to describe the anatomic extension of the tumor, as well as the progression of the disease, RCC is also classified into stages using the tumor-node-metastasis (TNM) system. This system is used for most of the solid tumors and was developed by the American Joint Committee on Cancer (AJCC). The “T” stands for the tumor and has three levels depending on the size and degree of local invasion. The “N” refers to whether the cancer has spread to regional lymph nodes. Finally, the “M” means if the cancer has metastasized to distant organs. RCC progression is divided into four stages (Table 3) (Greene et al., 2002).

Nowadays, there are no screening methods to detect renal cancer in early stages and, despite the existence of standard agents to treat the disease, most of patients tend to progress to a metastatic disease. In fact, one third of patients with RCC present locally advanced or metastatic disease at the time of diagnosis and one third of patients who undergo surgical resection for local disease will have a recurrence (Cairns, 2012).

In addition, data from the National Cancer Data Base (NCDB) reveals that the 5-year rate survival of RCC metastatic patients, which are at stage IV, represents only an 8% (Gupta

et al., 2008). This dramatic data poses metastasis as one of the most relevant processes to study in RCC, as well as the determination of predictive biomarkers.

STAGE	DESCRIPTION	SCHEMATIC REPRESENTATION	5-YEAR SURVIVAL RATE
<b>Stage I</b>	Tumor is only in the kidney and it is smaller than 7cm.		<b>81%</b>
<b>Stage II</b>	Tumor is still limited to the kidney but is larger than 7cm.		<b>74%</b>
<b>Stage III</b>	Tumor has extended into a major vein or adrenal glands, which are attached to the kidney. Cells spread beyond the Gerota's fascia, which is the layer of connective tissue that encapsulates the kidney and adrenal glands. It can also involve regional lymph nodes.		<b>53%</b>
<b>Stage IV</b>	It is the last and the most advanced stage of the disease. The tumor has invaded the Gerota's fascia and cancer has spread to the lymph system or distant organs.		<b>8%</b>

**Table 3. Stages of RCC.** RCC is classified into stages I to IV depending on the progression and the extension of the disease. Images are extracted and adapted from ("New Health Advisor," 2018). 5-year rate survival data has been extracted from the National Cancer Data Base (NCDB) ("American Cancer Society," 2018).

### **3.4 CLONAL HETEROGENEITY IN RENAL CELL CARCINOMA**

Intratumoral heterogeneity has been documented in various types of cancer and seems to be one of the main causes of therapeutic resistance. Acquired genetic and epigenetic alterations may determine differences in the therapeutic outcomes of a both local and systemic disease.

Despite some studies have demonstrated that there are shared features between the RCC subtypes that may provide prognostic markers and therapeutic targets (Ricketts et al., 2018), RCC is one of the cancers in which intratumor clonal heterogeneity has been reported at the genetic, transcriptomic and functional levels. Multiregional sequencing supports that both metastatic models, linear and parallel, are present in this type of tumor progression (Caswell and Swanton, 2017). In RCC, mutational burden varies depending on the region sampled, which leads to capturing genetic predictors of tumor behavior which do not represent the entire tumor (Sankin et al., 2014). This underestimation has been confirmed through exome-sequencing, chromosome aberration analysis and ploidy profiling on multiple independent samples from RCC primary tumors and metastases (Gerlinger et al., 2014, 2012).

There are already standard agents to manage advanced RCC. Nevertheless, treatments do not show high efficacy rates in most of the cases, and there is a deficiency of prognostic biomarkers. It is believed that the presence of clonal heterogeneity acts by limiting treatment outcomes, being the presence of chromosomal instability one of the main causes for this heterogeneity. This specific form of genome instability is characterized by an acquisition of whole-chromosome or segmental chromosomal aneuploidies (Venkatesan and Swanton, 2016; Voss et al., 2014).

## **4. MODELING METASTASIS IN THE MOUSE**

Nowadays, we can find several models allowing mechanistic and therapeutic research, approaching the different steps of the metastatic process.

Two different strategies in order to understand tumor development and progression *in vivo* are followed. On the one hand, genetically engineered mouse models have demonstrated to be useful to study events such as tumor progression, angiogenesis and local invasion or treatment responses. On the other hand, engraftment of human biopsies into mice has successfully generated appropriate models for studying metastatic dissemination and colonization of distant organs (Bos et al., 2010). In addition, there is a standard model used for studying hematogenous dissemination, which consists of intravenous injection of tumor cells through the tail vein of the mice, forcing cancer cells to lodge in lung capillaries. Even though this model presents some limitations, as the absence of a primary tumor, it shows experimental advantages such as a precise characterization of the last steps of the metastatic cascade (Labelle and Hynes, 2012).

A current challenge for metastasis research is to address the heterogeneous biology of this multistep process in the current models. The ideal cancer model would include both phenotypically and molecular features from human tumors.

### **4.1 PATIENT-DERIVED XENOGRAFT MOUSE MODELS**

Patient-derived xenografts (PDX) mouse models are generated by implanting human tumor pieces or human cancer cells isolated directly from the patients into immune-deficient mice. It has become an important model for cancer research because of its potential to generate most of human cancer types used in pre-clinical research studies.

These models have shown to be useful to study tumor and genetic evolution in metastasis due to their capacity of maintaining most of the important histomorphological features, gene expression profiles and also the genomic variations present in the original human tumor. Despite this method is more technically challenging

and its generation requires a bigger deal of time compared to cancer cell line xenograft models, it has been demonstrated that it better mimics human original tumors, both histologically and genetically. These differences could be explained because of the limited cellular heterogeneity in cell lines and the lack of stroma in cell culture, which fails at thoroughly representing the complexity of tumor clonal populations and tumor microenvironment (Katt et al., 2016; Lum et al., 2012). However, it is necessary to be considered that, when human tumor cells are implanted into the mice, the selection pressure exerted on them might cause changes in their original clonal composition. In addition, there is a downregulation of human stromal genes, which is compensated by an overexpression of the murine ones (Siolas and Hannon, 2013).

PDX models can be obtained by engrafting heterotopically or orthotopically (Kim et al., 2009). As for the former, it consists of the implantation of human tumor cells or pieces into the subcutaneous flank of the mouse. This method facilitates cell transfer and makes the monitoring of tumor growth and location easier. As for the latter, it involves the direct implantation of tumor cells or a piece of a human biopsy, also known of tumorgrafts or orthozenografts, where it was exactly located in the patient. These models normally present higher metastatic rates and are considered to better maintain histological and genetic features compared to the heterotopic ones, maybe due to the intrinsic properties of the tumor and the presence of a similar tumor microenvironment as one would find in the patient (Siolas and Hannon, 2013).

## **5. PREVIOUS DATA**

### **5.1 SPONTANEOUS GENERATION OF TWO VARIANTS OF A ccRCC PATIENT-DERIVED ORTHOXENOGRAFT MOUSE MODEL**

Previous work in the laboratory, performed by Mar Martínez-Lozano, developed a patient derived orthoxenograft (PDOX) murine model based on a human biopsy, named Ren 50, with a 4-grade Fuhrman from a patient who had ccRCC and a ganglionic metastasis at the time of diagnosis (pT3a pN1). Later on, the patient also developed lung

metastasis. This piece of tumor was implanted into the kidney of an athymic mouse (orthotopic) (Figure 11).

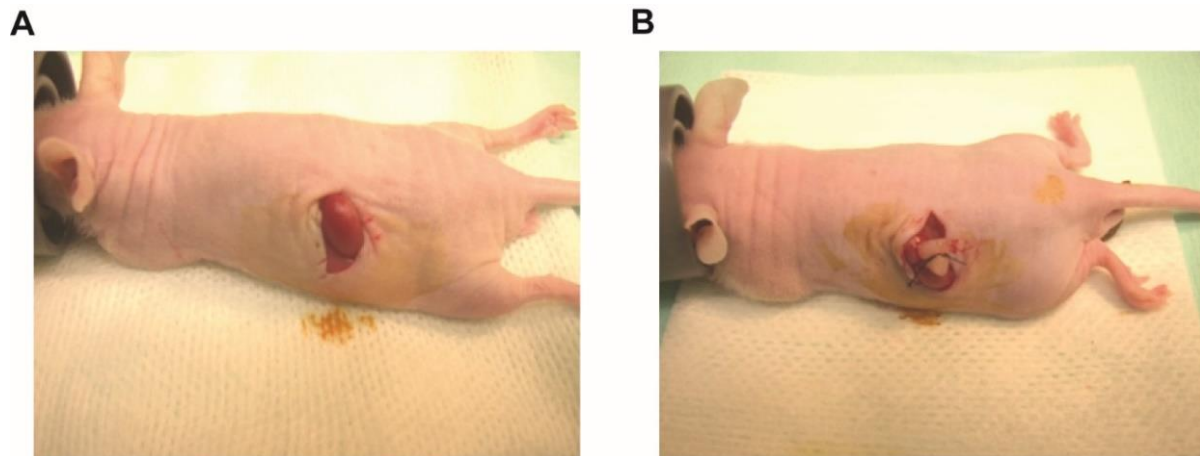


**Figure 11. PDOX mouse model of RCC.** Surgical implantation of a human kidney piece of tumor into an athymic mouse. A) A skin incision was performed on the kidney's area and the organ was externally exposed. B) A piece of tumor was surgically implanted into the kidney of the mouse.

At the time of sacrifice, this mouse had developed spontaneous micrometastases and also a macrometastasis in the lung (Figure 12).

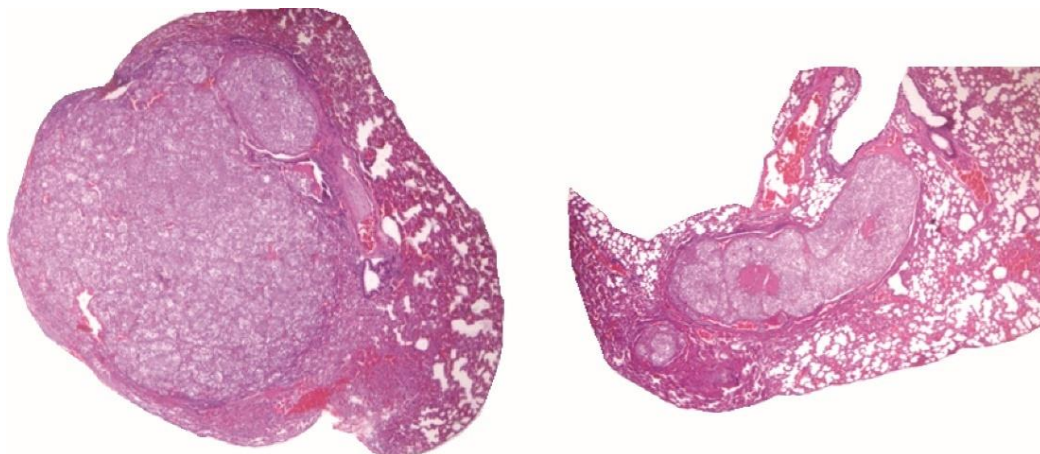


**Figure 12. The orthotopic mouse presented both micrometastases and macrometastases in the lung.** Pictures of hematoxylin-eosin staining (4X) of lung metastases from the orthotopic mouse.

First of all, a piece of the primary tumor was implanted into the kidney of a mouse, generating an orthoxenograft line named Ren 50. In parallel, we also decided to implant the spontaneous macrometastasis present in the lung of the orthotopic mouse into another animal, generating a different line named Ren 50M (Figure 13).

By perpetuating both lines during several passages, two different orthoxenograft group of tumors were created with shared mouse and patient origins. However, one of them had been generated from a natural selection of cells with the capacity to metastasize *in vivo*.

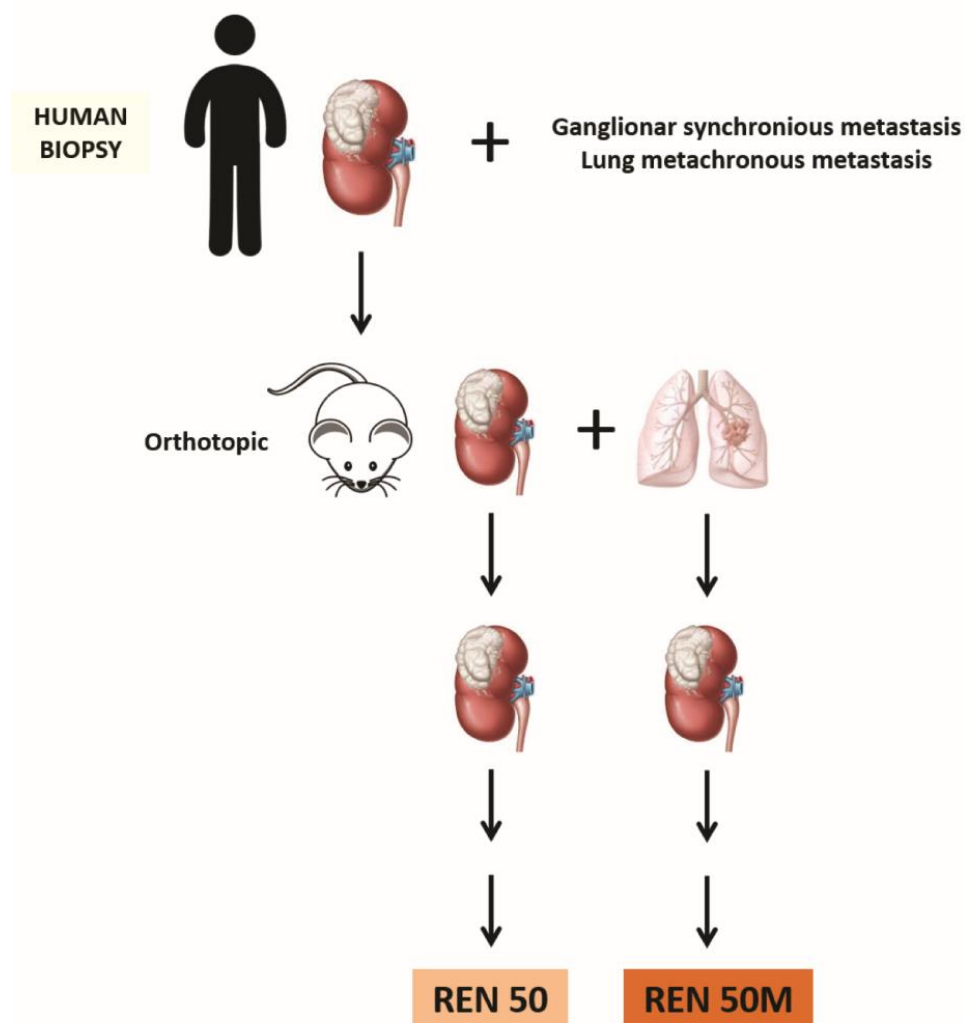


**Figure 13. Schematic representation of Ren 50 and Ren 50M mouse orthoxenograft lines.** A human biopsy from a ccRCC patient was implanted into the kidney of a mouse, which we called orthotopic. The tumor grown in this mouse was implanted into the kidney of another mouse, generating the Ren 50 line. In parallel, the lung macrometastasis from the orthotopic mouse was implanted into the kidney of another mouse, generating the Ren 50M line.



## 5.2 METASTATIC POTENTIAL OF REN 50 AND REN 50M TUMORS

Upon perpetuation of the primary ccRCC tumor into the kidney of mice during several passages (Ren 50), tumors generally presented clear cell phenotype and a very low metastatic potential. On the other hand, the line generated from the lung macrometastasis of the first orthotopic mouse (Ren 50M) developed ccRCC tumors and lung metastases at a higher frequency (Figure 14).

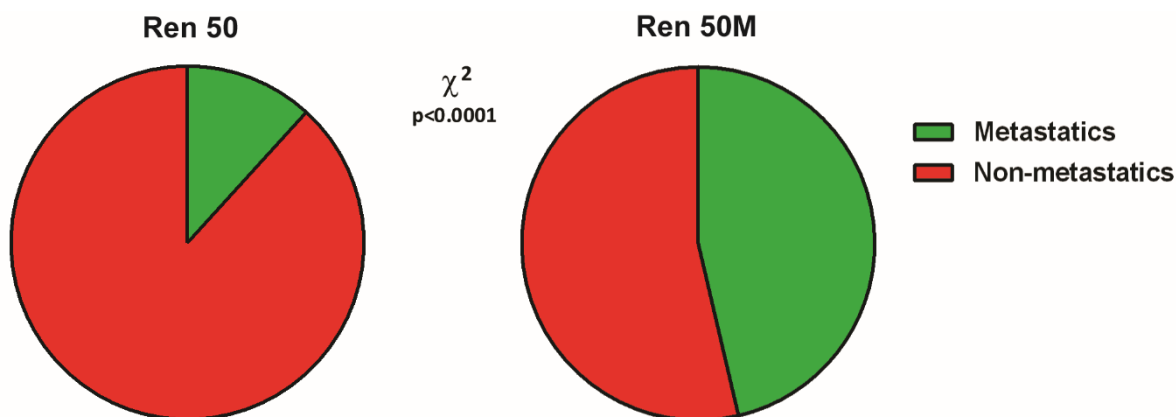


**Figure 14. Ren 50M did metastasis at a higher frequency compared to Ren 50.** Radial representation of the percentage of metastasis evaluated at 25-40 days. On the left, Ren 50 mice did metastasis in 8.33% of cases (n=24). On the right, Ren 50M mice did metastasis in 41.38% of the cases (n=29). Results showed a statistically significant difference between both groups by Chi-square test.

Moreover, we did not only observe differences in the incidence of metastasis, but also the type of lesions differed between both groups. Ren 50 always showed micrometastases, while Ren 50M mice presented more lesions within the lungs (Figure 15B), including both micrometastases and macrometastases (Figure 15A).

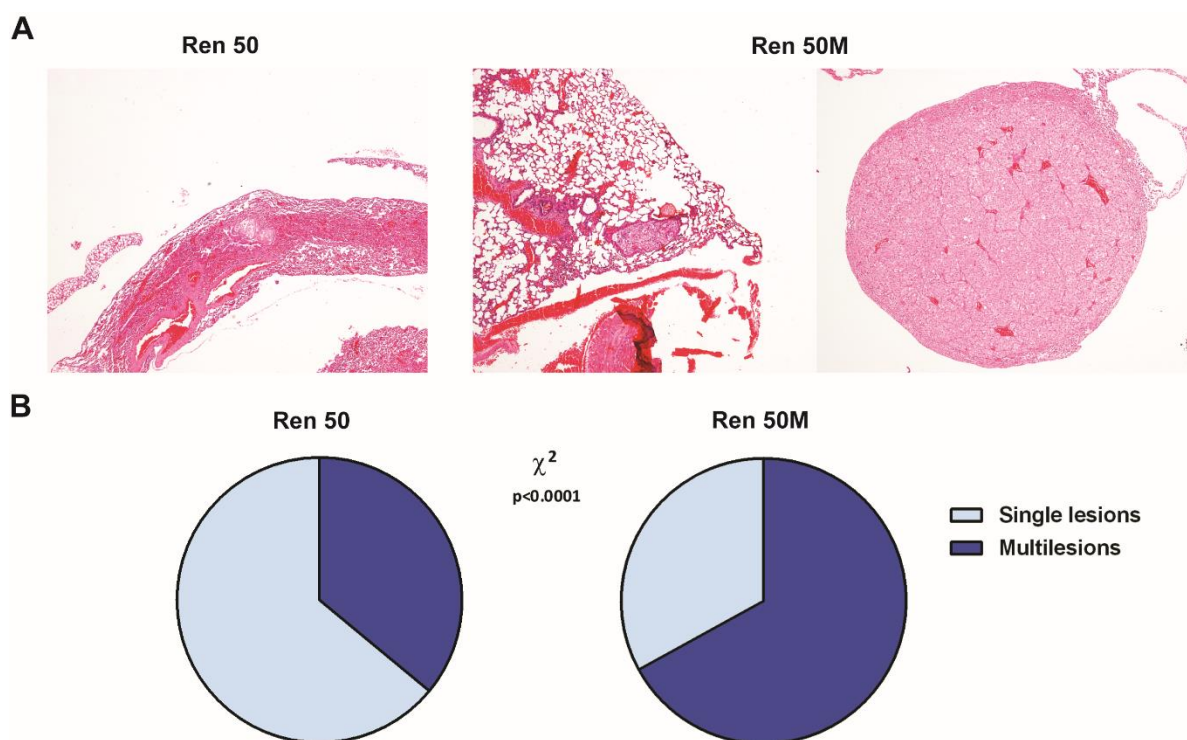


**Figure 15. Ren 50 always showed micrometastases, whereas Ren 50M mice presented more lesions in the lungs, including both micrometastases and macrometastases.** Metastasis parameter evaluated at 25-40 days. A) From left to right, pictures (4X) of a micrometastasis from a Ren 50 lung and a micrometastasis and macrometastasis from a Ren 50M lung. B) Radial representation of the percentage of single lesions or multilesions present in the lungs. Ren 50 had single lesions in the 64% of the cases (n=11), whereas Ren 50M mice did metastasis with more than one lesion in the 67% of the cases (n=18). Results showed a statistically significant difference between both groups by Chi-square test.

Altogether, these results demonstrated a clear difference in the metastatic capacity between Ren 50 and Ren 50 tumors, even though both came from the same orthotopic animal and the same cancer patient.

### **5.3 MOLECULAR CHARACTERIZATION**

A molecular approach was performed through Next Generation Sequencing (NGS) of RNA and exome in order to obtain information to generate pathways of interest and candidate gene lists that may be involved in the metastatic process.

#### **5.3.1 Exome sequencing analysis of the human biopsy, Ren 50 and Ren 50M tumors**

First, a whole exome sequencing was performed using HiSeq 1500 analyser (Illumina, Inc., San Diego, USA) at Cancer genomics Core Facility at Vall d'Hebrón Institut d'Oncologia (VHIO, Barcelona, Spain). Included samples comprised the Ren 50 human biopsy, three Ren 50 and three Ren 50M PDOX tumors. Intragroup samples were from animals of the same passage. SNV and indel characterization was performed using the public databases dbSNP (Sherry, 2001), Ensembl (Yates et al., 2016), COSMIC (Forbes et al., 2015) and ICGC Data Portal (International Cancer Genome Consortium (ICGC), 2018) using Genome of reference: GRCh37hg19.

We expected the results to provide us with information about common and differential mutations between groups that could account for the different metastatic phenotypes.

From this data, we could observe that most of the mutations were present in the biopsy and also in both groups, Ren 50 and Ren 50M. However, some mutations in the first human sample were not present either in the Ren 50 or in the Ren 50M. Interestingly, there were new mutations shared only by Ren 50 and Ren 50M lines and some exclusive mutations for both groups (Figure 16).

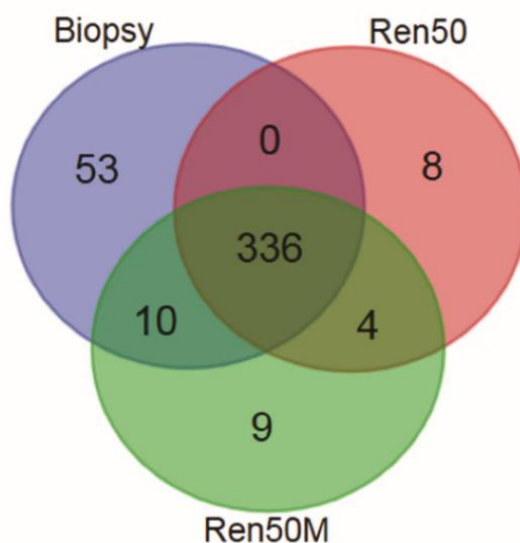
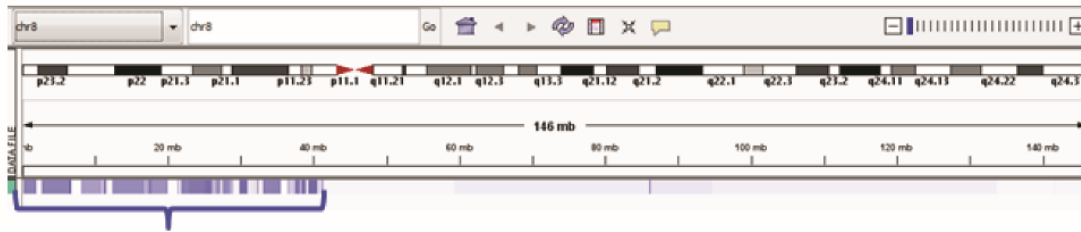


**Figure 16. Results from exome sequencing analysis revealed shared mutations between the human biopsy, Ren 50 and Ren 50M tumors. In addition, we observed specific mutations for each group.** Venn diagram of mutations found in the human biopsy (n=1), Ren 50 (n=3) and Ren 50M (n=3) tumors. In blue are represented specific mutations for the biopsy, in red the ones for Ren 50 tumors and in green the ones only present in Ren 50M tumors. Overlapped areas show common mutations between groups.

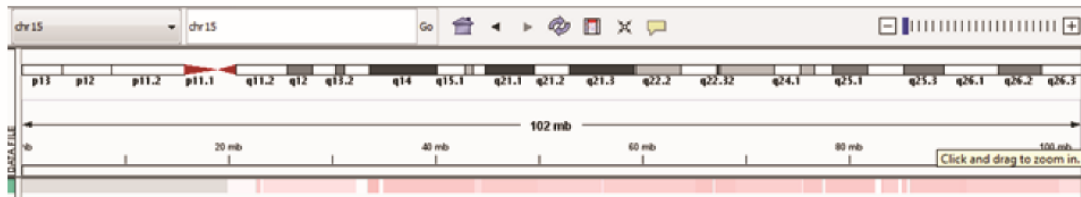
According to these data, we inferred that we obtained a human biopsy with clonal heterogeneity and, through clonal evolution, we obtained two variants of PDOX lines from a unique human tumor biopsy that also evolved a little during passages.

In addition, using the Integrative Genomic Viewer (IGV) software, we could confirm, by visual inspection of the regions with listed variants, that a lot of mutations were concentrated in specific chromosomal regions. These localizations led us to hypothesize on the presence of some loss of heterozygosity (LOH) and chromosomal rearrangements, especially in chromosomes 8, 15 and 18 (Figure 17).

## Chromosome 8



## Chromosome 15



## Chromosome 18

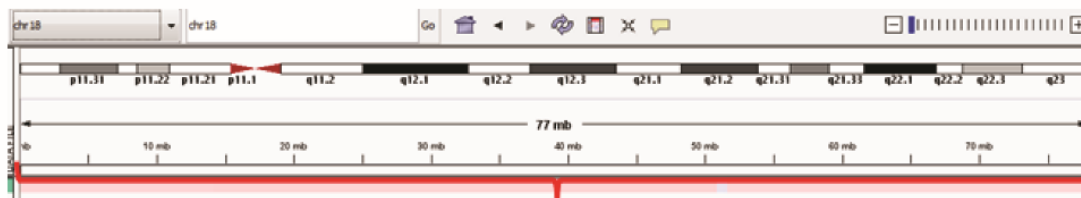


**Figure 17. Results from exome sequencing revealed an accumulation of mutations in chromosomes 8, 15 and 18.** From top to bottom, IGV presented an accumulation of deletions (represented in blue) in the p arm of chromosome 8 and amplifications (represented in red) in the q arm of chromosome 15 and whole chromosome 18 in Ren 50M tumors (n=3) compared to Ren 50 (n=3). Used data were from exome sequencing and the image has been extracted and adapted from IGV.

### 5.3.2 Fluorescent *In Situ* Hybridization analysis of Ren 50 and Ren 50M tumors, together with Ren 50M lung metastases

In order to address these hypothetical chromosomal rearrangements based on the exome sequencing results, a Fluorescence *in Situ* Hybridization (FISH) experiment was carried out in collaboration with Keyvan Torabi, from Dra. Rosa Miró laboratory at Universitat Autònoma de Barcelona.

Samples from Ren 50 and Ren 50M tumors were analyzed, together with metastases from Ren 50M mice. About 800 nuclei were quantified for each sample and the mean copy number was calculated using the following formula:

$$\text{Copy number (mean)} = \sum \text{copy number (n)} * \text{number of cells with this copy number (\%)}$$

Grounded on previous results, the first chromosome of choice was chromosome 8. Two different probes were used for its detection, one against the centromere and another against the chromosomal position 8q24, which corresponds to *MYC* gene (Figure 18A).

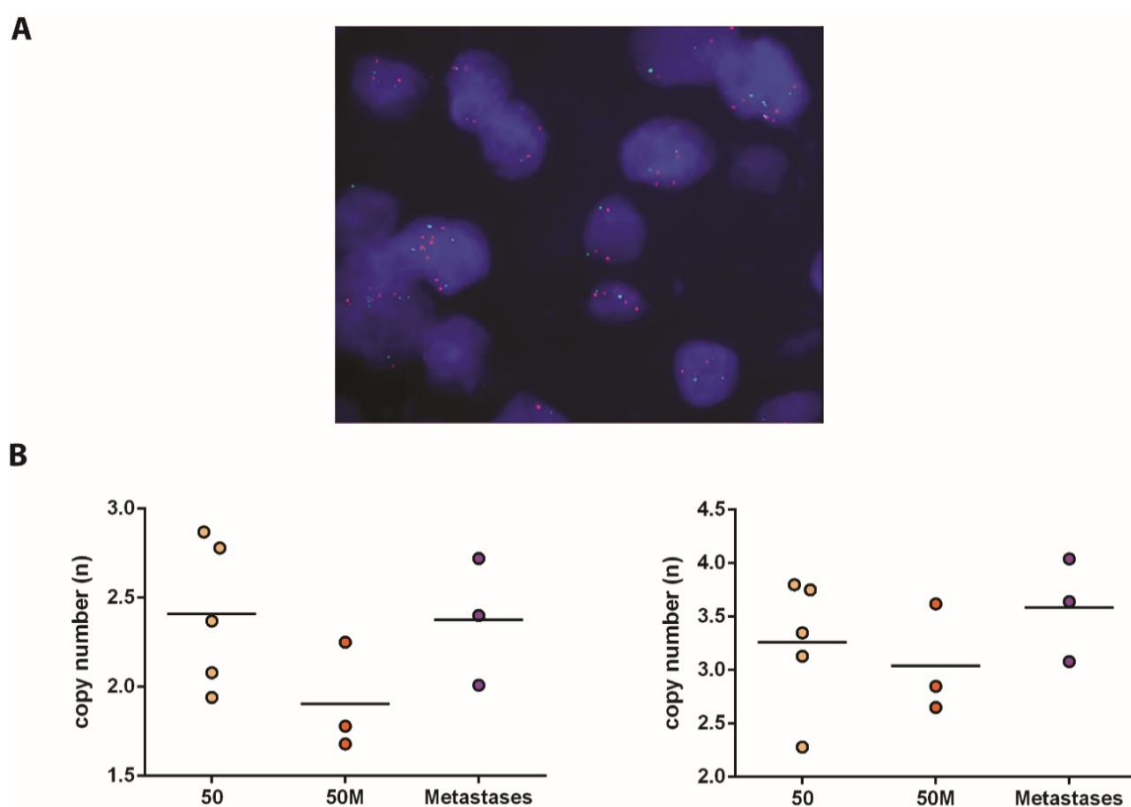


**Figure 18. Centromere of chromosome 8 and 8q24 analysis showed the same copy number expression pattern between them. Nevertheless, more copies of 8q24 were quantified.** A) Picture from FISH staining analysis. Green probe was bound to the centromere of chromosome 8. In order to detect the q arm of this chromosome, the *MYC* gene, located at chromosome 8q24, was detected in red. B) From left to right, quantification of the copy number of the chromosome 8 centromere and the 8q24 position. Results shown comprise five tumors of Ren 50, three tumors of Ren 50M and three lung metastases of Ren 50M animals.

Results showed that, despite the similarity in the copy number pattern obtained in the centromere and in the 8q24, the absolute quantification for both probes was different, always presenting more copies of 8q24 (Figure 18B).

With these results, we hypothesized that we probably had the presence of an isochromosome 8, which consists of a chromosomal unbalanced structural abnormality in which there are two identical arms due to duplication of one arm and loss of the other (Figure 19). In this case, we hypothesized that we probably had two copies of the long q arm of chromosome 8. Consequently, tumors from both lines carried a partial trisomy of the genes located at 8q and a partial monosomy of the genes located at 8p. Apart from the isochromosome, Ren 50 tumors seemed to present a total duplication of chromosome 8 in some cases (Figure 18).

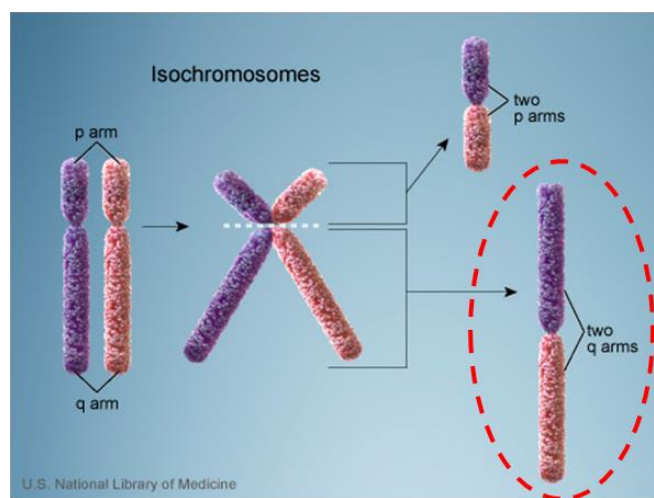


**Figure 19. Schematic representation of isochromosomes.** Isochromosome formation occurs after a division of the centromere, therefore obtaining monocentric isochromosomes containing arms which are specular images of each other. Image has been adapted from (NIH, 2018).

We next decided to study the copy number alterations present in chromosome 15. Despite they were not statistically significant, results showed an increase in the chromosome 15 copy number in Ren 50M tumors compared to Ren 50. However, the most interesting result was obtained from the metastases, which clearly presented higher levels of chromosome 15 copies (Figure 20).

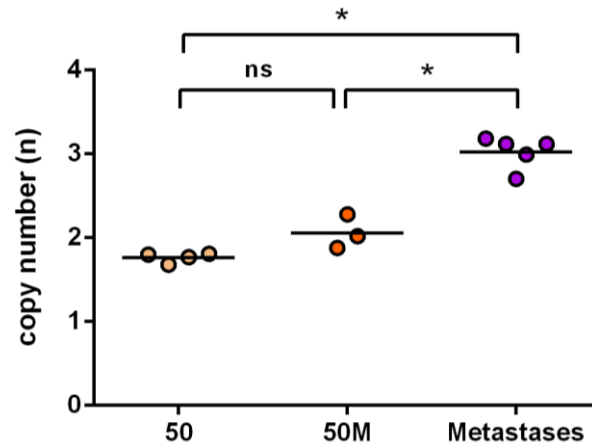


**Figure 20.** Ren 50M tumors showed a tendency of an accumulation of chromosome 15. Differences were statistically significant when comparing both groups to metastases, which presented a clear accumulation of this chromosome. Quantification of chromosome 15 centromere copy number. Results were obtained from four tumors of Ren 50, three tumors of Ren 50M and five Ren 50M lung metastases. Results were statistically significant by Mann-Whitney test.

Finally, the last chromosome of interest was chromosome 18. Results showed the same patterns observed in the previous one. Hence, we observed slight differences between chromosome 18 copy number in Ren 50 compared to Ren 50M. However, clear differences were found when analyzing metastases, which presented a higher accumulation of this chromosome (Figure 21).

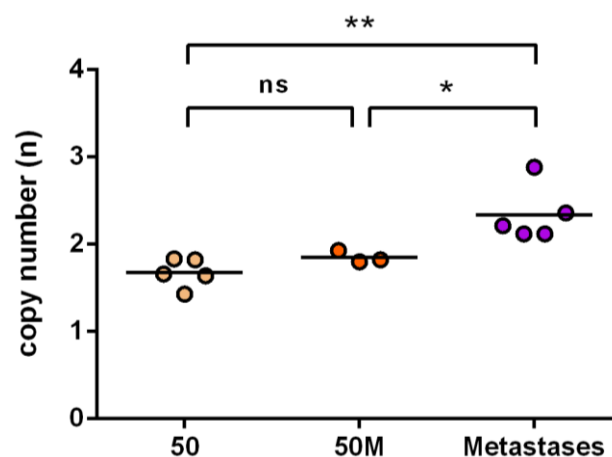


**Figure 21.** Ren 50M tumors showed a slight accumulation of chromosome 18. Differences were statistically significant when comparing both groups with metastases, which presented a clear accumulation of this chromosome. Quantification of the copy number of chromosome 18. Results were obtained from five tumors of Ren 50, three tumors of Ren 50M and five Ren 50M lung metastases. Results were statistically significant by Mann-Whitney test.



### **5.3.3 RNA sequencing and Gene Set Enrichment Analysis of Ren 50 and Ren 50 tumors**

In parallel to the exome sequencing, whole RNA sequencing was performed in order to detect mRNA expression differences between groups. Analyzed samples consisted of four Ren 50 and four Ren 50M tumors. Tumors were the same used in the exome sequencing analysis, with an extra tumor per group.

Samples were sequenced at Centro Nacional de Análisis Genómico (CNAG-CRG, Barcelona, Spain). RNAseq reads were aligned to the human (GRCh38/hg38) and mouse (GRCm38/mm10) reference genomes using STAR (version 2.5.1b) and GSNAP (version 2015-06-23), respectively, with ENCODE parameters for long RNA (Dobin et al, 2013). Transcripts were quantified using RSEM (version 1.2.28) and read counts were used as input for DESeq2 (version 1.10.1) (Love et al, 2014). The cut-off for considering a gene significantly up-sampled or down-sampled was FDR<5%.

When comparing one group to the other, results showed a long list of differentially expressed genes, presenting both downregulations and upregulations. Another interesting result to emerge from the RNA data, in line with exome sequencing and FISH results, was that genes in chromosome 8p seemed to be downregulated. On the contrary, most of genes located at chromosomes 15 and 18 were upregulated in Ren 50M tumors compared to Ren 50 (Figure 22).

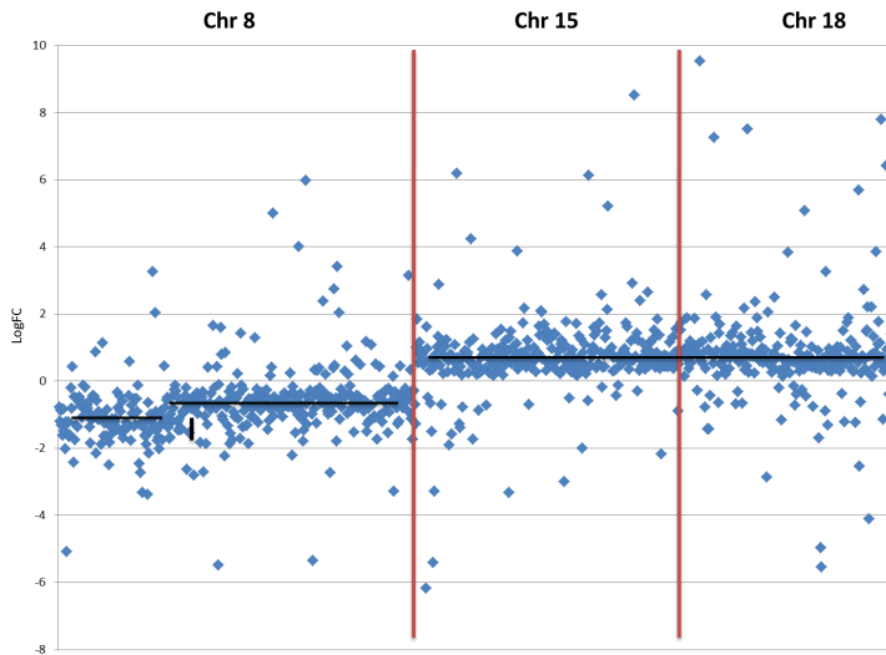


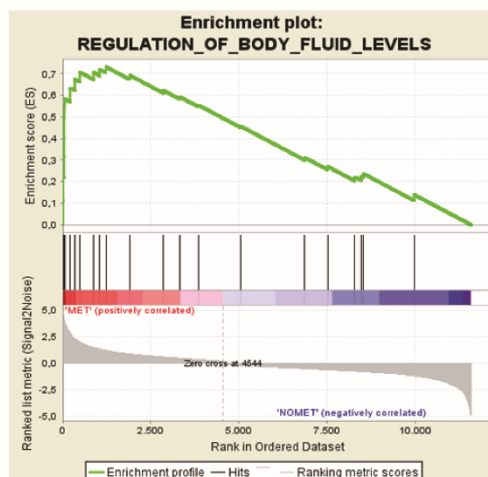
**Figure 22. Results from RNA Sequencing of Ren 50 and Ren 50M tumors showed an accumulation of alterations in the expression of genes from chromosomes 8, 15 and 18.** Representation of 993 genes expression located in chromosomes 8, 15 and 18. Data was extracted from RNA sequencing and values are the representation of a log fold change (LogFC) of gene expressions in Ren 50M (n=4) compared to Ren 50 (n=4) tumors.

Once data from RNA sequencing had provided differences in the expression of so many genes, expression profiles were subjected to a Gene Set Enrichment Analysis (GSEA) in order to analyze whether any gene signature was upregulated or downregulated in our samples.

GSEA is a computational method which determines whether a defined set of genes presents statistical significant concordant differences in gene expression levels when compared to another data set. Gene sets are available at Molecular Signatures DataBase (MolSigDB) and GSEA was run according to default parameters: collapses each probe set into a single gene vector (identified by its HUGO gene symbol), permutation number = 1000, and permutation type = "gene-sets". Calculation of the false discovery rate (FDR) was used to correct for multiple comparisons and gene set sizes (Subramanian et al, 2005).

In our case, RNA sequencing results were compared to all gene sets available (From C1 to C7). Interestingly, results from GSEA revealed an upregulation of genes related to hemostatic functions present in the signature *Regulation of blood and fluid levels* (from C5-Biological Process data set) in Ren 50M tumors compared to Ren 50 (Figure 23).

A



B

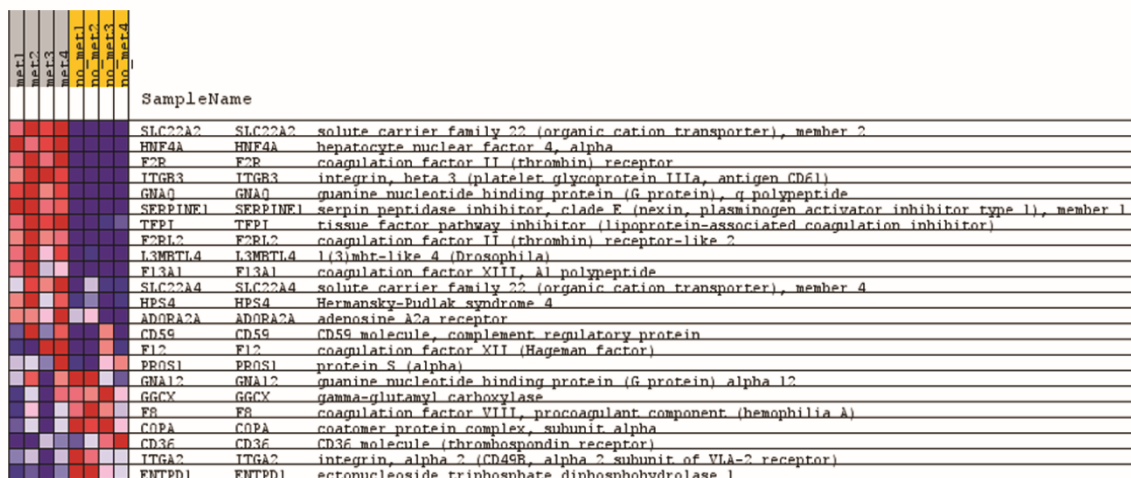
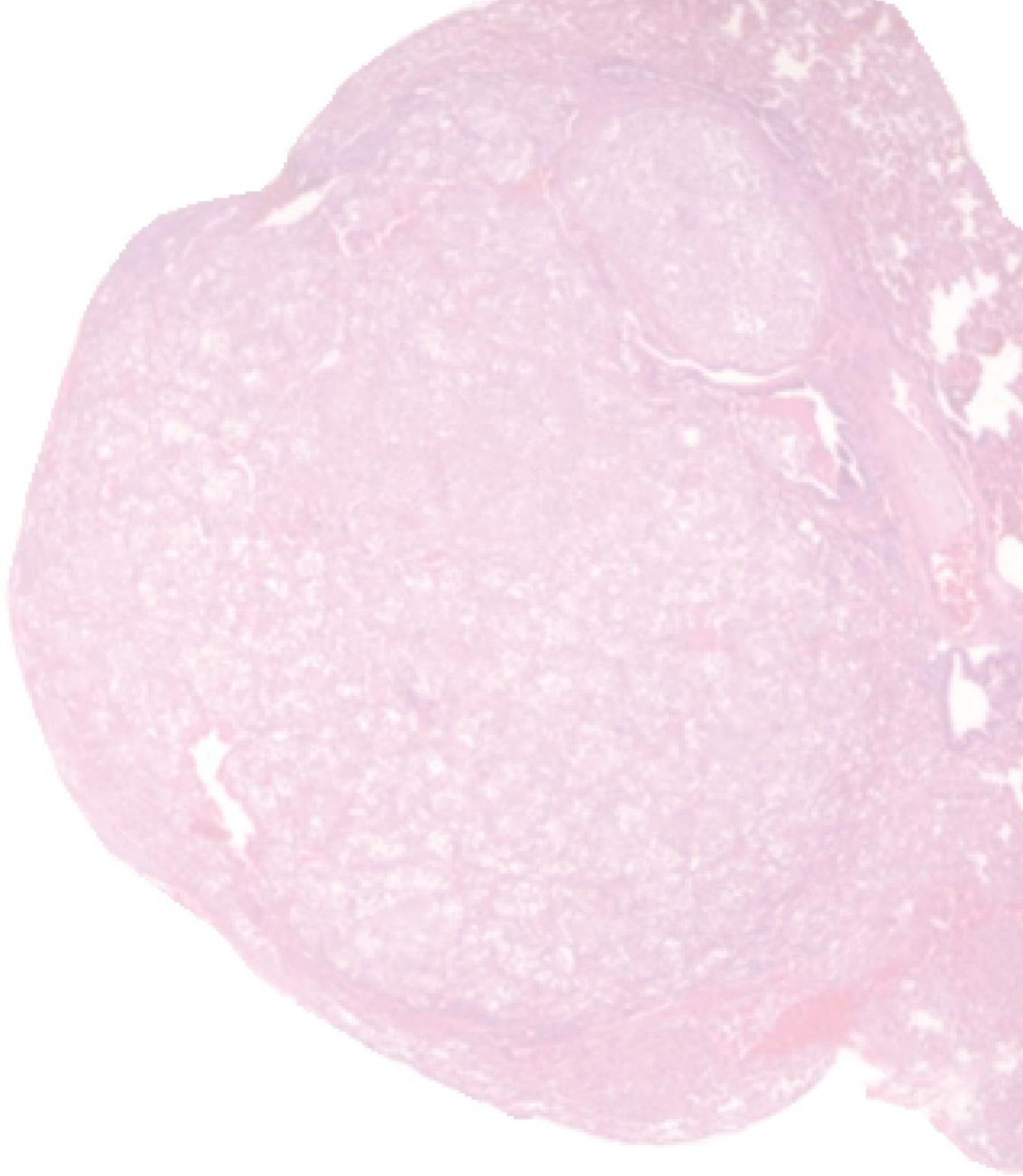


**Figure 23. Results from GSEA showed that Ren 50/50M samples highly correlated with the *Regulation of body fluid levels* signature. “MET” samples correspond to four tumors of Ren 50M and “NOMET” samples corresponded to four tumors of Ren 50, which were analyzed by RNA sequencing. Used data for running GSEA was the fold-change value of gene expression of Ren 50M versus Ren 50. A) *Regulation of blood fluid levels* enrichment plots. In red are represented enriched genes in our samples, which positively correlated with this signature. In blue are represented those genes which expression is negatively correlating. B) Heat map of gene expression from Ren 50 and Ren 50M samples corresponding to the *Regulation of body fluid levels* signature.**

In summary, previous data from our group have demonstrated molecular differences between Ren 50 and Ren 50M tumors. After exome, RNA and FISH analyses, differences in mutations, gene expression profiles and chromosomal rearrangements have been confirmed. Therefore, we hypothesize that these alterations can affect genes and pathways, leading to two clearly different metastatic phenotypes in the two variants of our orthoxenograft model.





## **OBJECTIVES**



The objectives of this thesis are:

1. To find some markers that could be useful as prognostic factors of metastatic potential of these tumors and also to identify therapeutic targets that could allow the inhibition of this process.
2. To validate our candidates both *in vitro* and *in vivo*.
3. Eventually, we want to validate the relevance of our candidates in human samples.

Finding the pathways involved in metastasis, together with the mechanisms involved in invasion and the resistance to current therapies, could enable the establishment of a new field of individual therapies to fight this type of cancer.







# **MATERIALS AND METHODS**



## 1. IN VITRO

### 1.1 CELL CULTURE

#### 1.1.1 Cell line maintenance

All media (Table 4) were supplemented with 10% fetal bovine serum (FBS) (Gibco), which was previously inactivated by heating at 56°C for 30min. Then, 50U/ml of penicillin, 50µg/ml of streptomycin sulfate, 2mM of L-glutamine, 10mM of HEPES, 1% pyruvate and 1% of non-essential aminoacids (all from Gibco, Life technologies) were added to all cell culture media. All cells were maintained at 37°C in humidified conditions with 5% CO<sub>2</sub>.

Medium	Reference	Manufacturer
RPMI Medium 1640	31870-025	Gibco (Thermo Fisher Scientific)
Dulbecco's Modified Eagle Medium (DMEM)	BE12614F	Lanza

**Table 4. Mediums used for cell culture.**

#### 1.1.2 Cell lines

All cell lines used in this thesis have human kidney tissue origin and are outlined in Table 5. pVHL-deficient 786O cell line was kindly provided by B. Jimenez (Instituto de Investigaciones Biomédicas CSIC-UAM, Madrid, Spain). The rest of them were kindly supplied by F. Setién from the cell culture facility of the Programa d'Epigenètica i Biologia del Càncer (PEBC).

Cell line	Disease	Medium
786O-	Renal Cell Adenocarcinoma	RPMI 1640
RCC4-	Clear Cell Carcinoma	RPMI 1640
RCC10-	Renal Cell Carcinoma	RPMI 1640
SN12C	Renal Cell Carcinoma	DMEM
Caki 1	Clear Cell Carcinoma	RPMI 1640
Caki 2	Clear Cell Carcinoma	RPMI 1640 (15% FBS)
ACHN	Renal Cell Adenocarcinoma	DMEM
A498	Renal Cell Carcinoma	DMEM

**Table 5. Cell lines derived from human kidney tissues used.**

### 1.1.3 Mycoplasma test

All cell lines were routinely tested for mycoplasma contamination by PCR using the following oligonucleotides:

Oligonucleotide	Sequence
MICO-1	5'- GGCGAATGGGTGAGTAACACG-3'
MICO-2	5'-CGGATAACGCTTGCGACTATG-3'

**Table 6. Oligonucleotides used for the detection of mycoplasma contamination.**

As a template for the PCR, media from cells which had been in overconfluence and absence of antibiotics for at least 5 days were used. If the result was positive, cells were treated with Plasmocin™ at 25µg/ml for 2 weeks, and then cells were tested again for contamination.

#### 1.1.4 Cell line treatments

Of CPE *in vitro*, its expression was upregulated through cumate (ABM) induction at 30µg/ml (see section 1.2.3.7). In addition, recombinant human CPE (Novoprotein) protein was used at 200nM (Murthy et al., 2013a).

For evaluating F2R inhibition, SN12C cells were treated with 1µM of SCH 79797 (Dihydrochloride) (Axon Medchem). This non-peptide is a selective F2R antagonist based on the natural alkaloid himbacine (Ahn et al., 2000).

#### 1.1.5 Cell counting

To determine cell concentrations, a manual counting method using trypan blue (Sigma) dying exclusion test was performed.

Adherent cells were detached by incubating them with pre-warmed trypsin (Gibco) for 5min at 37°C. Then, trypsin was inactivated by fresh medium supplemented with FBS. Cells were then centrifuged for 5min at 250G and resuspended with fresh full medium.

For cell counting, cells were diluted in trypan blue and viable cells were counted using a Neubauer chamber. Number of cells per ml was calculated according to the following formula:

$$\text{Concentration ( cells/ml )} = \text{Mean viable cells per quadrant} \times \text{Dilution factor} \times 10^4$$

#### 1.1.6 Cell freezing and cryopreservation

After trypsinization and centrifugation processes, cells were resuspended in cold freezing medium (90% FBS plus 10% DMSO (Sigma)) in a ½ or ⅓ dilution of a p100 plate, depending on the cell line.

Cell suspension was distributed in cryotubes at 1ml/tube and placed in a container filled with 2-propanol for its freezing at -80°C minimum for 24h. Then, cryotubes were stored in a liquid nitrogen tank.

For cell thawing, cells were quickly transported into dry ice from the nitrogen tank to a water bath at 37°C. Then, cells were diluted in pre-warmed medium and resuspended in a 15ml Falcon tube. They were centrifuged at 250G for 5min and the pellet was resuspended in fresh medium. Finally, they were plated normally onto a p100 plate to have a high confluence and optimize the recovery.

## **1.2 MOLECULAR ANALYSIS**

### **1.2.1 RNA detection**

#### **1.2.1.1 RNA extraction of cells**

Adherent cells were detached by incubating them with pre-warmed trypsin for 5min at 37°C. Then, trypsin was inactivated by fresh medium supplemented with FBS. Cells were then centrifuged for 5min at 250G and the pellet was washed with PBS (0.15 M NaCl, 0.9 mM Na<sub>2</sub>HPO<sub>4</sub> and 0.1 mM KH<sub>2</sub>PO<sub>4</sub>). They were centrifuged again and the pellet was directly stored at -80°C until the RNA extraction was performed. RNA was extracted using the RNeasy Plus kit (Qiagen) following manufacturer's instructions.

Obtained RNA was quantified in the spectrophotometer NanoDrop TM1000 (Thermo Scientific) and the quality of the RNA was finally validated by loading 500ng in a 1% agarose gel using a 1Kb Plus DNA ladder (Invitrogen) as a molecular weight marker.

In the case of gDNA contamination, an additional DNase treatment was performed, using DNA-free™ DNA removal kit (ThermoFisher Scientific), following manufacturer's instructions.

#### **1.2.1.2 Obtention of cDNA from RNA**

First of all, a 20µl mix composed of 2µg from each sample of RNA and sterile water was placed into a microcentrifuge tube and incubated for 10min at 65°C.

Then, using the High Capacity cDNA Reverse Transcription kit (Applied Biosystems), we prepared the following mix for each sample: 1µl of RNase inhibitor, 3µl of RT Buffer, 3µl

of Random primers, 1.2 µl of ddNTPs, 1µl of Reverse Transcriptase and 0.8µl of sterile water. 10µl of this mix was then added to each pre-warmed sample and the reverse transcription reaction took place with the following conditions: 10min at 65°C, 2h at 37°C, 5min at 85°C and ∞ at 4°C. Obtained cDNA was stored at -20°C until use.

### 1.2.1.3 Real-Time Quantitative PCR

In order to detect RNA expression, Real-Time quantitative PCR (RT-qPCR) analyses were performed using Taqman® Technology (Applied Biosystems). 25ng of cDNA obtained from different cell lines were loaded into each well of the plate mixed with 5µl of TaqMan® Universal PCR Master Mix (Applied Biosystems), 0.5µl of the Taqman® Probe of interest (Table 7) and ddH<sub>2</sub>O to a final volume of 10µl. The 384-well plate was read at the Plataforma de Centres Científics i Tecnològics de la Universitat de Barcelona (CCiT-UB). Results were visualized and analyzed using softwares RQ Manager 1.2.1 and SDS 2.4 (Applied Biosystems).

Gene	Specie	Dye-Label	Reference
CPE	Human	FAM™-MGB	Hs00175676_m1
F13A1	Human	FAM™-MGB	Hs01114178_m1
F2R	Human	FAM™-MGB	Hs0101692588_m1
HPRT1	Human	FAM™-MGB	Hs02800695_m1

**Table 7. Specific probes used in Taqman® analyses.**

The number of cycles obtained for detection of the fluorescent signal (Ct) for each gene was normalized against the same value of *HPRT1*, used as a housekeeping gene. Finally, RNA expression was calculated using the obtained ΔCt following this formula:

$$2^{-\Delta Ct} = 2^{-(Ct_{gene A} - Ct_{housekeeping gene})}$$



## **1.2.2 Protein detection**

### **1.2.2.1 Preparation of protein lysates from cell culture**

Cells were seeded in p100 plates and when they reached 90-100% confluence, they were lysed. After washing cells with PBS, 400µl of RIPA lysis buffer (0.1% SDS, 1% NP-40, 0.5% sodium deoxycholate, 50mM NeF, 5mM EDTA, 40mM β-glycerolphosphate, 200µM sodium orthovanadate, 100µM phenylmethylsulfonyl fluoride, 1µM pepstatin A, 1µg/ml leupeptin, 4µg/ml aprotin in PBS, pH 7.4) were added to the plate and swirled to distribute the buffer. The plate was kept on ice for 5min. After this, cells were scraped using a cell scraper (Sarstedt) and the lysate was transferred into a 1.5ml Eppendorf. It was incubated on ice for 5min and incubated in rotation during 30-40min at 4°C. Finally, the lysate was centrifuged at 14000rpm for 15min at 4°C and supernatants were stored at -20°C in order to titer them.

### **1.2.2.2 Quantification of protein extracts**

For protein quantification, the colorimetric Pierce™ BCA Protein Assay Kit (Thermo Scientific) was used.

First of all, a set of diluted standards ranging from 0 to 2mg/ml of Bovine Serum Albumin (BSA) were prepared in order to perform a standard curve. In addition, samples of interest were prediluted at 1:10.

Then, in order to do the quantification, a 96-well plate was used. First, 200µl of BCA Working Reagent (50:1, Reagent A:B) were loaded onto the wells. Then, 10µl of the known diluted concentrations of BSA or prediluted samples were added and mixed carefully without making bubbles. The plate was incubated at 37°C for 20-30mins and then absorbance was measured at 560nm wavelength by spectrophotometry (Power Wave XS, BIO-TEK) using the KCJr Win Software. Finally, protein concentration was calculated by extrapolation in the BSA standard curve.

Once quantified, each lysate was boiled in loading buffer (Laemmli buffer: 300mM Tris-HCl pH 6.8, 600mM DTT, 12% SDS, 0,6% bromophenol blue, 60% glycerol) at a final concentration of 1:4 for 5min at 95°C in order to reduce and denature the samples. They were stored at -20°C until use.

### **1.2.2.3 Conditioned media generation and trichloroacetic acid protein precipitation**

In order to obtain conditioned media from different 786O- CYMR cell lines, cells were seeded in p100 plates and left to grow. They were treated with or without cumate at 30µg/µl for 48h and then media was replaced with 7ml fresh medium maintaining the same conditions but with 2% FBS. 24h later, when cells had reached a confluence of 90-95% and they were at the time point at which they overexpressed CPE at highest levels, media was collected and filtered with a syringe filter with a PES membrane of 0.22µm (TRP). Then, it was centrifuged at 250G for 5min and filtered again. Finally, it was stored at -20°C until use.

In order to precipitate proteins present in these supernatants, a TCA protein precipitation protocol was followed.

1 volume of trichloroacetic acid (TCA) (Merck) was added to 4 volumes of protein sample. This was incubated for 10min at 4°C and then the tube was spun in a microcentrifuge for 5min at 14000rpm. The supernatant was removed and the pellet was washed with 200µl of cold acetone and spun again. These last two steps were repeated twice. The pellet was dried by placing the tube in a 95°C heat block for 5-10min to drive off the acetone. Finally, loading buffer to a final concentration 1:4 was added and the mix was boiled for 10min at 95°C.

### **1.2.2.4 Protein analysis by western blotting**

To further validate protein expression values, western blotting from cell samples was performed.

Sodium dodecyl sulphate-polyacrylamide gels (SDS-PAGE) for protein separation were prepared using 1.5mm glass plates (Bio-Rad). They consist of a mix of H<sub>2</sub>O, acrylamide-bisacrylamide, Tris-HCl 1.5M pH 6.8 or 8.8, APS and TEMED. Gels were composed of two parts: the stacking and the resolving gel. The percentage of acrylamide in the former was ranged from 7.5 to 12% and was determined depending on the molecular weight of the proteins of interest. 30µg of protein were loaded into the wells of SDS-PAGE gel along with a molecular weight marker (Page Ruler™ prestained, Thermo Scientific).

The gels with loaded proteins were submerged into the running buffer (25mM Tris, 192mM glycine, 0.1% SDS) and migration was carried out at a constant voltage of 120V. Then, acrylamide gels were transferred to a nitrocellulose membrane (Immobilon-P, Merck Millipore) at 100V for 120min. Membranes were then blocked to prevent unspecific binding of the antibody to the membrane with 5% skimmed milk (Nestle®) in TBS (Tris 50mM, NaCl 150mM) for 1h at room temperature (RT) in agitation. After blocking, membranes were incubated with appropriate dilutions of primary antibodies (Table 8) in TBS 1% skimmed milk overnight (O/N) at 4°C.

After washing in TBS- 0.1% Tween 20 (TTBS) thrice and once in TBS for 10 min each, blots were incubated with 1:5000 anti-rabbit IgG, 1:5000 anti-mouse IgG (GE Healthcare) or 1:2500 anti-mouse IgG light chain (Sigma-Aldrich) horseradish peroxidase (HRP) linked antibodies in 1% skimmed milk in TBS for 1 hour at RT.

Finally, after washing thrice with TTBS and once with TBS (10min each), blots were developed with Amersham ECL Select™ Western blotting detection reagent (GE Healthcare Life Sciences) according to manufacturer's instructions. Signals on blots were detected with ChemiDoc Touch (Bio-Rad) and quantified with Image Lab software (Bio-Rad).

Antibody	Antigen	Specie	Dilution	Manufacturer
HPA003819	CPE	Rabbit	1/250	Sigma-Aldrich
BD61059	CPE	Mouse	1/1000	BD Biosciences
17090002	F2R	Rabbit	1/500	Novus Biologicals
PA5-22110	FXIIA	Rabbit	1/1000	Thermo Fisher Scientific
180052 Clone V9	Vimentin	Mouse	1/200	Invitrogen
V9131, Clone hVIN-1	Vinculin	Mouse	1/2000	Sigma-Aldrich
T6074, Clone B-5-1-2	Tubulin	Mouse	1/2500	Sigma-Aldrich

**Table 8. Primary antibodies used for the Western blot detections.**

### 1.2.2.5 Protein detection by immunocytofluorescence

Aiming to detect protein levels through immunocytofluorescence assays, cells were seeded on glass coverslips previously deposited into 24-well plates with sterile tweezers after 2h UV of plate sterilization. When cells reached 80% confluence, they were washed with PBS and then fixed for 5min with 4% paraformaldehyde (PFA). The fixation process maintains cells in their current state and preserves the preparation by chemical reagents over an extended period.

After fixation, cells were washed thrice with PBS and then permeabilized for 15min with PBS-0.1% Triton (TPBS). As a result, intracellular structures become accessible for antibodies which are unable to pass through the lipid cell membranes if we need to detect intracellular antigens.

Afterwards, blocking was performed in order to avoid unspecific binding of the primary antibody to the cells. Normal Goat Serum diluted 1:5 in PBS for 30min at RT was used to carry out this process.

Then, cells were incubated with primary antibodies (Table 9) for 1h at RT diluted with blocking solution. After incubation, they were washed thrice with TPBS followed by a

second incubation with Alexa Fluor Secondary antibodies diluted 1/200 also with blocking solution for 1h at RT. All incubations were performed in a humidity chamber.

Coverslips were then washed thrice with TPBS and finally incubated for 10min at RT with DAPI in order to perform nuclear staining. Eventually, they were mounted on slides using Fluoromount™ Aqueous Mounting Medium (Sigma) to be suitable for microscopy. Cells were visualized using the Nikon Eclipse 80i microscope and images were taken with a Nikon DS-Ri1 digital camera using NIS-Elements BR 3.2 (64-bit) Software. Finally, they were analyzed using Image J Software.

Antibody	Antigen	Specie	Dilution	Manufacturer
BD61059	CPE	Mouse	1/100	BD Biosciences
Sc-13503	F2R	Mouse	1/200	Santa Cruz Biotechnology
PA5-22110	FXIIa	Rabbit	1/750	Thermo Fisher Scientific

**Table 9.** Primary antibodies used for protein detection by immunocytofluorescence.

### 1.2.3 Cell transfections and infections

#### 1.2.3.1 Handling of bacteria

In order to obtain sufficient amounts of plasmid DNA, its amplification in bacteria was required. For this reason, the plasmid of use should have a replication origin that allows its replication on the desired strain and a gene that confers resistance to an antibiotic in order to select the bacteria and avoid contaminations. In this work, One Shot® TOP10 Chemically Competent E. coli (Invitrogen) were used.

#### 1.2.3.2 Bacterial transformation using heat shock and competent cells

After 10min incubation in ice, a mixture of 500pg of chemically competent bacteria and 50ng of DNA were mixed and softly shaken at 42°C for 45s, a process known as heat shock. Afterwards, it was placed back in ice for 2min. Then, 450µl of SOC (Invitrogen) medium was added and transformed cells were incubated at 37°C for 1h in agitation at

200rpm. Finally, two different dilutions of transformed bacteria were plated in LB-antibiotic dishes and incubated O/N at 37°C.

### **1.2.3.3 Obtaining plasmidic DNA from bacterial cultures**

In this work, plasmidic DNA was obtained from saturated *E.Coli* cultures which grew in LB with antibiotic. DNA was prepared at large scale.

First of all, a colony grown in a LB-antibiotic dish was inoculated in 3ml of LB-antibiotic and incubated for 6-8h at 37°C in agitation (200-220rpm). Once this preculture was grown, 100µl of it were added to an Erlenmeyer with 100ml of LB-antibiotic and incubated O/N at 37°C in agitation at 200-250rpm.

### **1.2.3.4 Large scale DNA preparations**

DNA maxipreparations allow obtaining large amounts of highly pure plasmidic DNA from bacteria. Endotoxin-free maxipreps were prepared from 100ml of saturated bacteria culture using the Qiagen commercial EndoFree Plasmid Maxi Kit (Qiagen), following manufacturer's instructions. Obtained DNA concentration was measured by NanoDrop TM1000 (Thermo Scientific).

### **1.2.3.5 Characterization of the plasmid genome by DNA digestion with restriction enzymes**

In order to validate the resulting plasmid genomes, DNA digestions with restriction enzymes were performed.

As starting material for the digestion reactions, 300ng of DNA were used. To this amount of DNA, 1 unit of the enzyme, the appropriate buffer to each one (provided by the manufacturer at 10X), and ddH<sub>2</sub>O up to the desired final volume were added. The mixture was incubated for 2h in a water-bath at 37°C and then samples were resolved in a 1% agarose electrophoresis gel prepared in Tris-Acetate-EDTA (TAE) buffer, together with a 1Kb Plus DNA ladder (Invitrogen) as a molecular weight marker. Restriction

enzymes used in this work in order to assess correct plasmid genomes are outlined in Table 10.

Enzyme	Reference	Manufacturer
MluI (Buffer R)	ER0561	Thermo Fisher Scientific
KpnI (Buffer L)	1068AH	Takara Bio Inc (Clontech)
EcoRI (Buffer H)	11175084001	Roche
EcoRV (Buffer R)	ER0301	Fermentas (Thermo Fisher Scientific)
ApaI (Buffer B)	ER1411	Fermentas (Thermo Fisher Scientific)
XbaI (Buffer Tango)	ER0681	Fermentas (Thermo Fisher Scientific)

**Table 10. Restriction enzymes used to confirm correct plasmid genomes.**

### 1.2.3.6 Lipofectamine DNA Transfection

In order to transfect pCMV3 vectors (Table 11) to 786O- cells, a Lipofectamine® protocol was followed.

pCMV3 plasmids	Manufacturer	Reference
F13a	Sino Biological Inc.	HG11767-UT
CPE	Sino Biological Inc.	HG10069-UT
Empty Vector	Sino Biological Inc.	CV011

**Table 11. pCMV3 vectors used to transfect 768O- cell line.**

Cells of interest were previously seeded in order to be 70-90% confluent at the time of transfection. First of all, medium was replaced by 2ml of reduced serum Opti-MEM™ Medium (Gibco).

Then, two different solutions were prepared. First of all, Lipofectamine® (Invitrogen) was diluted in Opti-MEM™ medium at a 15:1 ratio 15:1. Then, 2.5µg of DNA (previously prepared at 1µg/µl) were also diluted in Opti-MEM™ medium. PLUS™ Reagent

(Invitrogen) was also added in order to increase transfection efficacy. The amount of both solutions was calculated to obtain a final volume of 320 $\mu$ l/well (160 $\mu$ l each). Finally, they were mixed at a 1:1 ratio and incubated 5 minutes at RT. 320 $\mu$ l of the final solution were added to each well of a 6-well plate at the time of transfection and plates were incubated O/N at 37 $^{\circ}$ C.

On the following day, medium was replaced with full 10% FBS medium. 24h later, cells were trypsinized and plated with full medium plus the antibiotic to which transfected cells should be resistant. Cells were maintained with antibiotic until resistant cells were selected. Non-transfected cells were also treated in parallel with antibiotic as reference. Survival curves with different antibiotic doses were previously tested in order to determine the optimal concentration for obtaining resistant cells.

### 1.2.3.7 Cumate system

In search of obtaining CPE-expressing cells through lentiviral infections, the cumate system was used. In this model and in normal conditions, cells express the CYMR gene. The resulting CYMR protein is able to bind the CMV-Cuo promoter and block *CPE* gene expression. When adding the small molecule cumate (ABM) to the medium, CYMR protein is arrested, leading to an activation of *CPE* gene expression (Figure 24).

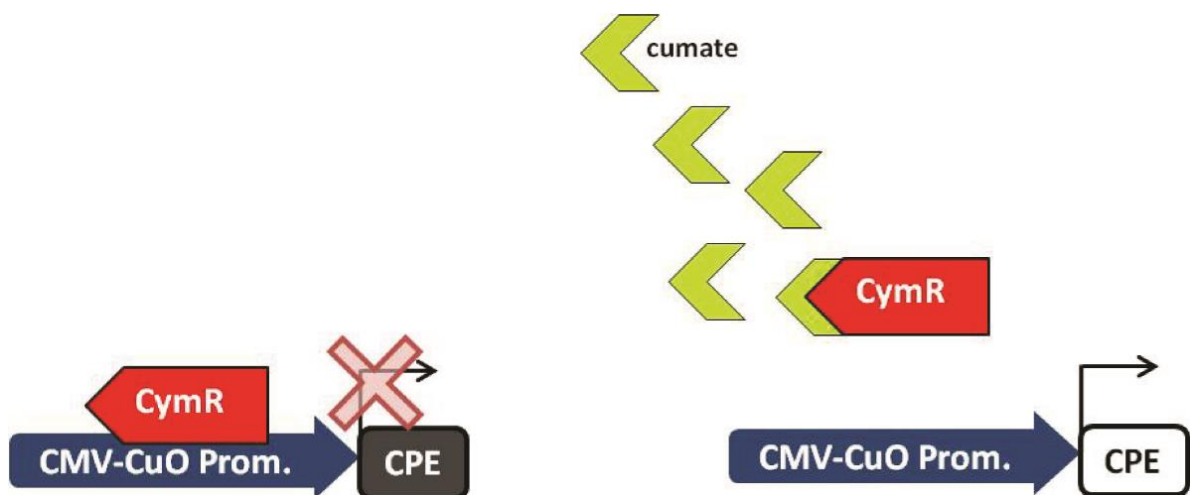


**Figure 24. Schematic representation of cumate system.** *CPE* gene is located under a CMV-CuO promoter which can be regulated by a CYMR repressor. When adding cumate into the medium, it binds the repressor, leading to an activation of *CPE* gene transcription.



### 1.2.3.7.1 Lentiviral production using polyethylenimine-mediated transfection

Lentiviruses in this work were generated by using the HEK293FT cell line. For transfection, cells were seeded at a confluence of 60-80% in a p100, previously coated with poly-L-Lysine (Sigma-Aldrich), and were transfected with the lentiviral plasmids outlined in Table 12 and shown in Figure 25.

Lentiviral vector	Manufacturer	Reference
CYMR	ABM	iCu999
CPE	ABM	iCU2028175
Blank	ABM	iCu008

Table 12. Lentiviral plasmids used to generate lentiviruses.

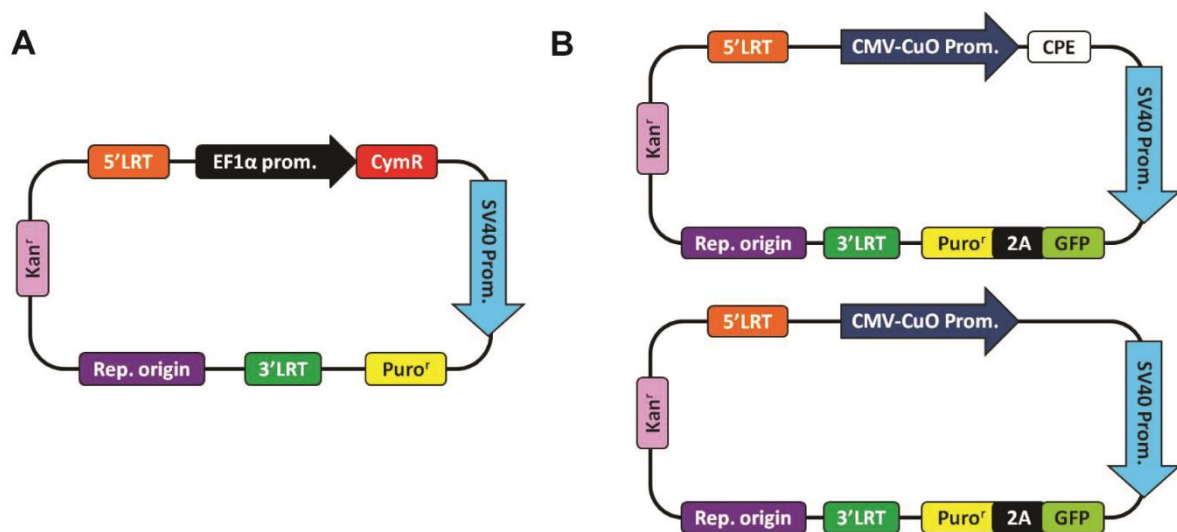


Figure 25. Schematic representation of lentiviral vectors. A) Schematic representation of the CYMR lentivirus plasmid. B) From top to bottom, schematic representations of CPE and Blank lentiviral vectors.

For each plasmid to be transfected, the following mixture was prepared in a 1.5ml tube: 25µg of plasmid DNA, 18.75µg pPAX2 vector, 6.25µg pMD2-G, 100µl polyethylenimine (PEI) (Polysciences) and Opti-MEM™ Medium to a final volume of 1ml.

First of all, DNA vectors and Opti-MEM™ medium were mixed and left at RT for 5min. Then, PEI was added and the mixture was vortexed for 15s, and then incubated for 15min

at RT. Finally, the mixture was added dropwise to the plates (1ml to the p100 plates and 100µl to each well of the 6-well plates) while shaking the plate softly to allow a homogenous distribution.

On the following day, cells were harvested and medium was replaced with 2% FBS medium and incubated O/N at 37°C. The day after that, supernatants were collected and centrifuged at 2500rpm for 10min at 4°C in order to collect any packaging cells. Then, they were filtered through a 0.45µm PES filter (TRP). Supernatants were then mixed 1:1 with full medium to a final concentration of 10% FBS and 4µg/ml of Polybrene® (Sigma-Aldrich).

#### **1.2.3.7.2 Lentiviral infections**

In the process of generating our cumate system, 786O- cells were firstly infected with CYMR viruses, hence obtaining cells that expressed CYMR gene in a constitutive fashion.

We then split the cells into two groups. One of them was reinfected with a lentivirus containing the *CPE* gene under the control of a CMV-Cuo promoter (Figure 25B top). The second group was reinfected with a second lentivirus which had exactly the same sequence but lacked the *CPE* gene sequence (Figure 25B bottom). Through this double infection, we expected to obtain two CYMR cell lines, with and without the *CPE* gene.

Previously, 786O- cells had been seeded to reach 70-75% confluence at the time of reinfection. Medium in these cell cultures was then replaced by the previous mixture in order to infect cells with lentiviruses. The incubation was performed O/N at 37°C.

Next morning, medium was replaced by 10% FBS full medium. 24h after the infection, puromycin was added in order to select effectively infected cells. Non-infected cells were always cultured in parallel and treated identically, as controls for antibiotic efficiency.

For the second selection, a new strategy was needed due to the already acquired puromycin resistance.

### **1.2.3.8 Cell Sorting**

In order to sort infected cells, they were trypsinized and the pellet was resuspended in PBS 2% FBS. Then, we passed both 100  $\mu$ l of PBS 2% FBS and cells through a 0.7 $\mu$ m PES filter (TRP). Finally, 100  $\mu$ l of extra PBS 2% FBS were passed through the filter again. We counted the cells in order to have less than  $6 \times 10^6$  cells/ml, which is approximately the maximum cell concentration that can be successfully sorted.

Infected cells with lentiviral vectors encoding GFP were sorted at the Plataforma de Centres Científics i Tecnològics at the Universitat de Barcelona (CCiT-UB). Cells were selected on the basis of their GFP fluorescence. On one hand, untransfected 786O- CYMR cell line was used as a negative control. On the other hand, both 786O- CYMR CPE and Blank were sorted by their GFP expression.

## **1.3 IN VITRO ASSAYS**

### **1.3.1 Migration assays**

#### **1.3.1.1 Wound healing assay**

For wound healing migration assays, cells were seeded in 6 well plates in order to be 90-95% confluent at the starting point. Number of cells and containing factors in the media were determined for each experiment depending on which parameters were to be evaluated. Therefore, monolayers were scratched with a 200 $\mu$ l tip to imitate a wound. After several steps involving washing and removal of floating cells, pictures of the distances between cell margins were taken at 0, 3, 6, 9 12 and 24 hours. Different pictures for each sample were taken from the same points of the scratch using an invert microscope (Leica DMI1). The percentage of opened area was then analyzed using Image J Software.

As a more precise technique, we also performed wound healing assays using 2-well culture inserts (Ibdi®) with a cell-free gap in the middle. Inserts were stacked into wells of 12-well plates and cells were plated inside both compartments in a final volume of

70 $\mu$ l. 500 $\mu$ l additional medium was added surrounding the insert. When cells reached confluence, inserts were removed with sterile tweezers and cells from both wells were separated by an empty line. Pictures and quantifications were performed as in the scratch assays.

### **1.3.1.2 Transwell migration assay**

In order to assess directional migration, transwell migration assays were performed. Cells were placed in 6.5mm inserts with an 8 $\mu$ m polycarbonate membrane of the Costar Transwell® Permeable Supports (Corning). The number of cells and the containing factors of both media were determined for each experiment depending on which parameters were to be evaluated. The chamber was incubated 24h at 37°C in a humidified atmosphere with 5% CO<sub>2</sub>. First of all, the membrane was wiped with a cotton swab to remove non-migrated cells on the upper part of the chamber and was fixed for 2 minutes with methanol. Then, it was washed with PBS and stained with hematoxylin (0.1% Hematoxylin, Merck Millipore, in ethanol 96%) for 90s. Finally, it was removed from the insert using a blade and mounted with sterile water on a slide.

Pictures of 11 representative fields of all the membrane were visualized using the Nikon Eclipse 80i microscope and images were taken at 20X magnification with a Nikon DS-Ri1 digital camera using NIS-Elements BR 3.2 (64-bit) Software. Finally, they were analyzed with Image J Software.

All control and experimental groups were performed in parallel in duplicates or triplicates. Migrated stained cells were manually counted using Image J Software and are represented as the total number of migrated cells/field for each condition.

### **1.3.2 Invasion assays**

To assess the invasive capability of cells, transwell Matrigel® invasion assays were performed. Cells were placed inside the inserts of the Corning® BioCoat™ Matrigel® Invasion Chamber with an 8 $\mu$ m polycarbonate membrane. The plate was incubated for

48h at 37°C in humidified conditions with 5% CO<sub>2</sub>. The rest of the protocol and the taking of images were performed exactly as in transwell migration assays.

Invaded stained cells were manually counted using Image J Software and represented as the total number of invaded cells/field for each condition.

## **2. IN VIVO**

### **2.1 ANIMALS AND CONDITIONS**

All animal studies were performed at the IDIBELL Animal Core Facility (AAALAC unit 1155) and approved by the Ethics Committee for Animal Experimentation from the Biomedical Research Institute of Bellvitge (IDIBELL) and the Generalitat de Catalunya. They were performed following the European directives on ethical usage of rodents for animal research (approval DARP #4899).

All mice used in this work were male athymic nude mice (Harlan Laboratories) and were maintained in individually ventilated cages on constant temperature (20-25°C) in SPF (Specific Pathogen Free) conditions and sterility. Animals were under an artificial circadian 12h light/dark cycle and received *ad libitum* standard diet and water. All experiments were performed inside a vertical laminar flow cabinet.

### **2.2 PATIENT-DERIVED ORTHOXENOGRAFT MOUSE MODEL FROM A RCC HUMAN BIOPSY**

In order to obtain our orthoxenograft mouse model, a small fresh piece of tissue from a biopsy of a patient who had ccRCC (chronologically named Ren 50) was obtained from the Bellvitge Hospital under local ethics committee's approved protocols (CEIC approvals ref. PR322/11).

The piece of tumor was orthotopically implanted into the right kidney of an athymic mouse and perpetuated throughout several passages. Normally, mice were sacrificed when their survival was compromised.

## **2.3 CELL LINES MOUSE MODELS**

Apart from orthoxenograft mouse models, *in vivo* experimental models using cell lines were performed.

### **2.3.1 Kidney tumors**

In order to establish both SN12C and 786O- human cancer cells as kidney tumors in athymic mice,  $10^6$  cells were directly injected into the right kidney of the animals using a 0.5ml needle (BD Micro-Fine). Once injected, tumor cells grew in the kidney, generating a palpable tumor in approximately 20-30 days. Then, tumors were perpetuated into successive passages and sacrificed as it was performed with the orthoxenograft model to obtain an experimental cohort.

### **2.3.2 Intravenous – Tail vein injection**

In order to determine if our genes of interest were involved in the last steps of the metastatic process, human cell lines were injected via tail vein.  $10^6$  cells were resuspended in 100  $\mu$ l of medium w/o FBS and other supplementary factors and were injected using a 1ml needle (Novico Medica) into the mice tail vein. Animals were sacrificed when symptoms of metastasis could be detected.

## **2.4 TUMOR AND ORGAN COLLECTION**

Tumors in the kidney and other organs were obtained from sacrificed animals and washed with sterile water. On the one hand, tumors in the kidney were split into different pieces. One piece was fixed in formaldehyde 4% O/N to be included in a cassette for paraffin embedding. The opposite part was included in OCT (Tissue-TEK® Sakura) for further analyses of frozen tissue. Finally, some peripheral tumor pieces, together with some pieces from cortex and medulla of the contralateral kidney, were directly frozen in cryotubes and maintained at -80°C in order to extract RNA or protein. In the end, lungs were divided into their five lobes and together with the spleen, the liver, half of the contralateral kidney and sometimes brain and diaphragm, were also fixed in formaldehyde 4% to be included in paraffin.

## **2.5 PARAFFIN INCLUSION**

Tissue fixation in formaldehyde 4% O/N was performed by rinsing them in tap water in order to eliminate the fixative agent. After that, tissue samples underwent a dehydration process through a battery of alcohols of crescent graduation (1h in ethanol 70%, 2 96% ethanol rounds of 1h and a new 96% ethanol O/N, 3 absolute ethanol rounds of 1.5h each) and finally submerged into xylene for 1.5h. Eventually, tissue samples were submerged into liquid paraffin at 65°C O/N. Next day, they were embedded in paraffin inside a block sharp ready to be cut and dried at RT.

## **2.6 DETERMINATION OF TUMOR BURDEN**

At the time of sacrifice and during organ extraction, tumor size (mm<sup>2</sup>) was measured using a caliper. Tumor weight (g) was calculated by a scale and tumor volume (mm<sup>3</sup>) was measured calculating the volume of PBS displaced inside a falcon, respectively.

## **2.7 INVASION STUDIES**

Paraffin-embedded samples were stained with hematoxylin and eosin (H&E) and used for the invasion quantification because only formaldehyde-fixed and paraffin-embedded tissues preserve their morphology and allow studying the architecture of the tissue.

Paraffin-embedded blocks were cut into 3-5µm thick sections using a microtome and deposited into poly-L-lysine pretreated slides. Sections were deparaffinized by subjecting them to a battery of 4 xylenes (10min each), 3 absolute ethanols, 3 96% ethanols, 1 70% ethanols, and 1 50% ethanol (5min each). Finally, sections were rehydrated by submerging them in dH<sub>2</sub>O.

Then, they were stained with H&E. Slides were submerged for 10min in hematoxylin and rinsed in tap water to eliminate the excess liquid. Afterwards, in some cases, they were submerged in HCl 1% until the tissue color shifted to red and then in ammonia water solution (200ml of dH<sub>2</sub>O with 1ml of ammonia 30%) until it turned back into blue. Sections were finally counterstained in eosin (2.5 g of eosin in 1L of ethanol 50%) for 10min.

Finally, slides were covered with coverslips and mounted using DPX (Merck). Tissues were visualized using the Nikon Eclipse 80i microscope and images were taken with a Nikon DS-Ri1 digital camera using NIS-Elements BR 3.2 (64-bit) Software. They were analyzed with Image J Software.

Apart from H&E stainings, vimentin immunohistochemistry assays (following the protocol depicted in the 2.10.2.3 section of this chapter) of tumors were also performed to analyze invasion. Pictures were taken using the Fluo Stereo Leica Macrofluor Lupa (0.57X magnification) and invasion was quantified using the Image J Software.

## **2.8 METASTASIS DETERMINATION**

The presence of metastases in the lungs and also in the liver or diaphragm, as other parts of the mice, was determined at the moment of sacrifice and was annotated as macrometastases.

Furthermore, aiming to detect micrometastases, H&E staining of slides from paraffin-included organ blocks were analyzed. Aiming to perform a further analysis of lungs and livers, 50µm deeper sections were also analyzed.

First of all, the incidence of metastasis was determined by scoring for presence or absence in each animal and counting the number of lesions, classifying them into single-lesions or multi-lesions. Also, the number of affected lobes were taken into account. In addition, all metastasis area density was calculated and normalized by total lung area using Image J software and expressed as a percentage. Finally, in order to corroborate the presence of tumor cells in other secondary organs, immunohistochemistry of vimentin was performed.

## **2.9 VORAPAXAR TREATMENT**

The administration of Vorapaxar (SCH 530348) (BOC Sciences) in order to inhibit F2R *in vivo* was started when tumor volume determined by palpation reached 1000mm<sup>3</sup>.



First, mice were randomized into two groups. Control group was treated with vehicle solution, composed of 0.9% Benzyl alcohol (Merck Millipore) diluted in NaCl 0.9% (Braun). The rest of the animals were treated with a Vorapaxar dose of 20mg/kg/day diluted in the vehicle solution used in controls.

Vorapaxar is a synthetic tricyclic 3-phenylpyridine which orthosterically inhibits F2R (Figure 26). As the *in vitro* inhibitor SCH 79797, it is based on the natural alkaloid himbacine. This drug has been demonstrated to be well absorbed in rats at a dosage of 10mg/kg/day and in monkeys at 1mg/kg/day. In addition, it has been approved by FDA for a human administration of 2.5mg/day (Chackalamannil et al., 2008; Flaumenhaft and De Ceunynck, 2017).

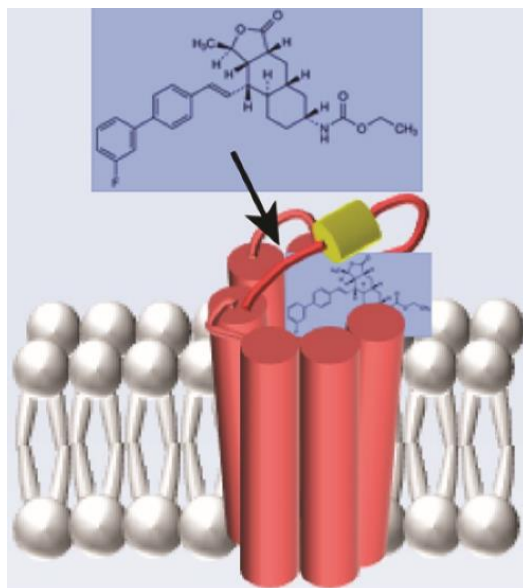


**Figure 26. Mechanism of action of Vorapaxar.** Vorapaxar is a competitive inhibitor that binds almost irreversibly to the extracellular ligand-binding pocket surface of F2R. Image has been adapted from (Flaumenhaft and De Ceunynck, 2017).

After taking into account the above-mentioned doses and applying a conversion of different animal models using the following formula (Km values based on data from FDA Draft Guidelines), we decided to use a dose of 20mg/kg/day in the mouse.

$$\text{Mouse dose (mg/kg)} = \text{Rat dose (mg/kg)} * (\text{rat Km/mouse Km}) = 10\text{mg/kg/day} * (6/3) = 20\text{mg/kg/day}$$

Both groups were treated orally on a daily basis and tumor growth was followed by palpation twice a week. Animals were finally sacrificed 17-19 days after treatment and tumor and organs were collected, processed and analyzed, as mentioned in aforementioned sections.

For the intravenous experiment, seven mice were selected as controls and were treated with vehicle. In parallel, seven mice were treated orally with 20mg/kg/day Vorapaxar for one month. Drug preparation and doses were the same as described previously. The treatment was started one day after injection and, at endpoint, mice were sacrificed and samples were collected and analyzed.

## **2.10 MOLECULAR ANALYSIS**

### **2.10.1 RNA detection**

#### **2.10.1.1 RNA extraction of tumor samples and cDNA obtention**

RNA was extracted from tumor samples stored at -80°C at the time of sacrifice.

Pieces were manually homogenized with RLT buffer from the RNeasy Plus kit (Qiagen) inside a glass homogenizer on ice. RNA extraction, quantification and cDNA obtention were performed using the same procedure detailed for cells (1.2.1.1 and 1.2.1.2).

#### **2.10.1.2 Real-Time Quantitative PCR**

In order to analyze RNA content in tumors, RT-qPCR using Taqman® System was also performed, using the aforementioned protocol and the quantification procedure described in section 1.2.1.3.

## 2.10.2 Protein detection

### 2.10.2.1 Tissue protein extraction and quantification

Protein extraction from tumor samples was performed from fresh or frozen tumor pieces stored at -80°C. Small pieces were mechanically disrupted using RIPA lysis buffer and a glass homogenizer on ice. The composition of RIPA buffer and the protocol used was the aforementioned one in cells in the section 1.2.2.1.

In order to quantify lysates from tumor pieces, the colorimetric Pierce™ BCA Protein Assay Kit (Thermo Scientific) depicted in section 1.2.2.2 was also used.

### 2.10.2.2 Protein analysis by western blotting

In order to analyze protein levels in tissues or tumors, western blots from the samples of interest were also performed. Antibodies and concentrations used for protein detection by western blotting were the ones previously described in *in vitro* protocols (1.1.2.2.4).

### 2.10.2.3 Immunohistochemistry in paraffinized sections

Paraffin-embedded blocks were cut and sections were deparaffinized following the protocol depicted in the 2.7 section of this chapter.

Afterwards, antigens masked during routine fixation were retrieved by submerging the slides in sodium citrate solution (0.38mg/ml) at pH 6.0 and heating for 15min. Then, samples were cooled down inside the citrate solution for 20-30min and washed with dH<sub>2</sub>O for 5min.

The endogenous peroxidase activity was blocked through a double incubation with 6% H<sub>2</sub>O<sub>2</sub> for 10min. Then, slides were washed with dH<sub>2</sub>O for 5min and cell membranes were permeabilized through immersion in TPBS thrice for 5min.

Next step was the blocking of the sections in order to reduce unspecific binding with Normal Goat Serum diluted 1:5 in PBS for 1h at RT, followed by incubation O/N at 4°C

with primary antibodies (Table 13). All incubations were performed in a humidity chamber.

On the following day, slides were tempered at RT for 20-30min and then washed thrice with TPBS for 5min. Then, they were incubated with secondary antibodies anti-mouse or anti-rabbit Envision<sup>+</sup>-System-HRP (Dako) and incubated 1h at RT in the humidity chamber.

After that, sections were washed thrice with TPBS for 5min. Then, they were developed by covering them with the chromogenic substrate DAB+ (EnVision™ Kit, Dako), from 30s to 10min, depending on the antibody and the samples used, until a brown precipitate appeared. The reaction was stopped by rinsing the slides with tap water for 10min.

Finally, sections were counterstained with hematoxylin, dehydrated, mounted and analyzed as depicted in section 2.7.

Antibody	Antigen	Specie	Dilution	Manufacturer
Ab28364	CD31	Rabbit	1/50	Abcam
HPA003819	CPE	Rabbit	1/50	Sigma-Aldrich
Sc-13503	F2R	Mouse	1/200	Santa Cruz Biothecnology
PA5-22110	FXIIa	Rabbit	1/750	Thermo Fisher Scientific
180052 Clone V9	Vimentin	Mouse	1/400	Invitrogen

**Table 13. Primary antibodies used for protein detection by immunohistochemistry**

### 3. CLINICAL VALIDATION: IN SILICO ANALYSES

Data from clinics were extracted from The Cancer Genome Atlas (TCGA) and analyses were performed in collaboration with Carlota Rubio-Pérez, from Núria López-Bigas laboratory at the Institut de Recerca Biomèdica (IRB), and Luis Palomero, from ProCURE (ICO-IDIBELL), both in Barcelona.

TCGA consists of a multidimensional genomics data generated through transcriptome profiling, exome sequencing, copy number alteration profiling and DNA methylation analysis, among other techniques. It compiles data from 33 cancer types and 11 thousand patient tumor samples (TCGA research network, 2018).

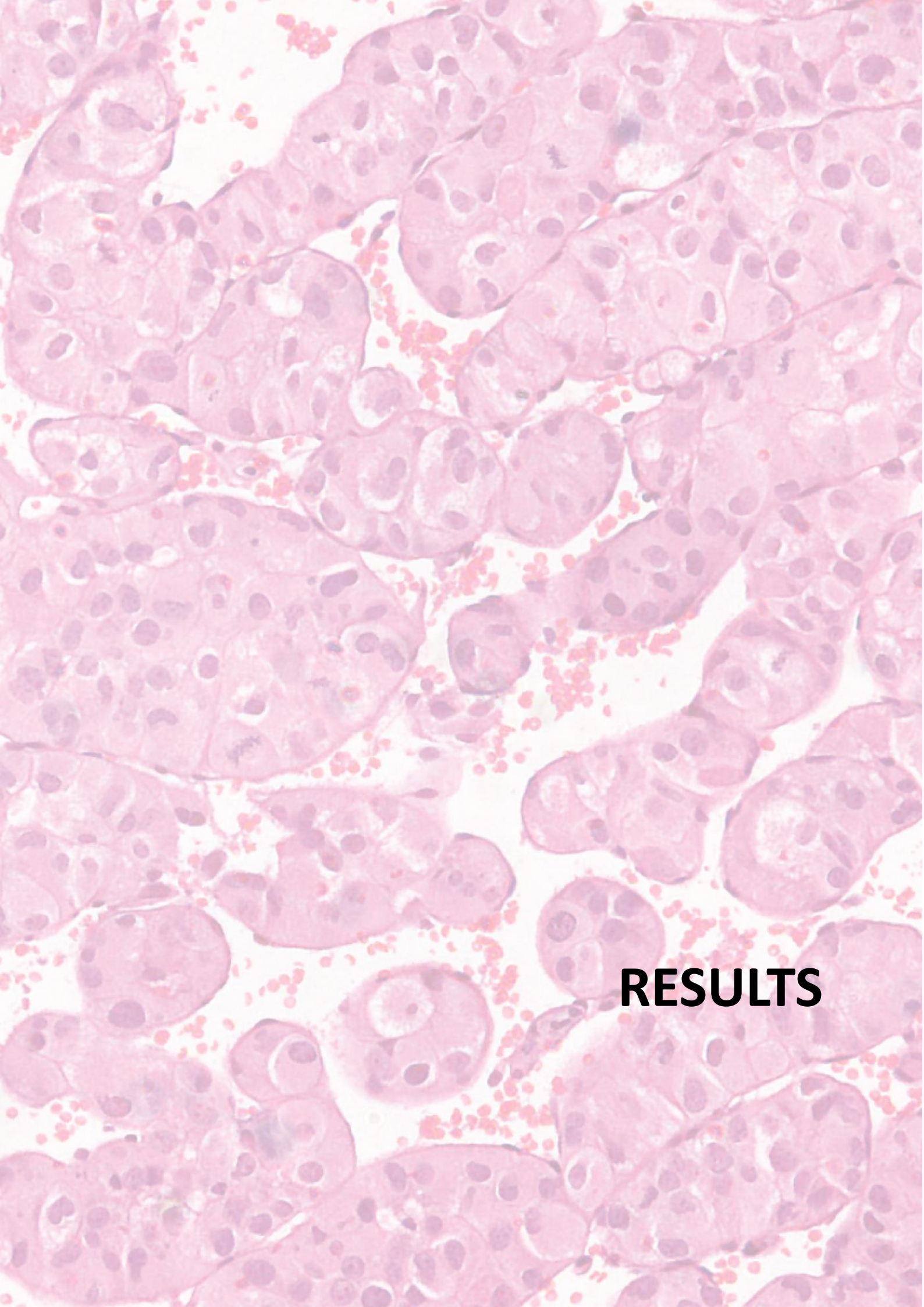
We analyzed TCGA RNA expression of our candidate genes across the main histological subtypes of RCC (TCGA, 2013). Then, we also validated their expression across all 33 TCGA cancer types and investigated whether their overexpression was influencing survival in RCC patients. Finally, we analyzed the correlation between our candidates and between their own correlating genes.

TCGA gene expression data (RSEM gene-normalized) and clinical annotations for 9,174 tumors across 33 cancer types was downloaded from the most recent freeze contained in the Firebrowse server (2016\_01\_28) (Broad Institute of MIT&Harvard, 2016). Next, expression data was log<sub>2</sub> transformed. Statistical analyses were performed using the Python scipy library (SciPY, 2018).

#### **4. STATISTICAL ANALYSIS**

Graphs and statistic tests were performed using GraphPad Prism v6 software (GraphPad Software, Inc. USA).

Due to the small samples size and the fact that not all the data were normally distributed, a non-parametric suitable test for each case was used (Mann-Whitney or Chi-Square). Two-sided and unpaired tests were used for data analysis. The statistical significance was defined at a *p* value lower than 0.05 (\*\**p*<0.01, \*\*\**p*<0.001, \*\*\*\**p*<0.0001).



**RESULTS**



## 1. METASTATIC CANDIDATES

Altogether, previous results confirmed heterogeneity between Ren 50 and Ren 50M tumors, even though they were derived from the same patient. The two variants of our model presented different mutations, gene expression profiles, and even differential chromosomal aberrations. Hence, these differences could account for the metastatic advantage of one group compared to the other.

The initial aim of our study was to generate a metastatic candidate gene list from the above-mentioned data we obtained.

### 1.1 CARBOXYPEPTIDASE E

Carboxypeptidase E (CPE) was the first gene chosen as a metastatic candidate. We decided to study it due to the interesting results obtained from the RNA Sequencing. When comparing *CPE* RNA expression between Ren 50 and Ren 50M tumors, the differences were evident. There was almost no expression in Ren 50 tumors, whereas in Ren 50M it was one of the most expressed genes in all the genome (Figure 27).

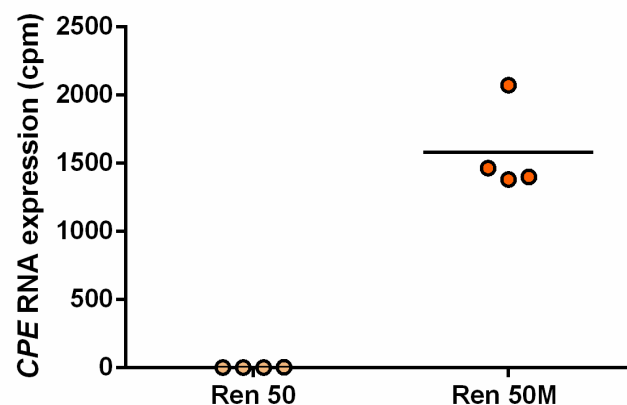


**Figure 27. *CPE* RNA was only detected in Ren 50M tumors.** *CPE* RNA expression obtained from RNA sequencing in four Ren 50 and four Ren 50M tumors. *CPE* RNA expression was quantified in counts per million (cpm). Results were statistically significant, p value 4.84 e-167, Fold Discovery Rate (FDR) 6.256 e-163.



Another interesting aspect of the data was the high fold change of *CPE* expression when comparing Ren 50M tumors to Ren 50 ones. In the metastatic group, *CPE* gene was expressed 437.31 more times. Regarding fold change (FC), *CPE* gene was on top of the list of more than 15,000 genes. Furthermore, it was relevant to consider that this difference was not explained by a low expression in one group, as we could see in some other genes, but because it was the most expressed gene in Ren 50M tumors. It was also explained by the extremely high RNA levels in Ren 50M tumors (Table 14). We could also confirm from the exome sequencing results, for both Ren 50 and Ren 50M, that *CPE* overexpression was not due to a mutation in this gene. In addition, *CPE* gene is located in chromosome 4, which is not one of the altered chromosomes confirmed by FISH analysis.

Gene Symbol	Description	Fold Change	PValue	FDR	Mean Ren 50	Mean Ren 50M
1 <i>APBB1IP</i>	Amyloid Beta Precursor Protein Binding Family B Member 1 Interacting Protein	3416,1349	7,83E-128	4,05E-124	0,0085	29,0560
2 <i>TSPAN18</i>	Tetraspanin 18	3250,2975	1,97E-33	3,07E-31	0,0260	84,6377
3 <i>TINAG</i>	Tubulointerstitial Nephritis Antigen	2615,4238	5,01E-77	4,18E-74	0,0022	5,7896
26 <i>F13A1</i>	Coagulation Factor XIII, A1 polypeptide	639,2797	1,04E-40	2,21E-38	0,6037	385,9226
33 <i>CPE</i>	Carboxypeptidase E	437,3084	4,84E-167	6,26E-163	3,6143	1580,5696

**Table 14.** *CPE* gene was one of the all genome with a highest fold change when comparing Ren 50M to Ren 50 tumors. Its expression in the metastatic group was extremely high. Table of selected genes regarding of their fold change when comparing Ren 50 and Ren 50M tumors. Fold change was obtained by comparing their expression levels and p value FDR represent the value of a test for statistical significance.

Therefore, the extremely high *CPE* expression in the metastatic tumors in our model and its absence in the non-metastatic ones, led us to hypothesize that it could be closely related to this process.

## 1.2 COAGULATION PATHWAY

On the other hand, we also decided to study the coagulation pathway. The interesting relation between our model and this cascade was obtained from the analysis of the RNA sequencing data using the computational GSEA method, analyzed by Dra. Susana Aguilar.

Among other signatures, obtained results revealed that the signature of *Regulation of blood fluid levels* showed the highest correlation with our data. Indeed, twelve genes from this signature presented a positive GSEA core enrichment (Table 15).

We decided to focus our studies on two of them, which correlated positively. Criteria for selecting candidates were both the presence of a high fold change between Ren 50 and Ren 50M tumors and also high expression levels in Ren 50M, ensuring detection of these genes at the protein level. Following these parameters, we chose Coagulation Factor XIII A1 (FXIII A1 or F13A1) and Coagulation Factor II Thrombin Receptor (F2R), also named Protease Activator receptor 1 (PAR1). In addition, F13A1 was also present in the FC-top list (Table 14). Our aim was to establish a relation between the expression of these genes and the metastatic capacity of tumors.

GENE_Symbol	Description	GSEA Core Enrichment	Fold Change	logFC	FDR	Mean Ren 50	Mean Ren 50M
<i>SLC22A2</i>	Solute carrier family 22 (organic cation transporter), member 2	YES	1322,4672	-10,217543	1,34867E-89	0,0347	45,9164
<i>F13A1</i>	Coagulation factor XIII, A1 polypeptide	YES	639,2797	-9,4197351	2,20957E-38	0,6037	385,9226
<i>HNF4</i>	Hepatocyte nuclear factor 4, alpha	YES	287,6259	-8,1279052	8,48E-46	0,0447	12,8683
<i>F2R</i>	Coagulation factor II (thrombin) receptor	YES	76,9164	-6,3448581	5,88396E-79	1,9530	150,2202
<i>GNAQ</i>	Guanine nucleotide binding protein (G protein), q polypeptide	YES	16,9633	-4,0843846	2,86803E-50	3,4701	58,8640
<i>ITGB3</i>	Integrin, beta 3 (platelet glycoprotein IIIa, antigen CD61)	YES	12,9162	-3,6904858	3,14963E-26	1,0127	13,0808
<i>SERPINE1</i>	Serpin peptidase inhibitor, clade E (nexin, plasminogen activator inhibitor type 1), member 1= PAI1)	YES	8,7405	-3,1277244	9,92251E-47	64,8592	566,9026
<i>F2RL2</i>	Coagulation factor II (thrombin) receptor-like 2	YES	8,4343	-3,0156571	5,92E-09	0,2238	1,8877
<i>TFPI</i>	Tissue factor pathway inhibitor (lipoprotein-associated coagulation inhibitor)	YES	3,6902	-1,8891136	5,38652E-13	28,4133	104,8516
<i>L3MBTL4</i>	l(3)mbt-like 4 (Drosophila)	YES	2,6331	-1,3965289	1,75413E-05	2,8373	7,4710
<i>SLC22A4</i>	Solute carrier family 22 (organic cation transporter), member 4	YES	1,8178	-0,8616226	0,038381746	1,5504	2,8183
<i>HPS4</i>	Hermansky-Pudlak syndrome 4	YES	1,6589	-0,7302649	0,001585276	342,4818	568,1597

**Table 15. Twelve genes from the *Regulation of body fluid levels* signature of GSEA were enriched in our data set. *F13A1* and *F2R* were two of the genes with a highest fold change and also high gene expression levels in Ren 50M tumors. Table of selected gene set enriched in samples from Ren 50M compared to Ren 50 tumors. FC was obtained by comparing their expression levels and p value and FDR represent the value of a test for statistical significance.**

Both *F13A1* and *F2R* genes, together with other genes from the obtained positive correlated genes list, codify for proteins that are involved in the coagulation pathway (Figure 28).

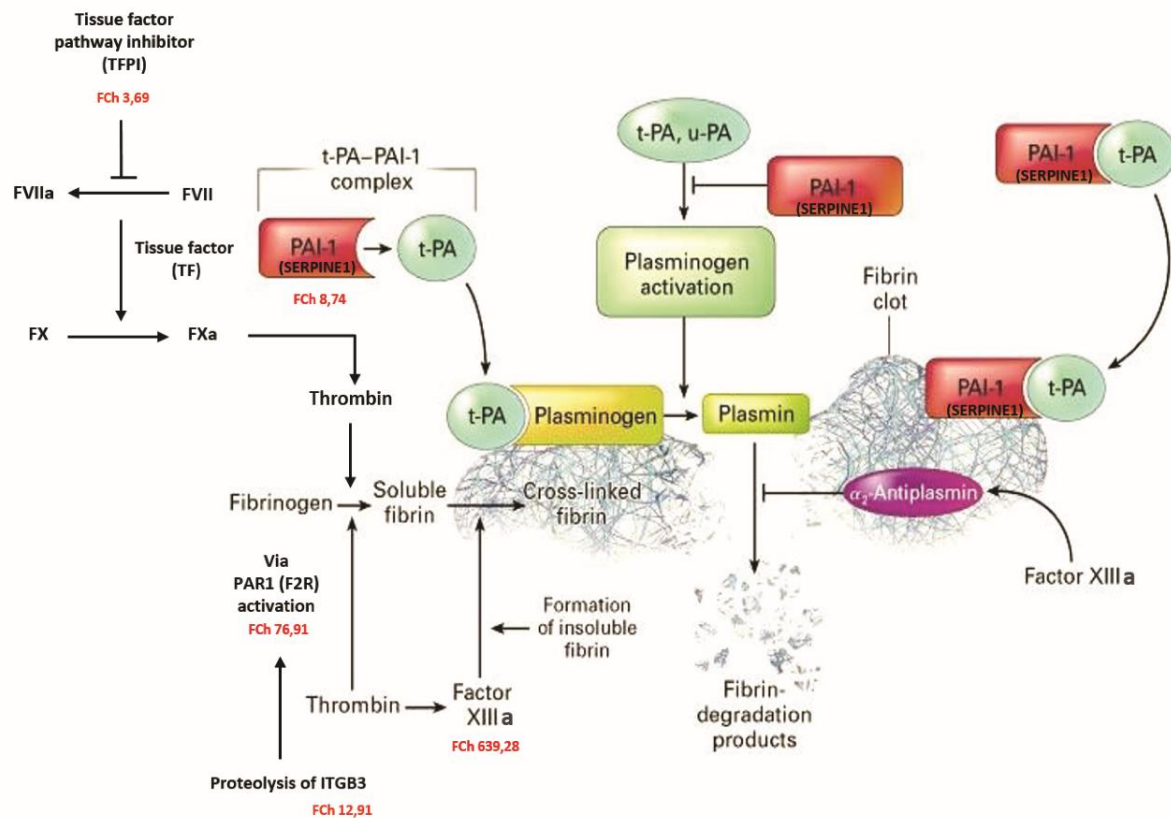


**Figure 28. Coagulation pathway.** Coagulation pathway consists of procoagulant and anticoagulant mechanisms aiming the maintenance of the hemostatic balance of blood clotting and vascular integrity. Several molecules are involved in these processes and are enriched in our GSEA results (highlighted in red). Image has been adapted from (Kohler and Grant, 2000).

From a detailed analysis of the data from the RNA sequencing, we could see that all tumors from Ren 50 group did not show expression of either *F13A1* or *F2R*. In contrast, RNA expression of these genes in Ren 50M tumors was very high (Figure 29).

Furthermore, from the exome sequencing results, we could confirm, for both Ren 50 and Ren 50M, that overexpression of *F13A1* and *F2R* was not because of a mutation. In addition, these genes are located in chromosomes 6 and 5, respectively, which are not among the altered chromosomes validated by FISH analysis.

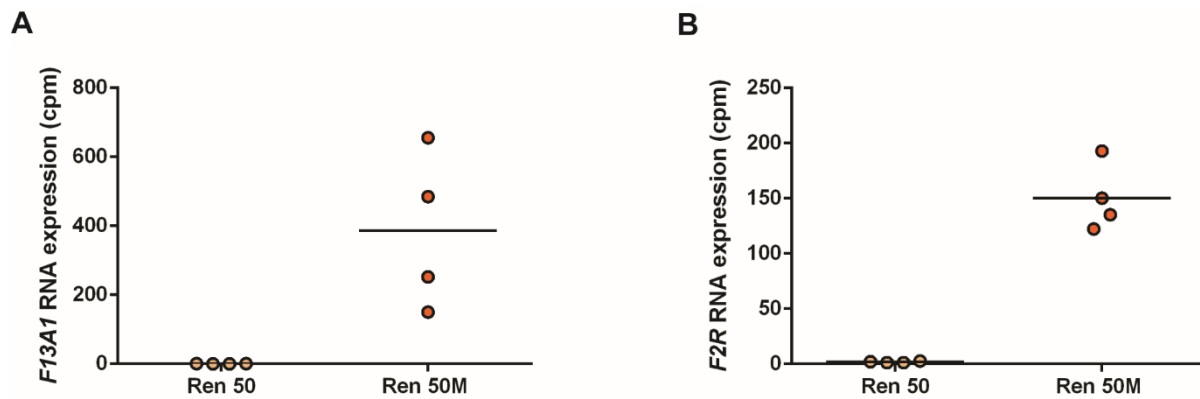


**Figure 29. *F13A1* and *F2R* were almost not expressed in Ren 50 tumors and highly expressed in Ren 50M.** RNA expression was quantified in cpm. A) Differences in *F13A1* RNA expression when comparing Ren 50M to Ren 50 tumors were statistically significant, p value  $1.04 \times 10^{-40}$ , FDR  $2.21 \times 10^{-38}$ , B) *F2R* RNA expression differences were statistically significant, p value  $5.92 \times 10^{-82}$ , FDR  $5.88 \times 10^{-79}$ .

In addition, we decided to follow the phenotype of the two variants of our orthoxenograft model in order to identify some features possibly related to the coagulation pathway.

During passages, we could observe that Ren 50M animals normally presented reddish skin. In contrast, any alteration in the color of the skin could be observed in mice from the Ren 50 line, suggesting a possible relation of this feature (Figure 30) with alterations in the coagulation pathway (Figure 28). However, analyses of the hematocrit from animals from both groups did not reveal any clear differences (data not shown).



**Figure 30. Ren 50 mice presented reddish skin, which could be related to coagulation pathway alterations.** Picture of mice from Ren 50 (on the left) and Ren 50M (on the right).

Furthermore, by microscopic analysis of the hematoxylin-eosin stainings, we observed some differences in the vascular phenotype between both lines. Detailed histological analyses using the endothelial marker CD31 revealed that Ren 50 tumors had long and thin vessels, whereas Ren 50M normally presented dilated vessels with big lumens (Figure 31A-B).

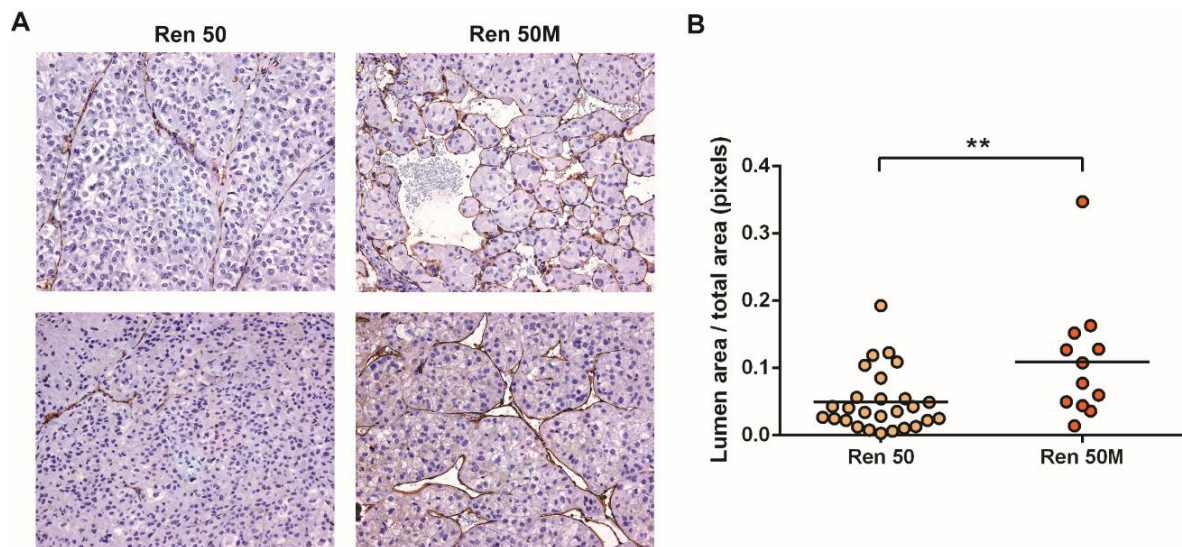


**Figure 31. Ren 50M tumors showed dilated vessels compared to long and thin vessels present in Ren 50.** A) CD31 endothelial marker immunohistological staining. From left to right, two pictures of Ren 50 tumors and two of Ren 50M (20X). B) Quantification of lumen vessels' area from 27 tumors of Ren 50 and 12 tumors of Ren 50M. Results were statistically significant by Mann-Whitney test.

In order to determine whether these differences could be associated to metastasis, a further analysis was performed. We grouped the animals regardless of the Ren line, based on two parameters: the vascular and the metastatic phenotype. We classified the tumors with long and thin vessels as Phenotype 1 and the ones with dilated vessels as Phenotype 2.

Through this classification, we found that Ren 50 tumors presented both phenotypes, whereas almost all tumors from the Ren 50M line presented phenotype 2 (Figure 32A). Furthermore, phenotype 1 could be associated to non-metastatic animals and almost all metastatic animals presented phenotype 2 (Figure 32B).

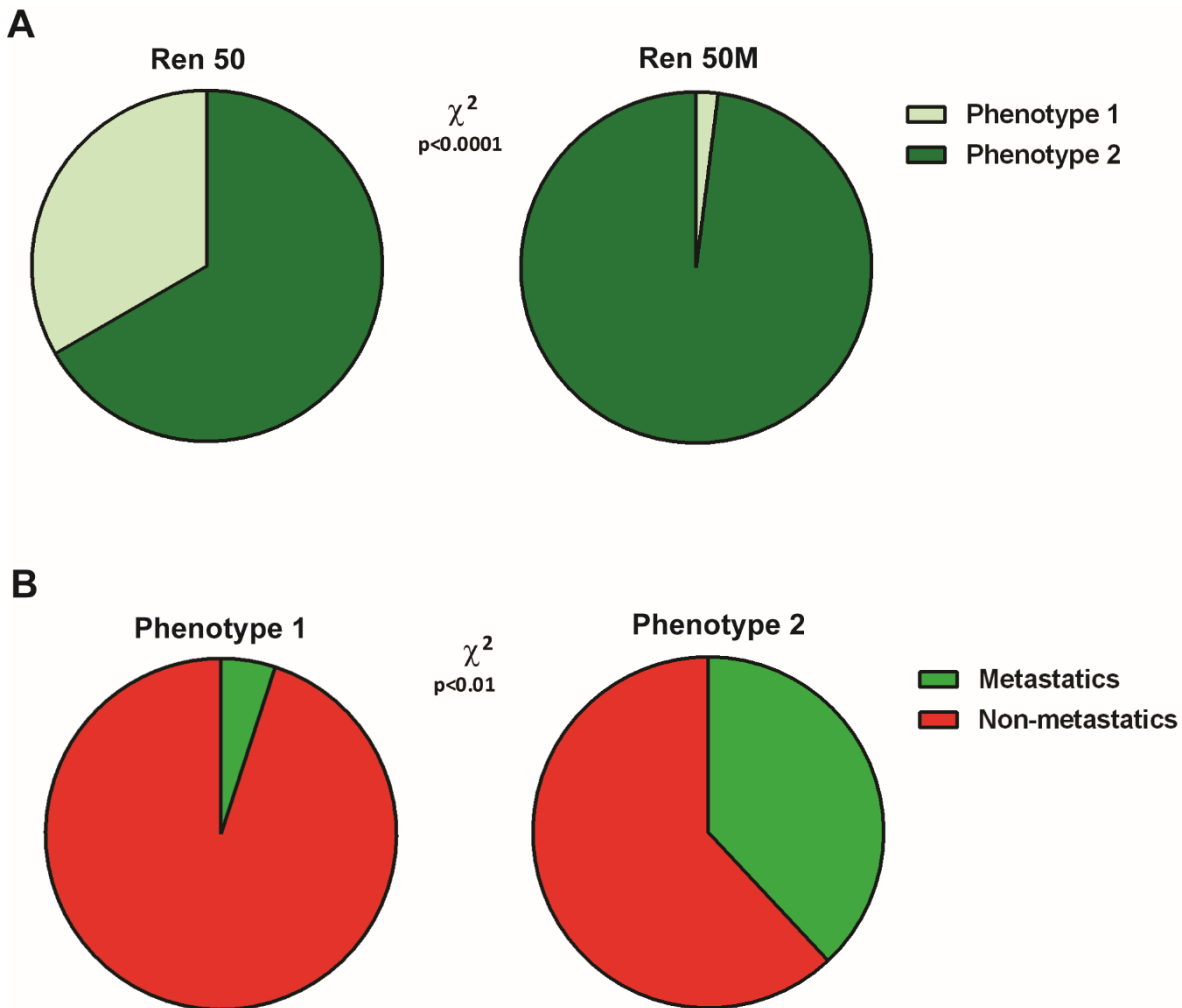


**Figure 32. Ren 50 tumors presented both phenotypes, whereas Ren 50M predominantly presented phenotype 2. Phenotype 1 was associated to non-metastatic animals and most of metastatic animals presented phenotype 2.** Quantifications were performed considering 112 mice in total. A) Quantification of mice classification regarding their Ren line and vascular phenotype. Results were statistically significant by Chi square test, \*\*\*\*p value <0.0001. B) Quantification of mice classification regarding of their vascular and metastatic phenotype. Results were statistically significant by Chi square test, \*\*p value 0.0041.

## **2. EXPRESSION VALIDATION**

Once we had selected some candidates on which to place our focus, we decided to test the maintenance of these huge differences during passages, both at RNA and at protein level, before starting to study their roles (later deciphered in sections 3.1, 3.2.1 and 3.2.2) and perform detailed functional analyses.

Expression of CPE was analyzed in tumors from Ren 50 and Ren 50M lines. In parallel, F13A and F2R expression was also tested in collaboration with Dra. Susana Aguilar.

### **2.1 EXPRESSION OF CPE, F13A AND F2R IN REN 50 AND REN 50M TUMORS**

First of all, we tried to confirm the strong differences found in RNA sequencing by Quantitative Taqman<sup>®</sup> Real Time-PCR assay. Expression validations confirmed that, for all cases, RNA expression levels of our candidates in Ren 50 tumors were very low. In contrast, RNA levels in Ren 50M tumors were clearly higher (Figure 33). Owing to these results, we could confirm the perpetuation of the RNA expression pattern for the three genes during passages, both in Ren 50 and in Ren 50M.



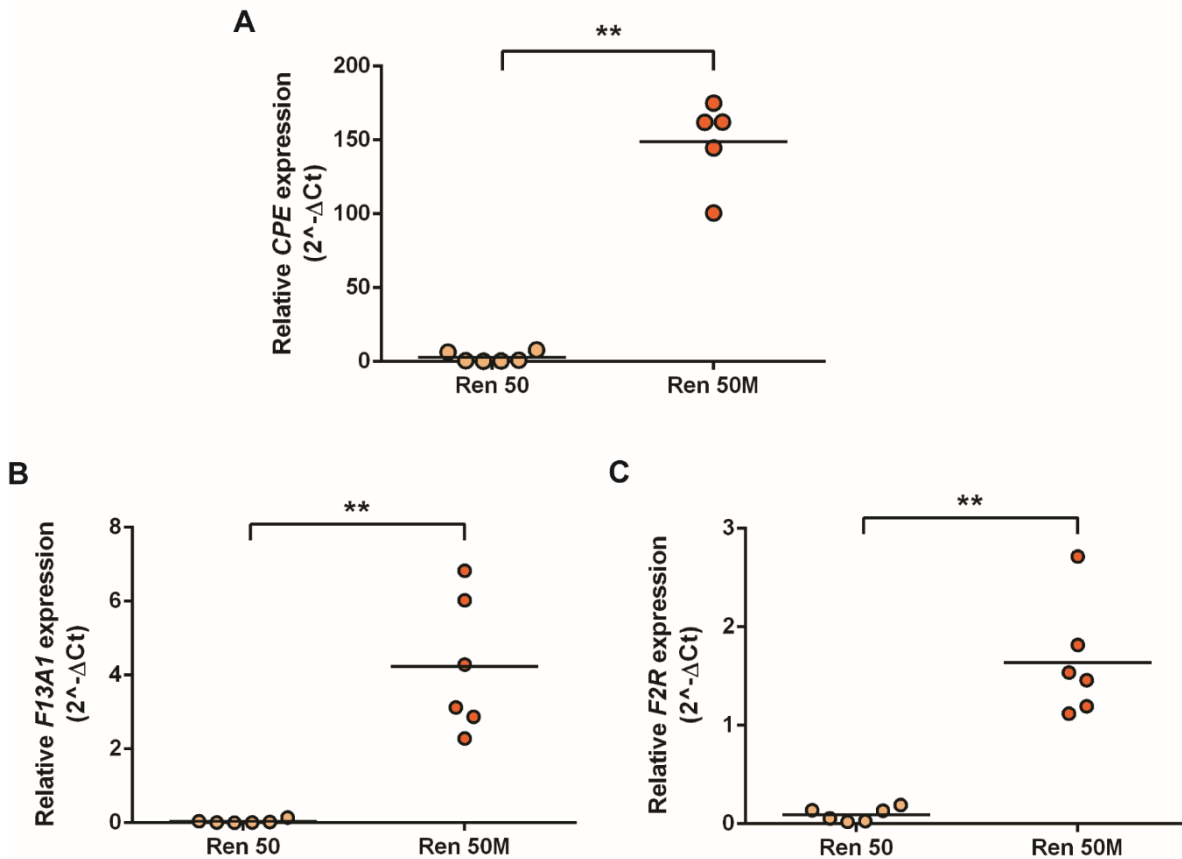


**Figure 33.** There was almost no relative *CPE*, *F13A1* and *F2R* expression in Ren 50 tumors and a very high expression in Ren 50M. Results obtained from a Taqman<sup>®</sup> Real-time PCR of six tumors of Ren 50 and six tumors of Ren 50M. RNA quantification of A) *CPE*, B) *F13A1* and C) *F2R* was normalized by *HPRT1* and measured by 2<sup>-ΔΔCt</sup>. Results were statistically significant by Mann-Whitney test in all the cases.

Once gene expression differences between both groups were validated, we decided to also validate these differences at the protein level. Results from two different techniques, western blot and immunohistochemistry, demonstrated no expression of CPE, F13A and F2R proteins in Ren 50 tumors. Contrarily, all Ren 50M tumors from different passages presented high levels of these three proteins (Figure 34).

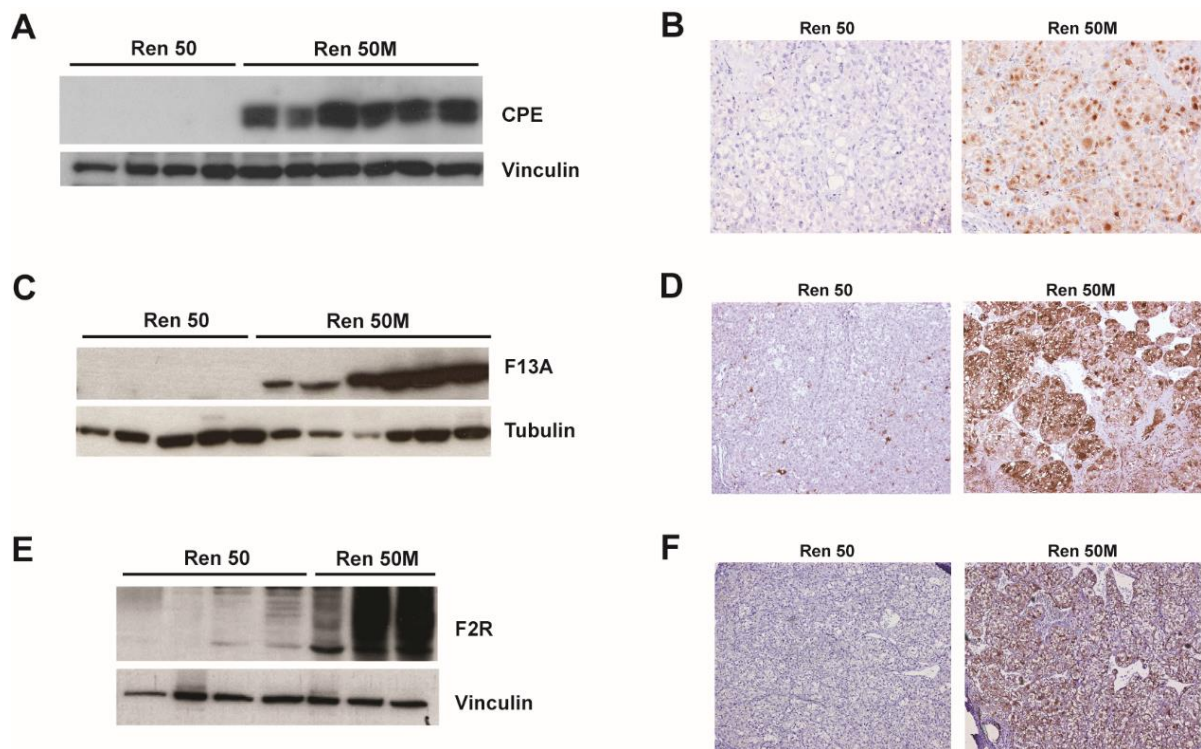


**Figure 34. Protein analyses confirmed absence of CPE, F13A and F2R protein expression in Ren 50 tumors and high expression in Ren 50M.** A) CPE protein was detected from lysates of four Ren 50 and six Ren 50M tumors. Vinculin was used as a housekeeping gene. B) CPE protein detection of Ren 50 and Ren 50M tumors by immunohistochemistry (20X). C) F13A protein was detected from lysates of five Ren 50 and six Ren 50M tumors using western blot. Tubulin was used as a housekeeping gene. D) F13A protein detection of Ren 50 and Ren 50M tumors by immunohistochemistry (20X). E) F2R protein was detected from lysates of four Ren 50 and three Ren 50M tumors. Vinculin was used as housekeeping gene. F) F2R protein detection of Ren 50 and Ren 50M tumors by immunohistochemistry (10X).

Therefore, we confirmed that the differences observed in RNA sequence from four animals of the same passages were maintained during the evolution of both lines.

## 2.2 PROTEIN EXPRESSION HETEROGENEITY OF CPE, F13A AND F2R IN THE ORTHOTOPIC MOUSE AND IN REN 50M TUMORS

Through immunohistochemistry staining, we confirmed that both the orthotopic and some Ren 50M tumors presented expression heterogeneity at the protein level (Figure 35).

These results prompted us to infer, in line with the exome sequencing results, that the human biopsy was probably clonally heterogeneous. Later on, this heterogeneity was probably perpetuated during the evolution of the metastatic line.

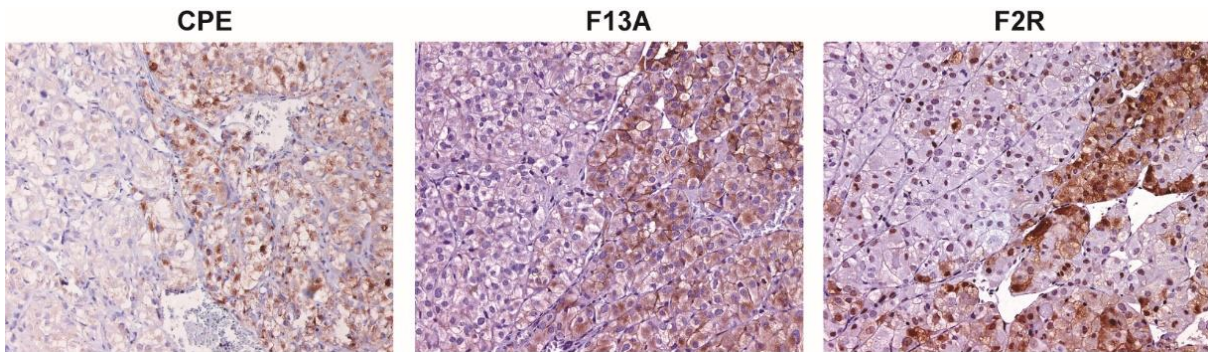


**Figure 35. Immunohistochemistry staining of our candidates confirmed protein expression heterogeneity in the orthotopic mouse and also in advanced passages of Ren 50M.** From left to right, immunohistochemistry of CPE of the OT tumor (20X) and immunohistochemistries of F13A and F2R of a Ren 50M tumor from passage 4, respectively (20X).

In order to assess whether this heterogeneity was distributed following the same pattern, we decided to overlap the staining of these proteins in order to compare positive and negative areas.

We could observe that, although they had some common areas with the same expression profile, they did not completely overlap, neither in the orthotopic, nor in Ren 50M tumors (Figure 36).

Hence, we can conclude that tumors are clonally heterogeneous and that proteins are not always distributed following the same patterns.

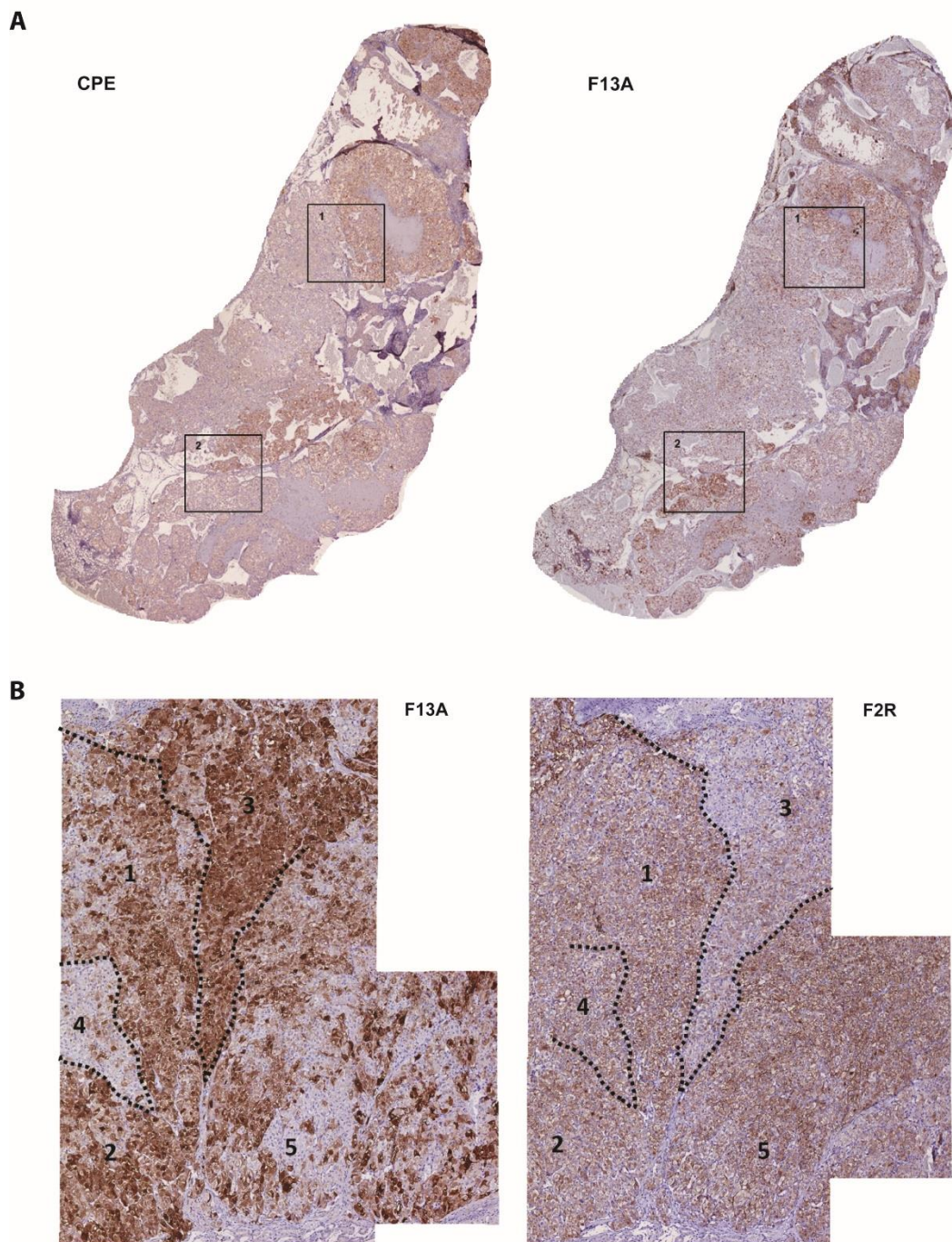


**Figure 36. When comparing the staining of the three proteins, they had some common areas but not all of them were completely overlapped.** A) Collage from pictures at 4X of immunohistochemistries of CPE and F13A from the orthotopic tumor. In this case, positivity in area 1 is overlapping, but in area 2, signal overlap does not occur. B) Collage from pictures at 10X of immunohistochemistries of F13A and F2R from a Ren 50M tumor from passage 11. In these compositions, areas 1 and 2 are overlapping, but areas 3 to 5 are excluded.

### 2.3 CPE, F13A AND F2R EXPRESSION IN REN 50 AND REN 50M LUNG METASTASES

At this point, we wanted to verify whether metastases were presenting the same protein pattern as their corresponding primary tumors. To do so, we tested the expression pattern of our proteins of interest in the metastases from both groups.

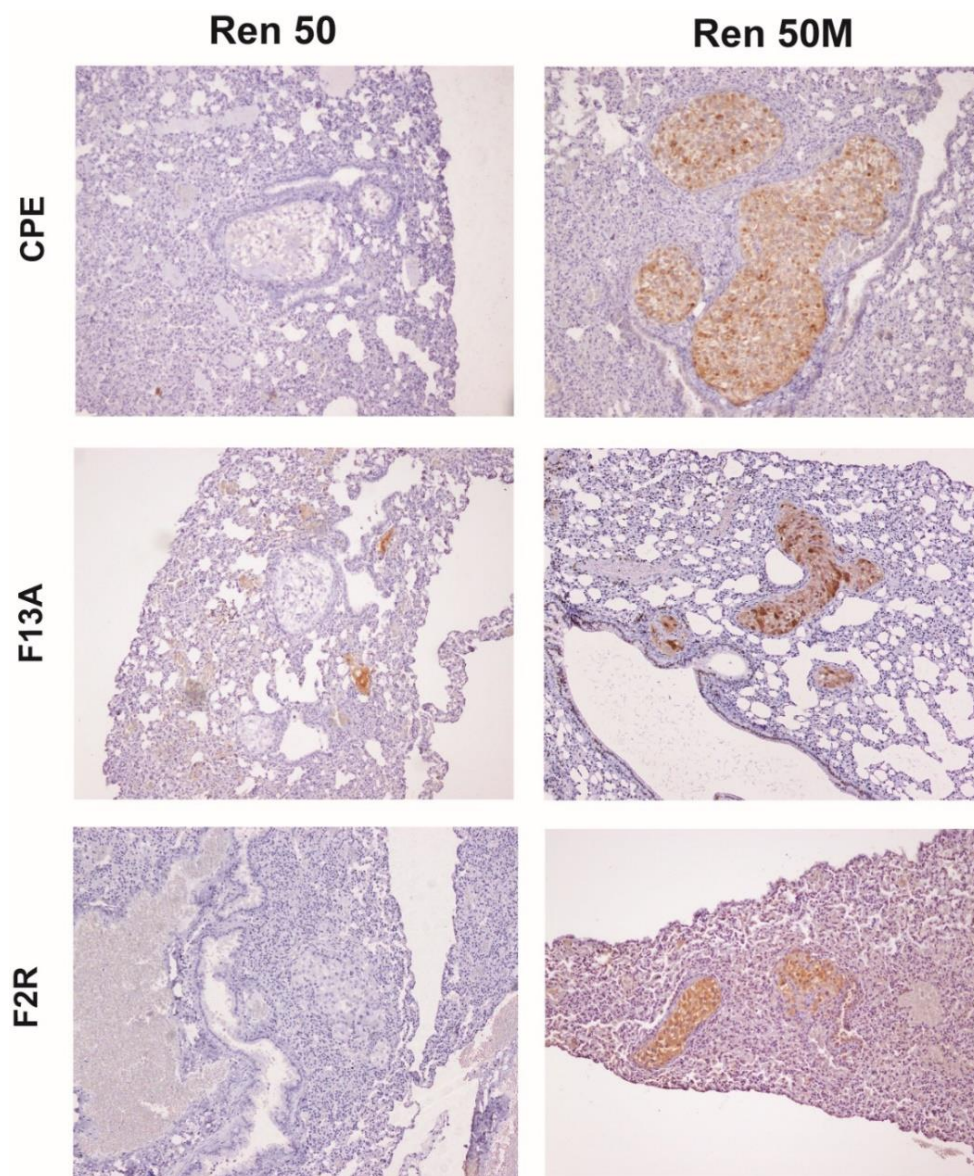


**Figure 37. Only Ren 50M metastases presented CPE, F13A and F2R protein expression.** From top to bottom and left to right CPE, F13A and F2R protein detection through immunohistological staining of lung metastases from Ren 50 and Ren 50M mice (10X).

Results confirmed absent expression of the three genes in Ren 50 lung metastases, in line with their primary tumors. On the contrary and, as expected, all metastases from Ren 50M mice did express CPE, F13A and F2R proteins (Figure 37). Furthermore, clonal heterogeneity could not be observed in Ren 50M metastases, suggesting that clones with the ability to generate metastasis seemed to always express our candidates.

With these results, we hypothesized that the few and small metastases in Ren 50 mice, as described in section 5.2 of the Introduction of this thesis, would probably have been generated through mechanisms with involved genes other than the Ren 50M driving ones.

As previously observed, the incidence and the size of the metastases between both groups are very different. In addition, there is a strong association between the expression of our candidates and Ren 50M tumors and metastases. Altogether, these results prompted us to further study our candidate genes and their putative role in the metastatic process.

### 3. FUNCTIONAL VALIDATION

#### 3.1 CARBOXYPEPTIDASE E

Carboxypeptidase E, also known as carboxypeptidase H, is a protein discovered in 1982 firstly named enkephalin convertase (Fricker and Snyder, 1982). CPE is one of the members of the M14-like superfamily of metallo-carboxypeptidases and is localized primarily in endocrine tissues and specific areas of the nervous system. It is a 476-amino acid peptide encoded by a nine-exon containing gene located in chromosome 4q32.3 (Manser et al., 1990).

CPE is a C-terminal cleaving carboxypeptidase involved in many biological processes, such as the synthesis and processing of a variety of bioactive peptides, like neuropeptides and hormones (Steiner, 1998).

Molecular modeling studies have revealed that CPE has a highly acidic C-terminal domain, which is an atypical amphipathic  $\alpha$ -helical domain under acidic conditions responsible for the specialized distribution of CPE in secretory granules. It also contains a catalytic domain and a signal peptide (SP), required for its direction to the RER cisternae. Finally, it has a cytoplasmic tail of about 5-10 amino acids, involved in the interactions with microtubules, thus mediating vesicle transport and its further recycling (Figure 38) (Ji et al., 2017).

CPE was described to play both enzymatic and non-enzymatic activities, and to exist in soluble (53KDa) and membrane-bound (55KDa) forms (Supattapone et al., 1984).

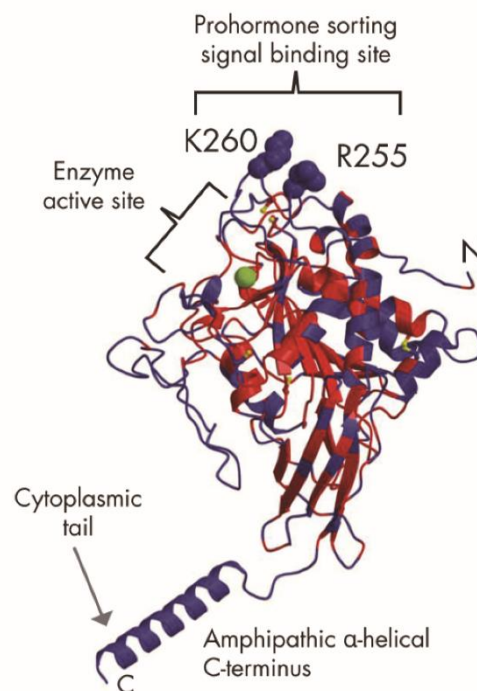


**Figure 38. Molecular model of CPE protein.** This model was based on the crystal structure of Carboxypeptidase D and overlapped homologous sequences are indicated in red. There are represented Arg255 and Lys260, which are the two basic residues demonstrated to interact with the acidic residue-based prohormone sorting-signal found in propeptides. The cytoplasmic tail and the C-terminal sequence that forms an amphipathic  $\alpha$ -helical domain are also represented. Finally, the green ball represents the zinc atom in the active site. This image has been adapted from (Cawley et al., 2012)

Many hormones and neuropeptides are synthesized in the rough endoplasmic reticulum (RER) as larger precursors. They are transported into vesicles to the golgi apparatus, where they are sorted at the TGN and packaged, together with their processing enzymes, into secretory immature granules before being released as bioactive peptides. Endocrine and neuroendocrine cells can be secreted through two different mechanisms. The first one, which is called constitutive secretory pathway (CSP), supports continuous protein secretion. In the second process, known as regulated secretory pathway (RSP), vesicles are released through a regulated process upon stimulation (Park and Loh, 2008).

The RSP starts with proteins binding to a sorting receptor in the TGN. Differently from other carboxypeptidases, CPE has an optimum pH at 5.5. Consequently, it is activated in the TGN and some CPE molecules would bind to the membrane (Figure 39) (Fricker et al., 1990; Greene et al., 1992).



Once inside the secretory granules, CPE is maximally active due to the acidic pH of 5-6 and binds to their membranes (Dhanvantari et al., 2002). In parallel, soluble CPE acts as an exopeptidase by removing the C-terminal basic arginine or lysine residues from pro-peptides, thereby activating them for their regulated secretion. For most peptides, this is their last needed modification before being released as biologically active peptides, whereas some need additional modifications (Figure 39) (Fricker and Snyder, 1983; Hook et al., 1982).

Then, secretory granules fuse to the plasma membrane, releasing mature peptides and both forms of CPE. Subsequently to granule exocytosis, the extracellular neutral pH reduces CPE activity. Finally, membrane CPE can recycle from the plasma membrane as a sorting receptor or exopeptidase through the early endosomes and back to the TGN, where it becomes active again. This mechanism is facilitated by the interaction of its cytoplasmic tail with ARF6 GTPase (Figure 39) (Arnaoutova et al., 2003).

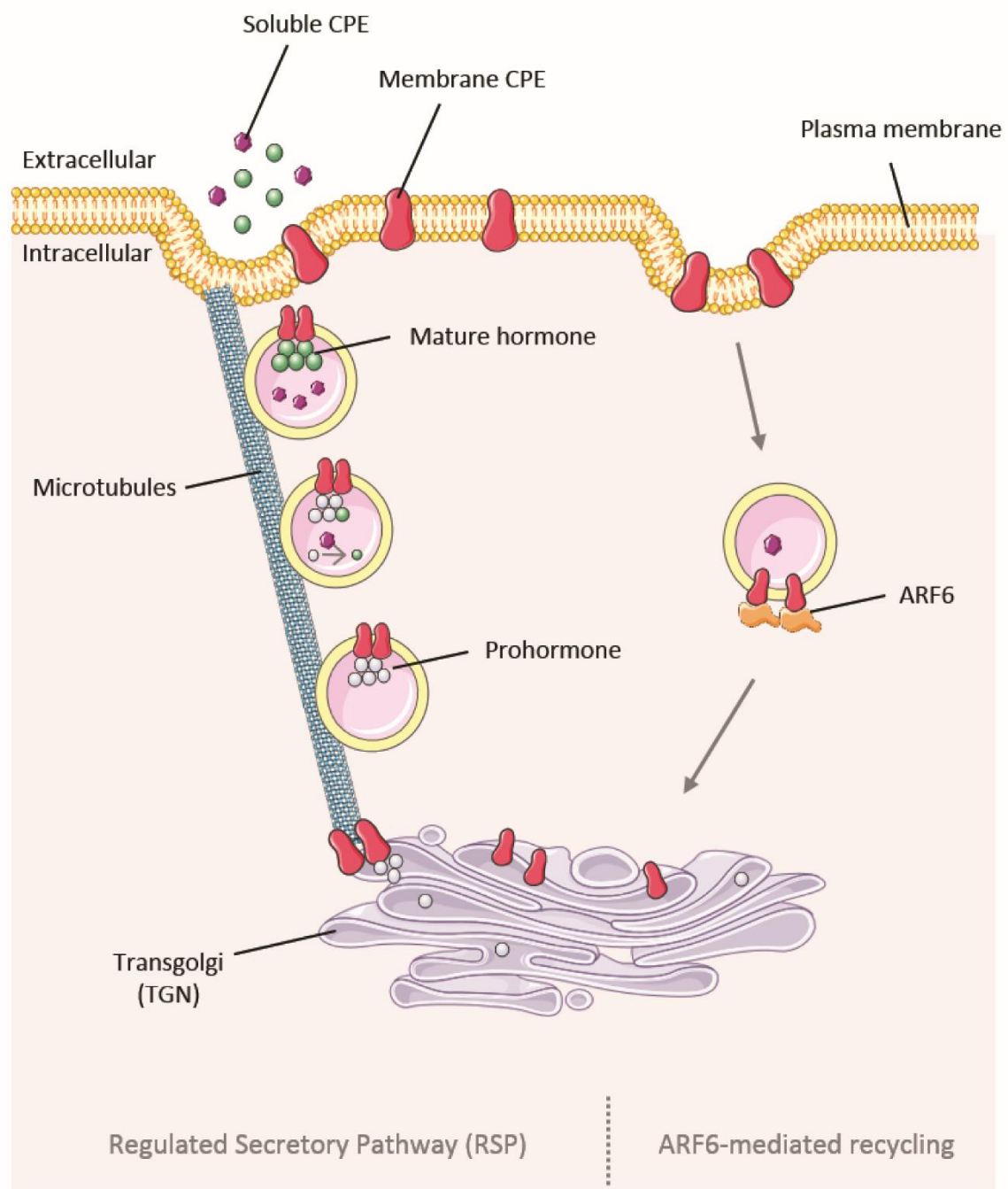


**Figure 39. Functionality of CPE.** CPE acts as a RSP sorting receptor at the TGN and is then packaged into dense core secretory granules for secretion, where it removes the C-terminal basic residues of prohormones for maturation. After exocytosis, it is recycled through an ARF6-mediated mechanism. Image has been adapted from (Ji et al., 2017).

Recent evidence suggests that CPE is related to cancer. In detail, a relationship between CPE expression and cell proliferation, tumorigenicity and also to metastasis in osteosarcoma cells has been described (Fan et al., 2016).

*In vivo* research has also described CPE as an overexpressed protein in different types of cancer, such as colorectal cancer (CRC) (Liang et al., 2013), pheochromocytomas (Murthy et al., 2010) and glioblastomas (Höring et al., 2012). Furthermore, its expression has been related to metastasis and poor prognosis in cervical cancer patients (Shen et al., 2016) and used as a prediction marker for tumor recurrence in early-stage hepatocellular carcinoma (Huang et al., 2016).

Recently, some effects produced by soluble CPE have been reported, extracellularly and independent of its enzymatic activity. Studies in pheochromocytoma and hepatocellular cancer have demonstrated that, in these type of cells, secreted or exogenous CPE promotes cell survival and has effects in migration and invasion (Murthy et al., 2013a). Furthermore, extracellular CPE has been shown to act as a neurotrophic factor by protecting neurons against oxidative or chronic stress (Cheng et al., 2013; Murthy et al., 2013b). It has also been related to the canonical Wnt pathway (Skalka et al., 2016).

### **3.1.1 CPE expression in RCC cell lines**

Therefore, adding up all the results from RNA and protein expression, we had confirmed the existence of a clear association between CPE and the metastatic group of tumors, Ren 50M. To address a functional relation between this protein and the metastatic capacity, we decided to evaluate its implication in the metastatic process both *in vitro* and *in vivo*.

First of all, we decided to test CPE expression in different RCC cell lines, both at RNA and at protein level. This approximation was necessary because no renal primary cell cultures, either from Ren 50 or from Ren 50M tumors, could be established.

Results from Taqman® Real-Time PCR and western blot showed almost no expression in any of the cell lines tested (Figure 40).

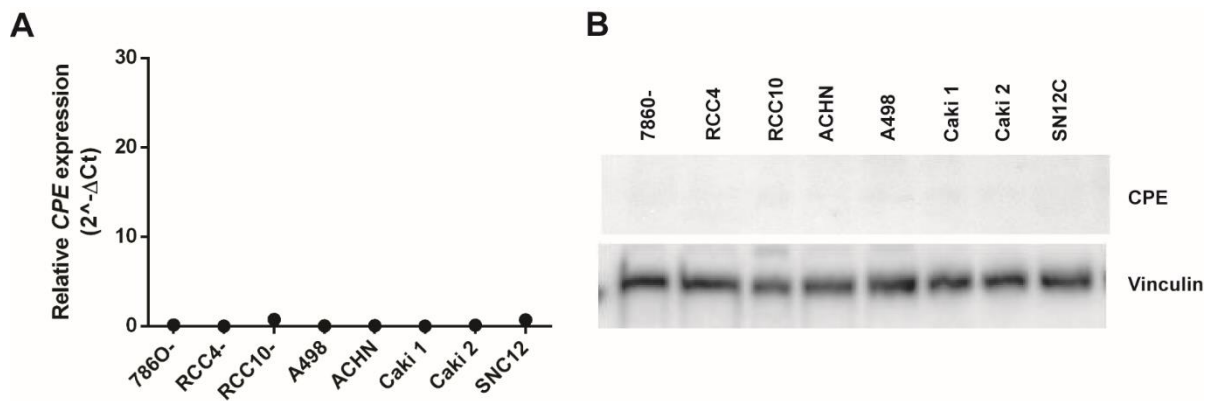


**Figure 40. None of the renal cell lines presented CPE relative RNA and protein expression.** A) Results obtained from Taqman® Real-time PCR of eight cell lines derived from RCC. RNA quantification of *CPE* was normalized by *HPRT1* measured by 2<sup>-ΔΔCt</sup>. B) *CPE* protein detection by western blot of the same samples.

Since we were not able to detect *CPE* in the tested cell lines, we decided to overexpress our gene of interest from the 786O- cell line. Previous validations performed in our group, both *in vitro* and *in vivo*, prompted us to choose these cells as an appropriate model for further experiments.

### 3.1.2 Generation of a *CPE*-expressing cell line

In an attempt to generate *CPE*-expressing 786O- cells, we decided to transfect them with two different pCMV3 vectors. On one hand, we transfected a group of 786O- cells with a pCMV3 vector containing the *CPE* gene. In parallel, another group of cells was transfected with a pCMV3 Empty vector to be used as a negative control. This second vector had the same sequence but lacking the *CPE* gene. After cell selection using antibiotics, *CPE* expression was evaluated. As expected, results from both immunofluorescence and western blot did not show expression of *CPE* in pCMV3-Empty vector cells. Nevertheless, modest *CPE* expression could be detected in pCMV3-*CPE* transfected cells (Figure 41).

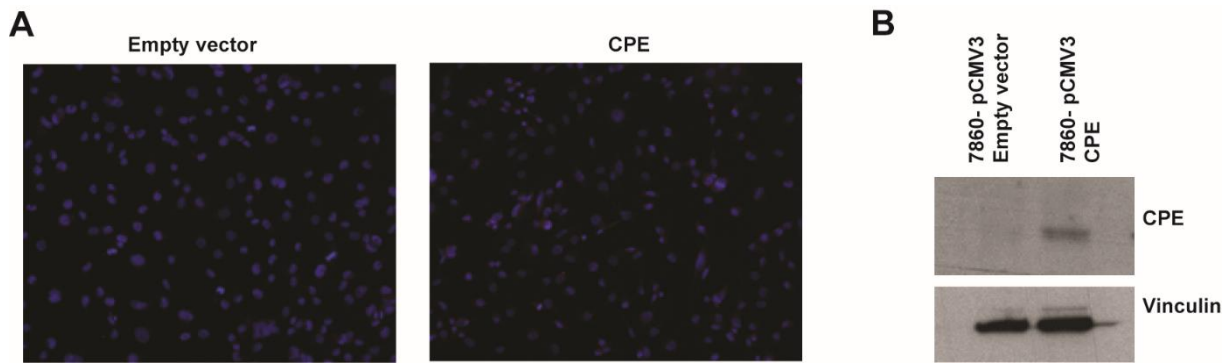


**Figure 41. CPE expression was not detected in cells transfected with the pCMV3-Empty vector. Almost no expression was either detected in cells transfected with the pCMV3-CPE vector.** A) Immunocytofluorescence of CPE protein in 786O- transfected cells (20X). B) CPE protein detection by western blot from lysates of both type of cells. Vinculin was used as housekeeping gene.

Aiming to obtain a better model to study the functional role of CPE, a new strategy using lentiviruses was used. This type of viruses is considered to be the most effective vehicle for transducing DNA, with a highly efficient transduction and a stable long-term expression.

In this line, we generated 786O- cells containing the cumate system. As depicted in section 1.2.3.7 of materials and methods of this thesis (page 89), it consists of the integration of the *CPE* gene under the control of a promoter which can be repressed by a CYMR protein. When adding cumate to the media, it binds the repressor and the transcription of *CPE* is activated.

Because of the presence of GFP in CPE and Blank vectors, we firstly decided to follow its signal during subsequent culture so that we could estimate the percentage of effectively transduced cells. We observed a population of not fully well-infected cells through GFP expression (Figure 42).

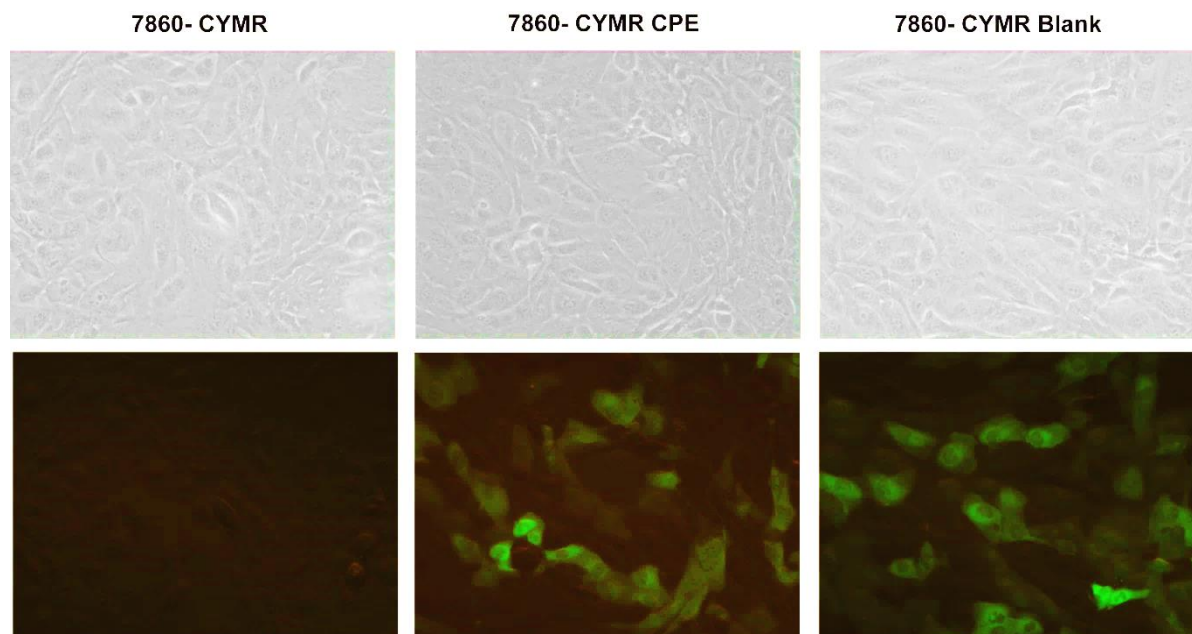


**Figure 42. 7860- CYMR cells did not show full infection efficiency of the CPE and Blank vectors.** From top to bottom and left to right, brightfield and green channel (GFP) images at 20X of 7860- CYMR, 7860- CYMR CPE and 7860- CYMR Blank cells.

Owing to these heterogeneous cell populations, we decided to sort both types of cells in order to obtain a pure CPE Inducible cell line and also a population with correctly integrated Blank vector. Aiming to obtain purer cell lines, cells were sorted based on their GFP fluorescence.

We decided to select and collect three different populations. We cultured the GFP negative population (1), the highly GFP positive population (3) and the rest of cells, composed by a population with an intermediate GFP-positive phenotype (2) (Figure 43).

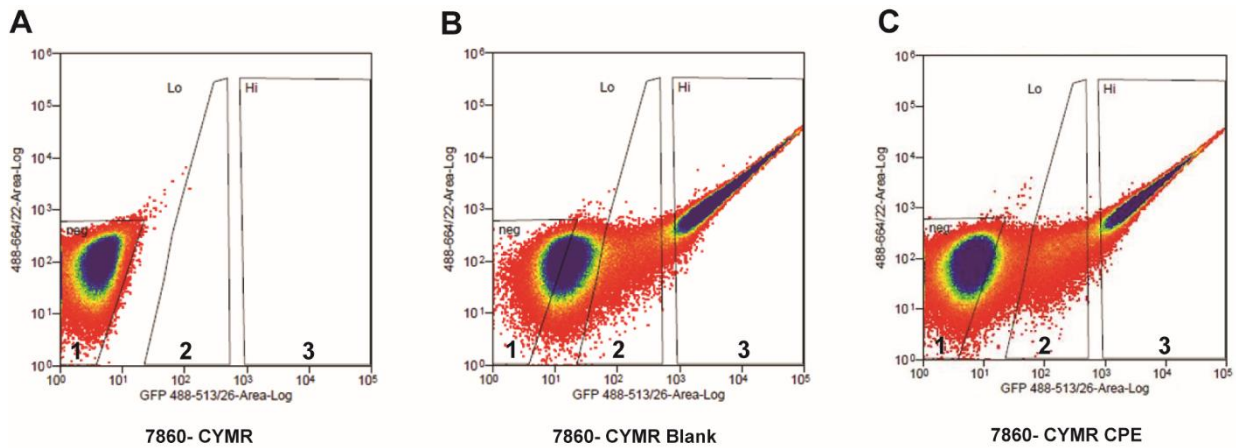


**Figure 43. Cell sorting of 786O- CYMR, CYMR Blank and CYMR CPE cells.** Cells were sorted applying gating parameters to select for GFP expression. A) 786O- CYMR cell line was used as a negative control due to its similarity to the other vectors but without GFP. Negative gate was determined using the parameters of this cell line detection. B) 786O- CYMR Blank cells were sorted and cells were split into three gates depending on the negative control, the highly GFP positive signal and cells with an intermediate phenotype. C) 786O- CYMR CPE cells were sorted following the same parameters used for Blank cells.

After sorting, we decided to check again GFP expression in order to confirm that we had been able to obtain a third population of each group of cells with an enrichment of GFP positive cells.

Results confirmed that group 1 from 786O- CYMR Blank and CPE cells were not expressing GFP, therefore confirming the selection of a negative population without the second plasmid. The second group of sorted cells, as expected, presented a GFP intermediate phenotype, forming a heterogeneous population of GFP expressing cells. Finally, following our purpose, we obtained a third cell population almost completely homogeneous for GFP expression (Figure 44).

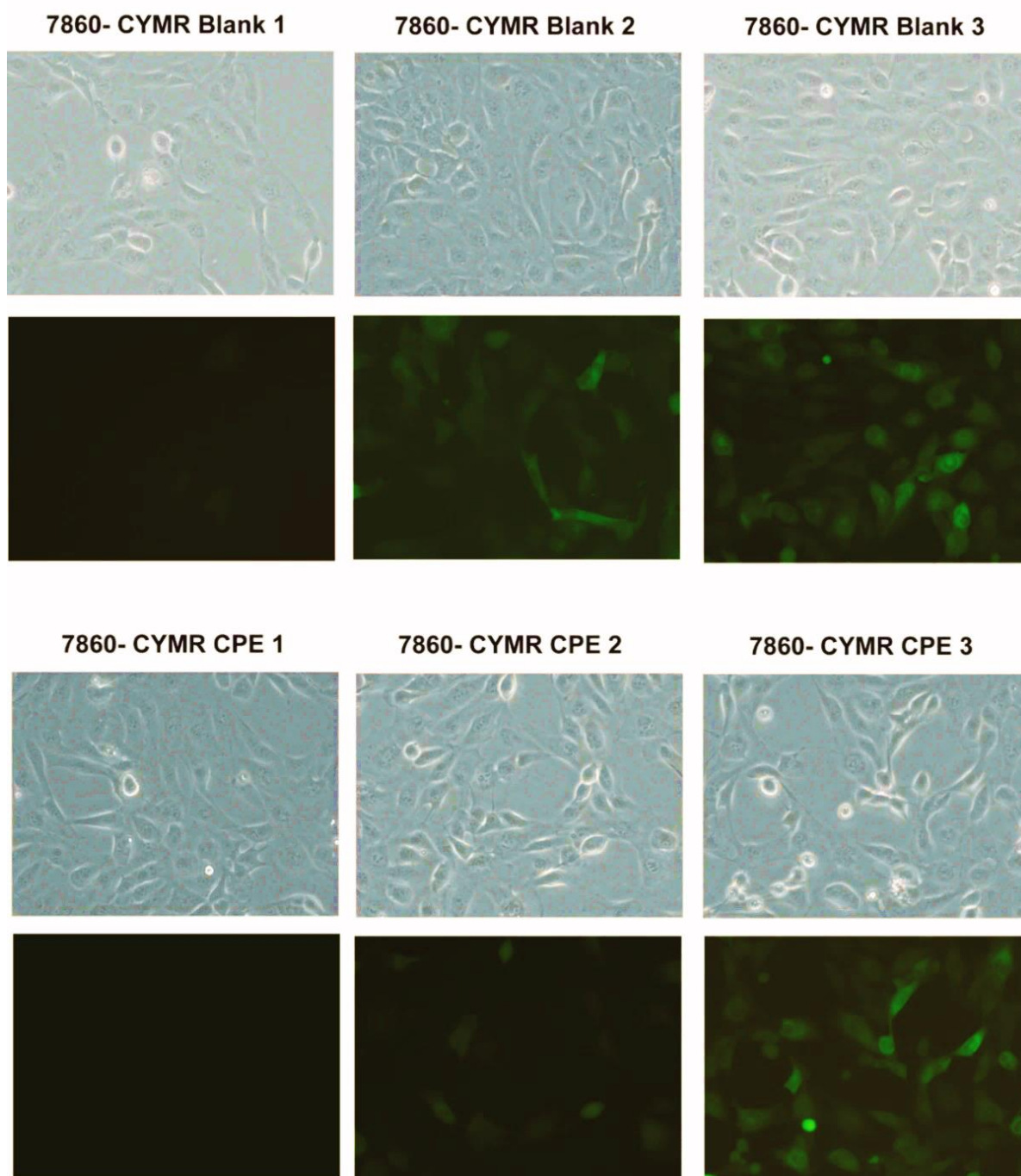


**Figure 44.** After cell sorting, we obtained three populations of 7860- CYMR Blank and CPE clearly differing in GFP expression. Group 1 was representing GFP-negative cells. Group 2 was a mix of negative and positive GFP expressing cells. Group 3 consisted of a selection of the highly GFP-positive cells. From top to bottom and left to right, brightfield GFP images at 20X of 7860- CYMR Blank and CPE sorted cells (1, 2 and 3, respectively).

Seeking to confirm CPE expression in all collected populations, we performed a Taqman<sup>®</sup> assay and also a western blot to detect CPE RNA and protein levels, respectively.



Results were consistent with the GFP expression patterns previously observed, hence confirming three different populations of CPE-expressing cells. Negative sorted cells never expressed CPE. The second group of cells, which were the cells between the negative and the highly positive GFP ones, presented expression of CPE, which was slightly increased when adding cumate. We decided to name these cells CPE Constitutive, due to their CPE expression without cumate induction. The third population presented CPE expression at a very low rate, but its expression was highly upregulated through cumate induction. We named these cells CPE Inducible. Finally, as expected, the third population of Blank cells did not show expression at either RNA or protein levels (Figure 45).

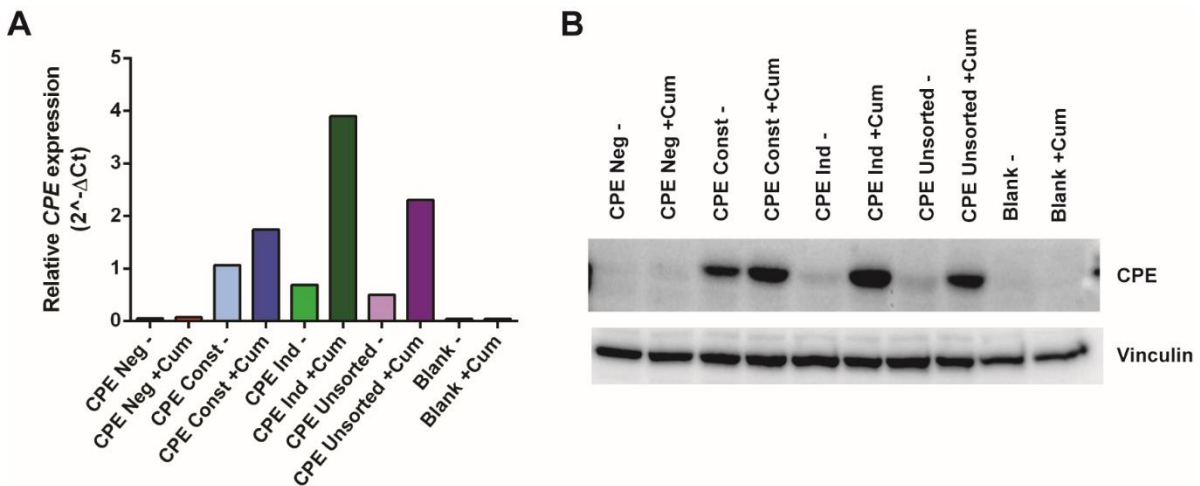


**Figure 45. 786O- CYMR Blank cells did not show CPE expression neither at RNA level, nor at protein level. CPE Constitutive cells expressed both CPE RNA and protein in a constitutive way. The expression slightly increased after cumate induction. CPE Inducible cells did almost not present expression and it was clearly upregulated with the addition of cumate.** All cells were incubated with or without cumate for 72h. A) RNA was then extracted and a Taqman<sup>®</sup> Real-time PCR was performed. Graph shows *CPE* RNA levels normalized by *HPRT1* and measured by  $2^{-\Delta C_t}$ . B) Western blot of CPE protein from lysates of the same cells under the same conditions previously tested for RNA. Vinculin was used as a housekeeping gene.

Finally, in order to determine at which time point we could obtain the highest CPE protein expression and how many hours were needed to lose its expression, we performed time-course assays testing both cumate induction and removal in CPE Inducible cells.

Results demonstrated that the highest CPE expression was at 72h of cumate incubation and was maintained high after 96h. Also, only 24h without cumate were necessary to utterly inhibit CPE expression (Figure 46). Owing to these results, from this point onwards, experiments were performed at 72h of cumate induction.

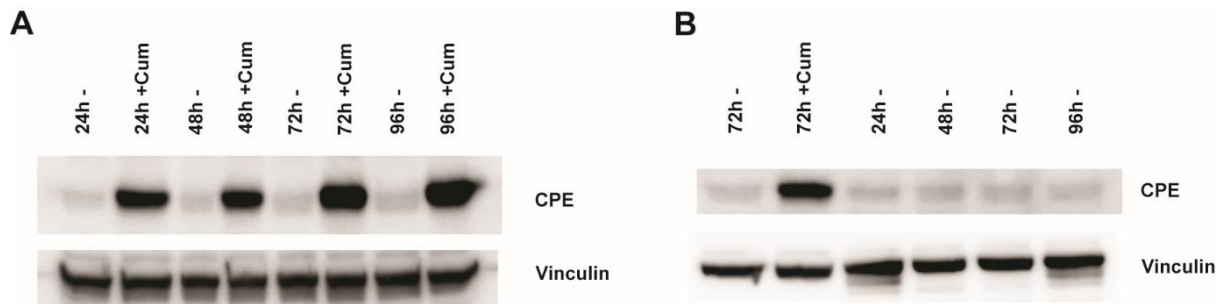


**Figure 46. CPE highest levels were obtained after 72h of cumate incubation. Its expression was completely reversed after 24h of its removal.** CPE protein was detected by western blot and vinculin was used as a housekeeping gene in both cases. A) 786O- CYMR CPE Inducible cells were incubated with cumate and cell lysates were obtained at 24, 48, 72 and 96h. B) Cells were incubated with cumate for 72h to obtain their highest expression. Then, cumate was removed and cell lysates were obtained at 24, 48, 72 and 96h.

Afterwards, we were prompted to relate its expression to a functional role in the metastatic process.

### 3.1.3 Effects of CPE expression in 786O- cells

To dissect the molecular mechanism that could be involved in metastasis, we started by evaluating migration. We performed it through a wound healing assay, hence validating whether CPE-expressing cells were able to non-directionally migrate faster than their corresponding controls.

We tested the migration capacity of CPE Constitutive, Inducible and Blank cells, with and without cumate induction. Results are shown in Figure 47, in which no significant differences were obtained regardless of CPE expression. Therefore, no relation between CPE expression and non-directional migration could be established.

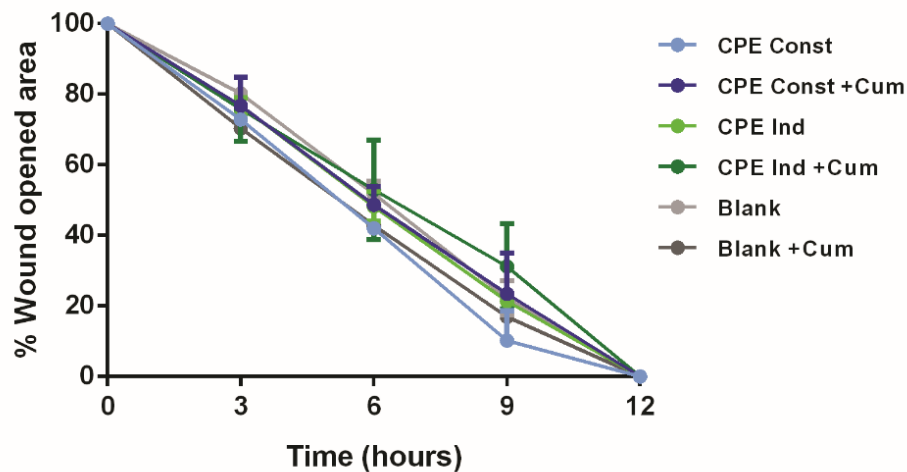


**Figure 47. CPE expression did not increase the migration capacity of 786O- cells.** Cell migration behavior was evaluated during a wound healing assay and images were taken every 3h until the wound was closed at 12h. CPE Constitutive, CPE Inducible and Blank cells were previously treated with or without cumate for 72 hours. At the beginning of the experiment, the scratch was performed and medium was replaced for fresh medium maintaining cumate conditions. Error bars represent S.D, n=2.

We next decided to alternatively evaluate the migration process, as well as the invasion capacity of the cells. To this purpose, we decided to treat cells with or without cumate and perform directional transwell migration and invasion assays.

Obtained results not only confirmed no relation between CPE expression and migration, but also a lack of correlation between the expression of our candidate and the invasion capacity of 786O- cells (Figure 48).

In conclusion, we were not able to confirm a functional direct relation between CPE expression and the migration or invasion *in vitro* processes.

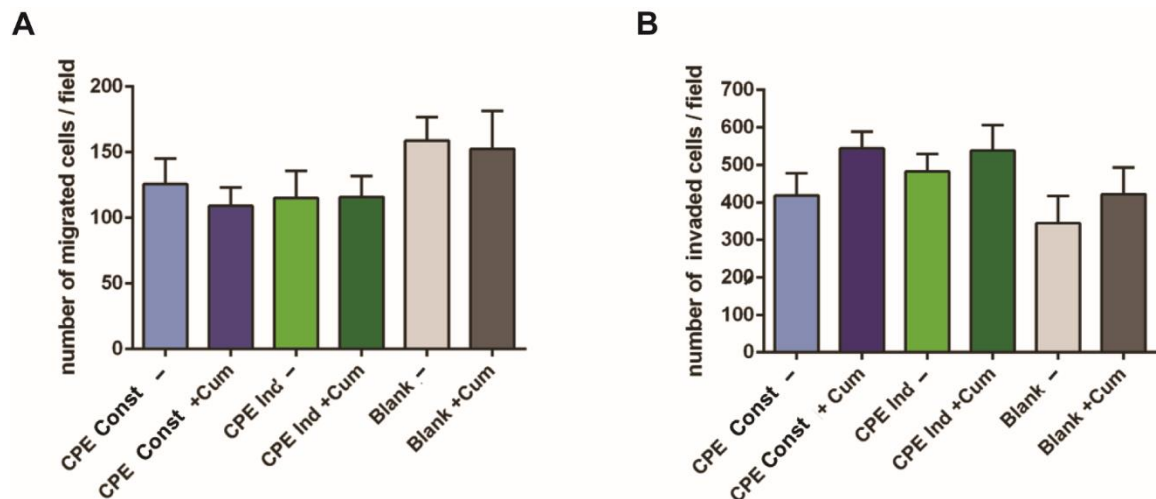


**Figure 48. CPE expression did not increase either the migration or the invasion capacity of 786O- cells.** 786O- CYMR CPE Constitutive, CPE Inducible and Blank cells were previously treated with and without cumate for 72h and then plated onto the transwells. No statistically significant differences were observed in any of the cases. Error bars represent S.D, wells/condition n=2. A) Transwell migration assay of the three cell lines with and without cumate. 10.000 cells were plated onto each well. B) Transwell Matrigel® invasion assay of the same cells and conditions validated in the migration assay. 20.000 cells were plated into the wells.

Since no correlation between CPE expression and the migration or invasion processes could be demonstrated so far, we hypothesized that CPE was maybe involved in the metastatic process acting as a chemoattractant or as a ligand, as it has been described in section 3.1.

### 3.1.4 CPE secreted protein detection and its effects *in vitro*

Firstly, we decided to test whether CPE-expressing cells were secreting the protein into the media. To approach this, protein precipitation of conditioned media was performed and assessed for the presence of CPE by western blot.

Results showed that both CPE Constitutive and CPE Inducible cells treated with cumate were secreting CPE protein into the media. Moreover, as it was expected, CPE could not be detected in medium from Blank cells (Figure 49).

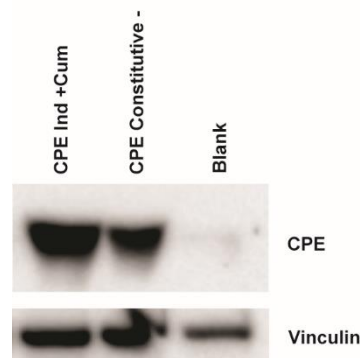


**Figure 49. CPE-expressing cells secreted the protein into the media.** Cells were maintained with or without cumate for 72h and then starved at 2% FBS with the same cumate conditions. Supernatants were collected 24h later and protein was detected by western blot. Vinculin was used as a housekeeping gene.

In order to study the possible function of CPE as a secreted protein, we started analyzing its effect on the migration capacity of the cells using a transwell migration assay.

Conditioned media from CPE Constitutive and Blank cells, used as a control, were collected. Then, they were placed in the bottom of the wells in order to assess whether it was affecting cell migration. We were not able to report differences in the migration capacity of the cells, regardless of the presence of CPE in the medium (Figure 50).

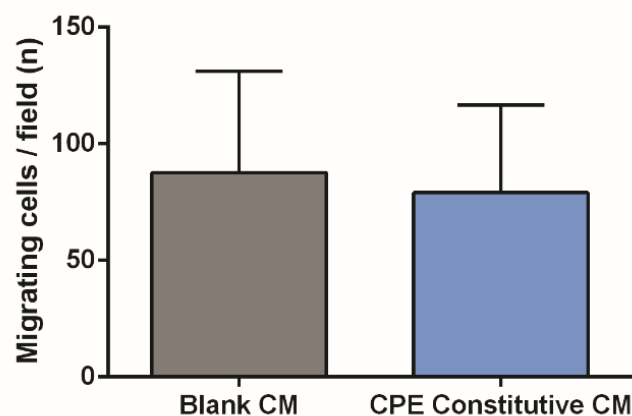


**Figure 50. Soluble CPE did not change cell migration capacity.** Transwell migration assay of 786O- CYMR Inducible cells without cumate. Conditioned mediums of 786O- CYMR Blank and CPE Constitutive cells were placed onto the bottom of the transwell. 10.000 cells were plated onto each well and the assay was performed at 24h. Error bars represent S.D, wells/condition n=3

Although no effects of soluble CPE in cell migration were reported, we decided to test whether this molecule could be involved in the invasion process. Aiming at this, we performed transwell Matrigel® invasion assays.

First of all, we placed conditioned media with or without soluble CPE into the bottom of the transwells. In addition, CPE recombinant protein was also used to test the invasion capacity of the cells. Results from experiments using three different settings led us to conclude that CPE was acting somehow by attracting cells and increasing their invasive potential (Figure 51).

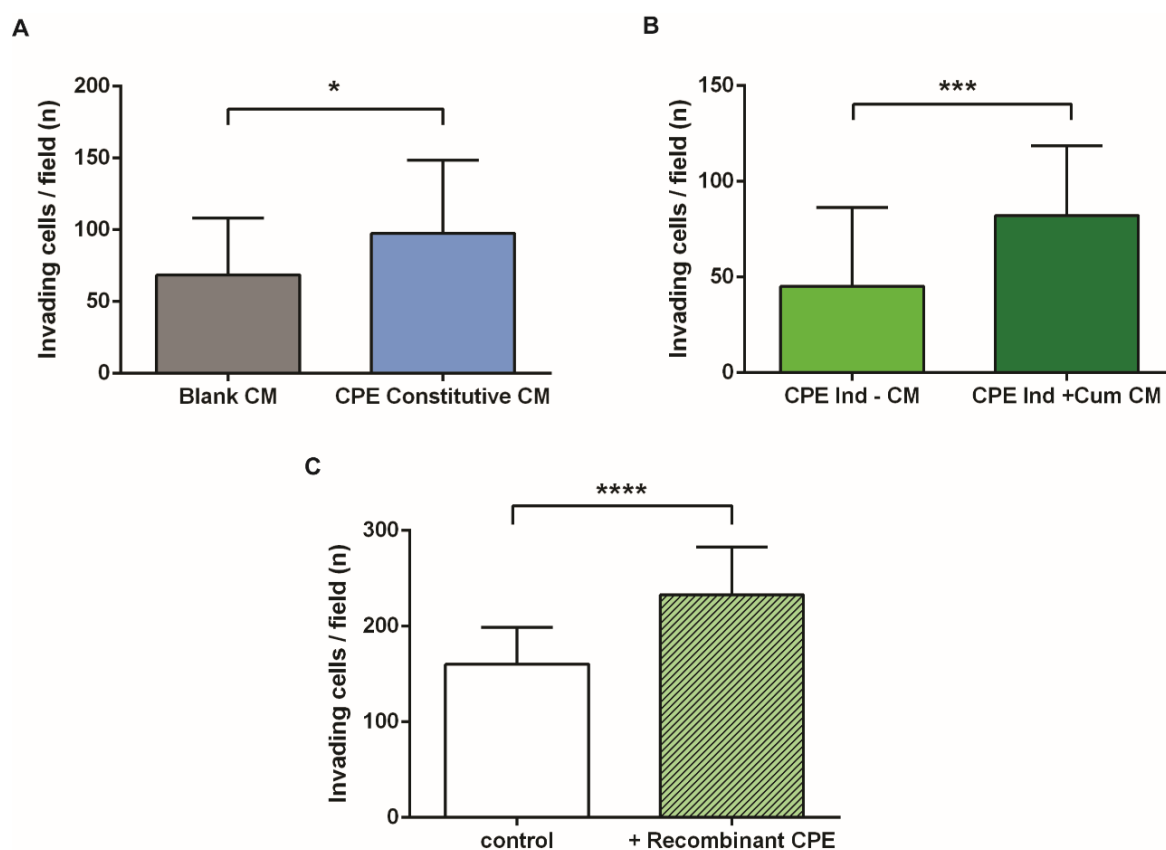


**Figure 51. CPE acted as a chemoattractant or as a ligand by increasing the invasion potential of 786O-cells.** 20.000 cells were plated onto each well and the assay was performed at 48h. Error bars represent S.D, wells/condition n=3. Differences were statistically significant in all the cases by Mann-Whitney test. A) Transwell Matrigel® invasion assay of 786O- CYMR Inducible cells without cumate. Conditioned media of 786O- CYMR Blank and CPE Constitutive cells were placed onto the bottom of the transwells. B) Transwell Matrigel® invasion assay of 786O- CYMR Blank cells without cumate. Conditioned media of 786O- CYMR CPE Inducible cells with and without cumate were placed onto the bottom of the transwells. C) Transwell Matrigel® invasion assay of 786O- cells. Fresh medium with or without CPE Recombinant at 200nM protein was placed onto the bottom of the transwells.

Because of its enzymatic activity, we hypothesized that CPE could be inducing invasion by degrading the ECM, thus facilitating cells to invade through Matrigel® *in vitro* and through the stroma *in vivo*. To approach this, we plated the cells after a previous incubation of the transwells with conditioned media for 48h.

Results demonstrated that cells invaded through Matrigel® regardless of the presence of CPE in pretreated mediums (Figure 52A). We also confirmed that the presence of cumate in conditioned mediums was not affecting invasion (Figure 52B), which is also useful as a control for previous experiments.

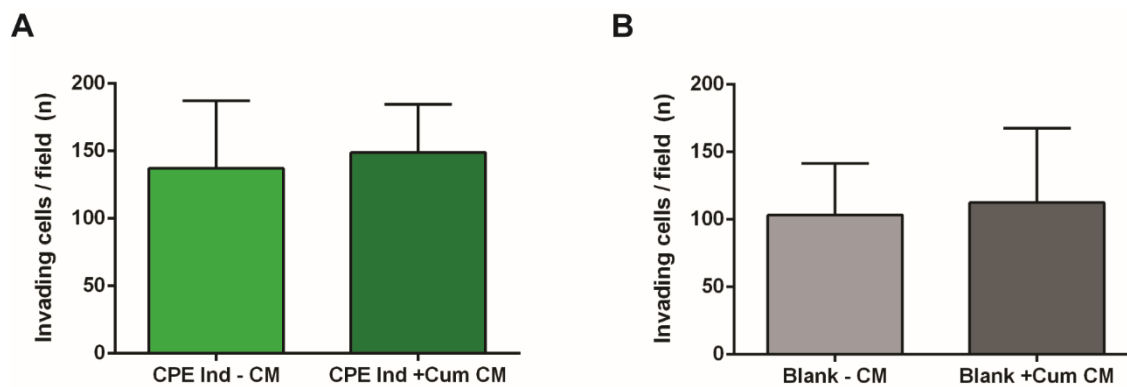


**Figure 52. Cells invaded through Matrigel® regardless of the presence of CPE in pretreated mediums.** A) Wells were previously treated for 48h with conditioned media of 786O- CYMR CPE Inducible cells with and without cumate. Then, 20.000 786O- CYMR Blank cells were plated into each well with fresh medium in both compartments and the transwell Matrigel® invasion assay was started. B) Wells were previously treated for 48h with conditioned mediums of 786O- CYMR Blank cells with and without cumate. Then, identical number of cells were plated into the wells and the same conditions were applied.

Furthermore, we decided to inhibit its enzymatic activity in order to evaluate whether it reversed the effects observed in invasion. We performed a transwell Matrigel® invasion assay using conditioned media of CPE Inducible cells with and without cumate and we added guanidinoethylmercaptosuccinic acid (GEMSA). This molecule was defined many years ago as the most potent CPE inhibitor (Fricker et al., 1983; Strittmatter et al., 1984).

As expected, results confirmed an increase of invasion due to secreted CPE as in previous experiments. However, the effect could not be reversed when GEMSA was added into

the media, suggesting that CPE was maybe acting as a chemoattractant or as a ligand by inducing cell invasion regardless of its enzymatic activity (Figure 53).

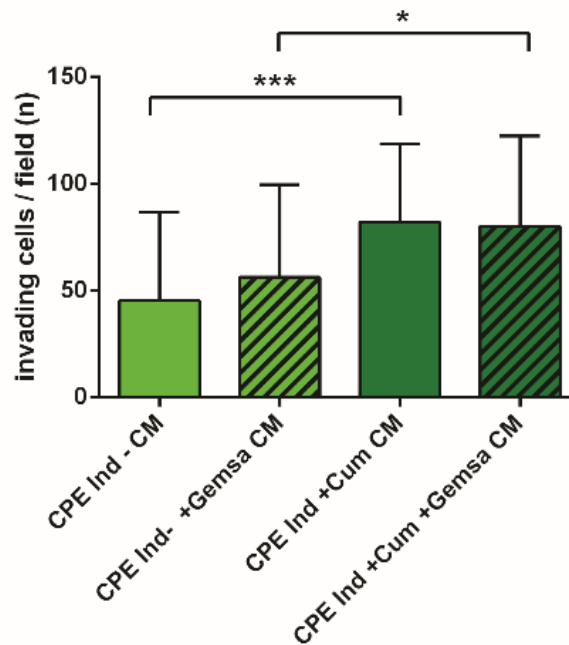


**Figure 53. Effects in invasion produced by soluble CPE were not reversed with an inhibitor of its enzymatic activity.** Transwell Matrigel® invasion assay of 20.000 786O- CYMR Blank cells plated into each well. Conditioned media of 786O- CYMR Inducible cells with and without cumate were placed into the bottom of the transwells. Gemsa at 20µM was added in order to inhibit CPE.

Altogether, these results confirmed a clear induction of 786O- cell invasion by secreted CPE through an already non-discovered mechanism which seemed not to involve its enzymatic activity.

Due to these encouraging results, we decided to validate a possible relation between our candidate and the metastatic process *in vivo*.

### 3.1.5 Effects of CPE expression in *in vivo* models of 786O-

We decided to start by performing intravenous injection of tumor cells, which is generally considered a standard model for studying hematogenous dissemination. Cancer cells were directly inoculated into the venous circulation through the tail vein of the mice in



order to force the seeding of cells in the lungs, thus focusing on the relation of tumor cells and the later phases of the metastatic process.

After 4 months, when some animals were presenting symptoms, mice were sacrificed and macrometastases were analyzed. Despite results were not statistically significant, it seemed that CPE Constitutive cells had been able to generate more macrometastases compared to Blank cells (Figure 54).

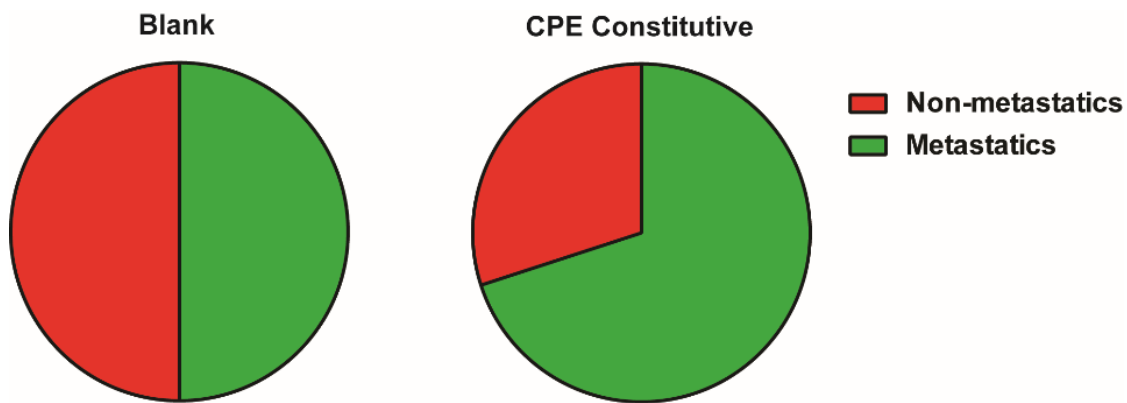


**Figure 54. CPE Constitutive cells seemed to have the ability to generate more macrometastases than Blank cells when being injected through tail vein.** Radial representation of the percentage of macrometastases evaluated at the time of sacrifice (after 4 months). Ten mice were evaluated from each group. Differences were not statistically significant.

In search of a more accurate measurement, lungs from mice were analyzed microscopically. Contrary to the macroscopic results, we observed that, regardless of CPE expression, no differences could be observed, either in the number of affected lung lobes (Figure 55A) or when quantifying the total metastasis area density (Figure 55B).



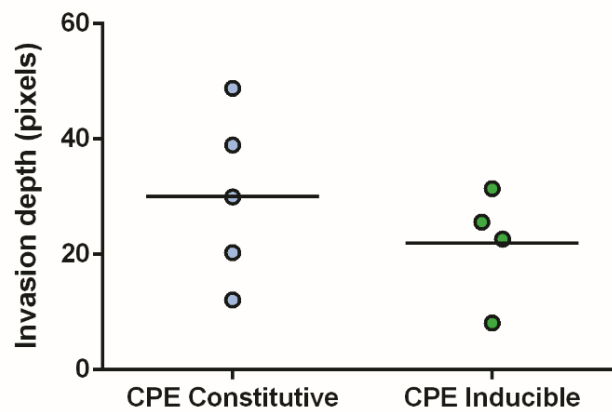


**Figure 56. CPE-expressing tumors did not show an increase in the invasive phenotype.** Five tumors generated with CPE Constitutive cells and four tumors generated with CPE Inducible cells were evaluated. Invasion depth was calculated from pictures at 0.57X of vimentin immunohistochemistry in order to evaluate the entire invasion front.

In addition, we wanted to determine whether CPE overexpression could increase the percentage of metastasis reported in 786O-. Hence, we analyzed the lungs of the mice during passages.

Results confirmed the already reported metastatic data from 786O- tumors. Nevertheless, CPE expression was not able to enhance the metastatic capacity of these animals (Figure 57).

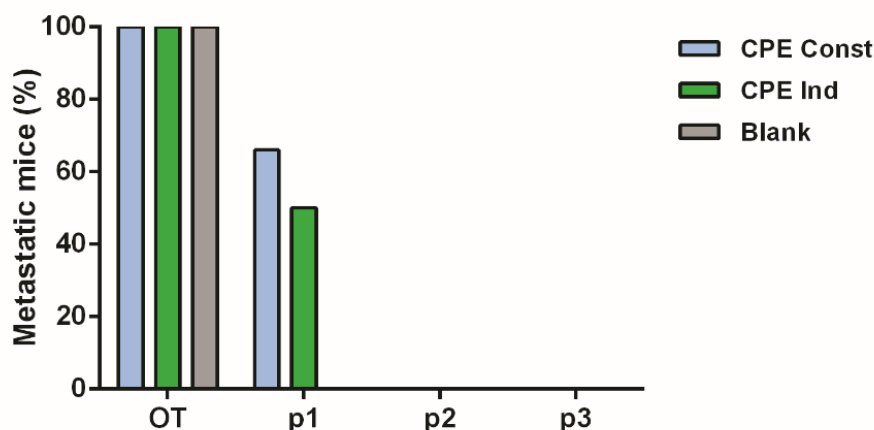


**Figure 57. CPE expression was not enough to enhance the metastatic potential of 786O- tumors.** Percentage of metastasis was calculated by microscopically analyzing the lungs from mice of the three groups (CPE Constitutive (n=8), CPE Inducible (n=8) and Blank (n=7)) from orthotopic to passage 3. Positivity was determined by vimentin immunohistochemistry.

At this point of the study, we had been able to report some effects of secreted CPE in 786O- cell invasion. However, these effects could not be later confirmed *in vivo*, since CPE overexpression was not enough to make 786O- cells more metastatic, neither when they were injected through the tail vein, nor when they generated kidney tumors.

One of the aims of our study was to validate our metastatic candidates at a functional level. Owing to these results, we were not able to confirm this functionality of CPE *in vivo*, probably due to the complexity of its underlying mechanism and the lack of knowledge about it in the field. Therefore, we were prompted to invest our available resources in validating other putative candidates involved in metastasis obtained from previous RNA and exome analyses of Ren 50 and Ren 50M tumors in order to fulfil our ultimate goal of finding prognostic markers and therapeutic targets with a clear relation to metastasis *in vitro* but also *in vivo*.

### **3.2 COAGULATION PATHWAY**

As depicted in section 1.2, the coagulation pathway was determined as a group of genes possibly related to metastasis, since they were found to be upregulated in Ren 50M metastatic tumors compared to Ren 50 in GSEA results obtained from processing RNA sequencing data. In addition, despite we have not been able to elucidate the underlying reason, we have also observed a clear difference in the color of the mice skin, which suggests an alteration in the coagulation pathway.

The coagulation system is known for its role in hemostasis. It is composed of vessel walls, platelets, coagulation factors, inhibitors and the fibrinolytic system, which altogether mediate blood clotting. There are several cascades involving coagulation proteins and enzymes which converge downstream in thrombin generation, the most important enzyme of this pathway. Overall, these contributions constitute a tightly controlled system of procoagulant and anticoagulation mechanisms, leading to a homeostatic balance of blood clotting and vascular integrity (Chan and Paredes, 2013).

Several studies have suggested an implication of blood coagulation in cancer progression. In fact, thrombosis is frequently diagnosed as one of the earliest manifestations in cancer patients and a significant correlation between thromboembolic events and tumor aggressiveness has been demonstrated, leading to worse prognosis (Lima and Monteiro, 2013). In RCC, hypercoagulability has been defined as a survival prognostic factor in metastatic patients (Tsimafeyu et al., 2009).

### 3.2.1 Coagulation Factor XIII

Blood coagulation factor XIII (FXIII or F13) is a 320 KDa protransglutaminase tetrameric protein. It is a zymogen harboring two identical catalytic A and two identical carrier/inhibitory B subunits ( $A_2B_2$ ), whose genes are located in chromosomes 6p24-25 and 1q31-32.1 and are named *F13A1* and *F13B*, respectively. Subunits A are believed to be synthesized in cells of bone marrow origin, although hepatocytes seem to also contribute. On the other hand, B subunits are synthesized in the liver (Muszbek et al., 1996)

FXIII circulates in the plasma as a tetramer ( $A_2B_2$ ), since B subunits are not stable in plasma on their own. Intracellular forms are synthesized in tissues and, in this localization, FXIII lacks B subunits and is therefore structurally a homodimer of potentially active A subunits ( $A_2$ ) (Muszbek et al., 1996).

FXIIIA is primarily expressed in cells of bone marrow origin, such as platelets, megakaryocytes, monocytes, monocyte-derived macrophages, as well as in their precursor cells. Its expression has also been detected in chondrocytes, osteoblasts and osteocytes. In contrast, FXIIIB is mainly expressed in the liver (Muszbek et al., 2011).

FXIII protein activation occurs at the final phase of the coagulation cascade by the proteolytic action of thrombin in the presence of calcium ( $Ca^{2+}$ ) (Lorand et al., 1974). This activation leads to a dissociation of the  $A_2$  and  $B_2$  subunits of the tetramer, resulting in identical forms of the tissue and plasma FXIIIA. At this point, FXIIIA acts by crosslinking fibrin  $\alpha$  and  $\gamma$  chains, thus stabilizing the clot by means of providing mechanical strength,

rigidity and elasticity, making it more resistant to fibrinolysis (Lorand, 2001) (Figure 58). In addition, it acts by cross-linking the major antifibrinolytic protein,  $\alpha 2$ -antiplasmin, to fibrin or fibrinogen, hence preventing the clot from premature degradation (Sakata and Aoki, 1980).

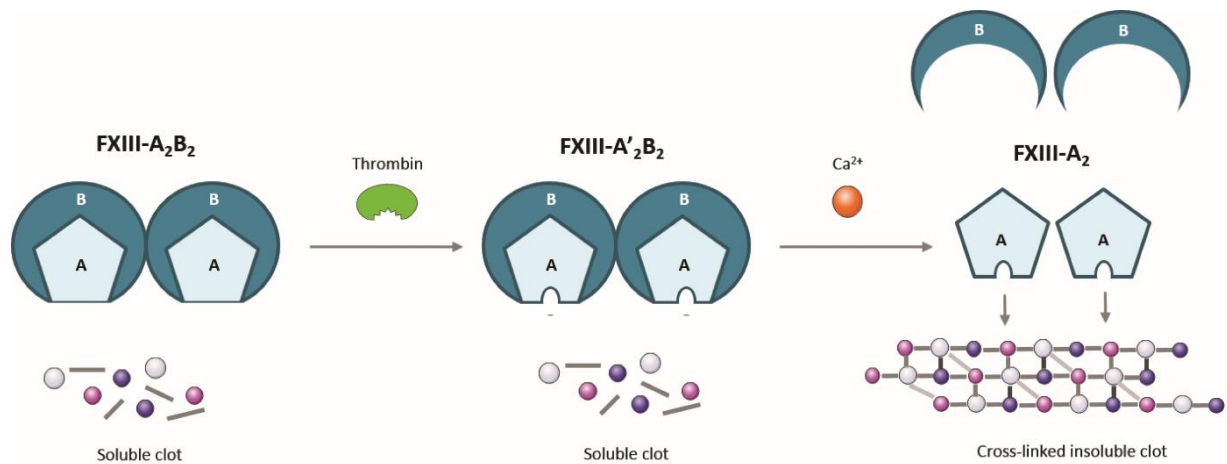


**Figure 58. Schematic representation of FXIII activation and its role in coagulation.** Tetrameric FXIII-A<sub>2</sub>B<sub>2</sub> protein is converted to activated FXIII-A<sub>2</sub> by thrombin in the presence of calcium and fibrin and acts by stabilizing the clot. Image has been adapted from (Corifact®, 2018).

Over the last two decades, it became evident that FXIII not only plays an essential role in clotting, but also has important biological roles outside of hemostasis.

FXIII<sub>A</sub> has been described to play some roles in angiogenesis, as it participates in tissue repair, tissue remodeling and wound healing. It promotes such processes by cross-linking ECM proteins and by promoting cellular signaling in leukocytes and endothelial cells. It acts by inducing endothelial cell proliferation and migration and inhibiting apoptosis, an action which depends on its transglutaminase activity, since the proangiogenic capacity was demonstrated to be abolished by blocking the active site (Dardik et al., 2005).

Apart from its role in angiogenesis, a broad range of substrates of FXIII have been identified, allegedly implying multiple functions for this factor (Richardson et al., 2013). FXIII plays an important role in ECM deposition and osteoblast differentiation. In addition,

it has been identified as a novel obesity gene and it has been described to participate in the modulation of immune responses (Schroeder and Kohler, 2016).

In the cancer field, A subunit of FXIII has been reported in some leukemias. Its expression has been found in leukemic lymphoblasts (Simon et al., 2012), as well as in myeloblasts and monoblasts from Acute Leukemias (Kiss et al., 2008). Furthermore, a correlation between higher FXIII activity and advanced stages in non-small cell lung cancer has been proved, which suggests that FXIII could be potentially used as a biomarker in this type of cancer (Lee et al., 2013). In addition, a mutation which increases FXIII activity has been associated to higher oral cancer risk (Vairaktaris et al., 2007). Finally, and as previously described in the Introduction of this thesis, FXIII is a thrombin substrate implicated in hematogenous dissemination of cancer cells, preventing NK-mediated clearance of CTCs (Palumbo et al., 2008).

### 3.2.1.1 F13A expression in RCC cell lines

As performed with CPE, we firstly decided to test F13A expression in different RCC cell lines, both at RNA and at protein level. Results from a Taqman® Real-Time PCR and a western blot did not show any expression of F13A in any of the cell lines tested (Figure 59).

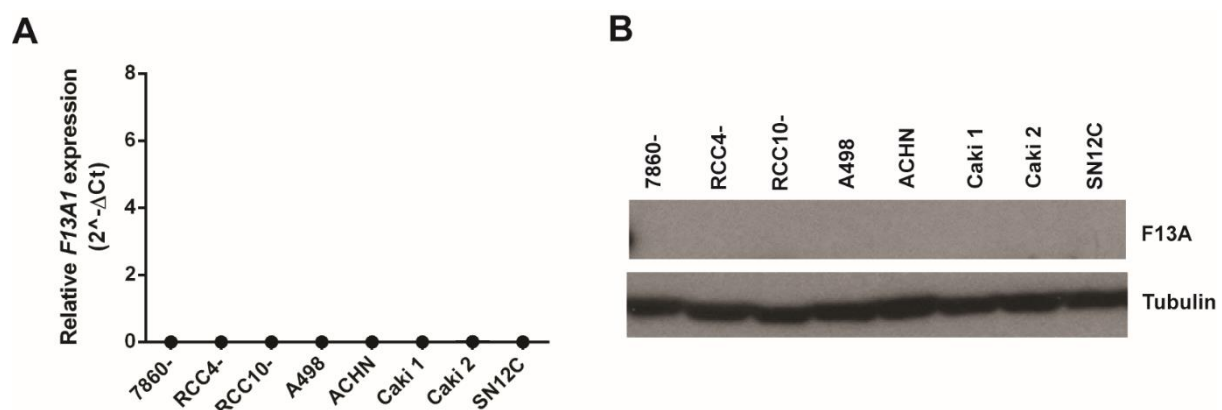


**Figure 59. F13A expression could not be detected in any of the renal cell lines tested.** A) Results obtained from Taqman® Real-time PCR of eight cell lines derived from RCC. RNA quantification of *F13A1* was normalized by *HPRT1* measured by 2<sup>-ΔΔCt</sup>. B) F13A protein detection by western blot. Analyzed samples were the same used in the Taqman® assay.

Following the same rationale as for the CPE results mentioned above, we decided to use the 786O- cell line in order to obtain F13A-expressing cells.

### 3.2.1.2 Generation of a F13A-expressing cell line

In order to obtain F13A-expressing 786O- cells, we transfected them with two different pCMV3 vectors. On one hand, a group of cells was transfected with a pCMV3-*F13A1* in order to obtain a constitutive F13A-expressing cell line. On the other hand, a second group of cells was transfected with a pCMV3-Empty vector as a negative control.

Once cells were selected using antibiotics, we tested F13A protein expression by immunofluorescence and by western blot. As expected, no protein expression was observed in cells transfected with the Empty vector, and a clear constitutive expression was detected in cells transfected with the pCMV3-*F13A1* vector (Figure 60).

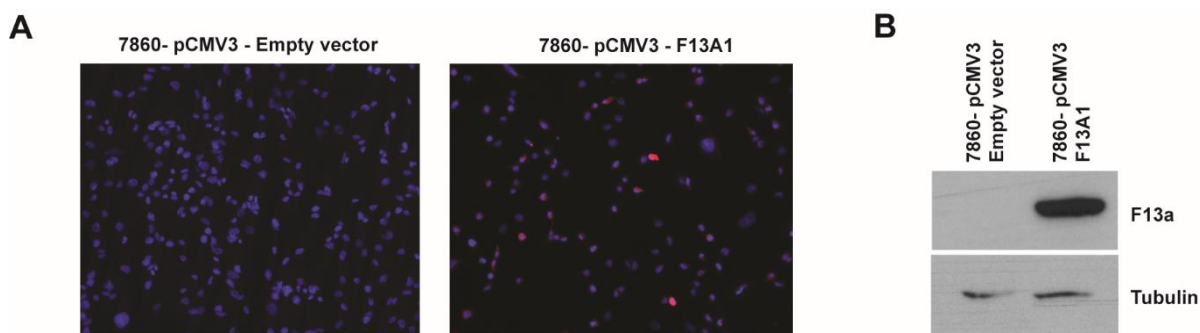


**Figure 60. Only cells transfected with the pCMV3-*F13A1* vector expressed the protein.** A) Immunocytofluorescence of F13A protein in 786O-pCMV3 Empty vector and *F13A1* transfected cells. Pictures were taken at 20X. B) F13A protein detection by western blot from lysates of both type of cells.

Given this detectable high expression of F13A in 786O- transfected cells, we decided to start to validate its possible roles in metastasis.

Since, in previous CPE results, we observed effects *in vitro* but could not reproduce them *in vivo*, we decided to directly validate whether F13A-expressing cells had an advantage in generating metastasis in the mice before starting *in vitro* investigations.



### 3.2.1.3 Generation of F13A-expressing tumors

Accordingly, both 786O- F13A and Empty vector cells were injected into the kidney of different mice and tumors were perpetuated during some passages.

First of all, it was necessary to confirm that F13A-expressing cells did maintain protein expression in tumors. Results from immunohistochemistry and western blot confirmed a very high expression of our candidate in tumors generated with F13A-expressing cells. On the other hand, no expression was detected in control tumors generated with Empty vector cells (Figure 61).

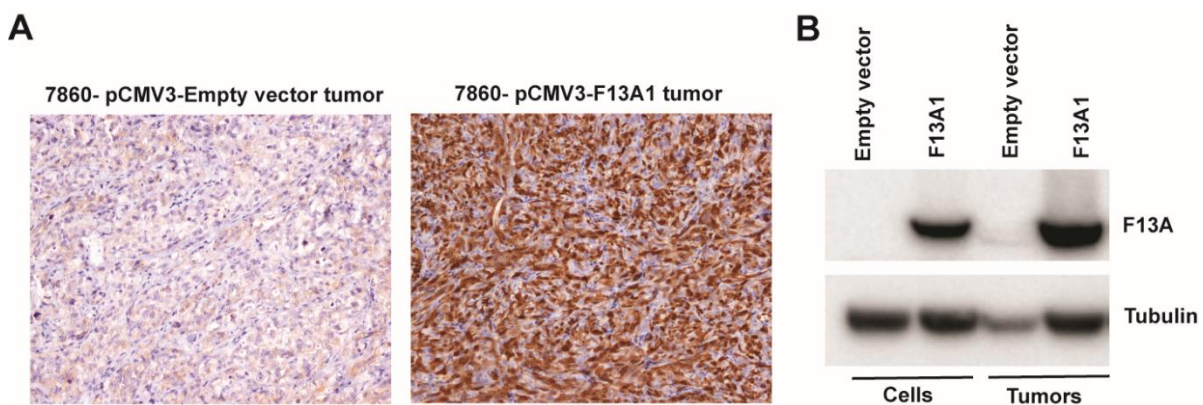


**Figure 61. Only 786O- tumors generated with pCMV3-F13A1 transfected cells expressed F13A protein.** A) Immunohistochemistry of F13A protein in 786O- tumors transfected with pCMV3 Empty Vector and F13A1 vectors. Pictures were taken at 20X. B) F13A protein detection by western blot from lysates of both types of cells and tumors.

Once F13A protein expression in tumors was validated, we decided to study *in vivo* its possible relation with metastasis.

### 3.2.1.4 Effects of F13A expression in 786O- tumors

In order to determine whether F13A-expressing tumors invaded more than their corresponding controls, invasion depth was quantified in tumors from both groups. Results did not show any advantage of F13A expression in relation to the invasion capacity (Figure 62).

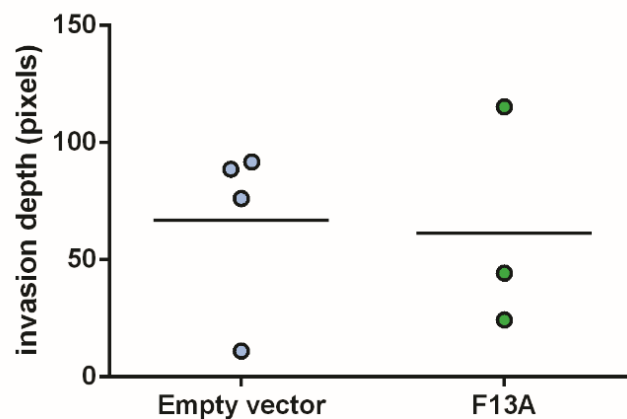


**Figure 62. F13A-expressing tumors did not show an increase of the invasion capacity.** A) Invasion depth was calculated from pictures of a vimentin immunohistochemistry. Samples of four 786O- pCMV3-Empty Vector tumors and three 786O- pCMV3-F13A1 tumors were analyzed. Pictures were taken at 0.57X in order to evaluate the entire invasion front.

Next, with the aim of evaluating whether F13A expression could increase the metastatic capacity of 786O- tumors, we analyzed the lungs from animals from both groups. As expected from previous studies, all the orthotopic mice had metastases. Nevertheless, the capacity was lost after passage 1, despite the presence of a random metastatic animal from the Empty Vector group appeared at passage 2 (Figure 63).

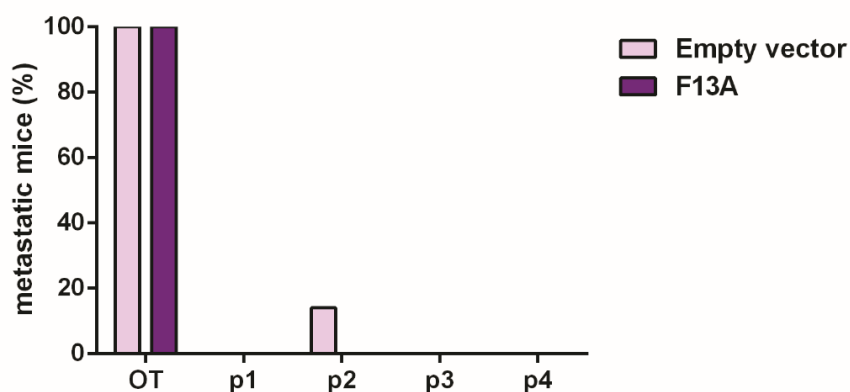


**Figure 63. F13A-expressing tumors did not show any metastatic advantage compared to controls.** Percentage of metastasis was calculated analyzing microscopically the lungs from mice of both groups (Empty vector n=15, F13A n=10). Positivity was determined by vimentin immunohistochemistry.

To sum up, we were not able to confirm that F13A expression was enough to generate metastasis in an *in vivo* model of 786O-.

### 3.2.1.5 CPE expression by F13A-expressing tumors

Despite discouraging results had been obtained up to this stage, F13A-expressing tumors did provide us with a highly unexpected result. Strikingly, we found that when tumors expressed F13A, they did also overexpress CPE. Furthermore, when testing the corresponding cell lines, we could confirm that the crosslink between these two proteins occurred *in vivo* but not *in vitro* (Figure 64).

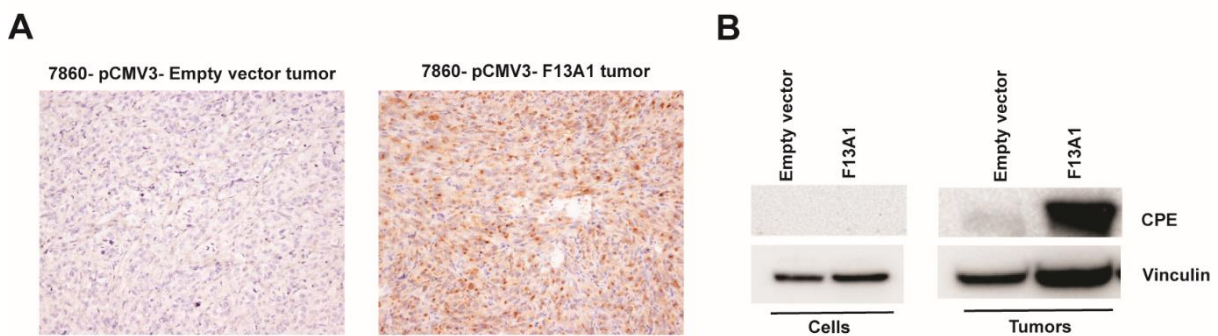


**Figure 64.** There was a crosslink between F13A and CPE *in vivo*. A) Pictures of an immunohistochemistry of CPE protein in 786O- tumors transfected with Empty Vector and F13A1 pCMV3 vectors (20X). B) CPE protein detection by western blot from lysates of both type of cells and tumors.

In conclusion, F13A upregulation was confirmed to be unexpectedly related to CPE expression. However, their expression was still not enough to engage the multistep metastatic process in 786O- tumors.

Therefore, we decided to evaluate the next putative candidate in search for a functionally direct effect in metastasis.

---

### 3.2.2 Coagulation Factor II Thrombin Receptor or Protease-Activated Receptor 1

Homeostasis of blood coagulation depends in part on protease activated receptor (PAR)-signaling (Isermann, 2017). Protease-activated receptors (PARs) are the largest family of signaling receptors expressed in mammalian cells. This family consists of seven-transmembrane G-protein coupled receptors (GPCRs) localized at cell surfaces that are activated uniquely by the cleavage of their extracellular N-terminus at a specific site, allowing the internal ligand to autoactivate (Alberelli and De Candia, 2014).

Four members of this family (PAR1 to PAR4) have been identified and, depending on each receptor, they can be activated by different proteinases. Thrombin is the physiologic activator of PAR 1/3/4, whereas PAR2 is activated by trypsin-like enzymes as well as coagulation factors VIIa and Xa (Coughlin, 2005). Nevertheless, recent work has confirmed PAR2 activation by high concentrations of thrombin (Mihara et al., 2016). The activation of these receptors triggers signaling mechanisms involved in different processes, such as migration, invasion, proliferation or the production of chemotactic and proangiogenic factors, regulating both physiological and pathological processes in multiple organs (Han et al., 2011).

Protease-activated receptor 1 (PAR1), also named Coagulation Factor Thrombin Receptor 2 (F2R), is a member of the PARs family composed of a sequence of 425 amino acids and a molecular mass of 68-80 kDa, with a reduction to a 36-40 kDa by deglycosylation (Soto et al., 2015; Soto and Trejo, 2010). The corresponding gene is located on chromosome 5q13.3 and it is 27 Kb long (Déry et al., 1998).

F2R is activated by thrombin, which cleaves its amino-terminal exodomain between residues Arg 41 and Ser 42 (LDPR41/42SFLLRN) in an irreversible way. When this occurs, a new N-terminal domain is unmasked and it can act as a tethered ligand by binding to the core of the receptor in order to initiate transmembrane signaling (Vu et al., 1991). No cofactor is needed for the induction of this signaling (Wojtukiewicz et al., 2015) (Figure 65).

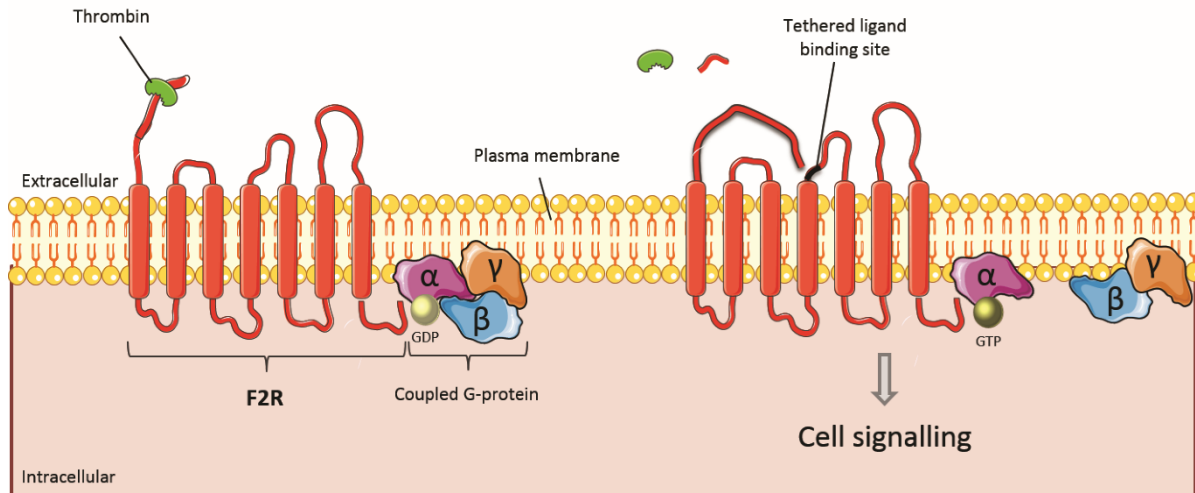


**Figure 65. Schematic representation of thrombin-mediated PAR1 activation.** After PAR1 cleavage by thrombin, a new amino-terminus domain binds to the body of PAR1 itself, thus signaling G-proteins. Image has been adapted from (Alberelli and De Candia, 2014).

Signaling from F2R is rapidly terminated by its phosphorylation and internalization. However, unlike classic GPCRs, which are eventually recycled, F2R is sorted to lysosomes for degradation. Nevertheless, some of the molecules are able to escape and return to cell surface (Trejo et al., 1998).

F2R expression was primarily found in endothelial cells and in fibroblasts. Later, it was also detected in other cell types, such as smooth muscle cells, T-cells, mast cells, glial cells and neurons (Isermann, 2017).

As previously described in the introduction of this thesis, F2R is also involved in cancer through different mechanisms. On the one hand, this receptor is involved in the early steps of the metastatic cascade, since its interaction with integrins has been demonstrated to enhance the invasive phenotype of tumor cells (Cohen Even-Ram et al., 2001). On the other hand, it also plays essential roles in tumor cell systemic circulation. It acts both in the surface of tumor cells by enhancing procoagulant activity and in the surface of platelets by facilitating the cohesion of heteroaggregates formed by themselves and tumor cells, thus preventing NK clearance (Gay and Felding-Habermann, 2011; Palumbo, 2008).

### 3.2.2.1 F2R expression in RCC cell lines

As previously performed with the above-described candidates, the first thing to evaluate was F2R expression in RCC cell lines.

In contrast to the results obtained for the other two candidates, Taqman® assay of *F2R* showed expression in some of the tested lines. The highest levels were expressed by RCC4- and SN12C cells (Figure 66).

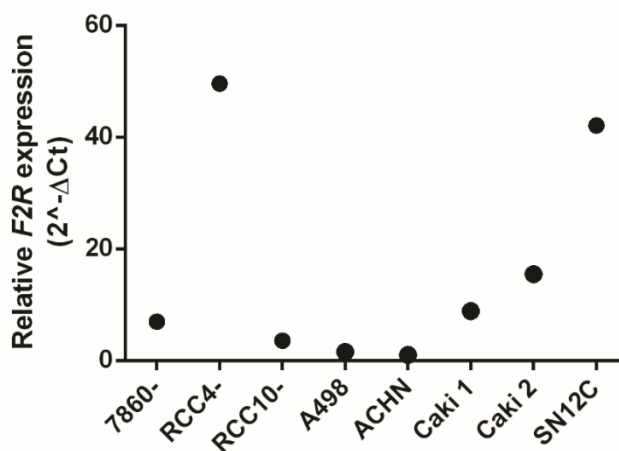


**Figure 66. RCC4- and SN12C cell lines presented the highest *F2R* RNA expression.** Results obtained from a Taqman® Real-time PCR of eight cell lines derived from renal carcinomas. RNA quantification of *F2R* was normalized by *HPRT1* and measured by  $2^{-\Delta CT}$ .

Due to the confirmation of previous studies in our group about their high aggressiveness and their elevated capacity to do metastasis *in vivo* (data not shown), SN12C cells were chosen to evaluate our candidate.

### 3.2.2.2 F2R protein expression in SN12C cells and tumors

In order to prove F2R expression in SN12C cells at the protein level, an immunocytofluorescence of SN12C cells and an immunohistochemistry of SN12C tumors were performed. Results confirmed a clear expression in both cases (Figure 67).

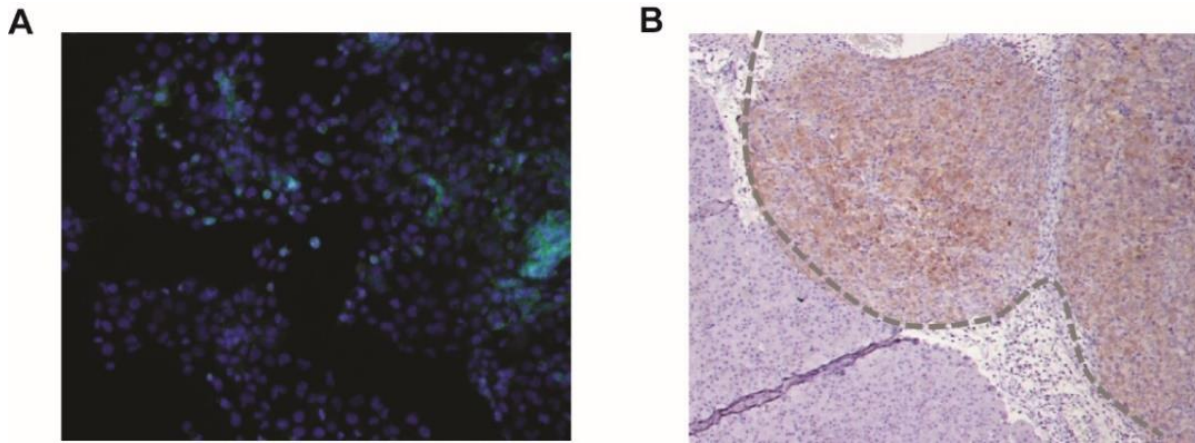


**Figure 67. Both SN12C cells and tumors expressed F2R protein.** A) Immunocytofluorescence of F2R in SN12C cells (10X). B) F2R Immunohistochemistry of a SN12C tumor. Cells were injected into the kidney of a mouse and then tumors were perpetuated. Grey line represents the tumor-kidney contact. Picture was taken at 10X.

After this validation, we decided to use these cells to perform *in vitro* experiments. In addition, Ren 50 and 50M tumors were not growing at that moment, so we determined SN12C as a proper *in vivo* model in order to study the roles of F2R in metastasis.

### 3.2.2.3 Effects of F2R inhibition in *in vivo* models of SN12C

Due to the large volume of published studies describing the role of PAR receptors in the last metastatic steps, we decided to study if we could see any effect in metastasis when inhibiting F2R.

We decided to inject SN12C cells through the tail vein. Then, mice were orally treated with vehicle or Vorapaxar, a competent selective F2R inhibitor already approved in patients for the antithrombotic treatment of coronary and peripheral vascular disease (Chackalamannil et al., 2008).

F2R inhibition did not show a decrease in the number of affected lung lobes. However, a clear decreasing tendency in the total metastasis area density was quantified in animals treated with the inhibitor (Figure 68).

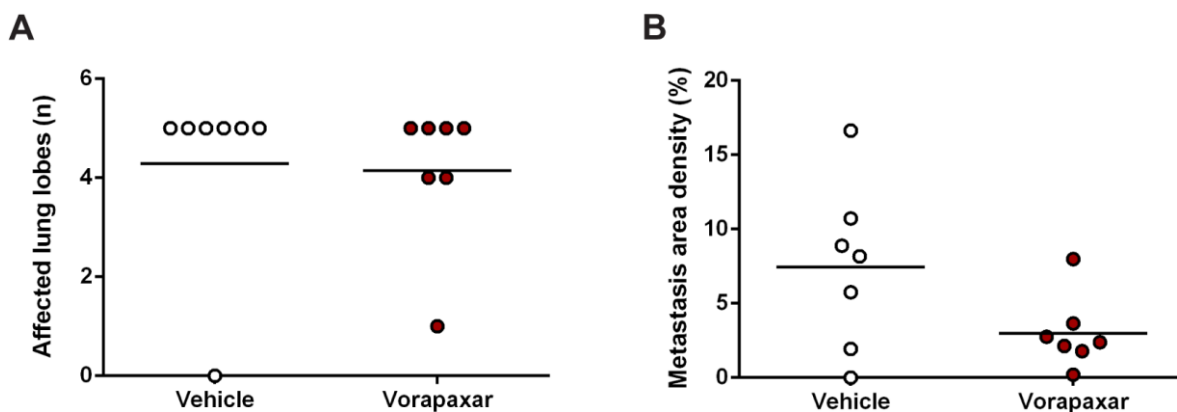


**Figure 68. F2R inhibition did not reduce the number of affected lung lobes but showed a reduction of the total metastasis area density.**  $10^6$  SN12C cells were injected through tail vein. Mice were split into two groups and were orally treated with vehicle (n=7) or Vorapaxar (n=7) at a dose of 20mg/kg/day since the day after injection. Analyses were performed using a vimentin immunohistochemistry. A) Microscopically determination of metastatic positive lung lobes. B) Quantification of the percentage of the total metastasis area density. For quantification, total metastasis area was normalized by the total lung area quantified for each animal.

For the same reasons than in F13A results and because of the implication of F2R in invasion described in the literature, we also decided to validate the entire metastatic process.

Seeking to tackle it, we injected SN12C cells into the kidney of mice and tumors were perpetuated during some passages. Then, two groups were orally treated with vehicle or Vorapaxar.

In order to study whether F2R was affecting tumor growth, tumor volume was monitored during all the treatment. We could determine that tumors presented the same progression rate regardless of F2R inhibition (Figure 69).



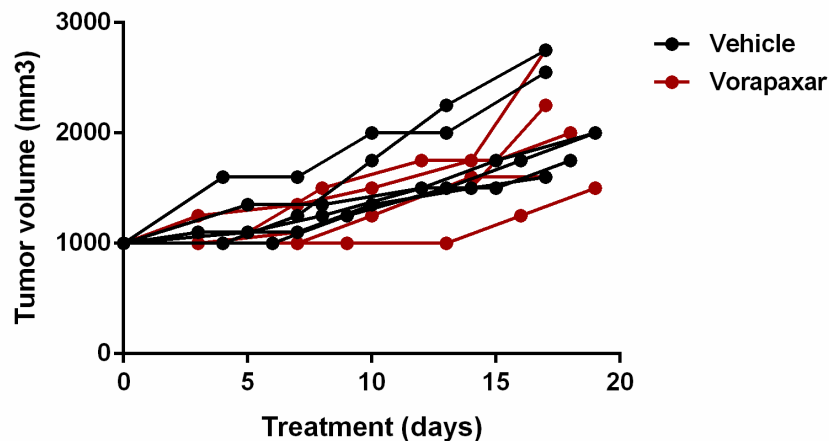


**Figure 69. F2R inhibition did not affect tumor growth.** Tumor volume was evaluated by palpation and treatment started when it measured 1000mm<sup>3</sup>. Six mice were treated with vehicle and five mice with Vorapaxar at a dose of 20mg/kg/day. Measurements were registered during all the experiment (17-19 days).

We next decided to test whether F2R inhibition was affecting tumor invasion. First, we qualitatively classified tumors regarding their invasive phenotype. F2R inhibition demonstrated a tendency of invasion reduction compared to controls (Figure 70).

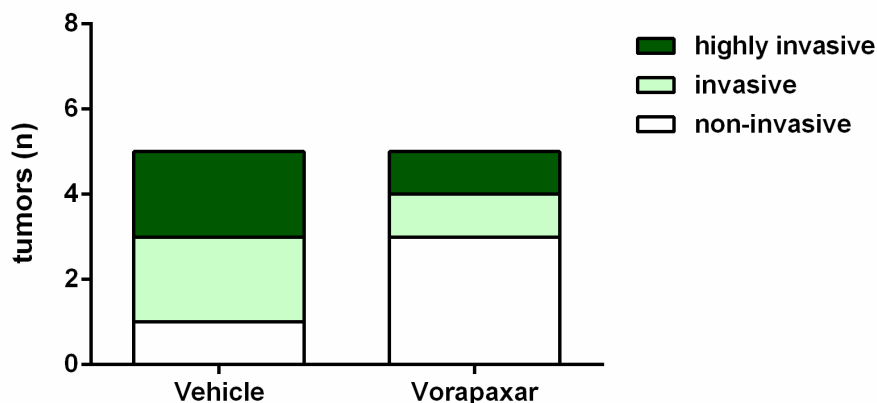


**Figure 70. F2R inhibition with Vorapaxar showed a decrease in the invasive phenotype.** Hematoxylin-eosin stainings were microscopically classified regarding their invasive phenotype into three groups. Tumors treated with F2R inhibitor showed a less invasive phenotype compared to controls. Five tumors from each group were analyzed. Differences were not statistically significant.

Then, we characterized tumor invasion by quantifying tumor invasive fronts (Figure 71A). Results did not show a significant difference between both groups. However, Vorapaxar-

treated animals showed a downward trend in tumor invasion compared to mice treated with vehicle solution (Figure 71B).

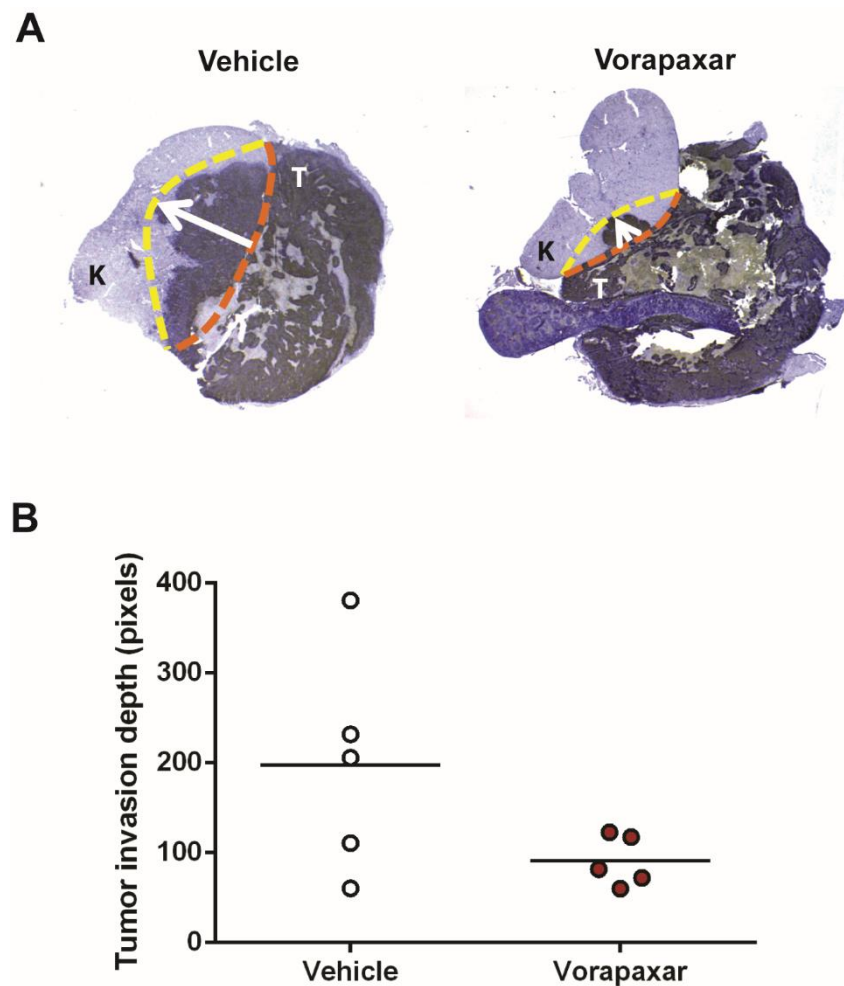


**Figure 71. F2R inhibition showed a decrease in invasion.** A) Pictures of a vimentin immunohistochemistry of five control tumors and five Vorapaxar-treated tumors. Pictures were taken at 0.57X and the invasive front was drawn and quantified. T: Tumor. K: Kidney. B) Tumor invasion depth quantification. Results were not statistically significant despite a clear tendency on invasion reduction.

We next wanted to study whether F2R inhibition had any effect on the metastatic capacity of SN12C tumors.

To this purpose, we performed a more thorough metastatic study analyzing lung metastases from treated and untreated mice.

We started by analyzing how many lobes were affected, and no differences could be observed (Figure 72A). However, we could quantify more and bigger lung colonies in controls compared to treated mice (Figure 72B-C).

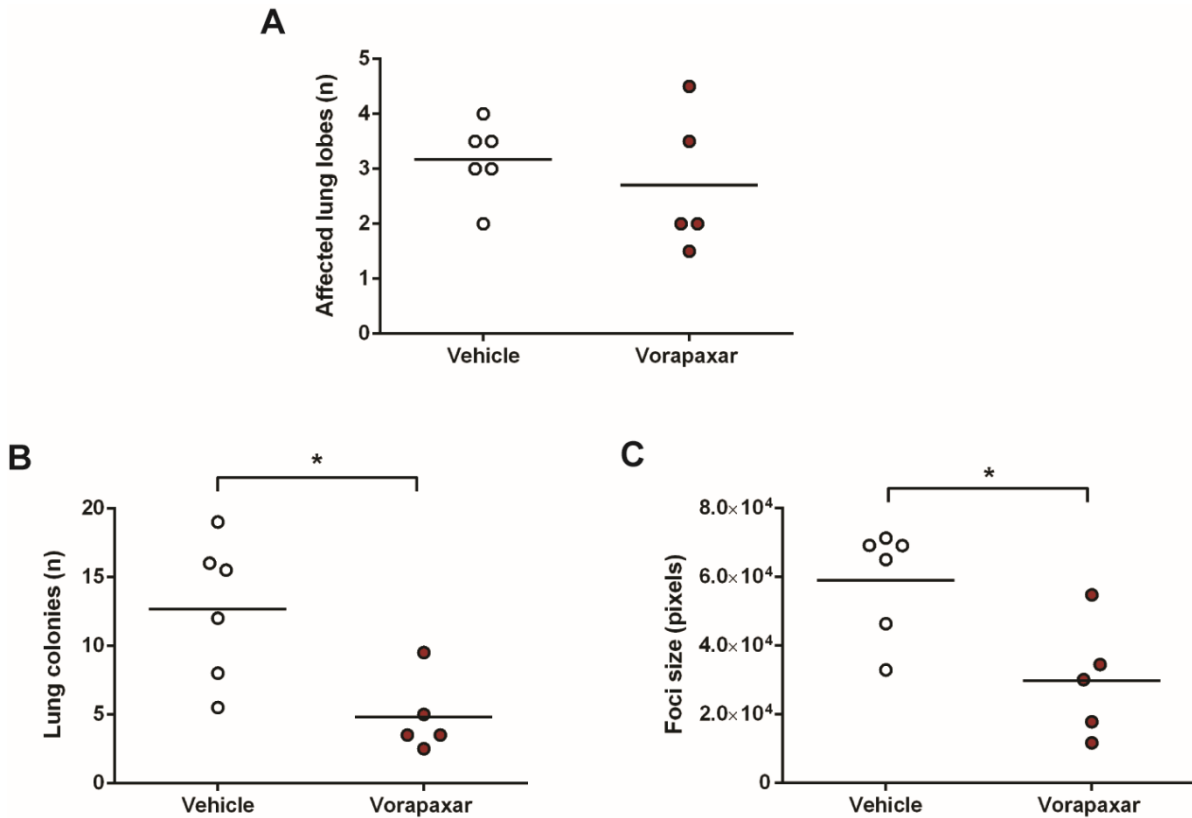


**Figure 72. F2R inhibition demonstrated a reduction of the metastatic capacity of SN12C tumors by reducing the number of lung colonies and their size.** All quantifications were performed by vimentin immunohistochemistry staining of each lung. A) Tumor cells were detected and quantification of affected lung lobes was performed. B) Number of lung colonies in each lung was determined. C) Foci size was calculated by quantifying all metastatic area normalized by the number of foci present in each lung.

Finally, F2R inhibition presented a clear reduction of total metastasis (Figure 73).

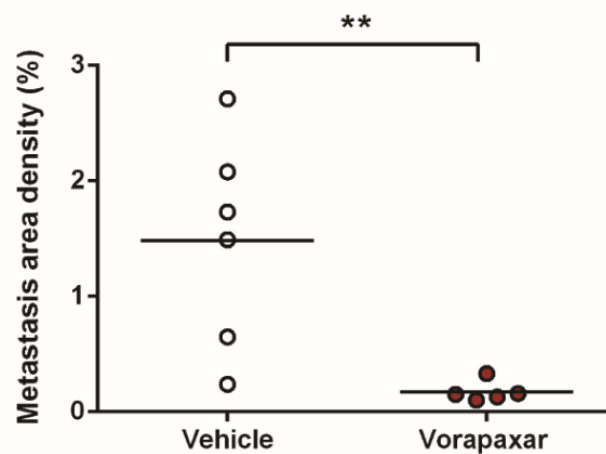


**Figure 73. F2R inhibition reduced metastasis.** Total metastasis area density was determined quantifying total metastatic area normalized by total lung area of each lung. Pictures of metastases were taken at 10X pictures of the lungs at 0.57X

Altogether, results from this experiment demonstrated that F2R inhibition clearly caused decreased metastasis in SN12C tumors, which, together with invasion, represents one of the hallmarks of cancer (Hanahan and Weinberg, 2011).

#### 3.2.2.4 Effects of F2R inhibition in SN12C cells

To assess the *in vitro* effects of F2R inhibition, we decided to use the SCH 79797 inhibitor, which is also a selective non-peptide F2R antagonist (Ahn et al., 2000). This F2R inhibitor has been established as an appropriate inhibitor *in vitro* because, unlike Vorapaxar, it does not need to be processed by the liver (Ghosal et al., 2011).

First of all, we decided to treat the cells and follow their phenotype. We could observe that when they were under SCH 79797 treatment, they completely changed their phenotype, losing some of their cell-cell contacts (Figure 74). Furthermore, the maintenance of their viability was confirmed by trypan blue staining.

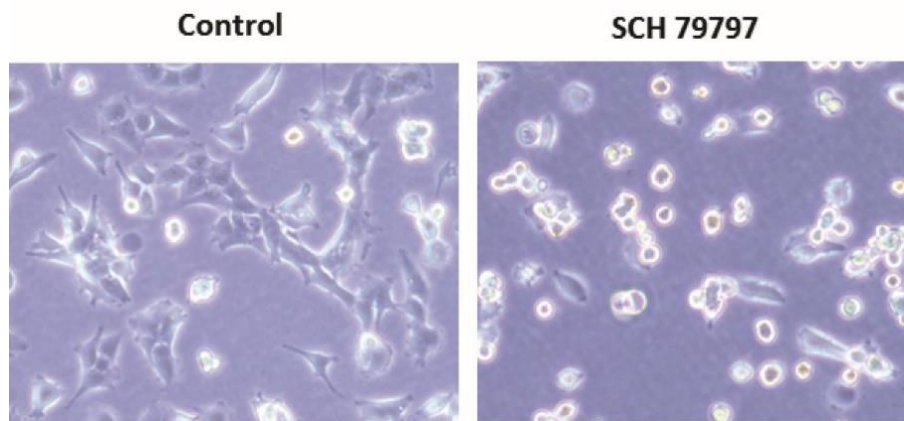


**Figure 74. F2R inhibition changed SN12C cells phenotype.** SN12C cells were plated and treated with SCH 79797 (1 $\mu$ M). Pictures at 10X were taken after 24h of treatment.

In order to assess whether these changes in cell phenotype could be enhancing their migration capacity, we performed a transwell migration assay. Results showed the same advantage in this process regardless of F2R inhibition (Figure 75).

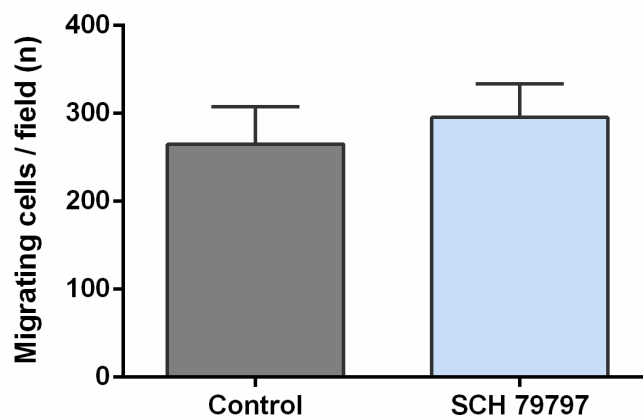


**Figure 75. F2R inhibition did not change the migration capacity of SN12C cells.** Transwell migration assay of SN12C cells with and without F2R inhibitor (SCH 79797 at 1 $\mu$ M). 100.000 cells were plated into each well and the assay was performed at 24h. Error bars represent S.D, wells/condition n=3.

Given that F2R expression has been associated to tumor invasion in the literature and that we had seen an effect in invasion when inhibiting the receptor *in vivo*, we also decided to evaluate the relation between the invasion process and our candidate *in vitro*.

Results confirmed a drastic decrease of SN12C cells invasion capacity (Figure 76) when inhibiting F2R, consistent with the effects observed with its inhibition *in vivo*.

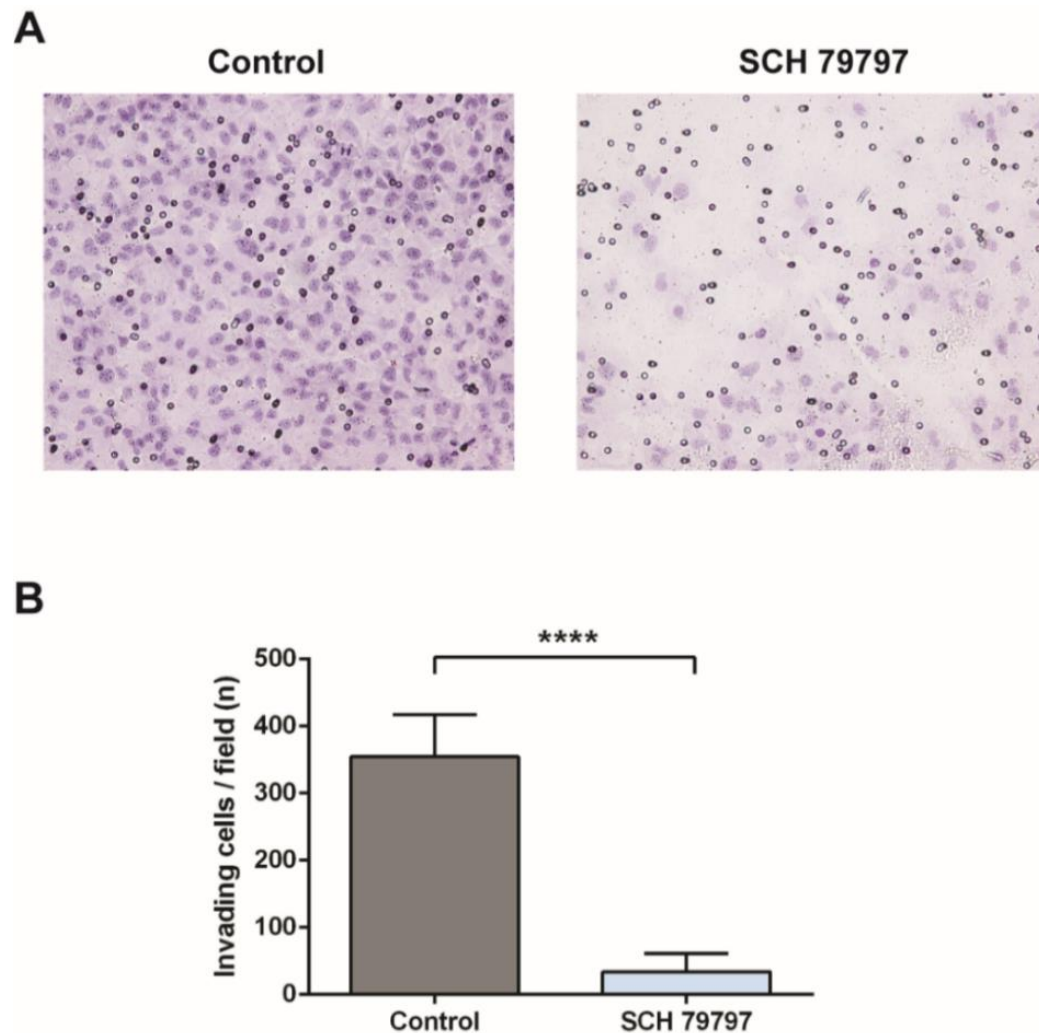


**Figure 76. F2R inhibition drastically decreased the invasion capacity of SN12C cells.** Transwell Matrigel® invasion assay of SN12C cells with and without F2R inhibitor (SCH 79797 at 1 $\mu$ M). 100.000 cells were plated into each well and the assay was performed at 48h. A) Representative images (20X) of transwell membranes hematoxylin stained from cells treated with vehicle and SCH 79797. B) Quantification of invading cells through transwell Matrigel® membranes. Error bars represent S.D, wells/condition n=3.

After gathering all the data at hand, we eventually wanted to confirm the potential of our results from one single patient in the clinic.

## 4. CLINICAL VALIDATION

In collaboration with Carlota Rubio-Pérez, from Núria López-Bigas laboratory in the Institut de Recerca Biomèdica (IRB), we further studied the relation between our candidates and clinical data from The Cancer Genome Atlas (TCGA).

### 4.1 EXPRESSION OF *CPE*, *F13A1* AND *F2R* IN ccRCC TUMORS COMPARED TO OTHER CANCER TYPES AND THE MAIN RCC SUBTYPES

First, we decided to check whether the expression distribution of our candidate genes is different across all 33 TCGA other cancer types, not only focusing on RCC.

Results revealed that ccRCC is one of the cancer types showing the highest expression rate. According to the median, *CPE* ranked sixth, *F13A1* fifth and *F2R* was the top ranked gene (Figure 77). This last result was highly remarkable and consistent, considering the overall *in vitro* and *in vivo* data reported in this work about this metastatic candidate.

We further analyzed whether RNA expression of our genes of interest could be associated to any RCC subtype. Using data from TCGA, we observed that expression of the three genes is higher in ccRCC (KIRC) compared to the other main histological subtypes, chromophobe (KICH) and papillary (KIRP) (Figure 78).

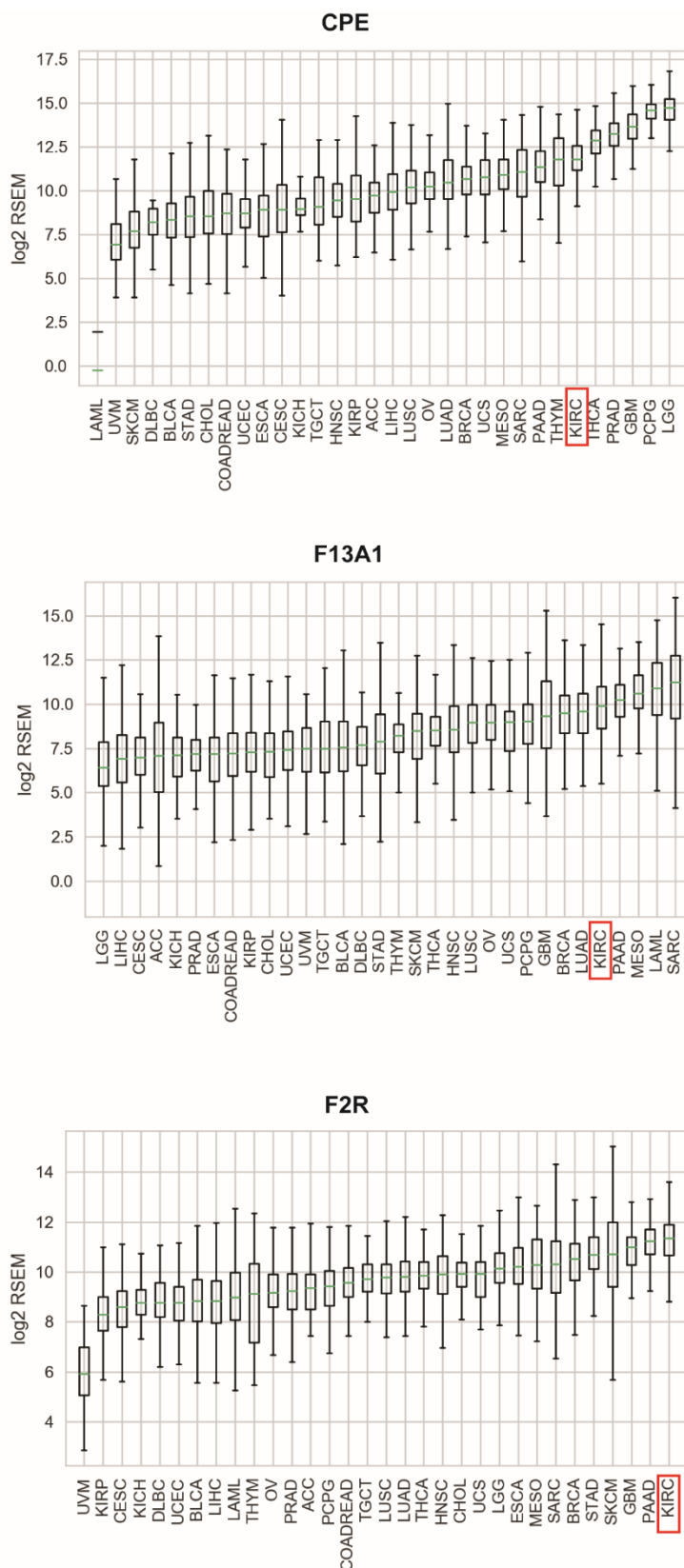


**Figure 77.** ccRCC is one of the cancer types showing the highest expression ranking of *CPE*, *F13A1* and *F2R*. Boxplots represent the distribution of expression of the three genes across all the 33 TCGA types of cancer. Expression values are expressed in log<sub>2</sub> RSEM (normalization measure of RNA seq counts).



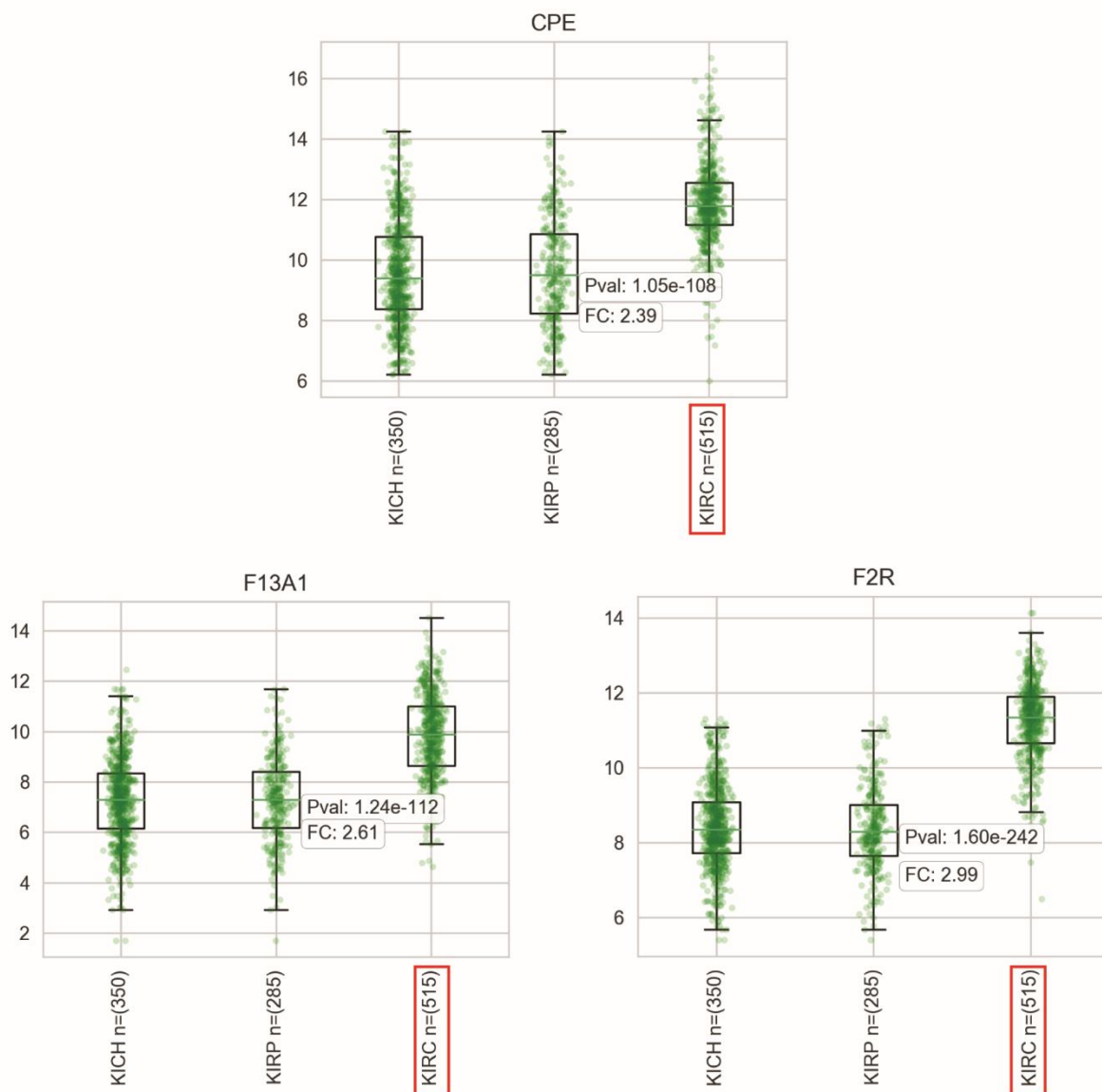


**Figure 78. CPE, F13A1 and F2R expression is higher in ccRCC compared to the other two main RCC subtypes.** Boxplots represent the distribution of expression of the three genes (each sample is represented as a dot) in KIRC, KIRP and KICH RCC subtypes. Expression values are expressed in log2 RSEM (normalization measure of RNA seq counts) and statistically significant differences were found using Mann-Whitney test when comparing KIRC expression to the other subtypes. P value and FC are represented inside the plot.

Taken together, these results suggest that there is a clear association between the overexpression of our three candidate metastatic genes and the type of cancer in which our study is focused on. Through data from patients, we have been able to confirm a specificity for these genes in the ccRCC subtype compared to the other main RCC. In addition, its expression is very high in ccRCC compared to other 33 different cancer types

available in TCGA. This combination of findings supports the conceptual premise that our model is not an isolated case and that our results can be extrapolated to, at least, other patients with ccRCC.

#### 4.2 EVALUATION OF CPE, F13A AND F2R IN RCC TISSUE SAMPLES

Provided the high RNA levels of expression of our metastatic genes in RCC, and especially in the ccRCC subtype, we decided to also validate their protein expression in a set of RCC tissue samples available in the laboratory. Results demonstrated that, for all the genes, nearly one third of samples presented positive staining for our metastatic candidates (Figure 79).

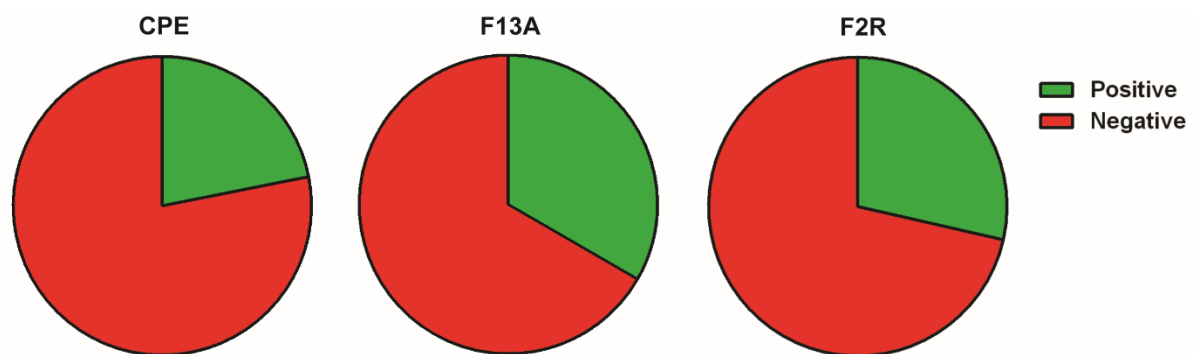


**Figure 79.** CPE, F13A1 and F2R were expressed in nearly one third of RCC tissue samples. From left to right, radial representation of the percentage of CPE, F13A and F2R positivity in RCC tissue samples. Evaluation was performed by immunohistochemistry. CPE protein was expressed in 21.8% of cases (n=32), F13A1 in the 33,3% (n=11) and F2R in the 28.5% (n=7).

Therefore, this evidence confirms again that overexpression of these proteins occurs in many RCC tumors.

#### 4.3 EVALUATION OF SURVIVAL IN ccRCC PATIENTS WITH OVEREXPRESSION OF CPE, F13A1 AND F2R

Finally, seeking to obtain more insight on the consequences of the overexpression of our metastatic candidates in the clinical setting, we wanted to investigate whether their overexpression has an impact on the prognosis of ccRCC patients. To do so, we ranked

the patients according to the expression of each individual gene and we compared the prognosis of the percentage 85 patients to the rest.

Results showed a significant correlation between *CPE* and *F13A1* RNA expression and worse prognosis in ccRCC patients (Figure 80A-B). These interesting results confirm once again that the overexpression of our metastatic candidates is not a unique fact in our Ren 50 patient and that they are clinically relevant in many patients with this cancer type. Furthermore, it is interesting to find that these two genes are related, since *F13A* overexpression induced *CPE* overexpression, and, eventually, they present similar clinical outcomes. Nevertheless, *F2R* expression is unexpectedly not influencing survival (Figure 80C).

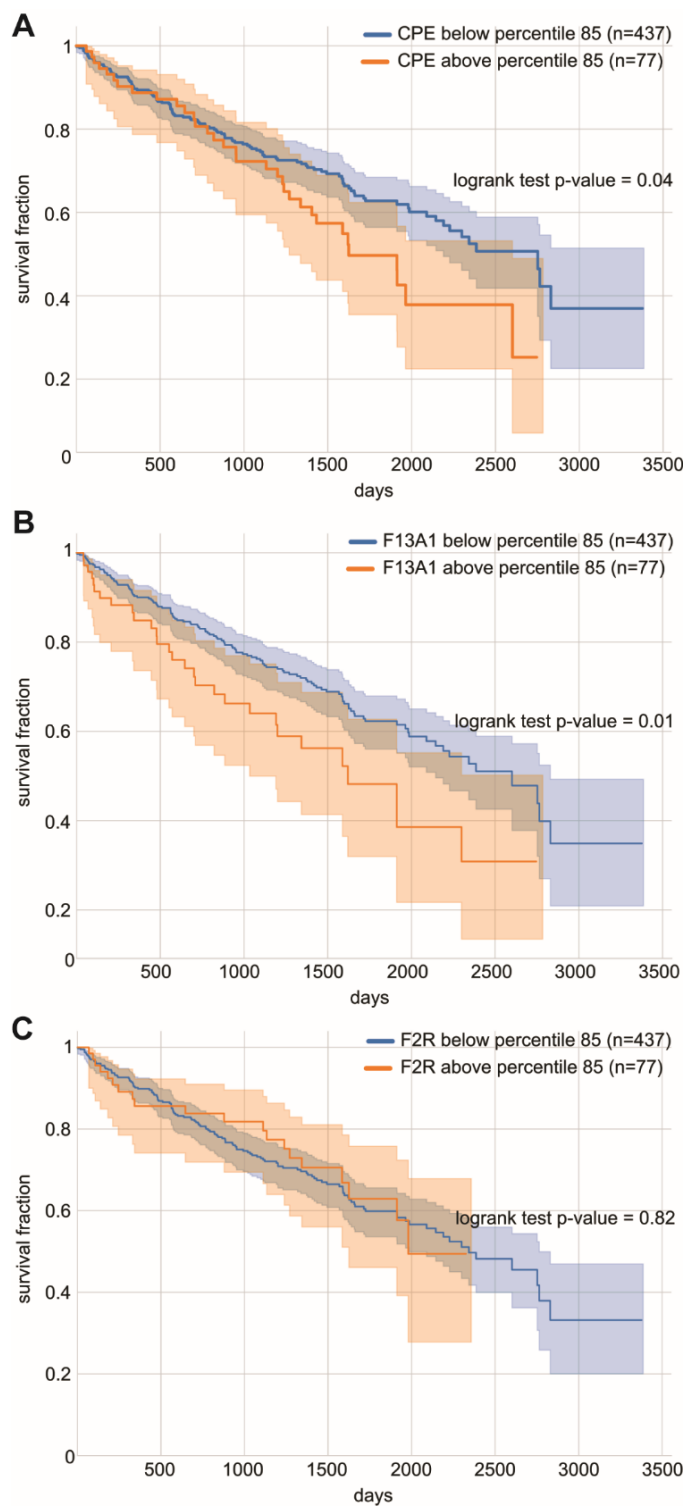


**Figure 80. ccRCC patients with an overexpression of *CPE* and *F13A1* present significant worse survival rates. On the contrary, *F2R* gene expression do not change ccRCC patient overall survival.** Kaplan-Meier plot of overall survival in 514 ccRCC patients (from TCGA). Patients were divided into two groups regarding their RNA expression levels. Blue line represents patients whose expression is below percentile 85. Orange line represents patients with an expression of these genes above percentile 85. Statistical significance is represented by the p value inside the plot, according to Log-rank test. A) *CPE* overall survival. B) *F13A1* overall survival. C) *F2R* overall survival.

Due to the lack of relation between F2R expression and patient survival, we decided to further check this parameter when considering all genes obtained in GSEA analysis with a positive enrichment core directly involved in the coagulation pathway (TFPI, SERPINE1, PAR1, F13A1 and ITGB3). These analyses were carried out in collaboration with Luis Palomero from ProCURE (ICO-IDIBELL), Barcelona.

Results did not show statistically significant differences. Nevertheless, we could observe a tendency of worse survival in patients when tumors present an overexpression of coagulation involved genes (Figure 81).

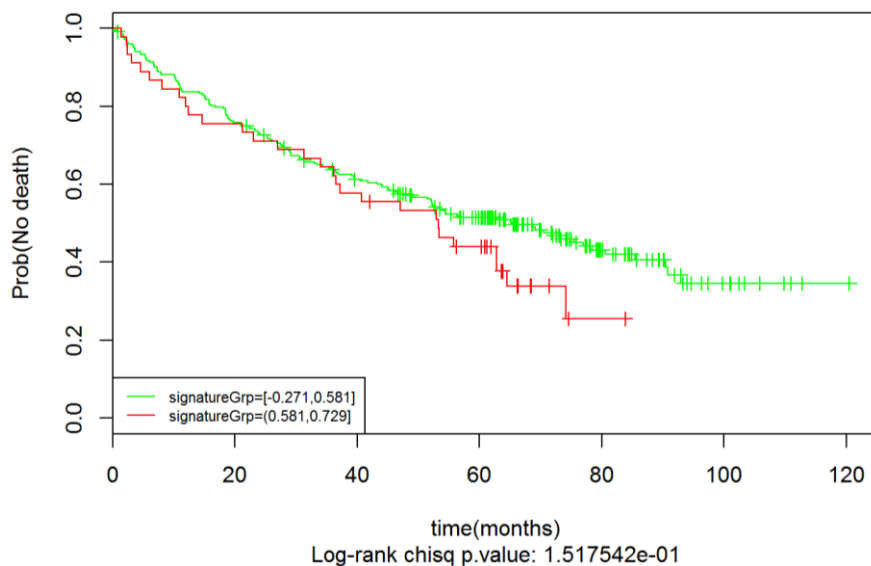


**Figure 81. Patients presenting an overexpression of genes involved in the coagulation pathway tend to present worse survival.** Kaplan-Meier plot of overall survival in 498 ccRCC patients (from TCGA). Patients were divided into two groups regarding of the gene set involved in coagulation (TFPI, SERPINE1, PAR1, F13A1 and ITGB3) RNA expression. Red line represents patients whose expression is above percentile 85. Green line represents patients with an expression of this data set genes below percentil 85. Data was analyzed by Log-rank test.

As for F2R, we could conclude that there is not a direct effect of its overexpression in survival in patients. However, it is interesting to highlight that some of the genes involved in the same pathway have implications in this outcome, since F13A alone presents worse survival and, when taking into account the coagulation-related group of genes altered in

Ren 50M tumors, we could see, at least, a tendency of lower survival rates in ccRCC patients.

#### **4.4 CORRELATION BETWEEN *CPE*, *F13A1* AND *F2R* GENE EXPRESSION AND THEIR CORRELATING GENES IN ccRCC PATIENTS**

Next, we also decided to correlate the expression of the three genes of interest in the ccRCC subtype. A Pearson correlation demonstrated a high correlation between them (Figure 82), suggesting that these three genes might be related and that they are co-overexpressed maybe acting in related pathways involved in the same processes.

Thus, recursively, the genes correlating between them may be correlating to similar extends (R-values), leading to the enrichment of similar functions.

To do so, we correlated the correlation values of genes from RNA sequencing data from TCGA and each gene of interest. Results showed that correlation values across the three genes and the rest of genes were very similar among them (Figure 83), further confirming a possible relation at the functional level. Following our study, we hypothesize that they might be acting together in pathways related to metastasis, eventually leading to worse prognosis in ccRCC patients.

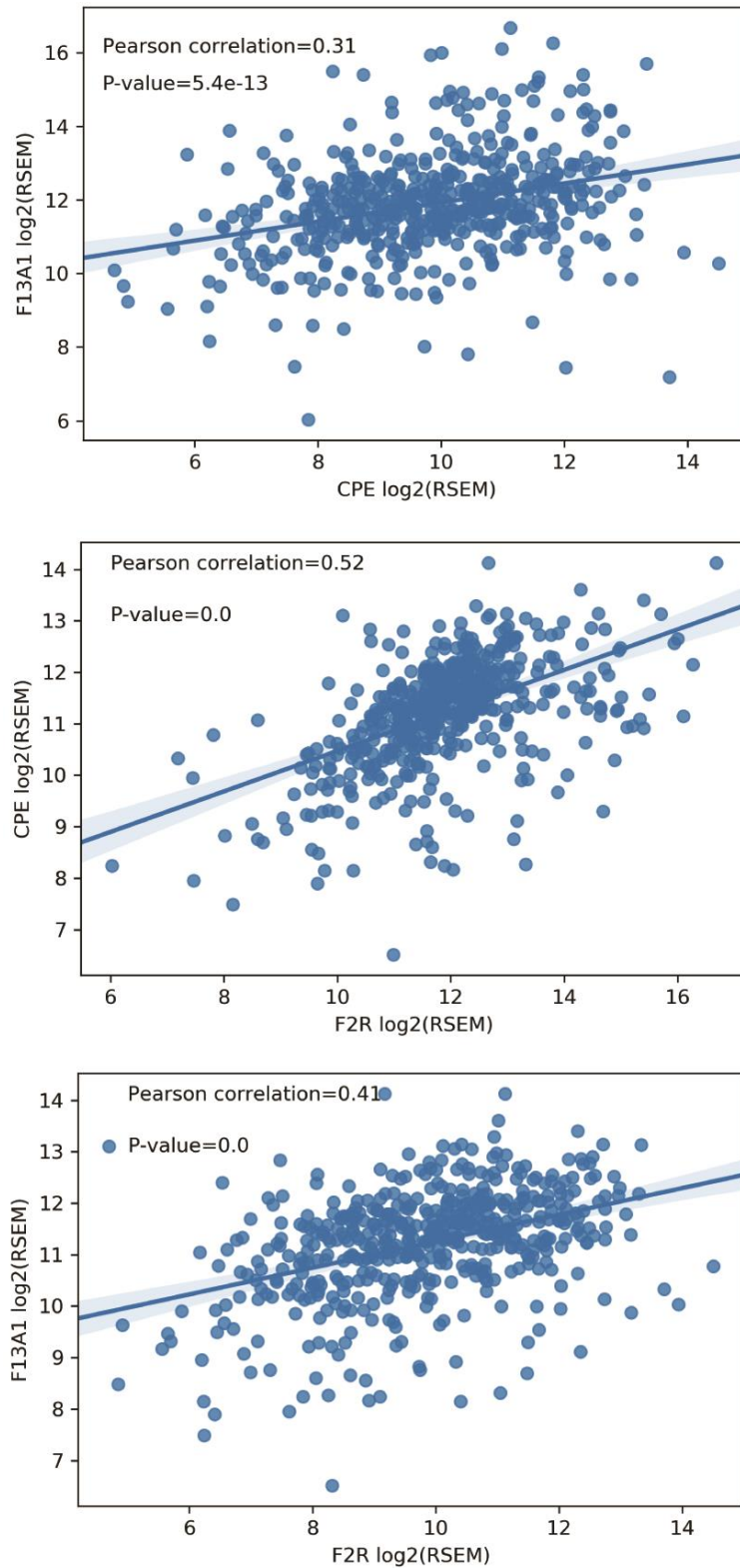


**Figure 82.** Data from TCGA demonstrated a correlation between *CPE*, *F13A1* and *F2R* in patients. Scatter plots of Pearson's correlation of the expression of the three genes between them. Analyzed data were extracted from TCGA and statistical significance is represented by the p value inside each plot, according to the corresponding Pearson correlation.

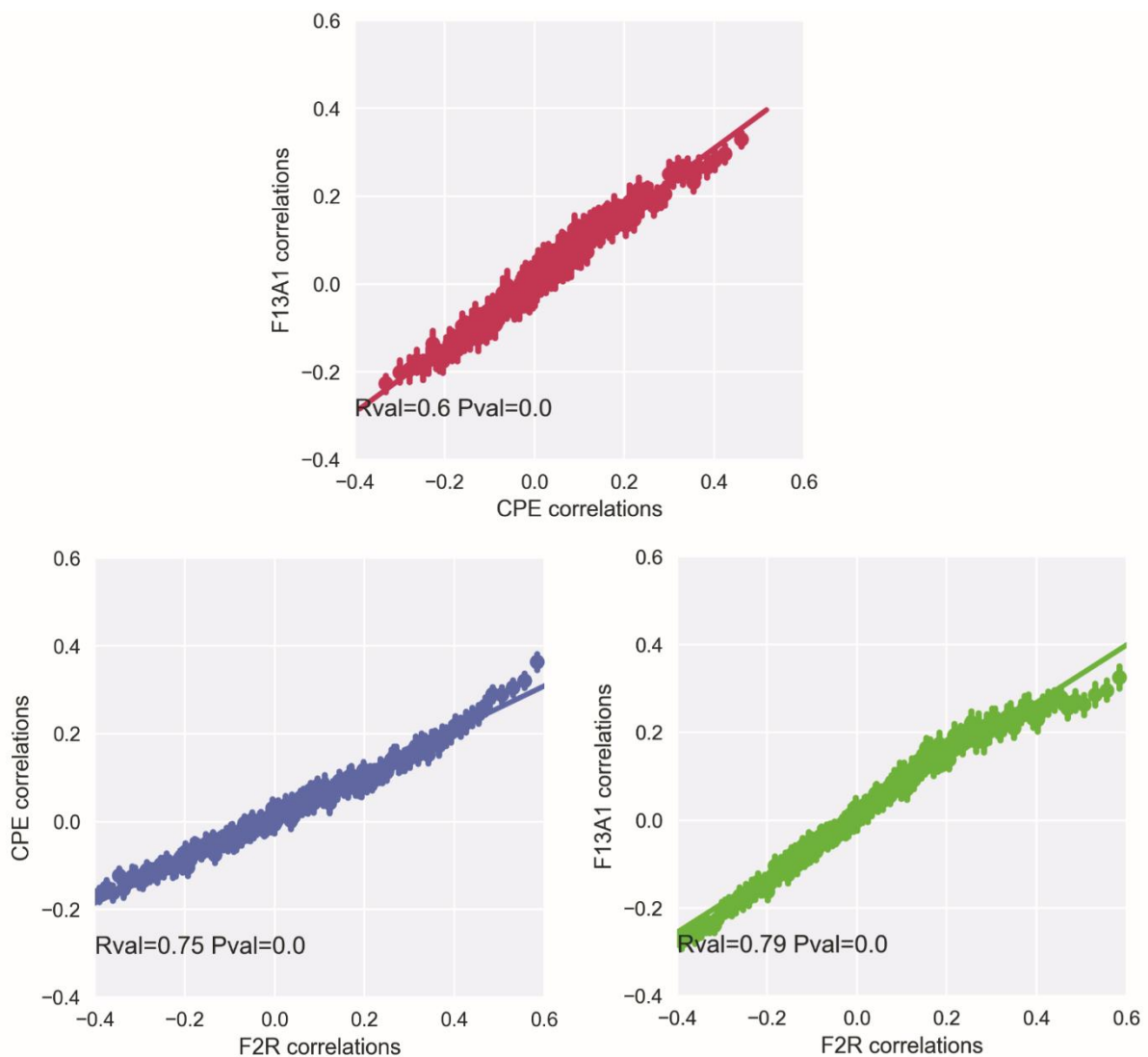
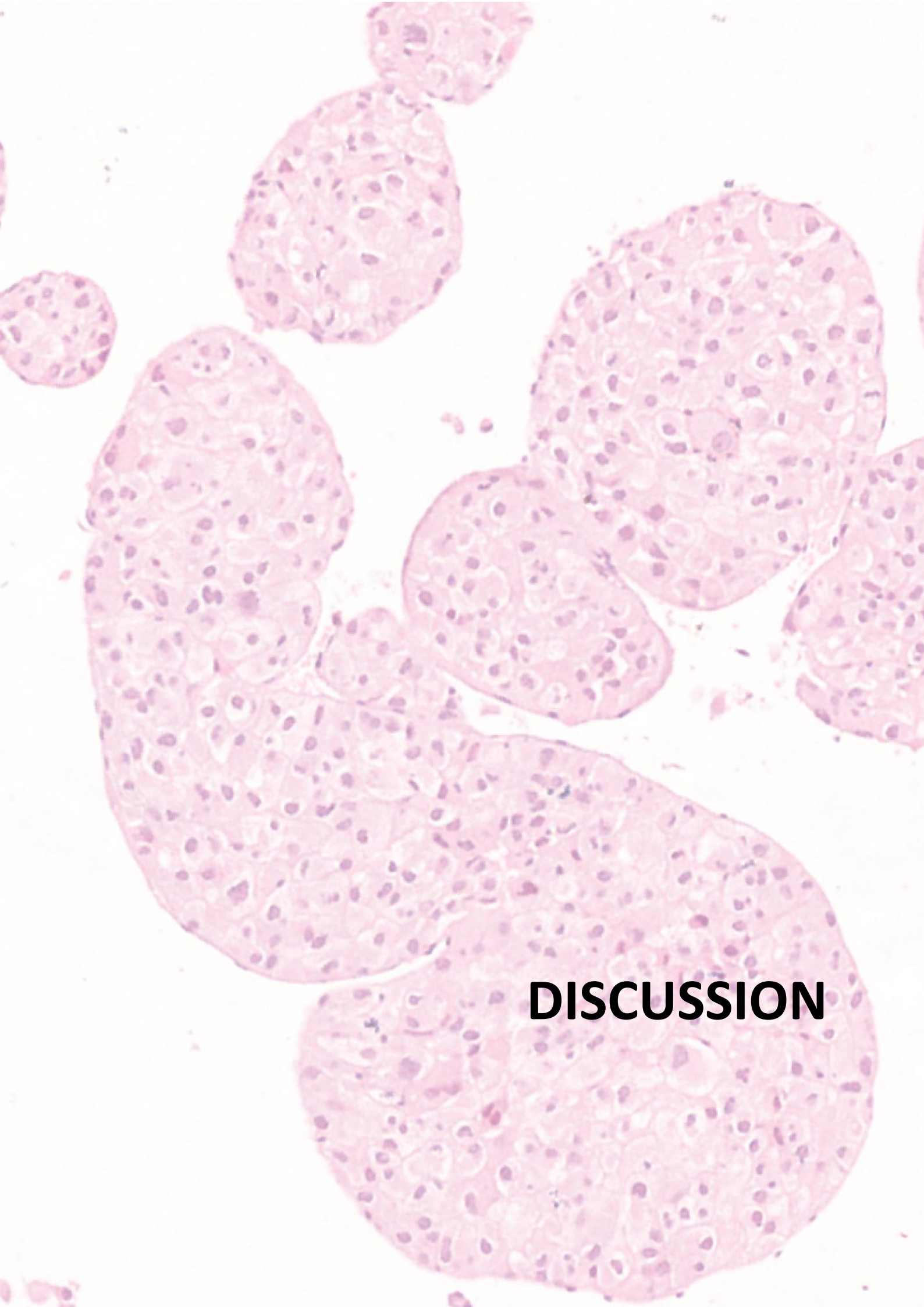


**Figure 83. Data from TCGA demonstrated a correlation between *CPE*, *F13A1* and *F2R* correlating genes in patients.** Scatter plots of Pearson's correlation divided in bins for a better representation. Correlation of the correlation values between 20,532 genes available in RNA sequencing data from TCGA and each gene of interest (*CPE*, *F13A1* and *F2R*). Statistically significance is represented by the p value inside each plot, according to the corresponding Pearson correlation.

Overall, these data from clinics support our metastatic candidates as proper markers and targets for RCC, since their overexpression is specific not only to our cancer type, but also to our clear cell subtype. Furthermore, both CPE and the coagulation pathway have been confirmed to affect overall survival in patients and to be functionally related.







**DISCUSSION**



## **1. METASTASIS, CLONAL HETEROGENEITY AND REN 50/50M MODEL**

Metastasis is one of the main processes of cancer progression, accounting for 90% of cancer deaths in patients (Gupta and Massagué, 2006). Therefore, targeting tumor metastasis has become an attractive target during the last years in cancer research in order to improve patients' overall survival. Kidney cancer represents the major of renal pathology and the discovery of early screening methods and biomarkers is still needed. Therefore, most of patients present metastatic disease at the time of diagnosis (Cairns, 2012) and data from the National Cancer Data Base reveal that their survival at this stage of progression is a dramatic 8%. Consequently, the focus of this thesis was to evaluate different potential metastatic candidate genes in an orthoxenograft animal model of ccRCC, which is the main RCC subtype and it accounts for the major cancer-related deaths (Moch et al., 2016b).

Metastasis consists of a multistep cascade in which many genes are involved, hence hampering the study of this complex process (Nguyen et al., 2009; Nguyen and Massagué, 2007). One of the main hurdles is the existence of clonal heterogeneity in primary tumors, which can develop advantage traits to a group of cells conferring them the ability to generate metastasis or resistance to current therapies. Furthermore, a problem arises with the underestimation of the existence of different clones composing both primary tumors and metastases, which finally leads to the selection of unappropriated treatments and undesired outcomes (Yap et al., 2012). Consistent with the literature about RCC, in which several studies have noted the importance of clonal heterogeneity in this type of cancer (Gerlinger et al., 2014, 2012; Sankin et al., 2014; Turajlic and Swanton, 2016; Voss et al., 2014), the staining of our metastatic candidates in tumors from our model has confirmed heterogeneity, both in the human biopsy and in mice samples from the orthotopic mouse and the metastatic line. Furthermore, we have confirmed at least one clone in Ren 50 tumors which lacks the expression of our candidates, allowing them to generate metastasis in a lower aggressive phenotype compared to Ren 50M. Several reports have confirmed that multiple metastatic clones can disseminate independently,

supported by differences in genetic profiles (Turajlic and Swanton, 2016). In our case, Ren 50 cells probably present a different gene expression profile which maybe lacks some of important metastatic genes, leading to the generation of a model with limited metastasizing capacity.

Depending on the time and the way tumor cells escape from the primary tumor, different metastatic models have been described. On one hand, cells can migrate both at the beginning and at later states of the metastatic process. On the other hand, they can travel alone or as polyclonal populations (Caswell and Swanton, 2017). Trying to understand what happened at the time of generation of the Ren 50/50M model, exome sequencing results have been analyzed (Figure 16). Despite most of mutations are shared between the human biopsy and both lines of the orthoxenografts tumors, the rest of mutations seem to provide useful information.

First, we can infer that the Ren 50M line is more similar to the biopsy, since the human specimen does not share exclusive mutations with Ren 50 tumors, but it does with the metastatic line. Therefore, it seems that the human biopsy was implanted to the orthotopic mouse maintaining the metastatic capacity of the patient. Then, a polyclonal group of cells would have travelled to the lung, generating a macrometastasis, which gave rise to the Ren 50M line. Secondly, we hypothesize that the small piece of tumor that generated the Ren 50 line lacked this high metastatic capacity, hence obtaining a variant of the model with a very low metastatic potential (Figure 84).

Regarding the 21 exclusive mutations only present in the orthoxenograft tumors, they could be attributed to the expected scarce evolution of these lines, since the analysis of Ren 50 and 50M was performed of tumors from passages 8 and 10, respectively. Another explanation could be the fact that the sequenced piece from the patient and the piece implanted into the orthotopic mouse were not exactly the same. Consequently, it may slightly differ clonally. This last scenario is the one that can generate clinical problems when human samples are biopsied. For instance, based on the prevalence of some mutations, Sankin et al. estimated that at least three different tumor regions should be

sampled in RCC in order to not underestimate the clonal composition of tumors (Sankin et al., 2014).

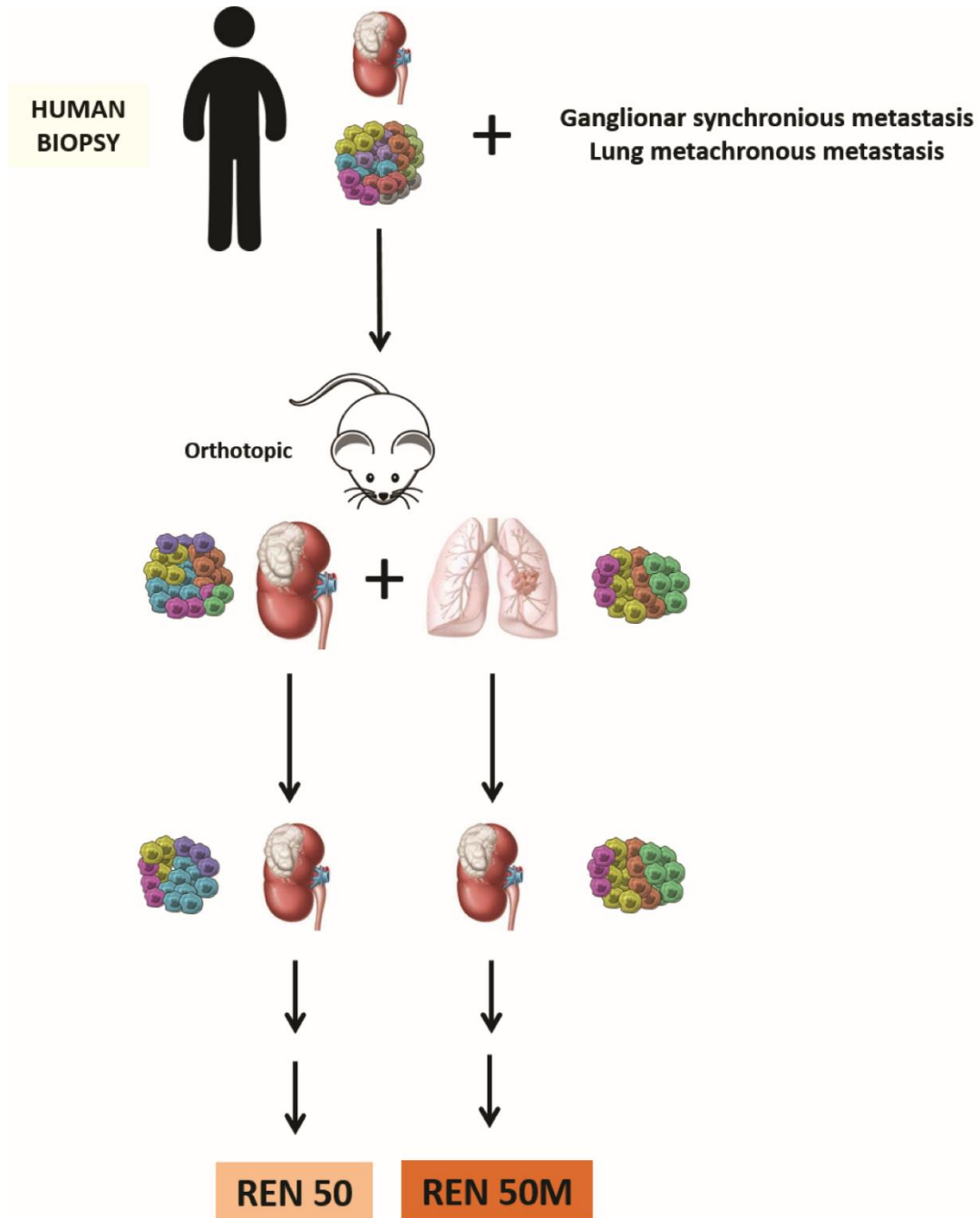


**Figure 84. Schematic representation of Ren 50 and Ren 50M, probably generated from a polyclonal metastasis.** A piece of a human biopsy composed of different subclones was implanted into a kidney of an athymic mouse (orthotopic). A piece of this tumor, which lacked the metastatic capacity of its tumor of origin, was implanted into the kidney of a mouse, generating the Ren 50 line. On the other side, a group of cells maintaining polyclonality would have migrated to the lung, generating the Ren 50M line.

To sum up, it can be suggested that the first metastasis in the orthotopic mouse that gave rise to the Ren 50M line was probably polyclonal, as it has been for instance described to occur in CRC (Wei et al., 2017). Then, the Ren 50 line lost the metastatic capacity of the patient, the orthotopic and the Ren 50M tumors. This type of multicellular metastatic travelling seems to be less common than single CTCs. However, it is thought to be exposed to less mechanical stress, which improves cell survival and decreases apoptosis, thus leading to an increase of the metastatic potential of tumor cells (Aceto et al., 2014; Strilic and Offermanns, 2017). In addition, the characterization of tumor cell clusters is very relevant in the clinical setting, since the composing cells can present different treatment resistance features and, as a consequence, different treatment responses (Cheung and Ewald, 2016).

Clonal heterogeneity is broadly considered to be a trait that allows tumor cells to survive against evolutionary pressures. Hence, our model is contrary to the common belief, since metastatic models are normally described as 'gain of function' events that allow cells to generate metastasis (Chiang and Massagué, 2008; Nguyen and Massagué, 2007; Turajlic and Swanton, 2016; Valastyan and Weingberg, 2011; Vanharanta and Massagué, 2013). In our case, this clonal advantage to generate metastasis seems to have occurred in the patient, but then, differences in the metastatic capacity seem to be a consequence of its loss in one of the lines of the orthoxenograft model. Therefore, we have confirmed that the availability of tumor sequencing, both from mice and from patients, is nowadays allowing to understand processes involved in cancer progression and to identify genes with essential roles in tumor progression and metastasis, as well as to further develop cancer targeted therapies.

Prompted by exome analyses, we also decided to validate chromosomic alterations, supported by prior studies which have already noted the relation of genetic aberrations and clinical outcome in RCC (Moch et al., 1996; Morita et al., 1991; Presti et al., 1993). The most common genetic abnormalities associated with ccRCC are the short p arm due to a chromosome 3 deletion (Zbar et al., 1987) and mutations involving the *VHL* gene

(Zbar, 1995). However, due to exome sequencing results, we decided to validate chromosomes 8, 15 and 18. In addition, data from exome analysis also confirmed a non-mutated *VHL* in the exomes of the gene, both in Ren 50 and Ren 50M tumors. However, we can confirm by RNA sequencing analyses that we do not have *VHL* RNA expression in our tumors. Therefore, we assume that we have VHL- tumors, maybe due to the presence of intronic or regulatory alterations, which our study has not been able to rule out.

We started analyzing the centromere of chromosome 8 and the position 8q24, in which the proto-oncogene *MYC* is located. This specific gene amplification has been demonstrated to be involved in the progression of cell carcinogenesis due to its influence on the expression of a wide range of genes (Neel et al., 1982). Using both probes, we have noted the presence of an isochromosome 8 in both Ren 50 and Ren 50M tumors. Therefore, we hypothesize the presence of an 8p monosomy and an 8q trisomy in primary tumors and in the metastases. Additionally, duplications of the entire chromosome 8 in some cells of Ren 50 tumors and metastases were detected.

First, the monosomy could be relevant considering what Rueckert, Devitt, and Gardner have just described. They propose the possibility of considering a new RCC subtype characterized by a chromosome 8 monosomy, together with other mutations and histological features (Rueckert et al., 2018). In parallel, in accordance to our findings, the gain of 8q has been detected in papillary and ccRCC. Mehrazin et al. have associated 8q amplifications with higher T stage, nuclear grade, nodal involvement, distant metastasis and worsened survival (Mehrazin et al., 2017). Our model broadly supports these findings, since Ren 50 patient presented high T stage, nuclear grade and lymph node metastasis at the time of diagnosis. However, we have not been able to confirm an association between a higher gain of 8q and metastasis.

In addition to chromosome 8, alterations in two other chromosomes have been studied for their possible association to the metastatic model. Our results have confirmed that both chromosome 15 and 18 amplifications are slightly related to metastatic tumors and strongly related to lung metastasis. Maleno et al. observed a frequent LOH in



chromosome 15 in CRC, bladder carcinoma and melanoma (Maleno et al., 2011). However, they were not able to demonstrate chromosome 15 alterations in RCC, which makes our study become newly relevant about the association between alterations in this chromosome and this type of cancer. In addition, a study of 89 ccRCC revealed several chromosomal imbalances related to, among other features, Fuhrman grade, necrosis and vascular invasion. Despite they did not report imbalances in chromosome 15, they interestingly associated losses of chromosome 18 with 4-Fuhrman grade, necrosis and T stage (Dagher et al., 2013). Besides, other studies have reported implications of losses of 18p in metastasis in esophageal squamous cell carcinoma (Ando et al., 2007) and losses of 18q as an unfavorable prognostic factor in CRC (Tanaka et al., 2009). Therefore, our study, while preliminarily, suggests a new possible association between the gain of chromosomes 15 and 18, contrary to what is described, and a very important step of cancer progression, as it is metastasis. We raise the possibility for future metastatic research to further investigate a possible association between the overexpression of genes located in these chromosomes and the metastatic process which, to date, have not been described in any type of cancer.

After exome and *FISH* analyses, RNA sequencing of tumors from both groups was also performed. During several years, the most used technique to measure gene expression has been microarrays. However, RNA sequencing has become also a widely used technique for this purpose (Cloonan et al., 2009; Sultan et al., 2008). Obtained results were in accord with the above-mentioned data, confirming an overexpression of genes located in altered chromosomes. Furthermore, we obtained a long list of thousands of genes located in other chromosomes differentially expressed in Ren 50M compared to Ren 50, suggesting new targets and pathways, as the coagulation cascade, involved in the metastatic process, which have further been analyzed.

To sum up, previous results from RNA and exome sequencing, together with their validation through *FISH* analysis and later validations in tissues, have confirmed the

presence of different clones with different genetic profiles, hence providing clues about the generation of our model and suggesting potential metastatic genes.

## **2. MODELLING METASTASIS IN THE MOUSE**

Finding the most effective treatment for different cancer types mostly relies on preclinical research in animal models that should reflect the human disease as faithfully as possible. Hence, the use of these preclinical models is essential in translational cancer research, especially when identifying biomarkers and therapeutic targets for the development of therapeutic agents (Pauli et al., 2017).

The rationale behind the *in vivo* design described in this work was based on the literature of metastatic studies. Several models have been developed in order to study this process. Until fairly recently, they did not successfully recapitulate the natural course of human cancer and normally failed at representing the entire tumor. However, more accurate models have been recently generated, which closely mimic tumor genetic composition, the interaction between cancer cells and stroma and also treatment responses and resistances (Francia et al., 2011; Gómez-Cuadrado et al., 2017; Kersten et al., 2016; Saxena and Christofori, 2013).

Experimental metastasis normally relies on the systemic injection of tumor cells. However, these models are criticized for not recapitulating all the metastatic process, as it occurs in patients. Depending on the site of tumor cells injection and their organ tropism, metastases will develop in different anatomic locations throughout the body (Khanna and Hunter, 2005). With regard to tail vein injections, tumor cells are forced to lodge in lung capillaries, thus facilitating the study of capillary extravasation and colonization processes (Hart and Fidler, 1980). In our study, this model has been very useful when studying which steps of the metastatic process are our candidates (CPE, F13A and F2R) affecting. Later, in order to solve these underestimations, we also inoculated tumor cells orthotopically, thus taking into account all the metastatic process. Despite their advantages, both techniques lack the representation of intratumoral heterogeneity present in human tumors, hence being poor predictors of clinical responses.

Therefore, PDOX models are indispensable for studying cancer progression and the metastatic process because they represent, at least initially, clearly advantageous against cell line inoculation considering heterogeneity of patient samples (Alizadeh et al., 2015). In addition, they better reproduce the histology, the metastatic capacity and treatment responses of human cancers (Gómez-Cuadrado et al., 2017).

However, the implantation of a small piece of tumor into the mouse also underestimates all populations composing the human specimen, and this problem is perpetuated along passages of a PDOX line. Nonetheless, our study reports evidence that this fact has led to the generation of two metastatic PDOX variants from a unique tumor. Therefore, this finding has important implications for developing cancer models from unique samples, which can present different metastatic capacities or, for instance, different responses to treatment, which in the end are the main problems of clinical outcomes due to clonal heterogeneity.

Related to the percentage of metastasis in Ren 50M mice (50%), it has to be considered that animals were normally sacrificed at 25-40 days, when they presented symptoms of illness and their survival was compromised. Hence, it is maybe not enough time to develop metastasis in some of the cases. Consequently, this feature only manifests in half of the mice. In addition, this non-genetic dependence is further supported by the fact that all the animals, regardless of their metastatic phenotype, always have successors that maintain the 50% metastatic rate. At the end, it is necessary to highlight that we have obtained a spontaneous metastatic model which is very challenging because, in most of cases, metastasis only occurs after resection of the primary tumor. Furthermore, in these cases, after a primary tumor is established, several months are required for metastasis to develop. Therefore, the time to manage these models extends a lot compared to our model. (Francia et al., 2011; Gómez-Cuadrado et al., 2017; Khanna and Hunter, 2005; Tohme et al., 2017).

Nowadays, different *in vivo* models can be chosen depending on the aim of the study and always taking into account the weaknesses of each one. Summing up, *in vivo* mouse

models are essential to better understand cancer progression and metastasis. Together with *in vitro* modelling and manipulation of tumor cells, these models allow research to progress in order to prevent or treat overt metastatic disease.

### **3. METASTATIC CANDIDATE GENES**

The main goal of this project was to find and validate putative genes that could be involved in the metastatic progression of kidney tumors. Concretely, we started validating metastatic candidates mainly from RNA sequencing results.

#### **3.1 CARBOXYPEPTIDASE E**

One of the most interesting genes from RNA sequencing data was *CPE*. We chose this gene due to its extremely high expression in metastatic tumors compared to the non-metastatic ones. Furthermore, we confirmed that such overexpression was not a consequence of a higher gene dose or a mutation in any of the groups. This enzyme, classically known for being involved in peptide and hormone processing (Fricker, 1988), has received increasing attention during the last years for its role in cancer.

It was in 2011 when, for the first time, an N-terminal-truncated CPE splice isoform (CPE- $\Delta$ N) was identified and associated to tumor growth in hepatocellular carcinoma (HCC) and pheochromocytomas/paragangliomas (PHEOs/PGLs). In these tumors, this isoform was proposed to be useful as a biomarker for predicting metastasis (Lee et al., 2011). Later, it has been continuously proposed as a prediction marker in other types of cancers. In 2013, Zhou et al. demonstrated that overexpression of CPE- $\Delta$ N predicted poor prognosis in CRC patients affecting tumor progression, tumor recurrence and lymph node metastasis (Zhou et al., 2013). More recently, it has been correlated with pelvic lymph node metastasis and poor prognosis in patients with early-stage cervical (Shen et al., 2016), and associated with the recurrence and metastasis of lung adenocarcinoma (Sun et al., 2016). Full-length CPE and  $\Delta$ N isoform may play opposite roles, since they have been described to regulate the canonical Wnt signaling pathway negatively and positively, respectively (Skalka et al., 2016, 2013). However, more evidence is needed to

confirm CPE- $\Delta$ N expression in different cancer types and there are still many unanswered questions about how these two isoforms are involved in cancer progression and metastasis.

The present study has been unable to demonstrate a relation between this truncated isoform and the metastatic process. CPE- $\Delta$ N has been described as a splice variant form of CPE lacking the N-terminal signal peptide. Thus, it translocates to the nucleus and, by interacting with histone deacetylase 1/2, upregulates *NEDD9* gene (Lee et al., 2011), which has been described to play roles in proliferation, invasion and migration (Kim et al., 2006; O'Neill et al., 2007). In order to study the truncated isoform, we started validating the protein by western blot. Regardless of the group, we detected two bands in some tumors. Then, we were not able to determine both isoforms by Taqman<sup>®</sup>, since the probe used for RNA analyses did not have the capacity to discriminate this N-truncated isoform. However, as seen in the Results section, we did not detect *CPE* in any of the Ren 50 tumors. In order to confirm the unspecificity of our second band, we decided to further validate it by using other techniques. Therefore, we can affirm from immunostainings that no CPE protein was present in the nucleus of the cells, neither *in vitro*, nor *in vivo*. Furthermore, we have tried to detect both isoforms through PCR and no evidence of CPE- $\Delta$ N presence was found (data not shown). Consequently, we can affirm that our study is thoroughly based on the full-length CPE form.

Several reports have shown the involvement of the full form of CPE in cancer and in the metastatic process. It has been demonstrated that CPE is upregulated in cell lines and tissues from CRC and that it correlates with cell proliferation and tumorigenicity (Liang et al., 2013). In addition, Murthy, Pacak, and Loh described a correlation between CPE expression and tumor growth and metastasis. In their study, they confirmed, through a microarray from the GEO profile database, an overexpression of *CPE* mRNA in many non-endocrine cancers, including RCC (Murthy et al., 2010). These results are in agreement not only with our Ren 50M model, but also with the clinical results obtained from the TCGA database. In accordance with them, we have confirmed that *CPE* RNA is

overexpressed in a variety of cancer types, especially in RCC. On the contrary, we have not noticed a difference in tumor growth neither between Ren 50 and Ren 50M tumors, nor between CPE-expressing tumors and controls during the perpetuation of the lines. Finally, we analyzed whether the extremely upregulation of this gene in our model and in patients could be a consequence of a mutation in a transcription factor, leading to a completely loss of its transcriptional regulation. Results did not show an alteration in a TF either in the Ren 50M tumors or in patients with overexpression of CPE (data not shown).

When relating CPE expression and patient prognosis, controversial findings have been described. On the one hand, two reports on patients with gliomas (Höring et al., 2012) and pulmonary neuroendocrine tumors (He et al., 2004) have associated low levels of CPE with poor prognosis. On the other hand, Huang et al. and Shen et al. have described CPE expression as a valid prognostic biomarker for tumor recurrence in early-stage hepatocellular carcinoma and have correlated it to lymph node metastasis and poor prognosis in patients with early-stage cervical cancer, respectively (Huang et al., 2016; Shen et al., 2016). In our study, we have been able to associate *CPE* overexpression and poor prognosis in ccRCC patients, in accordance to the latter above-mentioned study. Therefore, we hypothesize that CPE may act as an inducer or as a regulator of the metastatic cascade with a potential role as a RCC biomarker due to its clinical effects in poor prognosis. On the other hand, the presence of metastasis in other cancer types in which CPE is not present could be explained by independent mechanisms. In the end, further research should be undertaken in order to determine how CPE expression can be affecting clinical prognosis and recurrence in different cancer types.

In order to functionally validate that CPE expression is related to the metastatic capacity of RCC cells and tumors, a lentiviral system was successfully generated and CPE-expressing 786O- cells were obtained and tested. Firstly, we tried to find an effect of CPE expression and metastatic processes *in vitro*, such as migration and invasion. However, results of the current study do not reinforce what is described in the literature. Using our

renal CPE-expressing 786O- cells , we have not been able to confirm migration or invasion effects, as described for instance in pancreatic cells (Liu et al., 2014).

Following our purpose, we continued investigating possible roles of this protein in the metastatic process. Shortly after the discovery of CPE, it was seen that astrocytes and neurons both synthesize and secrete the protein extracellularly (Vilijn et al., 1989). In the recent years, some studies have noted the presence of secreted CPE and have defined some roles for this soluble protein. Since we could successfully detect soluble CPE in supernatants from CPE-expressing 786O- cells by western blot, we were encouraged to further investigate a possible role for this secreted protein in the metastatic cascade. Nonetheless, it seems that we have observed different effects of soluble CPE compared to what is described. Murthy et al. treated fibrosarcoma cells, which are highly invasive, with recombinant CPE protein. In this context, the migration capacity of the cells decreased by 50% and nearly a 22% reduction of the invasive capacity was also observed (Murthy et al., 2013a). Besides, Ilina et al. have proven evidence of a reduction of migration in glioblastoma cells due to soluble CPE (Ilina et al., 2017). In our setting, both by adding recombinant CPE or by using media containing soluble CPE, no effects in migration were observed. In fact, 786O- cells clearly increased their invasion capacity in both cases. Summing up, we have not reported evidence of what has been described in glioblastoma and we have found the opposite mechanism that has been described for fibrosarcoma. Therefore, our findings present a novel role for the soluble form of CPE in the invasion process of RCC.

At this point of the study, we wanted to elucidate the mechanism behind the invasion effects. Apart from the aforementioned functions, CPE has been described to act extracellularly by conferring neuroprotective effects not depending on its enzymatic activity (Cheng et al., 2013). In this report, they demonstrated that CPE effects did not revert either when adding the inhibitor of its enzymatic activity GEMSA, or when using an enzymatically inactive form of CPE. Since no effects of GEMSA in our setting were observed, we hypothesize that, in our model, a similar process to what they described

might be occurring. We think that CPE could bind an interacting target molecule to initiate the signaling, leading, in our case, to cell invasion. Furthermore, it should be considered that CPE has been described to enzymatically activate protein precursors, most of them absent in our tumors. Consequently, it is more difficult to relate the invasion effects to its enzymatic activity in our setting, at least considering the already described CPE-propeptide targets. After all, the underlying mechanism behind CPE-mediated tumor cell invasion remains unknown and further research is therefore recommended.

Owing to the encouraging *in vitro* results, we decided to move on to the *in vivo* setting. Following the aforementioned data, we expected that CPE could be somehow related to the invasion process. Therefore, we decided to validate the effects of CPE in metastasis both at the beginning of the process and at the last steps of the cascade. We expected a positive association only in the kidney cell inoculation experiment, so that the hypothesis that CPE is exclusively involved at the beginning of the metastatic process would be plausible. Contrary to our expectations, no positive results were observed in either of the cases. Albeit these results were rather disappointing, some considerations are worth discussing. First, we have been unsuccessful to develop primary cells from the orthoxenograft tumors of our model. In addition, none of the RCC cell lines tested expressed *CPE*. As a consequence, we successfully generated 786O- *CPE*-expressing cells, but gene expression levels were much lower than the observed in Ren 50M tumors. It is possible, therefore, that 786O- *CPE*-expressing tumors did not express enough *CPE* protein levels to reproduce the Ren 50M setting. For the same reason, *in vitro* migration and invasion assays could not have shown effects. Secondly, we did not obtain successful results when injecting the cells through the tail vein. As previously described, the metastatic cascade is an extremely inefficient process and, in animal models, it is important to bear in mind that only 0.01% or fewer of the total cancer cells that enter in the circulation finally develop metastases (Chambers et al., 2002). In line with this, we had already developed pilot studies in which we had confirmed that an injection of  $10^6$  cells through the tail vein was enough to generate metastases. Besides, we had tested



that one month was not enough to detect metastases and that after six months the lungs were full of colonies. Following these data and since some mice were presenting symptoms of lung metastases, we decided to sacrifice the animals four months after tail vein injection. By analyzing the results, we could observe numerous lung metastases in both groups. Therefore, we suggest ending tail vein experiments between one and four months in order to differentiate whether a group of 786O- cells have an advantage to generate metastases compared to others. We expect that, following this protocol, saturation of the model can be avoided, and only the cells with the best traits should be able to generate metastasis.

Finally, another possible explanation for these non-satisfactory results may be the lack of other molecules that may be needed to cooperate with CPE in order to enhance the metastatic process. Hence, one protein alone is not enough to trigger a whole multistep cascade in which several genes play different roles during different steps of the process. In summary, there is a lack of representation of the entire metastatic progression of cancer.

In conclusion, we have not been able to confirm a functional association between CPE and the metastatic capacity of 786O- cells *in vivo*. Nonetheless, our study supports evidence of an association between this gene and tumors with metastatic potential, together with a confirmation of a role of the secreted CPE protein in the invasion process in an *in vitro* setting of RCC. In addition, these results have been supported by clinical validations which have demonstrated the importance of this molecule in this type of cancer and its consequences in patient survival. Therefore, with further studies that could elucidate the underlying mechanism and improve *in vivo* validations, we envision that this molecule may be used as prognostic biomarker for metastatic RCC in a near future.

### **3.2 COAGULATION PATHWAY**

Nowadays, it is well-known that cancer patients present an activation of the coagulation system with a 4 to 7-fold increased risk for developing cancer-related venous

thromboembolism (VTE) compared to non-cancer patients. In fact, this clinical alteration represents the second leading cause of morbidity and mortality in this population (Donnellan and Khorana, 2017; Khorana, 2010; Streiff, 2016). In addition, thrombin generated during thrombosis has been demonstrated to enhance the malignant phenotype by inducing tumor growth, metastasis and angiogenesis (Nierodzik and Karpatkin, 2006). Altogether, the clinical hypercoagulated state itself and its consequences on cancer progression represents a high increase of cancer-related deaths. In our study, we have confirmed these data by analyzing TCGA data from patients. In accordance to what is described, we have seen that an overexpression of some genes involved in the coagulation pathway tends to reduce the overall survival of ccRCC patients.

In this part of the thesis, we have focused our research on determining the metastatic role of two molecules involved in the coagulation pathway. F13A and F2R became our main targets after the analysis of the RNA sequencing data using the computational GSEA method. Furthermore, from the exome sequencing and *FISH* analyses of both Ren 50 and Ren 50M tumors, we confirmed that overexpression of their codifying genes was not caused by either a mutation or an abnormal gene dose.

First of all, we think that affections in the coagulation pathway could be responsible for the alterations observed at the vascular level and in the mice skin. Despite we have not been able to confirm any evidence of this relation, since no alterations in the hematocrit of mice from both groups could be reported (data not shown), we think that at least F2R could be related to the dilated phenotype. It is known that F2R activation by thrombin can have effects on endothelial cells producing vasodilatation (Alberelli and De Candia, 2014). Therefore, it makes us think that F2R activation could be responsible for the dilated vascular phenotype observed in almost all Ren 50M tumors. However, other players should be involved in this vasodilation, since some Ren 50 tumors also present dilated vessels.

### 3.2.1 Coagulation Factor XIII

The first coagulation factor that we have validated is the F13A protein, codified by the *F13A1* gene. First of all, its overexpression in our model is in accordance to what it has been documented in other cancer types. Coagulation F13 has been associated, among others, to leukemias (Kiss et al., 2008), non-small cell lung cancer (Lee et al., 2013), oral cancer (Vairaktaris et al., 2007) and bone metastasis of prostate cancer (Morrissey et al., 2008).

One of the major challenges in this thesis was the *in vivo* evaluation of our metastatic candidates. Owing to previous CPE results, in which *in vitro* effects were not later reproduced *in vivo*, we decided to directly test the effects of F13A in a mouse model. By generating F13A-expressing 786O- cells, we successfully generated F13A-expressing 786O- tumors. Despite no advantages in the metastatic process could be detected, even considering the entire process, very surprising results were obtained. In our RCC model, we have confirmed that, when overexpressing F13A, an upregulation of CPE also occurs. In addition, we have validated that this crosstalk only takes place *in vivo*, since F13A-expressing cells did not express CPE *in vitro*. These findings raise intriguing questions regarding the connection between these two proteins, because no previous evidence of this association has been reported to date. In addition, due to the fact that no F13A protein was found in CPE-expressing 786O- cells and tumors (data not shown), we infer that CPE could be regulated by the F13A-signalling pathway.

It is known that F13 transglutaminase acts ultimately in the coagulation pathway by stabilizing the platelet/fibrin thrombi through the covalent crosslinking of thrombin. Hence, it supports hematogenous metastasis through a mechanism coupled to NK cell function and seems to not be required for tumor growth or tumor stroma formation (Palumbo, 2008; Palumbo et al., 2008). In our model, we have not confirmed advantages in the metastatic process regarding F13A expression. However, the *in vitro* and clinical results from CPE, together with the discovery of the F13A-CPE crosslink and the literature about the role of this coagulation factor and the metastatic process, led us to come to

terms with the fact that our *in vivo* model for both molecules is not the optimal one. After this part of the study, we inferred that, when investigating a multistep cascade, it would probably be more efficient to validate a protein which can be inhibited. Otherwise, it is very difficult to see effects on the entire process when expressing only one molecule while maybe lacking most of the rest. All in all, this kind of study is undoubtedly challenging.

Summing up, we have not been able to demonstrate *in vivo* effects, even when expressing both molecules. Nonetheless, despite these difficulties, we still think that these two molecules are potential useful plasma biomarkers for metastatic RCC. From a clinical point of view, as seen with *CPE*, *F13A1* expression has also demonstrated to have specificity for RCC and ccRCC in the clinical setting, together with worsened patient overall survival when it is overexpressed.

It would be interesting to confirm that F13A, as described, is involved in RCC tumor cells survival against NK cells. Then, it would also be relevant to study how CPE is affecting this process. Owing to the *in vitro* results obtained with this candidate, we hypothesize that CPE could be acting after F13A activity by cooperating on tumor cell extravasation and invasion of the new secondary organ parenchyma before the formation of micrometastases.

Altogether, these data provide novel insights to further validate the new connection between these two molecules and the underlying mechanism by which they could be affecting metastasis, hence defining an opportunity for early detection to prevent deaths from RCC metastatic disease.

### **3.2.2 Coagulation Factor II Thrombin Receptor or Protease-activated Receptor 1**

F2R, or PAR1, is the first member of the G protein-coupled receptors PARs family, which are expressed throughout the body. Activated by thrombin, this molecule is well-known

for its participation in normal biological functions, but roles for it in tumorigenesis in the recent years have been described.

In our clinical validations of TCGA data, we have observed a clear overexpression of this protein in ccRCC. More interestingly, among 33 types of cancer from TCGA, ccRCC was the one with the highest F2R levels. Hence, it seems that the overexpression of this receptor might be relevant in these patients. In accordance to our findings, F2R overexpression has been found in renal carcinomas, as well as in several types of cancer, such as breast, melanoma, gastric, colon, lung, pancreatic or prostate cancer (Liu et al., 2017). When analyzing its implication in patient survival, we did not report a direct correlation. However, we have to keep in mind that it is a receptor that needs to be activated, so its overexpression may not always be linked to its effects.

As a drug target, F2R has already shown enormous potential for the antithrombotic treatment of coronary and peripheral vascular disease (Chackalamannil et al., 2008), but its potential role in clinical cancer treatment is still limited. Vorapaxar was the first PAR1-inhibitor to be approved by the FDA in 2014 and, together with Atopaxar, are the current two clinical formulations of PAR1 inhibitors (Baker et al., 2014; Wang, 2015). These two small molecules present high oral bioavailability, potency and selectivity, and act as competitive inhibitors by binding the tethered ligand site of PAR1, competing with the endogenous agonist. However, Atopaxar never advanced to Phase III trials due to its adverse effects observed in the previous clinical phase (O'Donoghue et al., 2011; Wiviott et al., 2011). On the contrary, Vorapaxar demonstrated proved safe and well tolerated, prompting it to two pivotal Phase III clinical trials (Morrow et al., 2012; Tricoci et al., 2012).

Due to the extensive data reported for PAR1 in tumor development, invasion and metastasis, together with the overexpression of this molecule in our metastatic group, we decided to use Vorapaxar *in vivo* in order to find an anti-metastatic effect in RCC. Because of the aforementioned failure in the establishment of RCC primary cultures, coupled with troubles encountered at having Ren 50M tumors available at that moment,

we first validated the expression of F2R in RCC cell lines in order to find a F2R-expressing model. As shown in the Results section, we decided to use SN12C cells due to their high F2R expression, both *in vitro* and *in vivo*. When using Vorapaxar, we knew that the effects would be due to an inhibition of the human F2R and not because of an inhibitory effect of the mouse receptor (Zhang et al., 2012). In addition, it is known that PAR1 is not expressed in mouse platelets, contrary to what happens in humans (Coughlin, 2000). Hence, we can infer that our following discussed results are the consequence of a competitive inhibition of F2R from human tumor cells.

In our study, we have confirmed that, when tumor cells are in the circulation and PAR1 is inhibited, the ability to extravasate and generate metastases in the lungs clearly decreases, although the results were not statistically significant. We hypothesize that, by inhibiting PAR1 in tumor cells, we are hampering the formation of heteroaggregates between them and platelets. This would be in accordance with the fact that tumor cells can activate platelets and induce platelet aggregation, thereby mediating platelet-tumor cell interaction and facilitating different steps of the metastatic process (Gay and Felding-Habermann, 2011; Stegner et al., 2014; Strilic and Offermanns, 2017). It was confirmed several years ago that thrombin-treated tumor cells present an enrichment of lung metastases due to an increase of tumor cell adhesion to platelets, endothelial cells, fibronectin and von Willebrand factor, both *in vitro* and *in vivo* (Nierodzik et al., 1998). Later, Shi et al. also confirmed that thrombin-enhanced migration could be abolished by using anti-F2R antibodies that blocked the receptor by cleavage (Shi et al., 2004). Therefore, thrombin seems to enhance the metastatic potential of tumor cells by increasing their adhesive potential through PAR receptor signaling (Wojtukiewicz et al., 2016).

In our model, we think that we are affecting the PAR1-mediated interaction between tumor cells and platelets while they are in circulation by using a competitive antagonist of the receptor. However, this premise needs further investigation. For instance, *in vitro* assays should be performed in order to assess whether platelets changes their

aggregation rate when inhibiting PAR1 in SN12C:platelet co-cultures. Furthermore, we hypothesize that these interactions would also promote metastasis by the adhesion of these heteroaggregates to the endothelium, thus facilitating the extravasation of tumor cells (Gay and Felding-Habermann, 2011; Poggi et al., 1993). In order to explore this, *in vitro* experiments in which tumor cells migrate through an endothelial layer are also recommended.

Relevantly, we hypothesize that these effects would be maximized in patients, since Vorapaxar treatment in the clinical setting would also inhibit PAR1 in platelets. Therefore, the sum effect of both inhibitions would lead to a drastic decrease in the advantage of tumor cells to shield themselves by using platelets and would shrink their ability to make the last steps of the metastatic cascade succeed.

In order to inhibit the metastatic process from the beginning, we also decided to inject the cells into the kidney of mice, perpetuate SN12C tumors and treat the animals with Vorapaxar orally. When analyzing tumor invasion, although it was not statistically significant, we could confirm a clear decreasing tendency. These results further support the association between this receptor and tumor invasion that has been described in several tumors (Cohen Even-Ram et al., 2001; Wojtukiewicz et al., 2015). In addition, we have later reinforced these *in vivo* effects when inhibiting the receptor in cell culture.

In the *in vitro* setting, we have observed a huge decrease in SN12C cell invasion when inhibiting F2R. A possible explanation for these findings might be the changes observed in their phenotype after F2R inhibition. Nonetheless, we still do not know the underlying mechanism by which they seem to lose some of their cell-cell contacts. Owing to their conversion to a mesenchymal-like phenotype, we could hypothesize that cells are undergoing an EMT process. However, we would expect an increase of the invasive phenotype with a fibroblast-like morphology (Yang et al., 2016; Yilmaz and Christofori, 2009), which is completely the opposite to what we have observed. Therefore, there is abundant room for further progress in determining the pathways involved in this phenotype and process. When analyzing tumor cell migration, we have not seen the same

expected increase, as it has been reported in colon carcinoma cells (Darmoul et al., 2004). Therefore, in our setting, maybe PAR1 inactivation is not sufficient for inhibiting the migration process, as it occurs in human melanoma cells. In this cancer, PAR2 was demonstrated to also be necessary (Shi et al., 2004).

Finally, our most promising results come from the metastatic analysis of Vorapaxar-treated mice. In particular, Vorapaxar-treated SN12C tumors showed significantly reduced number of lung colonies and size compared versus controls. Altogether, these effects were translated into an evident reduction of the total metastasis area density by inhibiting F2R. These results make us think that we have obtained an added effect of F2R inhibition at the tumor invasion level, together with effects in the last steps of the process, thus clearly reducing the metastatic capacity of SN12C tumor cells.

Currently, anticoagulants are given to patients in order to solve thrombotic events related to cancer and treatments. Monotherapy with low-molecular-weight heparin (LMWH) is nowadays the first-line therapy for the long-term treatment of cancer-related VTE (Farge et al., 2013; Mandalà et al., 2011), over vitamin K antagonist (warfarin) due to its higher safety (Al-Samkari and Connors, 2018; Schmaier et al., 2018). However, both drugs require difficult dosage adjustments, present VTE recurrences, and hemorrhagic complications occur very often. For several years, some studies have suggested that LMWH treatment also has antitumor effects and increase the overall survival of cancer patients (Cosgrove et al., 2002; Klerk et al., 2005; Lee, 2007). However, a more recent systemic review and meta-analysis of randomized trials in cancer patients with VTE has not been able to show a survival benefit of treated patients, leaving the effect of LMWH on overall survival still unraveled (Sanford et al., 2014).

Nowadays, direct oral anticoagulants (DOAC) have presented efficacy, safety and availability in clinical trials. Concretely, inhibitors of thrombin and coagulation factor Xa have already replaced warfarin in non-cancer patients, demonstrating equivalent effects for VTE treatment with lower bleeding rates (Van Es et al., 2015). In addition, two clinical trials have compared direct factor Xa inhibitors in cancer patients, confirming non-



inferior effects compared to LMWH, although an increased risk of bleeding has been reported (Kahale et al., 2018; Li et al., 2018). DOACs clearly present an easy route of administration and lack of regular drug monitoring compared to LMWH and warfarin, respectively. Therefore, the use of DOACs may represent a treatment option, but there are still questions about their use in specific subsets of cancer patients that need to be answered (Al-Samkari and Connors, 2018; Farge et al., 2016; Rojas-Hernandez, 2018; Schmaier et al., 2018).

F2R receptor is an emerging anti-cancer drug target due to its overall roles in the progression of cancer. However, its inhibitors are currently in clinical use to treat acute coronary syndromes. Some studies are already under intensive investigations trying to demonstrate the use of F2R inhibitors in the preclinical setting of different types of cancer. Very recently, the use of a pepducin approach in breast, lung and ovarian cancer has been proposed. This peptide modulates GPCRs signaling allosterically but, being disadvantaged compared to Vorapaxar, this molecule is still under clinical phase II (Covic and Kuliopulos, 2018).

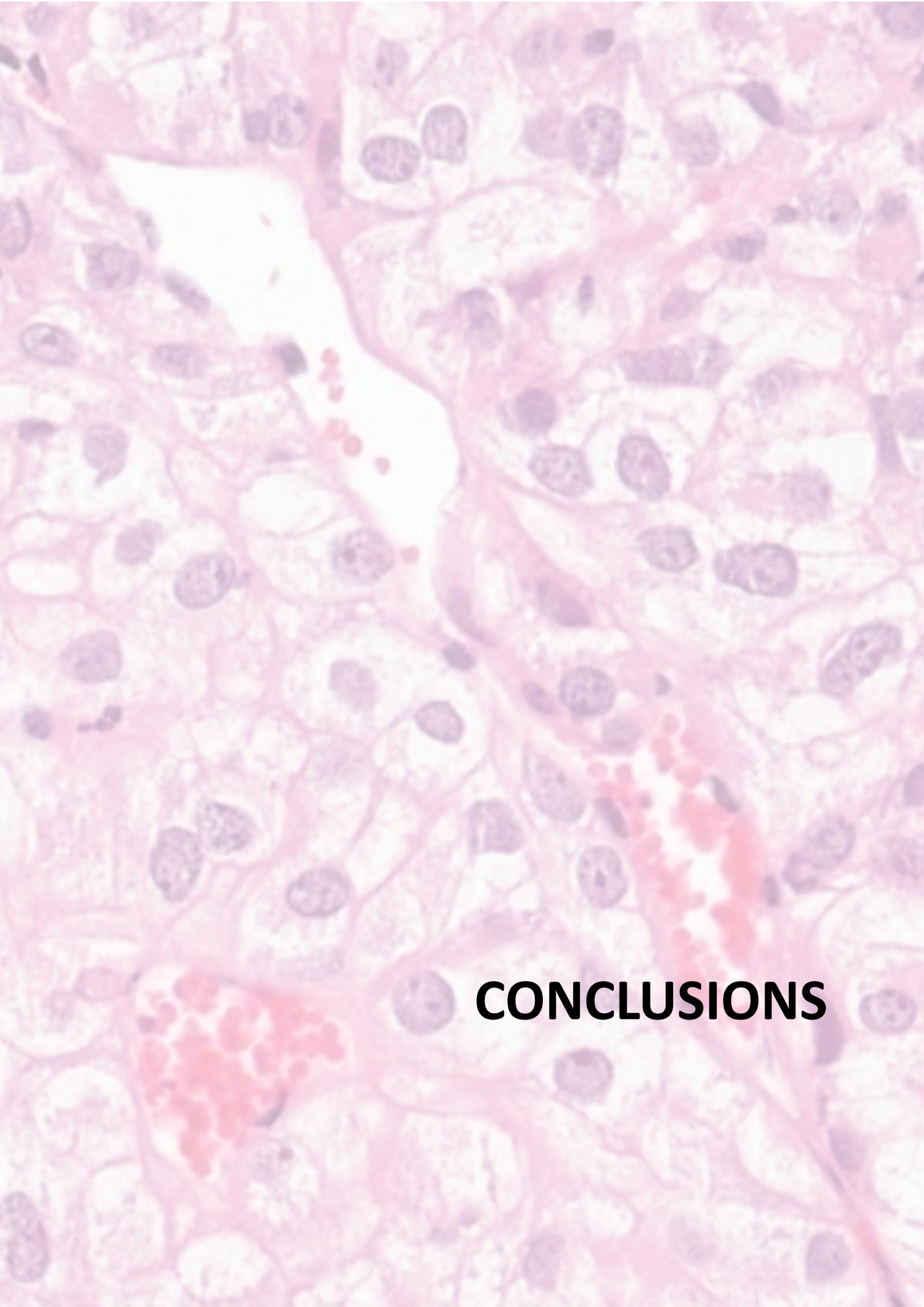
With our novel findings, we suggest the use of the already FDA-approved drug Vorapaxar, not only for its antithrombotic use, but also as a novel anti-cancer drug for targeting metastasis. First, our observed anti-metastatic effects should be reproduced in other RCC subtypes, together with a variety of cancers, both *in vitro* and *in vivo*. Then, it would be necessary to confirm the anti-metastatic effectivity in patients. Currently, there are many ongoing clinical trials using Vorapaxar, but none of them is focused on cancer and metastasis (Flaumenhaft and De Ceunynck, 2017). Besides, it is well known that LMWH is fully cleared by the kidneys, leading to accumulative effects in patients with impaired renal function (Boneu et al., 1990). On the contrary, the major route of elimination of Vorapaxar is through the feces, with minor renal excretion (Abdulsattar et al., 2011). Consequently, our suggestion becomes more relevant as a valid alternative for treating thrombosis and metastasis in RCC patients. However, further studies are recommended.

Ideally, we propose to develop a Vorapaxar experiment in a Ren 50M group of tumors, as long as we are still able to obtain Ren 50M tumors. We expect that, by inhibiting F2R in that setting, we would be able to inhibit the metastatic capacity of these tumors, mimicking what happens in the Ren 50 line. In addition, it would be interesting to assess whether there is a reversion of the reddish skin of the mice, together with a constriction of the dilated vascular phenotype. This reversion could not be analyzed in SN12C tumors because, despite their F2R expression, they do not present dilated vessels. Additionally, the establishment of Ren 50M primary cultures would also help discover the underlying mechanism. However, several protocols have been proven in order to obtain them and, despite their success for the establishment of primary cells from other RCC PDOX, they have not worked for this model. In the end, clinical trials are required to investigate the role of this molecule in the metastatic RCC process and the beneficial effects of its inhibition to the human being.

According to the overall data from our metastatic candidates, we can confirm that we have proven evidence that CPE is involved in the metastatic pathway *in vitro* and in the clinical setting, and that the coagulation pathway is related to the metastatic cascade *in vitro*, *in vivo* and in patients. From a clinical point of view, since the overexpression of these genes occurs in different tumors and in most of ccRCC patients, we have also proven that our model does not come from an outlier patient and that the overall results can be extrapolated and become useful for a large cohort of patients. Since data from TCGA have revealed a positive correlation between our candidate genes and their correlating genes, we should not rule out undiscovered interactions between them.

As a final conclusion, we suggest *CPE*, *F13A1* and *F2R* as potential genes with cooperating pivotal roles involved in the metastatic capacity of RCC tumors. Under further investigations, we expect them to be useful biomarkers for RCC, as well as to become potential targets to prevent and treat metastatic RCC disease.





**CONCLUSIONS**



1. We have established two variants of a RCC PDOX model which present different metastatic potential and distinct clonal heterogeneity, suggesting the loss of the metastatic capacity in one of them.
2. DNA and RNA sequencing, together with FISH analysis, have allowed the identification of CPE, F13A and F2R as possible metastatic candidates of RCC.
3. Validation of CPE has demonstrated a pro-invasive link between the soluble form of this molecule and the metastatic cascade, independent from its enzymatic activity. However, its overexpression alone is not sufficient to have effects *in vitro* and to generate metastasis *in vivo*.
4. Our studies of F13A and CPE have demonstrated a novel cross-link in RCC tumors. Nevertheless, upregulation of both molecules is not enough to initiate the whole metastatic cascade.
5. F2R has a role in metastasis, since its inhibition leads to a reduction of the early and later phases of metastasis. Hence, this molecule is suggested to be a new target in metastatic RCC.
6. *CPE*, *F13A1* and *F2R* genes are overexpressed in RCC, especially in the ccRCC subtype. Furthermore, *CPE* and *F13A1* overexpression has been related to poor prognosis in these patients, suggesting these genes as potential biomarkers in this type of cancer.
7. While *F2R* expression alone does not correlate with survival in ccRCC patients, the overexpression of a set of genes from the coagulation pathway tends to be associated with decreased survival in this clinical setting.
8. The three metastatic candidates and their associated genes correlate with each other, suggesting a new transcriptional program involved in metastatic RCC.



# REFERENCES





**A**

- Abdulsattar, Y., Ternas, T., Garcia, D., 2011. Vorapaxar: targeting a novel antiplatelet pathway. *P&T a peer-reviewed J. Formul. Manag.* 36, 564–8.
- Aceto, N., Bardia, A., Miyamoto, D., Donaldson, M., Wittner, B., Spencer, J., Yu, M., Pely, A., Engstrom, A., Zhu, H., Brannigan, B., Kapur, R., Stott, S., Shioda, T., Ramaswamy, S., Ting, D., Lin, C., Toner, M., Haber, D., Maheswaran, S., 2014. Circulating Tumor Cell Clusters Are Oligoclonal Precursors of Breast Cancer Metastasis. *Cell* 158, 1110–1122.
- Ahn, H., Foster, C., Boykow, G., Stamford, A., Manna, M., Graziano, M., 2000. Inhibition of cellular action of thrombin by N3-cyclopropyl-7-[[4-(1-methylethyl)phenyl]methyl]-7H-pyrrolo[3,2-f]quinazoline-1,3-diamine (SCH 79797), a nonpeptide thrombin receptor antagonist. *Biochem. Pharmacol.* 60, 1425–1434.
- Al-Samkari, H., Connors, J., 2018. The Role of Direct Oral Anticoagulants in Treatment of Cancer-Associated Thrombosis. *Cancers (Basel)*. 10, 271.
- Alberelli, M., De Candia, E., 2014. Functional role of protease activated receptors in vascular biology. *Vascul. Pharmacol.* 62, 72–81.
- Alizadeh, A., Aranda, V., Bardelli, A., Blanpain, C., Bock, C., Borowski, C., Caldas, C., Califano, A., Doherty, M., Elsner, M., Esteller, M., Fitzgerald, R., Korbel, J., Lichter, P., Mason, C., Navin, N., Pe'Er, D., Polyak, K., Roberts, C., Siu, L., Snyder, A., Stower, H., Swanton, C., Verhaak, R., Zenklusen, J., Zuber, J., Zucman-Rossi, J., 2015. Toward understanding and exploiting tumor heterogeneity. *Nat. Med.* 21, 846–853.
- American Cancer Society [WWW Document], 2018. URL <https://www.cancer.org/cancer/kidney-cancer/detection-diagnosis-staging/survival-rates.html>
- Ando, T., Ishiguro, H., Kimura, M., Mitsui, A., Mori, Y., Sugito, N., Tomoda, K., Mori, R., Harada, K., Katada, T., Ogawa, R., Fujii, Y., Kuwabara, Y., 2007. Frequent loss of the long arm of chromosome 18 in esophageal squamous cell carcinoma. *Oncol. Rep.* 17, 1005–11.
- Arnaoutova, I., Jackson, C., Al-Awar, O., Donaldson, J., Loh, Y., 2003. Recycling of Raft-associated Prohormone Sorting Receptor Carboxypeptidase E Requires Interaction with ARF6. *Mol. Biol. Cell* 14, 4448–4457.

**B**

- Baker, N., Lipinski, M., Lhermusier, T., Waksman, R., 2014. Overview of the 2014 food and drug administration cardiovascular and renal drugs advisory committee meeting about vorapaxar. *Circulation* 130, 1287–1294.
- Boneu, B., Caranobe, C., Sie, P., 1990. Pharmacokinetics of heparin and low molecular weight heparin. *Baillieres. Clin. Haematol.* 3, 531–44.

- Bos, P., Nguyen, D., Massague, J., 2010. Modeling metastasis in the mouse. *Curr. Opin. Pharmacol.* 10, 571–577.
- Brabletz, T., 2012. To differentiate or not-routes towards metastasis. *Nat. Rev. Cancer* 12, 425–436.
- Broad Institute of MIT&Harvard, 2016. Fire Browse [WWW Document]. URL <http://firebrowse.org>

## C

- Cairns, P., 2012. Renal cell carcinoma. *Cancer Biomarkers* 9, 461–473.
- Caswell, D., Swanton, C., 2017. The role of tumour heterogeneity and clonal cooperativity in metastasis, immune evasion and clinical outcome. *BMC Med.* 15, 1–9.
- Cawley, N.X., Wetsel, W.C., Murthy, S.R.K., Park, J.J., Pacak, K., Loh, Y.P., 2012. New roles of carboxypeptidase E in endocrine and neural function and cancer. *Endocr. Rev.* 33, 216–253.
- Chackalamannil, S., Wang, Y., Greenlee, W., Hu, Z., Xia, Y., Ahn, H., Boykow, G., Hsieh, Y., Palamanda, J., Agans-fantuzzi, J., Kurowski, S., Graziano, M., Chintala, M., 2008. Discovery of a Novel, Orally Active Himbacine-based Thrombin Receptor Antagonist (SCH 530348) with Potent Antiplatelet Activity. *J. Med. Chem.* 51, 3061–4.
- Chaffer, C.L., San Juan, B.P., Lim, E. I., Weinberg, R.A., 2016. EMT, cell plasticity and metastasis. *Cancer Metastasis Rev.* 35, 645–654.
- Chambers, A., Groom, A., MacDonald, I., 2002. Dissemination and growth of cancer cells in metastatic sites. *Nat. Rev. Cancer* 2, 563–72.
- Chan, A., Paredes, N., 2013. The Coagulation System in Humans. In: *Methods in Molecular Biology* (Clifton, N.J.). pp. 3–12.
- Cheng, Y., Cawley, N., Loh, Y.P., 2013. Carboxypeptidase E/NFalpha1: a new neurotrophic factor against oxidative stress-induced apoptotic cell death mediated by ERK and PI3-K/AKT pathways. *PLoS One* 8, e71578.
- Cheung, K., Padmanaban, V., Silvestri, V., Schipper, K., Cohen, J., Fairchild, A., Gorin, M., Verdone, J., Pienta, K., Bader, J.S., Ewald, A.J., 2016. Polyclonal breast cancer metastases arise from collective dissemination of keratin 14-expressing tumor cell clusters. *Proc. Natl. Acad. Sci. U. S. A.* 113, E854-63.
- Cheung, K.J., Ewald, A.J., 2016. A collective route to metastasis: Seeding by tumor cell clusters. *Science* 352, 167–9.
- Chiang, A., Massagué, J., 2008. Molecular Basis of Metastasis. *N. Engl. J. Med.* 359, 2814–2823.
- Cloonan, N., Xu, Q., Faulkner, G., Taylor, D., Tang, D., Kolle, G., Grimmond, S., 2009. RNA-MATE: A recursive mapping strategy for high-throughput RNA-sequencing data. *Bioinformatics* 25, 2615–2616.
- Cohen Even-Ram, S., Maoz, M., Pokroy, E., Reich, R., Katz, B., Gutweint, P., Altevogtt, P., Bar-Shavit, R., 2001. Tumor Cell Invasion Is Promoted by Activation of Protease Activated Receptor-1 in

- Cooperation with the  $\alpha\beta 5$  Integrin. *J. Biol. Chem.* 276, 10952–62.
- Corifact®, 2018. No Title [WWW Document]. URL <http://www.corifact.com>
- Cosgrove, R., Zacharski, L., Racine, E., Andersen, J., 2002. Improved cancer mortality with low-molecular-weight heparin treatment: a review of the evidence. *Semin. Thromb. Hemost.* 28, 79–87.
- Coughlin, S., 2005. Protease-activated receptors in hemostasis, thrombosis and vascular biology. *J. Thromb. Haemost.* 3, 1800–1814.
- Coughlin, S.R., 2000. Thrombin signalling and protease-activated receptors. *Nature* 407, 258–264.
- Covic, L., Kuliopulos, A., 2018. Protease-Activated Receptor 1 as Therapeutic Target in Breast, Lung, and Ovarian Cancer: Pepducin Approach. *Int. J. Mol. Sci.* 19, 2237.
- Criscuoli, M.L., Nguyen, M., Eliceiri, B.P., 2008. Tumor metastasis but not tumor growth is dependent on Src-mediated vascular permeability Tumor metastasis but not tumor growth is dependent on Src-mediated vascular permeability. *Vascular* 105, 1508–1514.

## D

- Dagher, J., Dugay, F., Verhoest, G., Cabillic, F., Jaillard, S., Henry, C., Arlot-Bonnemains, Y., Bensalah, K., Oger, E., Vigneau, C., Rioux-Leclercq, N., Belaud-Rotureau, M., 2013. Histologic prognostic factors associated with chromosomal imbalances in a contemporary series of 89 clear cell renal cell carcinomas. *Hum. Pathol.* 44, 2106–2115.
- Dardik, R., Loscalzo, J., Eskaraev, R., Inbal, A., 2005. Molecular mechanisms underlying the proangiogenic effect of factor XIII. *Arterioscler. Thromb. Vasc. Biol.* 25, 526–532.
- Darmoul, D., Gratio, V., Devaud, H., Peiretti, F., Laburthe, M., 2004. Activation of proteinase-activated receptor 1 promotes human colon cancer cell proliferation through epidermal growth factor receptor transactivation. *Mol. Cancer Res.* 2, 514–522.
- Déry, O., Corvera, C., Steinhoff, M., Bunnett, N., 1998. Proteinase-activated receptors: novel mechanisms of signaling by serine proteases. *Am. J. Physiol.* 274, C1429-52.
- Dhanvantari, S., Arnaoutova, I., Snell, C., Steinbach, P., Hammond, K., Caputo, G.A., London, E., Loh, Y., 2002. Carboxypeptidase E, a prohormone sorting receptor, is anchored to secretory granules via a C-terminal transmembrane insertion. *Biochemistry* 41, 52–60.
- Donnellan, E., Khorana, A., 2017. Cancer and Venous Thromboembolic Disease: A Review. *Oncologist* 22, 199–207.

## F

- Fan, S., Li, X., Li, L., Wang, L., Du, Z., Yang, Y., Zhao, J., Li, Y., 2016. Silencing of carboxypeptidase E inhibits cell proliferation, tumorigenicity, and metastasis of osteosarcoma cells. *Onco. Targets. Ther.* 9, 2795–2803.

- Farge, D., Bounameaux, H., Brenner, B., Cajfi, F., Debourdeau, P., Khorana, A.A., Pabinger, I., Solymoss, S., Douketis, J., Kakkar, A., 2016. International clinical practice guidelines including guidance for direct oral anticoagulants in the treatment and prophylaxis of venous thromboembolism in patients with cancer, *Lancet Oncol.*
- Farge, D., Debourdeau, P., Beckers, M., Baglin, C., Bauersachs, R.M., Brenner, B., Brillhante, D., Falanga, A., Gerotzafias, G.T., Haim, N., Kakkar, A.K., Khorana, A.A., Lecumberri, R., Mandala, M., Marty, M., Monreal, M., Mousa, S.A., Noble, S., Pabinger, I., Prandoni, P., Prins, M.H., Qari, M.H., Streiff, M.B., Syrigos, K., Bounameaux, H., Büller, H.R., 2013. International clinical practice guidelines for the treatment and prophylaxis of venous thromboembolism in patients with cancer. *J. Thromb. Haemost.* 11, 56–70.
- Fidler, I., 2003. The pathogenesis of cancer metastasis: The “seed and soil” hypothesis revisited. *Nat. Rev. Cancer* 3, 453–458.
- Flaumenhaft, R., De Ceunynck, K., 2017. Targeting PAR1: Now What? *Trends Pharmacol. Sci.* 38, 701–716.
- Forbes, S., Beare, D., Gunasekaran, P., Leung, K., Bindal, N., Boutselakis, H., Ding, M., Bamford, S., Cole, C., Ward, S., Kok, C., Jia, M., De, T., Teague, J., Stratton, M., McDermott, U., Campbell, P., 2015. COSMIC: Exploring the world’s knowledge of somatic mutations in human cancer. *Nucleic Acids Res.* 43, D805–D811.
- Francia, G., Cruz-Munoz, W., Man, S., Xu, P., Kerbel, R., 2011. Mouse models of advanced spontaneous metastasis for experimental therapeutics. *Nat. Rev. Cancer* 11, 135–141.
- Fricker, L., 1988. Carboxypeptidase E. *Annu. Rev. Physiol.* 50, 309–321.
- Fricker, L., Das, B., Angeletti, R., 1990. Identification of the pH-dependent Membrane Anchor of Carboxypeptidase E. *J. Biol. Chem.* 265, 2476–2482.
- Fricker, L., Plummer, T.J., Snyder, S., 1983. Enkephalin convertase: Potent, selective, and irreversible inhibitors. *Biochem. Biophys. Res. Commun.* 111, 994–1000.
- Fricker, L., Snyder, S., 1982. Enkephalin convertase: purification and characterization of a specific enkephalin-synthesizing carboxypeptidase localized to adrenal chromaffin granules. *Proc. Natl. Acad. Sci. U. S. A.* 79, 3886–90.
- Fricker, L., Snyder, S., 1983. Purification and characterization of enkephalin convertase, an enkephalin-synthesizing carboxypeptidase. *J. Biol. Chem.* 258, 10950–10955.
- Fuhrman, S., Lasky, L., Limas, C., 1982. Prognostic significance of morphologic parameters in renal cell carcinoma. *Am. J. Surg. Pathol.* 6, 655–63.

## G

- Gao, D., Nolan, D., Mellick, A., Bambino, K., McDonnell, K., Mittal, V., 2008. Endothelial Progenitor Cells Control the Angiogenic Switch in Mouse Lung Metastasis. *Science* (80-. ). 319, 195–198.

- Gay, L., Felding-Habermann, B., 2011. Contribution of platelets to tumour metastasis. *Nat. Rev. Cancer* 11, 123–134.
- Gerlinger, M., Horswell, S., Larkin, J., Rowan, A., Salm, M., Varela, I., Fisher, R., Mcgranahan, N., Matthews, N., Santos, C., Martinez, P., Phillimore, B., Begum, S., Rabinowitz, A., Spencer-Dene, B., Gulati, S., Bates, P., Stamp, G., Pickering, L., Gore, M., Nicol, D., Hazell, S., Futreal, P., Stewart, A., Swanton, C., 2014. Genomic architecture and evolution of clear cell renal cell carcinomas defined by multiregion sequencing. *Nat. Genet.* 46, 225–233.
- Gerlinger, M., Rowan, A., Horswell, S., Larkin, J., Endesfelder, D., Gronroos, E., Martinez, P., Matthews, N., Stewart, A., Tarpey, P., Varela, I., Phillimore, B., Begum, S., McDonald, N., Butler, A., Jones, D., Raine, K., Latimer, C., Santos, C.R., Nohadani, M., Eklund, A.C., Spencer-Dene, B., Clark, G., Pickering, L., Stamp, G., Gore, M., Szallasi, Z., Downward, J., Futreal, P., Swanton, C., 2012. Intratumor heterogeneity and branched evolution revealed by multiregion sequencing. *N. Engl. J. Med.* 366, 883–892.
- Ghosal, A., Lu, X., Penner, N., Gao, L., 2011. Identification of human liver cytochrome P450 enzymes involved in the metabolism of SCH 530348 (Vorapaxar), a potent oral thrombin protease-activated receptor 1. *Drug Metab. Dispos. Biol. fate Chem.* 39, 30–38.
- Giancotti, F., 2013. Mechanisms governing metastatic dormancy and reactivation. *Cell* 155, 750–764.
- Gómez-Cuadrado, L., Tracey, N., Ma, R., Qian, B., Brunton, V., 2017. Mouse models of metastasis: progress and prospects. *Dis. Model. Mech.* 10, 1061–1074.
- Gong, J., Maia, M., Dizman, N., Govindarajan, A., Pal, S., 2016. Metastasis in renal cell carcinoma: Biology and implications for therapy. *Asian J. Urol.* 3, 286–292.
- Greene, D., Das, B., Fricker, L., 1992. Regulation of carboxypeptidase E. Effect of pH, temperature and  $\text{CO}_2$  on kinetic parameters of substrate hydrolysis. *Biochem J* 285, 613–618.
- Greene, F., Page, D., Fleming, I., Fritz, A., Balch, C., Haller, D., Morrow, M., 2002. *AJCC Cancer Staging Manual*. Springer New York, New York, NY.
- Gundem, G., Van Loo, P., Kremeyer, B., Alexandrov, L., Tubio, J., Papaemmanuil, E., Brewer, D., Kallio, H., Högnäs, G., Annala, M., Kivinummi, K., Goody, V., Latimer, C., O'Meara, S., Dawson, K., Isaacs, W., Emmert-Buck, M., Nykter, M., Foster, C., Kote-Jarai, Z., Easton, D., Whitaker, H., Neal, D., Cooper, C., Eeles, R., Visakorpi, T., Campbell, P., McDermott, U., Wedge, D., Bova, G., 2015. The evolutionary history of lethal metastatic prostate cancer. *Nature* 520, 353–357.
- Gupta, G., Massagué, J., 2006. Cancer Metastasis: Building a Framework. *Cell* 127, 679–695.
- Gupta, K., Miller, J., Li, J., Russell, M., Charbonneau, C., 2008. Epidemiologic and socioeconomic burden of metastatic renal cell carcinoma (mRCC): a literature review. *Cancer Treat. Rev.* 34, 193–205.

## H

- Han, N., Jin, K., He, K., Cao, J., Teng, L., 2011. Protease-activated receptors in cancer: A systematic review. *Oncol. Lett.* 2, 599–608.
- Hanahan, D., Weinberg, R., 2011. Hallmarks of cancer: The next generation. *Cell* 144, 646–674.
- Hart, I., Fidler, I., 1980. Role of organ selectivity in the determination of metastatic patterns of b16 melanoma. *Cancer Res.* 40, 2281–2287.
- He, P., Varticovski, L., Bowman, E., Fukuoka, J., Welsh, J., Miura, K., Jen, J., Gabrielson, E., Brambilla, E., Travis, W., Harris, C., 2004. Identification of carboxypeptidase E and gamma-glutamyl hydrolase as biomarkers for pulmonary neuroendocrine tumors by cDNA microarray. *Hum. Pathol.* 35, 1196–209.
- Hiratsuka, S., Watanabe, A., Aburatani, H., Maru, Y., 2006. Tumour-mediated upregulation of chemoattractants and recruitment of myeloid cells predetermines lung metastasis. *Nat. Cell Biol.* 8, 1369–1375.
- Holmgren, L., O'Reilly, M., Folkman, J., 1995. Dormancy of micrometastases: balanced proliferation and apoptosis in the presence of angiogenesis suppression. *Nat. Med.* 1, 149–53.
- Hook, V., Eiden, L., Brownstein, M., 1982. A carboxypeptidase processing enzyme for enkephalin precursors. *Nature* 295, 341–2.
- Höring, E., Harter, P., Seznec, J., Schittenhelm, J., Bühring, H., S, B., Von Hattingen, E., Zachskorn, C., Mittelbronn, M., Naumann, U., 2012. The “go or grow” potential of gliomas is linked to the neuropeptide processing enzyme carboxypeptidase E and mediated by metabolic stress. *Acta Neuropathol.* 124, 83–97.
- Hsieh, J., Purdue, M., Signoretti, S., Swanton, C., Albiges, L., Schmidinger, M., Heng, D., Larkin, J., Ficarra, V., 2017. Renal cell carcinoma. *Nat. Rev. Dis. Prim.* 3, 17009.
- Huang, S., Wu, H., Chen, Y., Murthy, S., Chiu, Y., Chang, Y., Chang, I., Yang, X., Loh, Y., 2016. Carboxypeptidase E is a prediction marker for tumor recurrence in early-stage hepatocellular carcinoma. *Tumour Biol.* 37, 9745–9753.

## I

- Ilina, E., Armento, A., Sanchez, L., Reichlmeir, M., Braun, Y., Penski, C., Capper, D., Sahm, F., Jennewein, L., Harter, P., Zukunft, S., Fleming, I., Schulte, D., Le Guerroué, F., Behrends, C., Ronellenfisch, M., Naumann, U., Mittelbronn, M., 2017. Effects of soluble CPE on glioma cell migration are associated with mTOR activation and enhanced glucose flux. *Oncotarget* 8, 67567–67591.
- International Cancer Genome Consortium (ICGC), 2018. ICGC Data Portal [WWW Document]. URL <https://dcc.icgc.org/> (accessed 6.20.18).
- Isermann, B., 2017. Homeostatic effects of coagulation protease-dependent signaling and protease activated receptors. *J. Thromb. Haemost.* 15, 1273–1284.

**J**

- Ji, L., Wu, H., Qin, X., Lan, R., 2017. Dissecting carboxypeptidase E: properties, functions and pathophysiological roles in disease. *Endocr. Connect.* 6, R18–R38.
- Joose, S., Gorges, T., Pantel, K., 2015. Biology, detection, and clinical implications of circulating tumor cells. *EMBO Mol. Med.* 7, 1–11.

**K**

- Kahale, L., Hakoum, M., Tsolakian, I., Matar, C., Terrenato, I., Sperati, F., Barba, M., Yosucio, V., Schünemann, H., AKL, E., 2018. Anticoagulation for the long-term treatment of venous thromboembolism in people with cancer. *Cochrane database Syst. Rev.* 6, CD006649-CD006649.
- Kalluri, R., Zeisberg, M., 2006. Fibroblasts in cancer. *Nat. Rev. Cancer* 6, 392–401.
- Kaplan, R., Riba, R., Zacharoulis, S., Bramley, A., Vincent, L., Costa, C., MacDonald, D., Jin, D., Shido, K., Kerns, S., Zhu, Z., Hicklin, D., Wu, Y., Port, J., Altorki, N., Port, E., Ruggero, D., Shmelkov, S., Jensen, K., Rafii, S., Lyden, D., 2005. VEGFR1-positive haematopoietic bone marrow progenitors initiate the pre-metastatic niche. *Nature* 438, 820–827.
- Katt, M., Placone, A., Wong, A., Xu, Z., Searson, P., 2016. In Vitro Tumor Models: Advantages, Disadvantages, Variables, and Selecting the Right Platform. *Front. Bioeng. Biotechnol.* 4, 12.
- Kersten, K., de Visser, K., van Miltenburg, M., Jonkers, J., 2016. Genetically engineered mouse models in oncology research and cancer medicine. *EMBO Mol. Med.* 9, 137–153.
- Khanna, C., Hunter, K., 2005. Modeling metastasis in vivo. *Carcinogenesis* 26, 513–523.
- Khorana, A., 2010. Venous thromboembolism and prognosis in cancer. *Thromb. Res.* 125, 490–3.
- Kim, M., Evans, D., Wang, H., Abbruzzese, J., Fleming, J., Gallick, G., 2009. Generation of orthotopic and heterotopic human pancreatic cancer xenografts in immunodeficient mice. *Nat. Protoc.* 4, 1670–80.
- Kim, M., Gans, J., Nogueira, C., Wang, A., Paik, J., Feng, B., Brennan, C., Hahn, W., Cordon-Cardo, C., Wagner, S.N., Flotte, T.J., Duncan, L.M., Granter, S.R., Chin, L., 2006. Comparative Oncogenomics Identifies NEDD9 as a Melanoma Metastasis Gene. *Cell* 125, 1269–1281.
- Kiss, F., Simon, A., Csáthy, L., Hevessy, Z., Katona, E., Kiss, C., Kappelmayer, J., 2008. A coagulation factor becomes useful in the study of acute leukemias: studies with blood coagulation factor XIII. *Cytometry. A* 73, 194–201.
- Klerk, C., Smorenburg, S., Otten, H., Lensing, A., Prins, M., Piovella, F., Prandoni, P., Bos, M., Richel, D., van Tienhoven, G., Büller, H., 2005. The Effect of Low Molecular Weight Heparin on Survival in Patients With Advanced Malignancy. *J. Clin. Oncol.* 23, 2130–2135.
- Kohler, H.P., Grant, P.J., 2000. Plasminogen-Activator Inhibitor Type 1 and Coronary Artery Disease. *N. Engl. J. Med.* 342, 1792–1801.



**L**

- Labelle, M., Hynes, R., 2012. The initial hours of metastasis: The importance of cooperative host-tumor cell interactions during hematogenous dissemination. *Cancer Discov.* 2, 1091–1099.
- Lambert, A., Pattabiraman, D., Weinberg, R., 2017. Emerging Biological Principles of Metastasis. *Cell* 168, 670–691.
- Lee, A., 2007. The effects of low molecular weight heparins on venous thromboembolism and survival in patients with cancer, *Thrombosis Research*.
- Lee, S., Suh, I., Lee, E., Hur, G., Lee, S., Lee, S., Shin, C., Shim, J., In, K., Kang, K., Yoo, S., Kim, J., 2013. Relationships of coagulation factor XIII activity with cell-type and stage of non-small cell lung cancer. *Yonsei Med. J.* 54, 1394–1399.
- Lee, T., Murthy, S., Cawley, N., Dhanvantari, S., Hewitt, S., Lou, H., Lau, T., Ma, S., Huynh, T., Wesley, R., Ng, I., Pacak, K., Poon, R., Loh, Y., 2011. An N-terminal truncated carboxypeptidase E splice isoform induces tumor growth and is a biomarker for predicting future metastasis in human cancers. *J. Clin. Invest.* 121, 880–892.
- Li, A., Garcia, D.A., Lyman, G.H., Carrier, M., 2018. Direct oral anticoagulant (DOAC) versus low-molecular-weight heparin (LMWH) for treatment of cancer associated thrombosis (CAT): A systematic review and meta-analysis. *Thromb. Res.* 1–6.
- Liang, X., Li, L., Wu, G., Xie, Y., Zhang, G., Chen, W., Yang, H., Liu, Q., Li, W., He, W., Huang, Y., Zeng, X., 2013. Upregulation of CPE promotes cell proliferation and tumorigenicity in colorectal cancer. *BMC Cancer* 13, 412.
- Lima, L., Monteiro, R., 2013. Activation of blood coagulation in cancer: implications for tumor progression. *Biosci. Rep.* 33, 1–24.
- Linehan, W., Srinivasan, R., Schmidt, L., 2010. The genetic basis of kidney cancer: A metabolic disease. *Nat. Rev. Urol.* 7, 277–285.
- Liu, A., Shao, C., Jin, G., Liu, R., Hao, J., Shao, Z., Liu, Q., Hu, X., 2014. Downregulation of CPE regulates cell proliferation and chemosensitivity in pancreatic cancer. *Tumour Biol.* 35, 12459–12465.
- Liu, X., Yu, J., Song, S., Yue, X., Li, Q., 2017. Protease-activated receptor-1 (PAR-1): a promising molecular target for cancer, *Oncotarget*.
- Lorand, L., 2001. Factor XIII: structure, activation, and interactions with fibrinogen and fibrin. *Ann. N. Y. Acad. Sci.* 936, 291–311.
- Lorand, L., Gray, A., Brown, K., Credo, R., Curtis, C., Domanik, R., Stenberg, P., 1974. Dissociation of the subunit structure of fibrin stabilizing factor during activation of the zymogen. *Biochem. Biophys. Res. Commun.* 56, 914–922.

---

Lu, P., Weaver, V., Werb, Z., 2012. The extracellular matrix: a dynamic niche in cancer progression. *J. Cell Biol.* 196, 395–406.

Lum, D., Matsen, C., Welm, A., Welm, B., 2012. Human Primary Tumorgraft Models: Comparisons with Traditional Oncology Pre-Clinical Models and The Clinical Relevance and Utility of Primary Tumorgrafts in Basic and Translational Oncology Research. *Curr. Protoc. Pharmacol.* 84112, 1–11.

## M

Maddipati, R., Stanger, B., 2015. Pancreatic Cancer Metastases Harbor Evidence of Polyclonality. *Cancer Discov.* 5, 1086–97.

Maleno, I., Aptsiauri, N., Cabrera, T., Gallego, A., Paschen, A., Lopez-Nevot, M., Garrido, F., 2011. Frequent loss of heterozygosity in the beta2-microglobulin region of chromosome 15 in primary human tumors. *Immunogenetics* 63, 65–71.

Mandalà, M., Falanga, A., Roila, F., 2011. Management of venous thromboembolism (VTE) in cancer patients: ESMO clinical practice guidelines. *Ann. Oncol.* 22, 85–92.

Manser, E., Fernandez, D., Loo, L., Goh, P., Monfries, C., Hallt, C., Lim, L., 1990. Human carboxypeptidase E. *Biochem. J.* 267, 517–525.

Massagué, J., Obenauf, A., 2016a. Metastatic colonization by circulating tumour cells. *Nature* 529, 298–306.

Massagué, J., Obenauf, A., 2016b. Metastatic Colonization. *Nature* 529, 298–306.

Mehrazin, R., Dulaimi, E., Uzzo, R., Devarjan, K., Pei, J., Smaldone, M., Kutikov, A., Testa, J., Al-Saleem, T., 2017. The correlation between gain of chromosome 8q and survival in patients with clear and papillary renal cell carcinoma. *Ther. Adv. Urol.* 10, 3–10.

Mihara, K., Ramachandran, R., Saifeddine, M., Hansen, K., Renaux, B., Polley, D., Gibson, S., Vanderboor, C., Hollenberg, M., 2016. Thrombin-Mediated Direct Activation of Proteinase-Activated Receptor-2: Another Target for Thrombin Signaling. *Mol. Pharmacol.* 89, 606–14.

Moch, H., Cubilla, A., Humphrey, P., Reuter, V., Ulbright, T., 2016a. The 2016 WHO Classification of Tumours of the Urinary System and Male Genital Organs—Part A: Renal, Penile, and Testicular Tumours. *Eur. Urol.* 70, 93–105.

Moch, H., Humphrey, P., Ulbright, T., Reuter, V., 2016b. WHO Classification of Tumours of the Urinary System and Male Genital Organs, 4th ed. IARC.

Moch, H., Presti Jr., J., Sauter, G., Buchholz, N., Jordan, P., Mihatsch, M., Waldman, F., 1996. Genetic aberrations detected by comparative genomic hybridization are associated with clinical outcome in renal cell carcinoma. *Cancer Res.* 56, 27–30.

Morita, R., Ishikawa, J., Tsutsumi, M., Hikiji, K., Tsukada, Y., Kamidono, S., Maeda, S., Nakamura, Y., 1991. Allelotype of renal cell carcinoma. *Cancer Res.* 51, 820–823.

- Morrissey, C., True, L., Roudier, M., Coleman, I., Hawley, S., Nelson, P., Coleman, R., Wang, Y., Corey, E., Lange, P., Higano, C., Vessella, R., 2008. Differential expression of angiogenesis associated genes in prostate cancer bone, liver and lymph node metastases. *Clin. Exp. Metastasis* 25, 377–88.
- Morrow, D., Braunwald, E., Bonaca, M., Ameriso, S., Dalby, A., Fish, M., Fox, K., Lipka, L., Liu, X., Nicolau, J., Ophuis, A., Paolasso, E., Scirica, B., Spinar, J., Theroux, P., Wiviott, S., Strony, J., Murphy, S., 2012. Vorapaxar in the Secondary Prevention of Atherothrombotic Events. *N. Engl. J. Med.* 366, 1404–1413.
- Moserle, L., Casanovas, O., 2013. Anti-angiogenesis and metastasis: a tumour and stromal cell alliance. *J. Intern. Med.* 273, 128–137.
- Murthy, S., Dupart, E., Al-Sweel, N., Chen, A., Cawley, N., Loh, Y., 2013a. Carboxypeptidase E promotes cancer cell survival, but inhibits migration and invasion. *Cancer Lett.* 341, 204–213.
- Murthy, S., Pacak, K., Loh, Y.P., 2010. Carboxypeptidase E: elevated expression correlated with tumor growth and metastasis in pheochromocytomas and other cancers. *Cell Mol Neurobiol* 30, 1377–1381.
- Murthy, S., Thouennon, E., Li, W., Cheng, Y., Bhupatkar, J., Cawley, N., Lane, M., Merchenthaler, I., Loh, Y., 2013b. Carboxypeptidase e protects hippocampal neurons during stress in male mice by up-regulating prosurvival BCL2 protein expression. *Endocrinology* 154, 3284–3293.
- Muszbek, L., Ádány, R., Mikkolla, H., 1996. Novel Aspects of Blood Coagulation Factor XIII. 1. Structure, Distribution, Activation, and Function. *Crit. Rev. Clin. Laboratory Sci.* 33, 357–42.
- Muszbek, L., Bereczky, Z., Bagoly, Z., Komaromi, I., Katona, E., 2011. Factor XIII: A Coagulation Factor With Multiple Plasmatic and Cellular Functions. *Physiol. Rev.* 91, 931–972.

## N

- Nash, G., Turner, L., Scully, M., Kakkar, A., 2002. Platelets and cancer. *Lancet Oncol.* 3, 425–430.
- Neel, B., Jhanwar, S., Chaganti, R., Hayward, W., 1982. Two human c-onc genes are located on the long arm of chromosome 8. *Proc. Natl. Acad. Sci. U. S. A.* 79, 7842–6.
- New Health Advisor [WWW Document], 2018. URL <http://www.newhealthadvisor.com/What-Is-the-Difference-between-Pulmonary-Circulation-and-Systemic-Circulation.html>
- Nguyen, D., Bos, P., Massagué, J., 2009. Metastasis: From dissemination to organ-specific colonization. *Nat. Rev. Cancer* 9, 274–284.
- Nguyen, D.X., Massagué, J., 2007. Genetic determinants of cancer metastasis. *Nat. Rev. Genet.* 8, 341–352.
- Nierodzik, M., Chen, K., Takeshita, K., Li, J., Huang, Y., Feng, X., D’Andrea, M., Andrade-Gordon, P., Karpatkin, S., 1998. Protease-activated receptor 1 (PAR-1) is required and rate-limiting for thrombin-enhanced experimental pulmonary metastasis. *Blood* 92, 3694–3700.

- Nierodzick, M., Karpatkin, S., 2006. Thrombin induces tumor growth, metastasis, and angiogenesis: Evidence for a thrombin-regulated dormant tumor phenotype. *Cancer Cell* 10, 355–362.
- Nieswandt, B., Hafner, M., Echtenacher, B., Männel, D., 1999. Lysis of tumor cells by natural killer cells in mice is impeded by platelets. *Cancer Res.* 59, 1295–1300.
- NIH, 2018. U.S. National Library of Medicine [WWW Document]. URL <https://ghr.nlm.nih.gov/handbook/illustrations/isochromosomes> (accessed 6.19.18).
- Nowell, P., 1976. The clonal evolution of tumor cell populations. *Science* 194, 23–8.

## O

- O'Donoghue, M., Bhatt, D., Wiviott, S., Goodman, S., Fitzgerald, D., Angiolillo, D., Goto, S., Montalescot, G., Zeymer, U., Aylward, P., Guetta, V., Dudek, D., Ziecina, R., Contant, C., Flather, M., 2011. Safety and tolerability of atopaxar in the treatment of patients with acute coronary syndromes: The lessons from antagonizing the cellular effects of thrombin-acute coronary syndromes trial. *Circulation* 123, 1843–1853.
- O'Neill, G., Seo, S., Serebriiskii, I., Lessin, S., Golemis, E., 2007. A new central scaffold for metastasis: Parsing HEF1/Cas-L/NEDD9. *Cancer Res.* 67, 8975–8979.
- Obenauf, A., Massagué, J., 2015. Surviving at a Distance: Organ-Specific Metastasis. *Trends in Cancer* 1, 76–91.

## P

- Paget, S., 1889. The Distribution of Secondary Growths in Cancer of the Breast. *Lancet* 133, 571–573.
- Palumbo, J., 2008. Mechanisms Linking Tumor Cell – Associated Procoagulant Function to Tumor Dissemination 1, 154–160.
- Palumbo, J., Barney, K., Blevins, E., Shaw, M., Mishra, A., Flick, M., Kombrinck, K., Talmage, K., Sourj, M., Ichinose, A., Degen, J., 2008. Factor XIII transglutaminase supports hematogenous tumor cell metastasis through a mechanism dependent on natural killer cell function. *J. Thromb. Haemost.* 6, 812–819.
- Park, J., Loh, Y., 2008. Minireview: How Peptide Hormone Vesicles Are Transported to the Secretion Site for Exocytosis. *Mol. Endocrinol.* 22, 2583–2595.
- Pauli, C., Hopkins, B., Prandi, D., Shaw, R., Fedrizzi, T., Sboner, A., Sailer, V., Augello, M., Puca, L., Rosati, R., McNary, T., Churakova, Y., Cheung, C., Triscott, J., Pisapia, D., Rao, R., Mosquera, J., Robinson, B., Faltas, B., Emerling, B., Gadi, V., Bernard, B., Elemento, O., Beltran, H., Demichelis, F., Kemp, C., Grandori, C., Cantley, L., Rubin, M., 2017. Personalized in vitro and in vivo cancer models to guide precision medicine. *Cancer Discov.* 7, 462–477.
- Peinado, H., Lavotshkin, S., Lyden, D., 2011. The secreted factors responsible for pre-metastatic niche formation: Old sayings and new thoughts. *Semin. Cancer Biol.* 21, 139–146.

- Peinado, H., Zhang, H., Matei, I., Costa-Silva, B., Hoshino, A., Rodrigues, G., Psaila, B., Kaplan, R., Bromberg, J., Kang, Y., Bissell, M., Cox, T., Giaccia, A., Erler, J., Hiratsuka, S., Ghajar, C., Lyden, D., 2017. Pre-metastatic niches: Organ-specific homes for metastases. *Nat. Rev. Cancer* 17, 302–317.
- Pietras, K., Ostman, A., 2010. Hallmarks of cancer: interactions with the tumor stroma. *Exp. Cell Res.* 316, 1324–1331.
- Podlaha, O., Riester, M., De, S., Michor, F., 2012. Evolution of the cancer genome. *Trends Genet.* 28, 155–163.
- Poggi, A., Stella, M., Donati, M., 1993. The importance of blood cell-vessel wall interactions in tumour metastasis. *Baillieres. Clin. Haematol.* 6, 731–52.
- Polascik, T., Bostwick, D., Cairns, P., 2002. Molecular genetics and histopathologic features of adult distal nephron tumors. *Urology* 60, 941–6.
- Pollard, J., 2004. Opinion: Tumour-educated macrophages promote tumour progression and metastasis. *Nat. Rev. Cancer* 4, 71–78.
- Presti, J., Reuter, V., Cordon-Cardo, C., Mazumdar, M., Fair, W., Jhanwar, S., 1993. Allelic Deletions in Renal Tumors: Histopathological Correlations. *Cancer Res.* 53, 5780–5783.
- Psaila, B., Lyden, D., 2009. The metastatic niche: Adapting the foreign soil. *Nat. Rev. Cancer* 9, 285–293.

## R

- Reymond, N., D'Água, B., Ridley, A., 2013. Crossing the endothelial barrier during metastasis. *Nat. Rev. Cancer* 13, 858–70.
- Richardson, V., Cordell, P., Standeven, K., Carter, A., 2013. Substrates of Factor XIII-A: roles in thrombosis and wound healing. *Clin. Sci.* 124, 123–137.
- Ricketts, C., De Cubas, A., Fan, H., Smith, C., Lang, M., Reznik, E., Bowlby, R., Gibb, E., Akbani, R., Beroulhim, R., Bottaro, D., Choueiri, T., Gibbs, R., Godwin, A., Haake, S., Hakimi, A., Henske, E., Hsie, J., Ho, T., Kanchi, R., Krishnan, B., Kwiatkowski, D., Lui, W., Merino, M., Mills, G., Myers, J., Nickerson, M., Reuter, V., Schmidt, L., Shelley, C., Shen, H., Shuch, B., Signoretti, S., Srinivasan, R., Tamboli, P., Thomas, G., Vincent, B., Vocke, C., Wheeler, D., Yang, L., Kim, W., Robertson, A., Network, C.G.A.R., Spellman, P., Rathmell, W., Linehan, W., 2018. The Cancer Genome Atlas Comprehensive Molecular Characterization of Renal Cell Carcinoma. *Cell Rep.* 23, 313–326.
- Rini, B., Campbell, S., Escudier, B., 2009. Renal cell carcinoma. *Lancet* 373, 1119–1132.
- Rojas-Hernandez, C., 2018. The role of direct oral anticoagulants in cancer-related venous thromboembolism: a perspective beyond the guidelines. *Support. Care Cancer* 26, 711–720.
- Rueckert, J., Devitt, K., Gardner, J., 2018. Renal Cell Carcinoma with monosomy 8: A Case Series and Review of the Literature. *J. Assoc. Genet. Technol.* 44, 5–9.

## S

- Sakata, Y., Aoki, N., 1980. Cross-linking of alpha 2-plasmin inhibitor to fibrin by fibrin-stabilizing factor. *J. Clin. Invest.* 65, 290–297.
- Samaratunga, H., Gianduzzo, T., Delahunt, B., 2014. The ISUP system of staging, grading and classification of renal cell neoplasia. *J. kidney cancer VHL* 1, 26–39.
- Sanford, D., Naidu, A., Alizadeh, N., Lazo-Langner, A., 2014. The effect of low molecular weight heparin on survival in cancer patients: An updated systematic review and meta-analysis of randomized trials. *J. Thromb. Haemost.* 12, 1076–1085.
- Sankin, A., Hakimi, A., Mikkilineni, N., Ostrovnaya, I., Silk, M., Liang, Y., Mano, R., Chevinsky, M., Motzer, R., Solomon, S., Cheng, E., Durack, J., Coleman, J., Russo, P., Hsieh, J., 2014. The impact of genetic heterogeneity on biomarker development in kidney cancer assessed by multiregional sampling. *Cancer Med.* 3, 1485–1492.
- Saxena, M., Christofori, G., 2013. Rebuilding cancer metastasis in the mouse. *Mol. Oncol.* 7, 1–14.
- Schmaier, A., Ambesh, P., Campia, U., 2018. Venous Thromboembolism and Cancer. *Curr. Cardiol. Rep.* 10, 89–98.
- Schroeder, V., Kohler, H., 2016. Factor XIII : Structure and Function. *Semin. Thromb. Hemost.* 42, 422–428.
- SciPY, 2018. SciPy [WWW Document]. URL <https://www.scipy.org>
- Shen, H., Tan, J., Shang, J., Hou, M., Liu, J., He, L., Yao, S., He, S., 2016. CPE overexpression is correlated with pelvic lymph node metastasis and poor prognosis in patients with early-stage cervical cancer. *Arch. Gynecol. Obstet.* 294, 333–42.
- Sherry, S., 2001. dbSNP: the NCBI database of genetic variation. *Nucleic Acids Res.* 29, 308–311.
- Shi, X., Gangadharan, B., Brass, L., Ruf, W., Mueller, B., 2004. Protease-activated receptors (PAR1 and PAR2) contribute to tumor cell motility and metastasis. *Mol. Cancer Res.* 2, 395–402.
- Simon, Á., Bagoly, Z., Hevessy, Z., Csáthy, L., Katona, É., Vereb, G., Ujfalusi, A., Szerafin, L., Muszbek, L., Kappelmayer, J., 2012. Expression of coagulation factor XIII subunit A in acute promyelocytic leukemia. *Cytom. Part B - Clin. Cytom.* 82 B, 209–216.
- Siolas, D., Hannon, G., 2013. Patient-derived tumor xenografts: Transforming clinical samples into mouse models. *Cancer Res.* 73, 5315–5319.
- Skalka, N., Caspi, M., Caspi, E., Loh, Y., Rosin-Arbesfeld, R., 2013. Carboxypeptidase E: a negative regulator of the canonical Wnt signaling pathway. *Oncogene* 32, 2836–2847.
- Skalka, N., Caspi, M., Lahav-Ariel, L., Loh, Y.P., Hirschberg, K., Rosin-Arbesfeld, R., 2016. Carboxypeptidase E (CPE) inhibits the secretion and activity of Wnt3a. *Oncogene*.

- Soto, A., Smith, T., Chen, B., Bhattacharya, S., Cordova, I., Kenakin, T., Vaidehi, N., Trejo, J., 2015. N-linked glycosylation of protease-activated receptor-1 at extracellular loop 2 regulates G-protein signaling bias. *Proc. Natl. Acad. Sci. U. S. A.* 112, E3600-8.
- Soto, A., Trejo, J., 2010. N-Linked Glycosylation of Protease-activated Receptor-1 Second Extracellular Loop: a critical determinant for ligand-induced receptor activation and internalization. *J. Biol. Chem.* 285, 18781–93.
- Stegner, D., Dütting, S., Nieswandt, B., 2014. Mechanistic explanation for platelet contribution to cancer metastasis. *Thromb. Res.* 133, 149–53.
- Steiner, D., 1998. The proprotein convertases. *Curr. Opin. Chem. Biol.* 2, 31–39.
- Streiff, M., 2016. Thrombosis in the setting of cancer. *Hematology* 2016, 196–205.
- Strlic, B., Offermanns, S., 2017. Intravascular Survival and Extravasation of Tumor Cells. *Cancer Cell* 32, 282–293.
- Strittmatter, S., Lynch, D., Snyder, S., 1984. [3H]guanidinoethylmercaptosuccinic acid binding to tissue homogenates. Selective labeling of enkephalin convertase. *J. Biol. Chem.* 259, 11812–7.
- Sultan, M., Schulz, M., Richard, H., Magen, A., Klingenhoff, A., Scherf, M., Seifert, M., Borodina, T., Soldatov, A., Parkhomchuk, D., Schmidt, D., O’Keeffe, S., Haas, S., Vingron, M., Lehrach, H., Yaspo, M., 2008. A Global View of Gene Activity and Alternative Splicing by Deep Sequencing of the Human Transcriptome. *Science* (80- ). 321, 956–960.
- Sun, J., Meng, D., Li, L., Tian, X., Jia, Y., Wang, H., Yu, H., Sun, T., Qu, A., Shen, H., Bao, J., Zhang, G., 2016. N-terminal truncated carboxypeptidase E expression is associated with poor prognosis of lung adenocarcinoma. *Oncol. Lett.* 12, 4659–4664.
- Supattapone, S., Fricker, L., Snyder, S., 1984. Purification and Characterization of a Membrane-Bound Enkephalin-Forming Carboxypeptidase, “Enkephalin Convertase.” *J. Neurochem.* 42, 1017–1023.

## T

- Tanaka, T., Watanabe, T., Kitayama, J., Kanazawa, T., Kazama, Y., Tanaka, J., Kazama, S., Nagawa, H., 2009. Chromosome 18q Deletion as a Novel Molecular Predictor for Colorectal Cancer With Simultaneous Hepatic Metastasis. *Diagnostic Mol. Pathol.* 18, 219–225.
- TCGA, 2013. Comprehensive molecular characterization of clear cell renal cell carcinoma. *Nature* 499, 43–49.
- TCGA research network, 2018. The Cancer Genome Atlas [WWW Document]. URL <http://cancergenome.nih.gov/>. (accessed 3.15.18).
- Tesfamariam, B., 2016. Involvement of platelets in tumor cell metastasis. *Pharmacol. Ther.* 157, 112–119.
- Tohme, S., Simmons, R., Tsung, A., 2017. Surgery for cancer: A trigger for metastases. *Cancer Res.* 77, 1548–1552.

- Trejo, J., Hammes, S., Coughlin, S., 1998. Termination of signaling by protease-activated receptor-1 is linked to lysosomal sorting. *Cell Biol.* 95, 13698–13702.
- Tricoci, P., Huang, Z., Held, C., Moliterno, D., Armstrong, P., Van de Werf, F., White, H., Aylward, P., Wallentin, L., Chen, E., Lokhnygina, Y., Pei, J., Leonardi, S., Rorick, T., Kilian, A., Jennings, L., Ambrosio, G., Bode, C., Cequier, A., Cornel, J., Diaz, R., Erkan, A., Huber, K., Hudson, M., Jiang, L., Jukema, J., Lewis, B., Lincoff, A., Montalescot, G., Nicolau, J., Ogawa, H., Pfisterer, M., Prieto, J., Ruzylo, W., Sinnaeve, P., Storey, R., Valgimigli, M., Whellan, D., Widimsky, P., Strony, J., Harrington, R., Mahaffey, K., 2012. Thrombin-Receptor Antagonist Vorapaxar in Acute Coronary Syndromes. *N. Engl. J. Med.* 366, 20–33.
- Tsimafeyeu, I., Demidov, L., Madzhuga, A., Somonova, O., Yelizarova, A., 2009. Hypercoagulability as a prognostic factor for survival in patients with metastatic renal cell carcinoma. *J. Exp. Clin. Cancer Res.* 28, 30.
- Turajlic, S., Swanton, C., 2016. Metastasis as an evolutionary process. *Science* (80-. ). 352, 169–75.
- UK, C.R., 2012. Worldwide cancer incidence statistics [WWW Document]. URL <http://www.cancerresearchuk.org/health-professional/cancer-statistics/worldwide-cancer/incidence> (accessed 6.20.18).
- ## V
- Vairaktaris, E., Vassiliou, S., Yapijakis, C., Spyridonidou, S., Vylliotis, A., Derka, S., Nkenke, E., Fourtounis, G., Neukam, F., Patsouris, E., 2007. Increased risk for oral cancer is associated with coagulation factor XIII but not with factor XII. *Oncol. Rep.* 18, 1537–1543.
- Valastyan, S., Weingberg, R., 2011. Tumor Metastasis : Molecular Insights and Evolving Paradigms. *Cell* 147, 275–292.
- Van Es, N., Coppens, M., Schulman, S., Middeldorp, S., Harry, R., Es, N., Coppens, M., Schulman, S., Middeldorp, S., Harry, R., Van Es, N., Coppens, M., Schulman, S., Middeldorp, S., Harry, R., 2015. Direct oral anticoagulants compared with vitamin K antagonists for acute venous thromboembolism : evidence from phase 3 trials. *Blood* 124, 1968–1976.
- Vanharanta, S., Massagué, J., 2013. Origins of Metastatic Traits. *Cancer Cell* 24, 410–421.
- Venkatesan, S., Swanton, C., 2016. Tumor Evolutionary Principles: How Intratumor Heterogeneity Influences Cancer Treatment and Outcome. *Am. Soc. Clin. Oncol. Educ. B.* 35, 141–149.
- Vilijn, M., Das, B., Kessler, J., Flicker, L., 1989. Cultured Astrocytes and Neurons Synthesize and Secrete Carboxypeptidase E, a Neuropeptide-Processing Enzyme. *J. Neurochem.* 53, 1487–1493.



- Voss, M., Hakimi, A., Pham, C., Brannon, A., Chen, Y., Cunha, L., Akin, O., Liu, H., Takeda, S., Scott, S., Socci, N., Viale, A., Schultz, N., Sander, C., Reuter, V., Russo, P., Cheng, E., Motzer, R., Berger, M., Hsieh, J., 2014. Tumor genetic analyses of patients with metastatic renal cell carcinoma and extended benefit from mTOR inhibitor therapy. *Clin. Cancer Res.* 20, 1955–1964.
- Vu, T., Hung, D., Wheaton, V., Coughlin, S., 1991. Molecular cloning of a functional thrombin receptor reveals a novel proteolytic mechanism of receptor activation. *Cell* 64, 1057–1068.

## W

- Wang, A., 2015. Review of vorapaxar for the prevention of atherothrombotic events. *Expert Opin. Pharmacother.* 16, 1–14.
- Wang, H., Fu, W., Im, J., Zhou, Z., Santoro, S., Iyer, V., DiPersio, C., Yu, Q., Quaranta, V., Al-Mehdi, A., Muschel, R., 2004. Tumor cell alpha3beta1 integrin and vascular laminin-5 mediate pulmonary arrest and metastasis. *J. Cell Biol.* 164, 935–941.
- Wei, Q., Ye, Z., Zhong, X., Li, L., Wang, C., Myers, R., Palazzo, J., Fortuna, D., Yan, A., Waldman, S., Chen, X., Posey, J., Basu-Mallick, A., Jiang, B., Hou, L., Shu, J., Sun, Y., Xing, J., Li, B., Yang, H., 2017. Multiregion whole-exome sequencing of matched primary and metastatic tumors revealed genomic heterogeneity and suggested polyclonal seeding in colorectal cancer metastasis. *Ann. Oncol.* 28, 2135–2141.
- Weis, S., Cheresh, D., 2005. Pathophysiological consequences of VEGF-induced vascular permeability. *Nature* 437, 497–504.
- Wiviott, S., Flather, M., O'Donoghue, M., Goto, S., Fitzgerald, D., Cura, F., Aylward, P., Guetta, V., Dudek, D., Contant, C., Angiolillo, D., Bhatt, D., 2011. Randomized trial of atopaxar in the treatment of patients with coronary artery disease: The lessons from antagonizing the cellular effect of thrombin-coronary artery disease trial. *Circulation* 123, 1854–1863.
- Wojtukiewicz, M., Hempel, D., Sierko, E., Tucker, S., Honn, K., 2016. Thrombin-Unique coagulation system protein with multifaceted impacts on cancer and metastasis. *Cancer Metastasis Rev.* 35, 213–233.
- Wojtukiewicz, M.Z., Hempel, D., Sierko, E., Tucker, S.C., Honn, K. V., 2015. Protease-activated receptors (PARs)-biology and role in cancer invasion and metastasis. *Cancer Metastasis Rev.* 34, 775–796.
- World Health Organization, 2018. WHO | Cancer [WWW Document]. WHO. URL <http://www.who.int/cancer/en/> (accessed 6.25.18).

## X

- Xie, W., Leibl, M., Clark, M., Dohrmann, P., Kunze, T., Gieseler, F., 2005. Activation of the coagulation system in cancerogenesis and metastasation. *Biomed. Pharmacother.* 59, 70–75.

**Y**

- Yang, E., Cisowski, J., Nguyen, N., O'Callaghan, K., Xu, J., Agarwal, A., Kuliopulos, A., Covic, L., 2016. Dysregulated protease activated receptor 1 (PAR1) promotes metastatic phenotype in breast cancer through HMGA2. *Oncogene* 35, 1529–1540.
- Yap, T., Gerlinger, M., Yap, T., Gerlinger, M., Futreal, P., Pusztai, L., 2012. Intratumor Heterogeneity : Seeing the Wood for the Trees Intratumor. *Sci. Transl. Med.* 4, 1–5.
- Yates, A., Akanni, W., Amode, Mr., Barrell, D., Billis, K., Carvalho-Silva, D., Cummins, C., Clapham, P., Fitzgerald, S., Gil, L., Girón, C., Gordon, L., Hourlier, T., Hunt, S., Janacek, S., Johnson, N., Juettemann, T., Keenan, S., Lavidas, I., Martin, F., Maurel, T., McLaren, W., Murphy, D., Nag, R., Nuhn, M., Parker, A., Patricio, M., Pignatelli, M., Rahtz, M., Riat, H., Sheppard, D., Taylor, K., Thormann, A., Vullo, A., Wilder, S., Zadissa, A., Birney, E., Harrow, J., Muffato, M., Perry, E., Ruffier, M., Spudich, G., Trevanion, S., Cunningham, F., Aken, B., Zerbino, D., Flicek, P., 2016. Ensembl 2016. *Nucleic Acids Res.* 44, D710–D716.
- Yilmaz, M., Christofori, G., 2009. EMT, the cytoskeleton, and cancer cell invasion. *Cancer Metastasis Rev.* 28, 15–33.

**Z**

- Zbar, B., 1995. Von Hippel-Lindau disease and sporadic renal cell carcinoma. *Cancer Surv.* 25, 219–32.
- Zbar, B., Brauch, H., Talmadge, C., Linehan, M., 1987. Loss of alleles of loci on the short arm of chromosome 3 in renal cell carcinoma. *Nature* 327, 721–724.
- Zhang, C., Srinivasan, Y., Arlow, D., Fung, J., Palmer, D., Zheng, Y., Green, H., Pandey, A., Dror, R., Shaw, D., Weis, W., Coughlin, S., Kobilka, B., 2012. High-resolution crystal structure of human protease-activated receptor 1. *Nature* 492, 387–392.
- Zhou, K., Liang, H., Liu, Y., Yang, C., Liu, P., Jiang, X., 2013. Overexpression of CPE-DeltaN predicts poor prognosis in colorectal cancer patients. *Tumour Biol.* 34, 3691–3699.